

University of Patras
Department of Mechanical Engineering & Aeronautics
Stochastic Mechanical Systems & Automation (SMSA) Laboratory

Advanced Functional and Sequential Statistical Time Series Methods for Damage Diagnosis in Mechanical Structures

Ph.D. Thesis

Fotis P. Kopsaftopoulos

Submitted to the Department of Mechanical Engineering & Aeronautics
University of Patras, Greece

January 2012

Examining Committee

- **Spilios Fassois, Professor Ph.D. (supervisor)**
Department of Mechanical Engineering & Aeronautics
University of Patras, Greece
- **Dimitris Saravanos, Professor Ph.D. (advisor committee)**
Department of Mechanical Engineering & Aeronautics
University of Patras, Greece
- **Evangelos Dermatas, Associate Professor Ph.D. (advisor committee)**
Department of Electrical & Computer Engineering
University of Patras, Greece
- **John Sakellariou, Lecturer Ph.D.**
Department of Mechanical Engineering & Aeronautics
University of Patras, Greece
- **Tassos Bountis, Professor Ph.D.**
Department of Mathematics
University of Patras, Greece
- **Christos Papadopoulos, Professor Ph.D.**
Department of Mechanical Engineering & Aeronautics
University of Patras, Greece
- **Theodoros Philippidis, Associate Professor Ph.D.**
Department of Mechanical Engineering & Aeronautics
University of Patras, Greece

To my family and Maria.

Contents

Contents	v
Acknowledgements	vii
Summary	ix
Nomenclature	xi
1 Introduction	1
1.1 The general problem	1
1.1.1 Structural damage diagnosis	1
1.1.2 Identification of systems under multiple operating conditions	2
1.2 Critical review of the state-of-the-art	3
1.2.1 Structural damage diagnosis	3
1.2.2 Identification of systems under multiple operating conditions	6
1.3 Thesis goals	8
1.4 Thesis chapters and main contribution	8
1.4.1 Chapter II	8
1.4.2 Chapter III	10
1.4.3 Chapter IV	11
1.4.4 Chapter V	12
2 Experimental Assessment of Vibration Based Statistical Time Series Methods for Structural Health Monitoring	13
2.1 Introduction	14
2.2 Workframe of statistical time series methods for SHM	17
2.3 Concise overview of selected statistical time series methods for SHM	18
2.3.1 Non-parametric methods	19
2.3.1.1 A Power Spectral Density (PSD) based method	19

2.3.1.2	A Frequency Response Function (FRF) based method	19
2.3.2	Parametric methods	21
2.3.2.1	A model parameter based method	21
2.3.2.2	Residual based methods	21
2.3.2.3	The Sequential Probability Ratio Test (SPRT) based method	24
2.4	Application on a lightweight truss structure	24
2.4.1	The lightweight truss structure	25
2.4.2	The damage types and the experiments	25
2.4.3	Baseline phase: structural identification under various structural states (measurement position Y1)	26
2.4.3.1	Non-parametric methods	26
2.4.3.2	Parametric methods	27
2.4.4	Inspection phase (measurement position Y1)	28
2.4.4.1	PSD based method	28
2.4.4.2	FRF based method	29
2.4.4.3	Model parameter based method	31
2.4.4.4	Residual based methods	31
2.4.5	Summary results and discussion (all measurement positions)	34
2.5	Application on a scale aircraft skeleton structure	39
2.5.1	The scale aircraft skeleton structure	39
2.5.2	The damage scenarios and the experiments	39
2.5.3	Structural dynamics of the healthy structure	41
2.5.3.1	Non-parametric identification	41
2.5.3.2	Parametric identification	42
2.5.4	Application of scalar time series methods	43
2.5.4.1	The Power Spectral Density (PSD) based method	43
2.5.4.2	The Frequency Response Function (FRF) based method	45
2.5.4.3	The residual variance based method	45
2.5.4.4	The Sequential Probability Ratio Test (SPRT) based method	46
2.5.5	Application of vector time series methods	48
2.5.5.1	The model parameter based method	49
2.5.5.2	The residual likelihood function based method	51
2.5.6	Discussion	51
2.6	Concluding remarks	52

3 Identification of Stochastic Systems Under Multiple Operating Conditions: The

Vector-dependent Functionally Pooled (VFP) Parametrization	55
3.1 Introduction	56
3.2 Vector-dependent Functionally Pooled (VFP) model structure	58
3.2.1 The data set	58
3.2.2 The VFP-ARX model structure	59
3.2.3 The VFP-ARMAX model structure	62
3.2.4 The VFP model structure with innovations variance projection	64
3.3 Vector-dependent Functionally Pooled (VFP) model estimation	65
3.3.1 VFP-ARX model estimation	65
3.3.1.1 A Functionally Pooled (FP) linear regression framework	65
3.3.1.2 Least Squares (LS) based estimation methods	66
3.3.1.3 The Maximum Likelihood (ML) estimation method	68
3.3.2 VFP-ARMAX model estimation	70
3.3.2.1 The Prediction Error (PE) method	70
3.3.2.2 The two Stage Least Squares (2SLS) method	72
3.3.2.3 The Maximum Likelihood (ML) estimation method	72
3.4 Vector-dependent Functionally Pooled (VFP) model structure selection and validation	73
3.4.1 Model structure selection (identification)	74
3.4.1.1 Structure selection based on customary criteria	74
3.4.1.2 Genetic Algorithm (GA) based structure selection	74
3.4.2 Model validation	76
3.5 Asymptotic properties	77
3.5.1 Consistency analysis	77
3.5.2 Asymptotic distribution	78
3.6 Monte Carlo Studies	79
3.6.1 Test Case I: Complete parameter functional subspace	80
3.6.2 Test Case II: Non-complete parameter functional subspace	85
3.7 Concluding Remarks	93
Appendix A Bivariate Polynomials	97
Appendix B Proofs of Theorems	99
Appendix C Additional Monte Carlo Results	105
C.1 Test Case I: Complete parameter functional subspace	105
C.2 Test Case II: Non-complete parameter functional subspace	107

4	A Stochastic Functional Model Based Method for Vibration Based Damage Detection, Localization and Magnitude Estimation	109
4.1	Introduction	110
4.2	The VFP-ARX model based method	113
4.2.1	Baseline phase	113
4.2.1.1	Baseline modelling of the healthy structure	113
4.2.1.2	The notion of damage topology (mode)	114
4.2.1.3	Damage topology (mode) modelling	114
4.2.2	Inspection phase	117
4.2.2.1	Step I: Damage detection	117
4.2.2.2	Step II: Damage topology (mode) identification	118
4.2.2.3	Step III: Damage localization and magnitude estimation	119
4.3	The experimental set-up	120
4.3.1	The structure	120
4.3.2	The damage topologies and scenarios	120
4.3.3	The experimental procedure	121
4.3.4	The signals	122
4.4	Damage detection, localization, and magnitude estimation results	122
4.4.1	Baseline phase	124
4.4.1.1	Baseline modelling of the healthy structure	124
4.4.1.2	Modelling of the dynamics for damage topologies (modes) A, B, C	124
4.4.2	Inspection phase: damage detection, localization and magnitude estimation	126
4.5	Concluding remarks	129
5	A Sequential Statistical Time Series Method for Vibration Based Structural Health Monitoring	133
5.1	Introduction	134
5.2	Basic theory on sequential analysis	136
5.2.1	Binary hypotheses sequential testing	137
5.2.1.1	The Sequential Probability Ratio Test (SPRT)	137
5.2.1.2	The Operating Characteristic (OC) function	140
5.2.1.3	The Average Sample Number (ASN)	141
5.2.2	Sequential multihypothesis testing	142
5.2.2.1	The Armitage multihypothesis test	143
5.3	A sequential statistical time series method for SHM	143
5.3.1	The workframe	144

5.3.2	Baseline phase	144
5.3.2.1	Baseline modeling of the structure	144
5.3.3	Inspection phase	145
5.3.3.1	Damage detection	146
5.3.3.2	Damage identification and quantification	150
5.4	The experimental set-up	153
5.4.1	The structure	153
5.4.2	The damage types and the experiments	153
5.5	Damage detection, identification and quantification results	154
5.5.1	Baseline phase: structural identification under the healthy structural state . . .	155
5.5.1.1	Non-parametric identification	155
5.5.1.2	Parametric identification	155
5.5.2	Inspection phase	157
5.5.2.1	Damage detection	157
5.5.2.2	Damage identification and quantification	163
5.6	Concluding remarks	166
6	Conclusions	169
6.1	Thesis summary	169
6.2	Concluding remarks	171
6.2.1	General conclusions	171
6.2.2	Chapter conclusions	172
6.3	Future perspectives	174
	Bibliography	177
	List of Figures	187
	List of Tables	195
	Curriculum Vitae	197

Acknowledgements

This dissertation would not have been possible without the help and guidance of several individuals who in one way or another contributed and extended their valuable assistance in the preparation and completion of this study.

First and foremost I wish to thank my supervisor, Prof. Spilios Fassois, for giving me the chance, motivation and freedom to complete this thesis. Without his guidance, encouragement and technical support this dissertation would not have been possible.

I would also like to thank my advisory committee members, Prof. Dimitris Saravanos (Department of Mechanical Engineering & Aeronautics) and Associate Professor Evangelos Dermatas (Department of Electrical & Computer Engineering), for their guidance and support.

Lecturer John Sakellariou (Department of Mechanical Engineering & Aeronautics) and Dr. Dimitris Dimogiannopoulos (T.E.I. Piraeus) are greatly acknowledged for sharing their knowledge, expertise and enthusiasm with me.

The current and former members of the Stochastic Mechanical Systems & Automation (SMSA) laboratory have contributed immensely to my personal and professional evolution throughout the years of this dissertation. The SMSA group has been a source of friendships, advice and collaboration.

I am grateful that during my stay at the Department of Mechanical Engineering & Aeronautics and the SMSA laboratory I have had the chance to have next to me a friend and colleague like Minas Spyridonakos (Dipl-Eng. and soon to be Dr.). Words are not enough to express my gratitude for his presence and support. Thank you my friend.

I would also like to thank the current members of the SMSA laboratory, Dipl-Eng. Paul Michaelides and Dipl-Eng. Thodoris Mastrapostolis, for the time we spent together, both personal and professional. My journey was much more enjoyable with you guys on-board.

Furthermore, I would also like to thank the former members of the SMSA laboratory, and current friends, Dr. Aggelos Poulimenos, Dr. Demosthenes Rizos and Dr. John Hios for their numerous inspirational discussions and support during the first years of my thesis.

Lastly, I would like to thank my family for all their love and encouragement in all my pursuits. This thesis would have remained a dream had it not been for their support and understanding. And most of all for my loving, supportive and patient partner in life, Maria, whose faithful support during all the stages of this Ph.D. is so greatly appreciated. Thank you.

*Fotis P. Kopsaftopoulos
Patras, October 2011*

Summary

The past 30 years have witnessed major developments in vibration based damage detection and identification, also collectively referred to as damage diagnosis. Moreover, the past 10 years have seen a rapid increase in the amount of research related to Structural Health Monitoring (SHM) as quantified by the significant escalation in papers published on this subject. Thus, the increased interest in this engineering field and its associated potential constitute the main motive for this thesis.

The goal of the thesis is the development and introduction of novel advanced functional and sequential statistical time series methods for vibration based damage diagnosis and SHM. After the introduction of the first chapter, Chapter II provides an experimental assessment and comparison of vibration based statistical time series methods for Structural Health Monitoring (SHM) via their application on a lightweight aluminum truss structure and a laboratory scale aircraft skeleton structure. A concise overview of the main non-parametric and parametric methods is presented, including response-only and excitation-response schemes. Damage detection and identification are based on univariate (scalar) versions of the methods, while both scalar (univariate) and vector (multivariate) schemes are considered. The methods' effectiveness for both damage detection and identification is assessed via various test cases corresponding to different damage scenarios, multiple experiments and various sensor locations on the considered structures. The results of the chapter confirm the high potential and effectiveness of vibration based statistical time series methods for SHM.

Chapter III investigates the identification of stochastic systems under multiple operating conditions via Vector-dependent Functionally Pooled (VFP) models. In many applications a system operates under a variety of operating conditions (for instance operating temperature, humidity, damage location, damage magnitude and so on) which affect its dynamics, with each condition kept constant for a single commission cycle. Typical examples include mechanical structures operating under different environmental conditions, aircrafts under different flight conditions (altitude, velocity etc.), structures under different structural health states (various damage locations and magnitudes). In this way, damage location and magnitude may be considered as parameters that affect the operating conditions and as a result the structural dynamics. This chapter's work is based on the novel Functional Pooling (FP) framework, which has been recently introduced by the Stochastic Mechanical Systems & Automation (SMSA) group of the Mechanical Engineering and Aeronautics Department of University of Patras. The main characteristic of Functionally Pooled (FP) models is that their model parameters and innovations sequence depend functionally on the operating parameters, and are projected on appropriate functional subspaces spanned by mutually independent basis functions. Thus, the fourth chapter of the thesis addresses the problem of identifying a globally valid and parsimonious stochastic system model based on input-output data records obtained under a sample of operating conditions characterized by more than one parameters. Hence, models that include a vector characterization of the operating condition are postulated. The problem is tackled within the novel FP framework that postulates proper global discrete-time linear time series models of the ARX and ARMAX types, data pooling techniques, and statistical parameter estimation. Corresponding Vector-dependent Functionally Pooled (VFP) ARX and ARMAX models are postulated, and proper estimators of the Least

Squares (LS), Maximum Likelihood (ML), and Prediction Error (PE) types are developed. Model structure estimation is achieved via customary criteria (Bayesian Information Criterion) and a novel Genetic Algorithm (GA) based procedure. The strong consistency of the VFP-ARX least squares and maximum likelihood estimators is established, while the effectiveness of the complete estimation and identification method is demonstrated via two Monte Carlo studies.

Based on the postulated VFP parametrization a vibration based statistical time series method that is capable of effective damage detection, precise localization, and magnitude estimation within a unified stochastic framework is introduced in Chapter IV. The method constitutes an important generalization of the recently introduced Functional Model Based Method (FMBM) in that it allows, for the first time in the statistical time series methods context, for complete and precise damage localization on continuous structural topologies. More precisely, the proposed method can accurately localize damage anywhere on properly defined continuous topologies on the structure, instead of pre-defined specific locations. Estimator uncertainties are taken into account, and uncertainty ellipsoids are provided for the damage location and magnitude. To achieve its goal, the method is based on the extended class of Vector-dependent Functionally Pooled (VFP) models, which are characterized by parameters that depend on both damage magnitude and location, as well as on proper statistical estimation and decision making schemes. The method is validated and its effectiveness is experimentally assessed via its application to damage detection, precise localization, and magnitude estimation on a prototype GARTEUR-type laboratory scale aircraft skeleton structure. The damage scenarios considered consist of varying size small masses attached to various continuous topologies on the structure. The method is shown to achieve effective damage detection, precise localization, and magnitude estimation based on even a single pair of measured excitation-response signals.

Chapter V presents the introduction and experimental assessment of a sequential statistical time series method for vibration based SHM capable of achieving effective, robust and early damage detection, identification and quantification under uncertainties. The method is based on a combination of binary and multihypothesis versions of the statistically optimal Sequential Probability Ratio Test (SPRT), which employs the residual sequences obtained through a stochastic time series model of the healthy structure. In this work the full list of properties and capabilities of the SPRT are for the first time presented and explored in the context of vibration based damage detection, identification and quantification. The method is shown to achieve effective and robust damage detection, identification and quantification based on predetermined statistical hypothesis sampling plans, which are both analytically and experimentally compared and assessed. The method's performance is determined a priori via the use of the analytical expressions of the Operating Characteristic (OC) and Average Sample Number (ASN) functions in combination with baseline data records, while it requires on average a minimum number of samples in order to reach a decision compared to most powerful Fixed Sample Size (FSS) tests. The effectiveness of the proposed method is validated and experimentally assessed via its application on a lightweight aluminum truss structure, while the obtained results for three distinct vibration measurement positions prove the method's ability to operate based even on a single pair of measured excitation-response signals.

Finally, Chapter VI contains the concluding remarks and future perspectives of the thesis.

Nomenclature

Important conventions and symbols

- Bold-face upper/lower case symbols designate matrix/column-vector quantities, respectively.
- Matrix transposition is indicated by the superscript T .
- Definition is indicated by \triangleq .
- A functional argument in parentheses designates function of a real variable; for instance $x(t)$ is a function of analog time $t \in \mathbb{R}$.
- A functional argument in brackets designates function of an integer variable; for instance $x[t]$ is a function of normalized discrete time ($t = 1, 2, \dots$). The conversion from discrete normalized time to analog time is based on $(t - 1)T_s$, with T_s designating the sampling period.
- A functional argument including the imaginary unit designates complex function; for instance $X(j\omega)$ is a complex function of ω .
- A hat designates estimator/estimate of the indicated quantity; for instance $\hat{\theta}$ is an estimate of θ .
- The subscripts “o” and “u” designate quantities associated with the nominal (healthy) and current (unknown) state of the structure, respectively.

Symbols

$A[\mathcal{B}, \mathbf{k}]$: AutoRegressive (AR) polynomial
$B[\mathcal{B}, \mathbf{k}]$: eXogenous (X) polynomial
$C[\mathcal{B}, \mathbf{k}]$: Moving Average (MA) polynomials
arg min	: minimizing argument
arg max	: maximizing argument
$\mathbf{a}, \mathbf{b}, \mathbf{c}, \mathbf{s}$: AR, X, MA, and innovations variance projection coefficients vectors
a_i, b_i, c_i	: AR, X and MA i -th parameter, respectively
$a_i(\mathbf{k}), b_i(\mathbf{k}), c_i(\mathbf{k})$: AR, X and MA i -th parameter under \mathbf{k} operating parameter vector
$a_{i,j}, b_{i,j}, c_{i,j}$: AR, X and MA coefficients of projection
d	: parameter vector dimensionality
$e_{\mathbf{k}}[t]$: residual sequence under \mathbf{k} operating parameter vector at time t
\mathcal{F}	: Fisher information matrix

$\mathcal{F}\langle\cdot\rangle$: functional subspace of the indicated quantity
F	: F statistic
$f(\cdot)$: probability density function of the indicated quantity
$f_{(1-\alpha)}(K_1, K_2)$: F -distribution's $(1 - \alpha)$ critical point with (K_1, K_2) degrees-of-freedom
f_s	: sampling frequency (Hz)
\mathcal{G}	: set of transfer functions obtained in a given structure
$G_j(\mathbf{k})$: basis functions ($j = 1, 2, \dots, p$)
$H(j\omega)$: frequency response function
H_o, H_1	: null and alternative hypothesis
H_V	: hypothesis V
$\mathbf{J}(\cdot)$: Jacobian matrix of indicated vector
J	: estimation criterion
j	: complex unit
\mathbf{k}	: operating parameter vector $\mathbf{k} = [k_i^1 \ k_j^2]$
$k_{i,j}$: operating parameter vector values $k_{i,j} = (k_i^1, k_j^2)$
k_{\min}, k_{\max}	: minimum and maximum values of operating parameter
$L(\theta)$: operating characteristic function (Chapter VI)
$L(\cdot), \mathcal{L}(\cdot)$: likelihood function of the indicated quantity
\mathcal{M}	: model structure (a mapping from a parameter space to a set of models)
$\mathcal{M}(\theta)$: particular model corresponding to the parameter value θ
M	: stochastic model
$\min \inf$: minimizing infimum (greatest lower bound)
\mathbf{m}	: integer valued model structure
\mathbf{m}_{bin}	: binary integer valued model structure
M_1, M_2	: values of the first and second externally measurable variables k^1 and k^2
\hat{N}	: stopping rule
N	: data record length
$\mathcal{N}(\cdot, \cdot)$: normal (Gaussian) distribution with indicated mean and covariance
na, nb, nc	: AR, X and MA model orders
$P_{mn}(x, y)$: bivariate orthogonal polynomials of total degree mn
$\mathbf{P}(\theta)$: covariance matrix of vector θ
pa, pb, pc, ps	: AR, X, MA, and innovations variance functional subspace dimensionalities
$p(\cdot)$: Gaussian probability density function
S	: system/structure
$S_{xy}(\omega)$: cross spectral density
$S_{yy}(\omega)$: power spectral density
T_s	: sampling period (s)
w_n	: natural frequency (Hz)
$\mathbf{w}[t]$: cross-section innovations vector at time t
$w_{\mathbf{k}}[t]$: innovations sequence under \mathbf{k} operating parameter vector at time t
$x_{\mathbf{k}}[t]$: excitation signal under \mathbf{k} operating parameter vector at time t
$y_{\mathbf{k}}[t]$: response signal under \mathbf{k} operating parameter vector at time t
$z_V[t]$: excitation–response signal pair under structural state V at time t
Z_V	: complete ($\forall t$) excitation–response signal pair under structural state V

$Z_{1-\alpha}$: standard normal distribution's $1 - \alpha$ critical point
α	: type I risk level (false alarm probability)
β	: type II risk level (missed damage probability)
$\mathbf{\Gamma}_{\mathbf{w}[t]}$: cross-section innovations covariance matrix
γ_w	: innovations covariance
$\gamma^2(\omega)$: coherence function
Δf	: frequency resolution (Hz)
δ	: decision rule
$\delta[\tau]$: Kronecker delta ($\delta[0] = 1$, $\delta[\tau] = 0$ for $\tau \neq 0$)
ζ	: damping ratio (%)
$\boldsymbol{\theta}$: projection coefficients vector (VFP models) or parameter vector (ARX models)
$\boldsymbol{\theta}_o$: "true" projection coefficients vector or parameter vector
$\boldsymbol{\theta}$: projection coefficients vector including innovations covariance
$\boldsymbol{\vartheta}$: vector containing the AR and X coefficients of projection $\boldsymbol{\vartheta} = [\mathbf{a} : \mathbf{b}]$
Λ	: likelihood function ratio
$\rho[\tau]$: normalized autocovariance function
$\boldsymbol{\Sigma}$: residual covariance matrix
σ_e^2	: residual variance
τ	: discrete time lag
$\boldsymbol{\phi}, \boldsymbol{\varphi}$: regression vectors
$\chi_{1-\alpha}^2(d)$: $1 - \alpha$ critical point of the chi-square distribution with d degrees-of-freedom
$\chi_{(\cdot)}^2$: χ^2 -distributed test statistic of the indicated characteristic quantity
ω	: frequency

Operators

\otimes	: Kronecker product
$*$: Khatri-Rao product
$ \cdot $: Euclidian norm of a vector
∂	: partial derivative
\triangleq	: definition (the left side is defined by the right side)
\mathcal{B}	: backshift operator ($\mathcal{B}^i \cdot y[t] = y[t - i]$)
cov[.]	: covariance of the indicated quantity
D	: differential operator
$\det\{\cdot\}$: determinant of the indicated quantity
$\dim \boldsymbol{\theta}$: dimension (rows) of the column vector $\boldsymbol{\theta}$
$E\{\cdot\}$: statistical expectation
\ln	: natural logarithm
var[.]	: variance of the indicated quantity

Abbreviations and acronyms

ACF	:	AutoCovariance Function
AIC	:	Akaike Information Criterion
AR	:	AutoRegressive
ARMA	:	AutoRegressive Moving Average
ARX	:	AutoRegressive with eXogenous excitation
ARMAX	:	AutoRegressive Moving Average with eXogenous excitation
a.s.	:	almost surely (with probability one)
ASN	:	Average Sample Number
BIC	:	Bayesian Information Criterion
BLUE	:	Best Linear Unbiased Estimate
CCF	:	Cross Correlation Function
CM	:	Condition Monitoring
CP	:	Classical Pooling
CPU	:	Central Processing Unit
CSD	:	Cross Spectral Density
DP	:	Damage Prognosis
FE	:	Finite Element
FMBM	:	Functional Model Based Method
FP	:	Functionally Pooled
FRF	:	Frequency Response Function
FSS	:	Fixed Sample Size
GA	:	Genetic Algorithm
iid	:	identically independently distributed
LPV	:	Linear Parameter Varying
LS	:	Least Squares
LTI	:	Linear Time Invariant
MA	:	Moving Average
ML	:	Maximum Likelihood
NDE	:	Non-Destructive Evaluation
NLS	:	Nonlinear Least Squares
OC	:	Operating Characteristic
OLS	:	Ordinary Least Squares
pdf	:	Probability density function
PE	:	Prediction Error
PSD	:	Power Spectral Density
RSS	:	Residual Sum of Squares
SHM	:	Structural Health Monitoring
SPC	:	Statistical Process Control
SPP	:	Samples Per Parameter
SPRT	:	Sequential Probability Ratio Test
SQP	:	Sequential quadratic programming
SSS	:	Signal Sum of Squares
SUR	:	Seemingly Unrelated Regressions
VARX	:	Vector AutoRegressive with eXogenous excitation
VFP	:	Vector-dependent Functionally Pooled
WLS	:	Weighted Least Squares
w.p.	:	with probability

Chapter 1

Introduction

1.1 The general problem

1.1.1 Structural damage diagnosis

The past 30 years have witnessed major developments in vibration based damage detection and identification, also collectively referred to as damage diagnosis. Moreover, the past 10 years have seen a rapid increase in the amount of research related to Structural Health Monitoring (SHM) as quantified by the significant escalation in papers published on this subject. Thus, the increased interest in this engineering field and its associated potential constitute the main motive for this thesis.

Damage diagnosis in vibrating structures, such as aerospace and mechanical structures, buildings, bridges and offshore platforms, is of paramount importance for reasons associated with proper operation, improved maintenance, reduced costs and increased safety. The process of implementing a damage diagnosis strategy is referred to as Structural Health Monitoring (SHM – Doebling *et al.* 1996, Doebling *et al.* 1998, Farrar *et al.* 2001, Farrar and Worden 2007, Fassois and Sakellariou 2007, Fassois and Sakellariou 2009, Rytter 1993). This process involves the observation of a system/structure over time using periodical measurements, the extraction of damage sensitive quantities (features) from these measurements, and the statistical analysis of these quantities in order to determine the current structural health state. Damage may be defined as changes to the material and/or geometric properties of these systems, including changes to the boundary conditions and system connectivity, which adversely affect the system's performance (Farrar and Worden 2007). Implicit in this definition is the concept that damage is not meaningful without a comparison between two different states of the system, one of which is assumed to represent the initial, often undamaged (healthy), state.

Damage diagnosis is carried out in conjunction with five closely related disciplines that include SHM, condition monitoring (CM – Bently and Hatch 2003), non-destructive evaluation (NDE – Doebling *et al.* 1996, Doebling *et al.* 1998, Doherty 1987, Shull 2002, Staszewski *et al.* 2004), statistical process control (SPC – Montgomery 1997, Sohn *et al.* 2000, Fugate *et al.* 2001, Zepico-Valle *et al.* 2011), and damage prognosis (DP – Farrar *et al.* 2003, Farrar and Lieven 2007). Typically, SHM is associated with online-global damage diagnosis in structural systems such as aeronautical, engineering, civil and marine structures. CM is analogous to SHM, but addresses damage diagnosis in rotating and reciprocating machinery, such as those used in manufacturing and power generation. NDE is usually carried out off-line in a local manner after the damage has been located. There are exceptions to this rule, as NDE is also used as a monitoring or SHM tool for in situ structures such as pressure vessels, rails and wind turbines (Shull 2002, Razi *et al.* 2011, Zak *et al.* 2012). NDE is therefore primarily used for damage characterization and as a severity check when there is a priori

knowledge of the damage location. SPC is process based rather than structure based and uses a variety of sensors to monitor changes in a process, one cause of which can result from structural damage. Once damage has been detected, DP is used to predict the remaining useful life of a system. This thesis primarily addresses the issue of vibration based SHM with potential applications to CM.

The need for global damage detection at the earliest possible time is pervasive throughout the aeronautical, mechanical, civil and manufacturing engineering communities. Such detection requires the need to perform some form of SHM and is motivated by the increased potential life and safety, as well as the economic impact of this technology. Therefore, the ability to monitor the health state of structures is becoming increasingly important. Most current structural and mechanical system maintenance is done in a time-based mode. SHM is the technology that will allow the current time-based maintenance philosophies to evolve into potentially more cost effective condition-based maintenance philosophies (Farrar and Worden 2007). The concept of condition-based maintenance is that a sensing system on the structure will monitor the system response and notify the operator that damage has been detected. Life-safety and economic benefits associated with such a philosophy will only be realized if the monitoring system provides sufficient warning such that corrective action can be taken before the damage evolves to a failure level. The trade-off associated with implementing such a philosophy is that it requires a more sophisticated monitoring hardware to be deployed on the system and it requires a sophisticated data analysis procedure that can be used to interrogate the measured data. Furthermore, SHM has the potential to extend the maintenance cycles and, hence, keep the system operating without interruptions for longer time intervals.

A system of classification for damage diagnosis methods, as presented in Rytter (1993), defines four levels of damage diagnosis, as follows:

- Level 1: Damage detection – Determination that damage is present in the structure
- Level 2: Damage localization – Determination of the geometric location of the damage
- Level 3: Damage quantification – Quantification of the severity of the damage
- Level 4: Remaining life estimation – Prediction of the remaining service life of the structure

The relevant literature for this thesis can be classified mostly as Level 1, Level 2, or Level 3 methods, as these levels are most often related directly to structural dynamics testing and modeling issues. Level 4 is generally categorized within the fields of fracture mechanics, fatigue life analysis, or structural design assessment and, as such, is not addressed in the structural vibration or modal analysis literature. Hence, the current thesis focuses on the first three damage diagnosis levels.

1.1.2 Identification of systems under multiple operating conditions

System identification deals with the problem of building mathematical models of dynamic systems based on experimental data obtained from the system. Since dynamic systems are abundant in our environment, the techniques of system identification have a wide application area, such as the identification of dynamic properties of aeronautical, mechanical and civil structures, identification of systems and control, performance study of aerospace and automotive vehicles, modeling of stock prices in economics, and analysis of dynamic biological functions. The foundation of modern system identification is based on the combination of linear systems theory, time series analysis and asymptotic theory (Söderström and Stoica 1989, Mendel 1995, Andersen 1997, Ljung 1999, Lütkepohl 2005).

There are two categories of model structures: (i) non-parametric and (ii) parametric. Non-parametric model structures are characterized by the property that the resulting models are curves

or functions that do not explicitly employ a finite-dimensional parameter vector, since they use direct techniques without first selecting a confined set of possible models (Ljung 1999, Chapter 6),(Söderström and Stoica 1989, Chapter 3). Non-parametric methods include time domain models, such as the autocorrelation (ACF) and cross-correlation (CCF) functions, as well as frequency domain models, such as the power spectral density (PSD) and the frequency response function (FRF). On the other hand, parametric model structures suppose that a set of candidate models is selected and it is parametrized as a model structure using a parameter vector θ (Ljung 1999, Chapter 7),(Söderström and Stoica 1989, Chapter 6). The search for the best model within the set becomes a problem of determining or estimating θ . Typical parametric model structures include among others the AutoRegressive Moving Average (ARMA), AutoRegressive with eXogenous excitation (ARX), AutoRegressive Moving Average with eXogenous excitation (ARMAX), and state space models.

Classical system identification aims at deriving a model representing a system under a specific operating condition. Yet, in many applications a system may operate under different operating conditions at different occasions (time periods), during different service intervals or commission cycles, with the dynamics depending in a pseudo-static fashion on certain operating parameter(s). As is often the case in practice, each operating condition may affect the system and its dynamics. Typical examples include aeronautical, civil and mechanical structures under different environmental conditions such as temperature and humidity, aircrafts under different flight conditions such as altitude and velocity, rotating machinery operating at various speeds, hydraulic systems operating under different temperatures or fluid pressures, mechanical systems under different load or lubrication conditions, physiological systems under different conditions, and so on.

With respect to the aims of the current thesis, system identification under different operating conditions is related to the identification of structures under different *structural health states*, such as various damage locations and/or damage magnitudes. In this way, damage location and magnitude may be considered as parameters that affect the operating conditions and as a result the underlying structural dynamics. In such cases, it is important to identify a *global* and *compact* (parsimonious) model describing a structure under *any* admissible operating condition, based on input and noise-corrupted output vibration data records corresponding to a *sample* of those conditions. Hence, part of this thesis aims at achieving effective and accurate (statistically efficient) identification of a global and compact parametric, linear, time invariant, stochastic time series model describing structures under different health states characterized by varying damage locations and damage magnitudes.

1.2 Critical review of the state-of-the-art

1.2.1 Structural damage diagnosis

Over the past several years, a wide variety of local non-destructive testing tools have been developed (Farrar *et al.* 2001, Doebling *et al.* 1996, Doebling *et al.* 1998). Although recent advances in NDE methods propose a global solution with respect to damage diagnosis (Shull 2002, Lim *et al.* 2006, Kirikera *et al.* 2007, Razi *et al.* 2011, Zak *et al.* 2012), the majority of the methods based on ultrasound, acoustic, radiography, eddy current, and thermal field principles, generally require access to the vicinity of the suspected damage location, while they are typically time consuming and costly. The need for global damage diagnosis methods that can be applied to realistic structures has led to the development of methods that examine changes in the structural vibration characteristics. Vibration based methods for damage diagnosis are among the most accurate and effective (Doebling *et al.* 1998, Farrar *et al.* 2001, Montalvão *et al.* 2006, Alvandi and Cremona 2006, Fassois and Sakellariou 2007, Fassois and Sakellariou 2009, Fan and Qiao 2011). They offer a number of potential advantages, such as no

requirement for visual inspection, “automation” capability, “global” coverage (in the sense of covering large areas of the structure), and the ability to work at a “system level”.

Statistical time series methods for SHM form an important, rapidly evolving, category within the broader vibration based family of methods. They are fundamentally of the inverse type, as the models used are *data based* rather than physics based, and inherently account for uncertainties. They offer a number of potential advantages such as (Fassois and Sakellariou 2007, Fassois and Sakellariou 2009, Basseville *et al.* 2004, Mevel *et al.* 2003, Sakellariou and Fassois 2008, Kopsaftopoulos and Fassois 2010a, Bodeux and Golinval 2001):

- (i) No requirement for complicated, large size physical or analytical, such as tuned Finite Element (FE), models.
- (ii) No requirement for complete structural models; in fact they may operate on partial models based on a limited number, or even a *single pair*, of excitation and/or response signals.
- (iii) Inherent accounting for uncertainties (measurement, environmental, operational and so on) through statistical tools.
- (iv) Statistical decision making with specified performance characteristics.

Statistical time series methods utilize (i) random excitation and/or response signals (time series), (ii) statistical model building, and (iii) statistical decision making for inferring the health state of a structure. As with all vibration based methods, the fundamental principle upon which they are founded is that small changes (damage) in a structure cause discrepancies in its vibration response, which may be detected and associated with a specific cause (damage type). Non-parametric time series methods for SHM are those based on corresponding time series representations, such as power spectral estimates (Ljung 1999, Söderström and Stoica 1989, Fassois and Sakellariou 2007, Fassois and Sakellariou 2009), and have received limited attention in the literature (Fassois and Sakellariou 2007, Fassois and Sakellariou 2009, Kopsaftopoulos and Fassois 2010a, Kopsaftopoulos and Fassois 2011b, Benedetti *et al.* 2011). Parametric time series methods for SHM are those based on corresponding time series representations, such as the AutoRegressive Moving Average (ARMA) representation (Ljung 1999, Söderström and Stoica 1989, Fassois and Sakellariou 2007, Fassois and Sakellariou 2009). This type of methods has attracted considerable attention and their principles have been used in a number of studies (Fassois and Sakellariou 2007, Fassois and Sakellariou 2009, Kopsaftopoulos and Fassois 2010a, Kopsaftopoulos and Fassois 2011b).

Nevertheless, and despite the fact that statistical time series methods generally tend to treat damage detection (Level 1) effectively, *no mature solutions* yet exist for the damage localization (Level 2) and quantification (magnitude estimation – Level 3) subproblems. To date, vibration based damage diagnosis methods that have shown promise to detect, locate (identify), and quantify damage are based on the basic idea that modal parameters (natural frequencies, mode shapes and modal damping) are functions of the physical properties of the structure (mass, damping and stiffness) (Doebbling *et al.* 1998, Farrar *et al.* 2001, Montalvão *et al.* 2006, Farrar and Jauregui 1998a, Farrar and Jauregui 1998b). Therefore, changes in the physical properties will cause detectable changes in the modal properties. The majority of these methods is established on, or presumes, access to detailed and large size Finite Element (FE) models and utilize intensive model updating techniques (for tuning the model to the obtained data records) and pre- and post-damage data records (Farrar *et al.* 2001, Zimmerman *et al.* 2001, Nauerz and Fritzen 2001, Liberatore and Carman 2004, Perera *et al.* 2007). Furthermore, as complete FE models are utilized, these techniques require a significant number of measurement sensors and thus tend to be computationally and experimentally elaborate, while problems may be introduced

by the measurement constraints imposed by actual testing conditions (Farrar *et al.* 2001, Farrar and Jauregui 1998*a*, Farrar and Jauregui 1998*b*, Zimmerman *et al.* 2001). Moreover, some of these methods appear to be inconsistent and unable to clearly identify the damage location when they are applied to less severe damage cases, while it may be ambiguous at times to determine whether they indicate damage at more than one location (Montalvão *et al.* 2006, Farrar and Jauregui 1998*a*).

As statistical time series and related methods are *data based* (inverse type) rather than physics based, they offer the important advantage of being based on simple, *partial* models of the structural dynamics, which are identified based on a potentially “small” number of vibration signals – sometimes even on a single signal or a single signal pair (Fassois and Sakellariou 2007, Fassois and Sakellariou 2009). They may be thought of as generalizations of earlier techniques using deterministic models and identification techniques – a classical early approach being that of damage detection based on natural frequency changes in modal models. Statistical time series type methods utilize statistical models and identification techniques taking uncertainties into account, they may operate on normal operating vibration signals, in an output-only mode, and also on structures of any size and geometry. They may be thought of as including the related class of statistical pattern recognition type methods (Worden 1997, Sohn *et al.* 2001, Mattson and Pandit 2006*a*, Manson *et al.* 2003, Lee *et al.* 2006, Xi *et al.* 2000, Jung and Koh 2009). This family of methods utilizes techniques related to time series and outlier analysis (Sohn *et al.* 2001, Mattson and Pandit 2006*a*, Manson *et al.* 2003), neural network analysis (Manson *et al.* 2003, Lee *et al.* 2006), and analysis of statistical parameters (Xi *et al.* 2000, Jung and Koh 2009). Neither sophisticated FE models nor modal parameters are employed in the implementation of these methods, while they are reportedly capable of achieving effective damage detection. Nevertheless, while damage detection may be potentially treated effectively by many of these methods, the damage localization problem is typically treated as a *classification problem*, meaning that a damage location is selected among a *finite* number of potential damage locations. This is a simplification and a much simpler problem than precise damage localization over properly defined *continuous topologies* on a structure – that is to say infinite possible damage locations – which essentially corresponds to the actual SHM problem. Furthermore, damage magnitude estimation is generally not possible (except for maybe some “rough” characterization) – a method offering an approach for properly tackling this problem was only recently introduced by the Stochastic Mechanical Systems & Automation (SMSA) laboratory of the Mechanical Engineering & Aeronautics Department at University of Patras (Sakellariou 2005, Sakellariou and Fassois 2008, Sakellariou *et al.* 2002).

The vast majority of the previously outlined literature on vibration based statistical time series methods for SHM is based on Fixed Sample Size (FSS) hypothesis testing procedures, which are used during the statistical decision making phase for inferring the actual health state of the structure. FSS hypothesis testing employs a constant amount of observations, which is determined *a priori* of the experimental data acquisition. On the other hand, hypothesis testing may be also treated via sequential analysis, which is a method of statistical inference whose characteristic feature is that the number of observations required by the procedure is not determined in advance of the experiment. The decision to terminate the experiment depends, at each stage, on the results of the observations previously made, thus the number of observations required by the test is not pre-determined, but a *random variable*. If samples can be taken one at a time and the information from them accumulated, one would expect to be in a better position to make decisions than if no attempt were made to look at the data until a sample of fixed size had been taken. A merit of the sequential method, as applied to testing statistical hypotheses, is that test procedures can be constructed which require, on average, a substantially smaller number of observations than equally reliable test procedures based on a predetermined (fixed) number of observations (Wald 1947, Ghosh and Sen 1991, Lehmann and Romano 2008). Moreover, a potential advantage of a damage diagnosis method which is based on sequential analysis for testing hypotheses is its straightforward extension for online implementation,

which may be of great interest with respect to SHM applications.

Although statistical hypothesis testing methods based on sequential analysis were introduced over half a century ago, the engineering applications based on sequential testing have been limited to the surveillance of nuclear power plant components (Humenik and Gross 1990, Gross and Humenik 1991), while some numerical investigations of its performance with respect to anomaly detection in nuclear reactor noise signals have been presented in Schoonewelle *et al.* (1995), Schoonewelle *et al.* (1996) and Glöckler (1991). Furthermore, in the context of vibration based damage diagnosis and SHM, only a limited number of studies taking advantage of the sequential hypothesis testing merits exists (Sohn *et al.* 2003, Oh and Sohn 2009).

1.2.2 Identification of systems under multiple operating conditions

In recent years limited attention has been paid to the identification of “global” models representing systems under multiple or varying operating conditions. System identification traditionally aims at deriving a model capable of representing a system at a specific operating condition. Yet, in many cases, a system may operate under different, though constant, conditions at different time intervals and data records, each one corresponding to a distinct such condition, are obtained. In such cases, it is important to identify a *global* and *compact* (parsimonious) model describing the system under *any* admissible operating condition, based on input and noise-corrupted output data records corresponding to a *sample* of those conditions.

The most significant efforts for the development of models for the identification of dynamical systems under multiple operating conditions are found in sciences of statistics, economics and econometrics, where several families of models have been proposed in the past (Dielman 1989, Greene 2003, Lois 1989). Nevertheless, in all cases either the model structure preserves the restrictive assumption of equal number of parameters among all operating conditions or employs an individual set of parameters for each distinct operating condition, hence being incapable of accurately representing the system in an intermediate operating condition, for which data is not available, and as a result for all the admissible operating conditions. Indicative such model structures include among others the linear regression models based on aggregated data (Dielman 1989), which are very simple system representations that combine information from different operating conditions in single linear regression expressions, the Classical Pooling (CP) models (Dielman 1989, Lois 1989) summarizing data information from all operating conditions in a single mathematical representation of the linear regression form, without aggregation, preserving a common set of parameters for all operating conditions, and the Seemingly Unrelated Regressions (SUR) models (Dielman 1989, Greene 2003, Lois 1989), which are considered as extensions of the CP models implementing an individual set of parameters for each operating condition and accounting for correlated disturbances of different operating conditions at the same time instant (for a brief review of these model structures see Sakellariou (2005)). All these types of models do not explicitly account for each operating condition, but rather attempt to either “average out” their effects by providing representations characterized by constant parameters, or to provide a measure of model “spread” by treating the model parameters as random variables.

A “feasible” approach for solving this identification problem could be along the lines of the “multi-model” principle. The problem could be handled using a number of “pseudo-independent” conventional mathematical models and customary identification techniques that could artificially split the problem into a number of seemingly unrelated subproblems. Each model could be then obtained based on data records corresponding to each operating condition. Models corresponding to other (intermediate) operating conditions would not be readily available, but could be “interpolated” based on those identified. Nevertheless, such a two-stage “multi-model” approach is statistically suboptimal

and leads to decreased accuracy. The reasons for this are: First, the artificial splitting of the problem into disjoint subproblems (separate identification for each data record) leads to the estimation of an unnecessarily high number of parameters (due to the fact that each model is identified separately from any other), a fact violating the principle of *statistical parsimony* and leading to decreased accuracy. Second, any *interrelations* that may exist among the different data records are neglected, a fact leading to further loss of information. Third, the separate (subsequent) treatment of the parameter interpolation stage leads to further (unnecessary) estimation errors.

In order to effectively handle such problems, a novel *Functional Pooling (FP) framework* has been recently introduced by the Stochastic Mechanical Systems & Automation (SMSA) laboratory of the Mechanical Engineering & Aeronautics Department at University of Patras (Kopsaftopoulos and Fassois 2006a, Sakellariou 2005, Sakellariou and Fassois 2007, Sakellariou and Fassois 2007b, Hios and Fassois 2009b). This framework circumvents the above difficulties and allows for effective and accurate (statistically efficient) identification of a global and parsimonious model describing the system under any admissible operating condition. It is based on the novel concept of functional pooling that introduces functional dependencies (in terms of the operating parameter) in the postulated model structure. It is this specific characteristic that, unlike in conventional pooling used in fields such as econometrics (Dielman 1989, Lois 1989, Greene 2003) where the effects of “operating conditions” are “smoothed out”, allows for both precise and parsimonious modeling.

The class of FP models could be in the most general terms considered to belong to the broader family of Linear Parameter Varying (LPV) models (for details in LPV model identification see Toth (2010), Bamieh and Giarre (2003) and the references therein). Nevertheless and despite their superficial resemblance, these two model classes address somewhat different identification issues with quite different perspectives. LPV identification is achieved via two major approaches: (i) the local approach and (ii) the global approach. In the local approach LTI models are identified in a number of (local) operating points corresponding to constant scheduling signals and the resulting local linear models are interpolated (possibly by using data from an additional global experiment) to an LPV model (Toth 2010). For the interpolation various techniques and approaches have been introduced, varying from interpolation on pole estimates to the technique where each local (LTI) model is converted to a state space model in canonical form, and subsequently the coefficients in this model are interpolated. The local approach would, nevertheless, suffer from a number of problems as it would fail to provide a single global and parsimonious model valid under all admissible operating conditions, while it would be suboptimal, characterized by reduced statistical accuracy, as it would result in a large number of estimated parameters and ineffective use of the information available in the totality of the data records. For instance, the *interrelations* among the different data records would be ignored, as a result of separating the problem into seemingly unrelated subproblems. In the global approach though one has to determine a global LPV model structure and an identification criterion and data from a *single global experiment* are employed in order to estimate an LPV model (Toth 2010).

In the FP framework the only essential practical, but necessary, condition for identifying parsimonious global system models is the availability of data records from each operating condition (point) with each such condition corresponding to a specific value of one (or more) measurable variable. Furthermore, this framework circumvents the aforementioned difficulties that the LPV local approach faces and allows for effective and accurate (statistically efficient) identification of a global and parsimonious model describing the system under any admissible operating condition. Moreover, the interrelations among the different data records belonging to the various operating conditions are fully taken into account, as the FP model structure employs appropriate data pooling techniques. Furthermore, an extremely important difference is that the LPV global approach employs data obtained from a single experiment, which is not the case in the FP framework, as it employs data records obtained under a sample of the operating conditions. From all the above it is obvious that, despite

their phenomenal similarities, the FP and LPV model structures constitute distinct representations that have important differences and therefore should be clearly distinguished.

1.3 Thesis goals

The main goals of this thesis may be summarized as follows:

- (i) Experimental assessment and critical comparison of the main vibration based statistical time series methods for SHM via their application to paradigm laboratory structures. Discussion of the methods' main features, operational characteristics and applicability under uncertainties, as well as investigation of their pros and cons.
- (ii) Evolution and improvement of the recently introduced FP framework for the identification of stochastic dynamic systems under multiple/varying operating conditions. Postulation of the Vector-dependent Functionally Pooled (VFP) parametrization that includes a *vector* characterization of the admissible operating conditions and development of effective parameter estimation and model structure selection methods. Investigation of the asymptotic properties of the developed estimators and Monte Carlo assessment.
- (iii) Extension, generalization, and experimental validation and assessment of the recently introduced stochastic Functional Model Based Method (FMBM), which is now based on the novel VFP model structure, and is – for the first time – capable of achieving unified and effective damage detection (Level 1), along with *complete* and *precise localization* (Level 2) and *magnitude estimation* (Level 3).
- (iv) Introduction and experimental validation and assessment of a sequential, statistically optimal, time series method for vibration based SHM. The method is able to achieve *robust* and effective damage detection (Level 1), along with damage identification (Level 2) and quantification (Level 3) under uncertainties. It operates under predetermined type I (false alarm) and II (missed damage) error probabilities achieving *early* detection of damage. Moreover, the method is characterized by computational simplicity and thus may be easily implemented for online SHM in “real” structures.

The thesis chapters and their specific contribution are analytically presented in the next section.

1.4 Thesis chapters and main contribution

The thesis chapters are summarized in Table 1.1.

1.4.1 Chapters II: Experimental Assessment of Vibration Based Statistical Time Series Methods for Structural Health Monitoring

The *goal* of this chapter is to provide an experimental assessment and comparison of vibration based statistical time series methods for Structural Health Monitoring (SHM) via their application to a lightweight aluminum truss structure and a scale aircraft skeleton structure.

In spite of the progress achieved so far, the literature on vibration based statistical time series methods for SHM remains relatively *sparse*. In particular, no application studies that experimentally

Chapter	Title
II	Experimental Assessment of Vibration Based Statistical Time Series Methods for Structural Health Monitoring
III	Identification of Stochastic Systems Under Multiple Operating Conditions: The Vector-dependent Functionally Pooled (VFP) Parametrization
IV	A Stochastic Functional Model Based Method for Vibration Based Damage Detection, Localization, and Magnitude Estimation
V	A Sequential Statistical Time Series Method for Vibration Based Structural Health Monitoring

Table 1.1: Thesis chapters.

compare and assess the various methods are available. The *goal* of the present chapter is the experimental comparison and assessment of a number of *univariate* (scalar) and *multivariate* (vector) statistical time series methods via their application on a lightweight laboratory aluminum truss structure and a scale aircraft skeleton structure. Two non-parametric methods, namely a Power Spectral Density (PSD) and a Frequency Response Function (FRF) based method, as well as five parametric methods, namely a model parameter based, a residual variance, a residual likelihood function, a residual uncorrelatedness and a Sequential Probability Ratio Test (SPRT) based method, are reviewed and experimentally assessed. The damage cases considered correspond to loosening of various bolts connecting certain of the elements of the structures. Random force excitation is provided via an electromechanical shaker, while the vibration responses are measured at various positions via dynamic strain gauges and accelerometers.

Both *univariate* (scalar response) and *multivariate* (vector responses) versions of the methods are used, while assessment results are presented for *two* laboratory structures, namely an aluminum truss structure and a scale aircraft skeleton structure. The methods' main features and operational characteristics are discussed along with practical issues, while their effectiveness is demonstrated via various test cases corresponding to different experiments, damage scenarios, and vibration measurement positions.

Original contributions:

- Experimental assessment and critical comparison of non-parametric and parametric statistical time series methods for SHM, employing both scalar (univariate) and vector (multivariate) schemes.
- Discussion of the methods' main features, operational characteristics, and performance under experimental uncertainties and multiple experiments under various damage scenarios.
- Identification of the main advantages and disadvantages of the methods under practical situation in order to determine future research focus.

The part of the chapter concerning the experimental assessment of the scalar methods for SHM in a truss aluminum structure has been published in the Mechanical Systems & Signal Processing journal (Kopsaftopoulos and Fassois 2010a), while the part of the chapter concerning the vector methods assessment in a scale aircraft skeleton structure has been published in the Journal of Theoretical and Applied Mechanics (invited paper) journal (Kopsaftopoulos and Fassois 2011b). Preliminary results of

the methods' assessment have been published in the proceedings of four conferences (Kopsaftopoulos and Fassois 2008, Kopsaftopoulos *et al.* 2010, Kopsaftopoulos and Fassois 2010*b*, Kopsaftopoulos and Fassois 2010*c*).

1.4.2 Chapter III: Identification of Stochastic Systems Under Multiple Operating Conditions: The Vector-dependent Functionally Pooled (VFP) Parametrization

The *goal* of this chapter is the identification of stochastic systems under multiple operating conditions via Vector-dependent Functionally Pooled (FP) models. In many applications a system operates under a variety of operating conditions which affect its dynamics, with each condition kept constant for a single commission cycle. Hence, damage location and damage magnitude may be considered as parameters that affect the operating conditions and thus may be effectively parametrized. This chapter's work is based on the novel *Functional Pooling (FP) framework*, which has been recently introduced by the SMSA group, and specifically in Sakellariou (2005), Sakellariou and Fassois (2007) and Sakellariou and Fassois (2007*b*).

Thus, the third chapter of the thesis addresses the problem of identifying a globally valid and parsimonious system model based on input-output data records obtained under a sample of operating conditions characterized by more than one parameters (for instance operating temperature and humidity or damage location and magnitude). Thus, models that include a *vector* characterization of the operating conditions (referred to as *operating parameter vector*) are postulated. The problem is tackled within the novel Functional Pooling (FP) framework that postulates proper global models of the ARX and ARMAX types, data pooling techniques, and statistical parameter estimation. Corresponding Vector-dependent Functionally Pooled (VFP) ARX and ARMAX models are postulated, and proper estimators of the Least Squares (LS), Maximum Likelihood (ML), and Prediction Error (PE) types are developed. Model structure estimation is achieved via customary criteria (Bayesian Information Criterion) and a Genetic Algorithm (GA) based procedure. The strong consistency of the estimators is established, whereas the effectiveness of the complete estimation and identification method is demonstrated via Monte Carlo experiments.

Original contributions:

- Extension of the FP models employing a scalar operating parameter to the Vector-dependent FP (VFP) models employing the *operating parameter vector*.
- Establishment of the strong consistency of the proposed estimators.
- Model structure estimation is achieved via a Genetic Algorithm (GA) based procedure.
- The innovations sequence variance is projected to a functional subspace, so now it may be available not only for the sample of operating conditions (available data records), but it may be efficiently estimated for all admissible operating conditions.
- Assessment of the proposed estimators and structure selection procedures via Monte Carlo experiments.

The VFP-ARX model estimation and identification part has been published in conference proceedings (Kopsaftopoulos and Fassois 2006*a*). The complete VFP parametrization journal paper version is under preparation for publication (Kopsaftopoulos and Fassois 2011*a*).

1.4.3 Chapter IV: A Stochastic Functional Model Based Method for Vibration Based Damage Detection, Localization, and Magnitude Estimation

The *aim* of this chapter is the introduction and experimental validation and assessment of a stochastic Functional Model Based Method (FMBM) that is – for the first time – capable of achieving effective damage detection along with *complete* and *precise localization* and *magnitude estimation*.

The proposed method constitutes an important generalization of the original FMBM (Sakellariou 2005, Sakellariou and Fassois 2008), with its main innovative element being its unique ability to achieve – for the first time within the context of statistical time series type methods – *complete* and *precise* damage *localization* over *continuous topologies* (infinite number of potential locations) on a structure, combined with damage *magnitude estimation*. Furthermore, estimator uncertainties are fully taken into account in all phases of the diagnostic procedure, and uncertainty ellipsoids are provided for combined damage location and magnitude. Like the original FMBM, the method utilizes a partial and reduced size identified model, and is capable of operating on a “low” number of measurement sensors – even on a single pair for “small” structures – and any type of vibration response signals (acceleration, velocity, displacement).

The method is based in the new extended class of *Vector-dependent Functionally Pooled* (VFP) models developed in the previous thesis chapter, as well as on proper statistical estimation and decision making schemes. VFP models allow for the analytical inclusion of *both* damage location and magnitude in the dynamics, thus permit the extension of the notion of *damage mode/fault mode* to include damage not only of all possible magnitudes, but also of all possible *locations* in a specific continuous topology on a structure. More precisely, the proposed method can accurately localize damage anywhere on properly defined continuous topologies on the structure, instead of pre-defined specific locations. The method is validated and its effectiveness is experimentally assessed via its application to damage detection, precise localization, and magnitude estimation on a prototype GARTEUR-type laboratory scale aircraft skeleton structure. The damage scenarios considered consist of varying size small masses attached at various continuous topologies on the structure. The method is shown to achieve effective damage detection, precise localization, and magnitude estimation based on even a single pair of measured excitation-response signals.

Original contributions:

- The feasibility of achieving precise damage localization and magnitude estimation based on only a *single* excitation-response signal pair is, for the first time, investigated and demonstrated.
- Localization and damage magnitude *uncertainties* are explicitly considered and estimated, with *uncertainty ellipsoids* corresponding to specified probability levels being constructed.
- The method’s operation and effectiveness is examined for *both* “local” and “remote” (with respect to the sensor location) damage. This is critical in view of the need for effective diagnosis with the smallest possible number the available sensors.
- The effectiveness of the method in properly detecting and “negatively” localizing (that is excluding all considered structural topologies) damage that does *not* belong to any of the modelled types/topologies (referred to as *unmodelled damage*) is examined.

This chapter has been accepted for publication in the Mechanical Systems & Signal Processing journal (Kopsaftopoulos and Fassois 2011*e*). Initial results have been published in Kopsaftopoulos and Fassois (2006*b*) and Kopsaftopoulos and Fassois (2007).

1.4.4 Chapter V: A Sequential Statistical Time Series Method for Vibration Based Structural Health Monitoring

The *goal* of the final chapter is the development of a sequential statistically optimal time series method for vibration based Structural Health Monitoring (SHM). The method is based on the statistically optimal Sequential Probability Ratio Test (SPRT) introduced by Wald (1947), which is for the first time employed for vibration based damage detection, identification and quantification. SPRT utilizes likelihood ratio hypotheses tests on model residuals, which – as the Neyman-Pearson lemma implies – for a given amount of information they are the most powerful tests (Ghosh and Sen 1991, Lehmann and Romano 2008).

The method is able to achieve effective damage detection, along with damage identification and quantification, based on sequential multihypothesis testing. Furthermore, unlike conventional hypothesis testing, the method operates under predetermined type I (false alarm) and II (missed damage) error probabilities, while the number of observations required to reach a decision is a random variable, rather than a fixed quantity. The method's performance is determined *a priori* via the analytical expressions of the Operating Characteristic (OC) and the Average Sample Number (ASN) functions, while it requires on average the minimum number of samples in order to reach a decision compared with fixed sample size most powerful tests.

The method's effectiveness is validated and experimentally assessed via its application to damage detection, identification and quantification on a lightweight aluminum truss structure using a single pair of measured excitation-response signals.

Original contributions:

- Use – for the first time in the context of vibration based SHM – of the statistically optimal multihypothesis SPRT in order to propose a complete SHM method able to achieve *early, robust* and effective damage detection, identification and quantification under uncertainties.
- The method's performance is determined *a priori* via the use of the operating characteristic and average sample number functions, selected type I (false alarm) and II (missed damage) error probabilities, and available data records of the structure.
- Assessment of the operating characteristic function, average sample number function, and performance characteristics of the method via a Monte Carlo study.
- Assessment of the method's performance under experimental uncertainties using multiple experiments under various damage scenarios via its application on a paradigm laboratory structure.
- Potential online SHM implementation, as the method may be based on simple conventional time series models (ARX, ARMAX, state space, and so on) and is characterized by computational simplicity.

Initial results of this chapter have been published in the Journal of Theoretical and Applied Mechanics (Kopsaftopoulos and Fassois 2011*b*) and in conference proceedings (Kopsaftopoulos and Fassois 2011*d*). The complete journal version is under preparation for publication (Kopsaftopoulos and Fassois 2011*c*).

Chapter 2

Experimental Assessment of Vibration Based Statistical Time Series Methods for Structural Health Monitoring

The goal of the second chapter is to provide an experimental assessment and comparison of vibration based statistical time series methods for Structural Health Monitoring (SHM) via their application on a lightweight aluminum truss structure and a scale aircraft skeleton structure. An overview of the principles and techniques of the main non-parametric and parametric methods is provided, including response-only and excitation-response schemes. Damage detection and identification are based both on scalar (univariate) and vector (multivariate) versions of the methods, while results for various vibration measurement positions on the structures are presented. The non-parametric and parametric identification is presented, while the damage diagnosis methods' effectiveness is assessed via multiple experiments under various damage scenarios. The results of the chapter confirm the high potential and effectiveness of statistical time series methods for SHM.

2.1 Introduction

Vibration based structural damage detection, identification (localization) and magnitude estimation, also collectively referred to as damage diagnosis, is of paramount importance for reasons associated with proper operation, maintenance and safety. The process of implementing a damage diagnosis strategy is referred to as Structural Health Monitoring (SHM). This process involves the observation of a structure/system over time using periodical measurements, the extraction of damage sensitive quantities (features) from these measurements, and the statistical analysis of these quantities in order to determine the current structural state.

Over the past several years, a wide variety of local non-destructive testing tools have been developed (Farrar *et al.* 2001, Doebling *et al.* 1996, Doebling *et al.* 1998). These are mainly based on ultrasound, acoustic, radiography, eddy current, and thermal field principles, and require access to the vicinity of the suspected damage location, while they are typically time consuming and costly. Aiming at overcoming the aforementioned drawbacks, SHM methods attempt to achieve damage diagnosis on a more “global” basis, with no requirement for visual inspection and potential automation capability. Among them, vibration based methods (Farrar *et al.* 2001, Doebling *et al.* 1996, Doebling *et al.* 1998, Montalvão *et al.* 2006, Fan and Qiao 2011, Salawu 1997) appear promising, as they tend to be time effective and less expensive than many alternatives.

Statistical time series methods for SHM form an important, rapidly evolving, category within the broader vibration based family of methods (Fassois and Sakellariou 2007, Fassois and Sakellariou 2009, Basseville *et al.* 2004, Mevel *et al.* 2003, Sakellariou and Fassois 2008, Kopsaftopoulos and Fassois 2007, Bodeux and Golinval 2001, Kopsaftopoulos and Fassois 2010*a*, Kopsaftopoulos and Fassois 2011*b*, Loh *et al.* 2011, Gul and Catbas 2011). They utilize (i) random excitation and/or response signals (time series), (ii) statistical model building, and (iii) statistical decision making for inferring the health state of a structure. As with all vibration based methods, the fundamental principle upon which they are founded is that small changes (damage) in a structure cause discrepancies in its vibration response, which may be detected and associated with a specific cause (damage type).

Statistical time series methods for SHM are fundamentally of the inverse type, as the models used are *data based* rather than physics based. Furthermore, they offer a number of important advantages, including inherent accounting for uncertainties, no need to interrupt normal operation, no requirement for physics-based or finite element type models, no requirement for complete modal models, and statistical decision making with specified performance characteristics. On the other hand, as complete structural models are not employed, time series methods may identify damage only to the extent allowed by the type of model used. Other limitations include the need for proper “training”, adequate user expertise and potentially limited physical insight. For an extended overview of the principles and techniques of statistical time series methods for SHM, the interested reader is referred to the recent overviews of Fassois and Sakellariou (2007) and Fassois and Sakellariou (2009).

Statistical time series methods for SHM use scalar or vector random signals from the structure in its healthy state, as well as from a number of potential damage states, identifying suitable (parametric or non-parametric) statistical time series models describing the structure in each state, and extracting a statistical quantity (characteristic quantity) characterizing the structural state in each case (baseline phase). Damage diagnosis is then accomplished via statistical decision making consisting of comparing, in a statistical sense, the current characteristic quantity with that of each potential state as determined in the baseline phase (inspection phase).

Non-parametric time series methods for SHM are those based on corresponding time series representations, such as power spectral estimates (Fassois and Sakellariou 2007, Fassois and Sakellariou 2009). This type of methods has received limited attention in the literature. Sakellariou *et al.* (2001)

present the application of a Power Spectral Density (PSD) based method to fault detection in a railway vehicle suspension. The method is applied within a statistical framework, utilizing interval spectral estimates and statistical decision making schemes, while its effectiveness is assessed via experimental data. Furthermore, the application of a PSD analysis based method to a simply supported aluminum beam is presented by Liberatore and Carman (2004), although the effectiveness of the method is demonstrated in conjunction with an analytical model, without employing statistical tools. Rizos *et al.* (2008) treat the problem of damage detection in stiffened aircraft panels via a non-parametric Frequency Response Function (FRF) based method. The FRF estimates are demonstrated to exceed their normal variability bounds under skin damage, while the method accounts for uncertainties and statistical variabilities. Finally, Hwang and Kim (2004) present an FRF based method, whose effectiveness is numerically demonstrated via simulation examples based on Finite Element (FE) models of a simple cantilever and a helicopter rotor blade. Although no statistical framework is incorporated, the method is reported to achieve a satisfactory level of precision with respect to damage diagnosis.

Parametric time series methods for SHM are those based on corresponding time series representations, such as the AutoRegressive Moving Average (ARMA) representation (Fassois and Sakellariou 2007, Fassois and Sakellariou 2009, Ljung 1999, Söderström and Stoica 1989, Lütkepohl 2005). This type of methods has attracted considerable attention and their principles have been used in a number of studies. Sohn *et al.* (2001) and Sohn *et al.* (2003) use the prediction errors of a so-called AutoRegressive and AutoRegressive with eXogenous inputs (AR-ARX) model, a sequential hypothesis testing technique (sequential probability ratio test), and extreme value statistics for damage diagnosis. The method is assessed via numerical simulations and its application to an eight degree-of-freedom mass-spring system, data obtained from a patrol boat, and a three-storey building model. In a related work, Sohn and Farrar (2001) employ the standard deviation ratio of the residual errors from a two-stage AR-ARX model, obtained from healthy measured signals, as the damage sensitive feature. Under the normality assumption this feature is shown to follow F distribution based on which a hypothesis test is developed to infer the structural health state of an eight degree-of-freedom mass-spring system. Adams and Farrar (2002) discuss the use of the autoregressive and exogenous coefficients of a frequency domain ARX model and their implementation for damage diagnosis. The model coefficients are utilized for detecting damage with some level of statistical confidence by applying a standard statistical measure (Mahalanobis distance), while the proposed method is applied to data obtained from a three-storey building model.

Furthermore, the first three autoregressive coefficients of an ARMA model constitute the feature vector employed by Nair *et al.* (2006) and Nair and Kiremidjian (2007) to tackle damage detection. A Gaussian mixture model is used to model the feature vector, while damage is detected via the gap statistic. The postulated method is applied to analytical and experimental data from the ASCE benchmark structure. Carden and Brownjohn (2008) propose a damage detection method based on the ARMA model residual sum of squares and a statistical classifier utilizing a χ^2 distribution. The experimental assessment of the method is achieved via its application to the IASC-ASCE four-storey frame structure, the Z24 bridge, and the Malaysia-Singapore Second Link bridge. Fugate *et al.* (2001) fit an AR model to the measured data obtained from a healthy structure and the corresponding model residuals are used as damage sensitive features. Next, statistical process control methods, such as the X-bar and S control charts, are employed to monitor the mean and variance of the selected features in order to detect damage. For demonstration, the method is applied to vibration test data acquired from a concrete bridge column. An estimate of the standard deviation along with higher-order moments of the residuals obtained from vector AR models are used to detect damage by Mattson and Pandit (2006b). A damage detection threshold level is identified from available training data, while the method is assessed via data obtained from an eight degree-of-freedom test bed. Gao and Lu (2009) present a formulation that enables the construction of residual generators, via state-space representations, as

damage indicators. Then, damage detection is transformed into a disturbance decoupling problem, so that a geometric technique can be employed to detect damage. Numerical results and experimental examples on a laboratory test frame are used to assess the effectiveness of the method. A two-stage damage diagnosis strategy is proposed by Zheng and Mita (2007). Damage existence is determined in the first stage using a damage indicator defined as the distance between two ARMA models, while, in a second stage, damage localization is achieved via pre-whitening filters. The method does not incorporate a statistical framework, while it is applied to a five-storey steel structure. Sakellariou and Fassois (2006) employ Output Error (OE) models and statistical hypothesis testing procedures utilizing the corresponding model parameter vectors, in order to achieve damage diagnosis in structures under earthquake excitation. Damage identification (localization) is achieved via a geometric method, where the parameter vector is used as an initial feature vector, while the method's effectiveness is assessed via a six-storey building model.

A method based on subspace identification and state space model residuals is reported in Basseville *et al.* (2004) and Mevel *et al.* (2003), while methods based on the novel class of stochastic Functionally Pooled (FP) models are reported in Sakellariou and Fassois (2008) and Kopsaftopoulos and Fassois (2007). The FP model based methods are capable of offering an effective solution to the damage detection, localization and magnitude estimation (quantification) subproblems within a unified framework. Nevertheless, these methods are somewhat more elaborate.

In spite of the progress achieved so far, the literature on vibration based statistical time series methods for SHM remains relatively sparse. In particular, no application studies that experimentally compare and assess the various methods are available. The *goal* of the present study precisely is the experimental comparison and assessment of a number of *univariate* (scalar) statistical time series methods to a lightweight laboratory aluminum truss structure. The damage cases considered correspond to loosening of various bolts connecting certain of the truss elements. Random force excitation is provided via an electromechanical shaker, while the vibration responses are measured at various positions via dynamic strain gauges. Two non-parametric methods, namely a Power Spectral Density (PSD) and a Frequency Response Function (FRF) based method, as well as four parametric methods, namely a model parameter based, a residual variance, a residual likelihood function, and a residual uncorrelatedness based method, are briefly reviewed and experimentally assessed.

As already indicated, *univariate* (scalar response) versions of the methods are used, while results are presented for *three* distinct vibration response positions designated as Y1, Y2 and Y3. The methods' main features and operational characteristics are discussed along with practical issues, while their effectiveness is demonstrated via various test cases corresponding to different experiments, damage scenarios, and vibration measurement positions.

The main issues addressed in the study are:

- (a) Assessment of the methods in terms of their damage detection capability under various damage scenarios and different vibration measurement locations (classified as either "local" or "remote" with respect to damage location).
- (b) Assessment of the ability of the methods to accurately identify (classify) the damage type through "local" or "remote" sensors.
- (c) Comparison of the performance characteristics of *scalar* and *vector* statistical time series methods with respect to damage diagnosis: false alarm, missed damage, and damage misclassification rates are investigated.

The rest of the chapter is organized as follows: The experimental set-up is presented in Section 2.4, while the general workframe of statistical time series methods for SHM is briefly outlined in Section

Baseline Phase				
<i>Structural state</i>	S_o (healthy structure)	S_A (damage type A) [†]	S_B (damage type B) [†]	...
<i>Vibration signals</i>	$z_o[t] = (x_o[t], y_o[t])$	$z_A[t] = (x_A[t], y_A[t])$	$z_B[t] = (x_B[t], y_B[t])$...
	$Z_o = (X_o, Y_o)$	$Z_A = (X_A, Y_A)$	$Z_B = (X_B, Y_B)$...
<i>Charact. quantity</i>	Q_o	Q_A	Q_B	...
Inspection Phase				
<i>Structural state</i>	S_u (current structure in unknown state)			
<i>Vibration signals</i>	$z_u[t] = (x_u[t], y_u[t])$			
	$Z_u = (X_u, Y_u)$			
<i>Charact. quantity</i>	Q_u			

[†]Normally various damage magnitudes are considered.

Table 2.1: Workframe setup: structural state, vibration signals used, and the characteristic quantity (baseline and inspection phases).

2.2. A concise overview of the methods is given in Section 2.3, and the experimental assessment and comparison is presented in Sections 2.4 and 2.5. Concluding remarks are finally summarized in Section 2.6.

2.2 Workframe of statistical time series methods for SHM

Let S_o designate the structure under consideration in its *nominal* (healthy) state, S_A, S_B, \dots the structure under damage of *type (mode)* A, B, \dots and so on, and S_u the structure in unknown (to be determined) state. Each damage type may include a continuum of damages which are characterized by common nature or location (for instance, damage in a specific structural element) but varying degree of damage.

Statistical time series methods are commonly based on discretized excitation $x[t]$ and/or response $y[t]$ (for $t = 1, 2, \dots, N$) random vibration data records. Note that t refers to discrete time, with the corresponding actual time being $(t - 1)T_s$, where T_s stands for the sampling period. Let the complete excitation and response signals be presented as X and Y , that is $Z = (X, Y)$. Like before, a subscript (o, A, B, \dots, u) is used for designating the corresponding state of the structure that provided the signals.

Note that all collected signals need to be suitably pre-processed (Doebeling *et al.* 1998, Fassois and Sakellariou 2007, Fassois 2001). This may include low or band-pass filtering within the frequency range of interest, signal subsampling (in case the originally used sampling frequency is too high), sample mean subtraction, as well as proper scaling (in the linear dynamics case). The latter is not only used for numerical reasons, but also for counteracting –to the extent possible– different operating (including excitation levels) and/or environmental conditions.

The obtained signals are subsequently analyzed by parametric or non-parametric time series methods and appropriate models are identified and properly validated (Fassois and Sakellariou 2007, Fassois and Sakellariou 2009, Ljung 1999). Such models are identified on the basis of data Z_o, Z_A, Z_B, \dots in the *baseline phase* and based on Z_u in each *inspection phase*. From each estimated model, the corresponding estimate of a *characteristic quantity* Q is extracted ($\hat{Q}_o, \hat{Q}_A, \hat{Q}_B, \dots$ in the baseline phase; \hat{Q}_u in the inspection phase – see Table 2.1).

Damage detection is then based on proper comparison of the true (but not precisely known) Q_u to the true (but also not precisely known) Q_o via a binary statistical hypothesis test that uses the corresponding estimates – see Table 2.2. *Damage identification* is similarly based on the proper

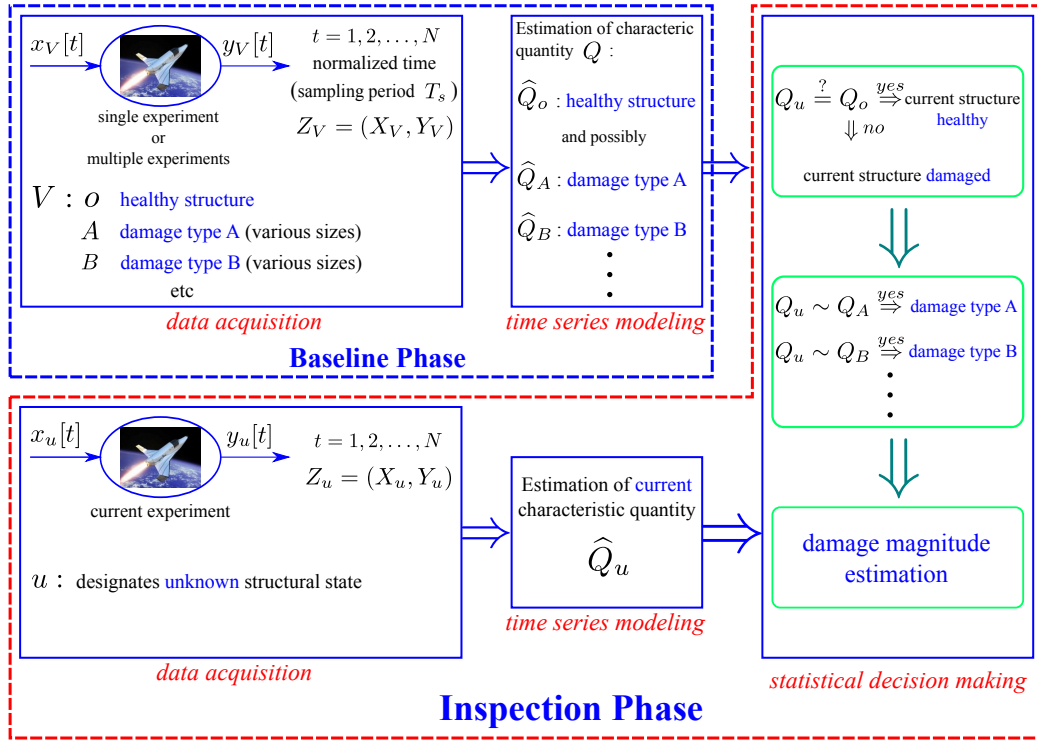


Figure 2.1: Workframe for statistical time series methods for Structural Health Monitoring.

comparison Q_u to each one of Q_A, Q_B, \dots via statistical hypothesis testing procedures that also use the corresponding estimates (Table 2.2). *Damage magnitude estimation*, when considered, is based on interval estimation techniques. The general workframe for statistical time series methods for SHM is depicted in Figure 2.1.

Note that the design of a binary statistical hypothesis test is generally based on the probabilities of *type I* and *type II* error, or else the *false alarm* (α) and *missed damage* (β) probabilities. The designs presented in this work are based on the former, but in selecting α it should be born in mind that as α decreases (increases) β increases (decreases).

2.3 Concise overview of selected statistical time series methods for SHM

A concise overview of selected statistical time series methods for SHM is presented – for further details the reader is referred to Fassois and Sakellariou (2007) and Fassois and Sakellariou (2009). Statistical

<i>Damage detection</i>	
$H_o : Q_u \sim Q_o$	null hypothesis – healthy structure
$H_1 : Q_u \not\sim Q_o$	alternative hypothesis – damaged structure
<i>Damage identification</i>	
$H_A : Q_u \sim Q_A$	hypothesis A – damage type A
$H_B : Q_u \sim Q_B$	hypothesis B – damage type B
\vdots	\vdots

Table 2.2: Statistical hypothesis testing problems for the damage detection and identification tasks.

time series methods may be classified as *non-parametric* or *parametric*, depending on the way the characteristic quantity Q is constructed (Fassois and Sakellariou 2007, Fassois and Sakellariou 2009). Non-parametric methods utilize a statistic based on non-parametric time series representations, such as spectral models (Fassois and Sakellariou 2007, Fassois and Sakellariou 2009). On the other hand, parametric methods utilize a statistic Q based on parametric time series representations, such as AutoRegressive with eXogenous excitation (ARX) or other representations (Fassois 2001, Ljung 1999, Söderström and Stoica 1989). Depending on whether the response only or the excitation and the response signals are employed, the methods are also classified as *response-only* or *excitation-response*, respectively.

2.3.1 Non-parametric methods

2.3.1.1 A Power Spectral Density (PSD) based method

Damage detection and identification is tackled via changes in the Power Spectral Density (PSD) of the measured vibration response signals when the excitation is not available (*response-only* case). The method's characteristic quantity thus is $Q = S_{yy}(\omega) = S(\omega)$, with ω designating frequency. The main idea is based on the comparison of the current (*unknown*) structural response's PSD $S_u(\omega)$ to that of the healthy structure's $S_o(\omega)$ – or, in fact, to that corresponding to any other structural condition. The following hypothesis testing problem is then set up for damage detection:

$$\begin{aligned} H_o & : S_u(\omega) = S_o(\omega) && \text{(null hypothesis – healthy structure)} \\ H_1 & : S_u(\omega) \neq S_o(\omega) && \text{(alternative hypothesis – damaged structure).} \end{aligned} \quad (2.1)$$

As the true PSDs, $S_u(\omega), S_o(\omega)$, are unknown, their estimates $\hat{S}_u(\omega), \hat{S}_o(\omega)$ obtained via the Welch method (with K non-overlapping segments; refer to Table 2.3) are used (Kay 1988, pp. 3 and 76). Then, the following quantity follows (for each frequency ω) F distribution with $(2K, 2K)$ degrees of freedom (Fassois and Sakellariou 2007, Fassois and Sakellariou 2009):

$$F = \frac{\hat{S}_o(\omega)/S_o(\omega)}{\hat{S}_u(\omega)/S_u(\omega)} \sim F(2K, 2K). \quad (2.2)$$

Under the null (H_o) hypothesis the true PSDs coincide ($S_u(\omega) = S_o(\omega)$) and $F = \hat{S}_o(\omega)/\hat{S}_u(\omega)$. This should then be in the range $[f_{\alpha/2}, f_{1-\alpha/2}]$ with probability $1 - \alpha$, and decision making is as follows at a selected α risk level (type I error probability of α):

$$\begin{aligned} f_{\frac{\alpha}{2}}(2K, 2K) \leq F \leq f_{1-\frac{\alpha}{2}}(2K, 2K) \quad (\forall \omega) & \implies H_o \text{ is accepted} \quad \text{(healthy structure)} \\ \text{Else} & \implies H_1 \text{ is accepted} \quad \text{(damaged structure),} \end{aligned} \quad (2.3)$$

with $f_{\alpha/2}, f_{1-\alpha/2}$ designating the F distribution's $\alpha/2$ and $1 - \alpha/2$ critical points.

Note that damage identification may be similarly achieved by performing hypotheses testing similar to the above for damages from each potential damage type (see Table 2.2).

2.3.1.2 A Frequency Response Function (FRF) based method

This method is similar, but requires the availability of both the excitation and response signals (*excitation-response* case) and uses the FRF magnitude as its characteristic quantity $Q = |H(j\omega)|$. The main idea is the comparison of the FRF magnitude $|H_u(j\omega)|$ of the current state of the structure

Quantity	Power Spectral Density (PSD)	Cross Spectral Density (CSD)	Frequency Response Function (FRF)
<i>Estimator</i>	$\widehat{S}_{yy}(\omega) = \frac{1}{K} \sum_{i=1}^K \widehat{Y}_L^i(j\omega) \widehat{Y}_L^i(-j\omega)$ $\widehat{Y}_L^i(j\omega) = \frac{1}{\sqrt{L}} \sum_{t=1}^L a[t] \widehat{y}^i[t] e^{-j\omega T_s}$ $\widehat{y}^i[t] = y^i[t] - \widehat{\mu}_y$ (ith segment of length L)	$\widehat{S}_{yx}(\omega) = \frac{1}{K} \sum_{i=1}^K \widehat{Y}_L^i(j\omega) \widehat{X}_L^i(-j\omega)$ $\widehat{X}_L^i(j\omega) = \frac{1}{\sqrt{L}} \sum_{t=1}^L a[t] \widehat{x}^i[t] e^{-j\omega T_s}$ $\widehat{x}^i[t] = x^i[t] - \widehat{\mu}_x$ (ith segment of length L)	$\widehat{H}(j\omega) = \widehat{S}_{yx}(j\omega) / \widehat{S}_{xx}(j\omega)$
<i>Properties</i>	$2K \widehat{S}_{yy}(\omega) / S_{yy}(\omega) \sim \chi^2(2K)$	$E\{ \widehat{S}_{yx}(j\omega) \} \approx S_{yx}(j\omega) $ $\text{var}[\widehat{S}_{yx}(j\omega)] \approx \frac{ S_{yx}(j\omega) ^2}{\gamma^2(\omega)K}$	$E\{ \widehat{H}(j\omega) \} \approx H(j\omega) $ $\text{var}[\widehat{H}(j\omega)] \approx \frac{1-\gamma^2(\omega)}{\gamma^2(\omega)2K}$
<i>Comments</i>	K : number of data segments $a[t]$: time window	Welch method (no overlap) For $N \rightarrow \infty$, $a[t] = 1$ $\gamma^2(\omega) \rightarrow 1$ or $K \rightarrow \infty$	

Remarks:
 $\omega \in [0, 2\pi/T_s]$ stands for frequency in radian per second; j stands for the imaginary unit; K stands for the number of segments used in Welch spectral estimation.
 $\gamma^2(\omega)$ stands for the coherence function (Bendat and Piersol 2000, p. 196).
 The frequency-domain estimator distributions may be approximated as Gaussian for small relative errors (that is $\gamma^2(\omega) \rightarrow 1$ or $K \rightarrow \infty$) (Bendat and Piersol 2000, pp. 274–275).
 MATLAB functions: *pwelch.m* for \widehat{S}_{yy} , *csd.m* for \widehat{S}_{yx} , *tfestimate.m* for \widehat{H} , *mscohere.m* for $\widehat{\gamma}^2$

Table 2.3: Estimation of non-parametric statistical time series models.

to that of the healthy structure $|H_o(j\omega)|$. The following hypothesis testing problem is then set up for damage detection:

$$\begin{aligned}
 H_o & : \delta |H(j\omega)| = |H_o(j\omega)| - |H_u(j\omega)| = 0 && \text{(null hypothesis – healthy structure)} \\
 H_1 & : \delta |H(j\omega)| = |H_o(j\omega)| - |H_u(j\omega)| \neq 0 && \text{(alternative hypothesis – damaged structure)}.
 \end{aligned} \tag{2.4}$$

As the true FRFs, $H_u(j\omega)$ and $H_o(j\omega)$, are unknown, their respective estimates, $\widehat{H}_u(j\omega)$ and $\widehat{H}_o(j\omega)$, obtained as indicated in Table 2.3, are used. The FRF estimator may, asymptotically ($N \rightarrow \infty$), be considered as approximately following Gaussian distribution (Bendat and Piersol 2000, p. 338). Under the null (H_o) hypothesis the true FRF magnitudes coincide ($|H_u(j\omega)| = |H_o(j\omega)|$), hence $\delta |\widehat{H}(j\omega)| = |\widehat{H}_o(j\omega)| - |\widehat{H}_u(j\omega)| \sim \mathcal{N}(0, 2\sigma_o^2(\omega))$. The variance $\sigma_o^2(\omega) = \text{var}[|\widehat{H}_o(j\omega)|]$ is generally unknown, but may be estimated in the baseline phase (Table 2.3).

Equality of the two FRF magnitudes may be then examined at the selected α (type I) risk level through the statistical test:

$$\begin{aligned}
 Z = |\delta |\widehat{H}(j\omega)|| / \sqrt{2\widehat{\sigma}_o^2(\omega)} \leq Z_{1-\frac{\alpha}{2}} \quad (\forall \omega) & \implies H_o \text{ is accepted} \quad \text{(healthy structure)} \\
 \text{Else} & \implies H_1 \text{ is accepted} \quad \text{(damaged structure)},
 \end{aligned} \tag{2.5}$$

with $Z_{1-\alpha/2}$ designating the standard normal distribution's $1 - \alpha/2$ critical point.

Damage identification may be similarly achieved by performing hypotheses testing similar to the above for damages from each potential damage type (see Table 2.2).

2.3.2 Parametric methods

2.3.2.1 A model parameter based method

This method bases damage detection and identification on a characteristic quantity $Q = f(\boldsymbol{\theta})$ which is function of the parameter vector $\boldsymbol{\theta}$ of a parametric time series model ($Q = \boldsymbol{\theta}$ in the typical case).

Let $\hat{\boldsymbol{\theta}}$ designate a proper estimator of the parameter vector $\boldsymbol{\theta}$ (Fassois 2001),(Ljung 1999, pp. 212–213). For sufficiently long signals the estimator is (under mild assumptions) Gaussian distributed with mean equal to its true value $\boldsymbol{\theta}$ and a certain covariance $\mathbf{P}_{\boldsymbol{\theta}}$ (Ljung 1999, p. 303), hence $\hat{\boldsymbol{\theta}} \sim \mathcal{N}(\boldsymbol{\theta}, \mathbf{P}_{\boldsymbol{\theta}})$.

Damage detection is based on testing for statistically significant changes in the parameter vector $\boldsymbol{\theta}$ between the nominal and current state of the structure through the hypothesis testing problem (Fassois and Sakellariou 2007, Fassois and Sakellariou 2009):

$$\begin{aligned} H_o & : \delta\boldsymbol{\theta} = \boldsymbol{\theta}_o - \boldsymbol{\theta}_u = \mathbf{0} && \text{(null hypothesis – healthy structure)} \\ H_1 & : \delta\boldsymbol{\theta} = \boldsymbol{\theta}_o - \boldsymbol{\theta}_u \neq \mathbf{0} && \text{(alternative hypothesis – damaged structure).} \end{aligned} \quad (2.6)$$

The difference between the two parameter vector estimators also follows Gaussian distribution (Fassois and Sakellariou 2007), that is $\delta\hat{\boldsymbol{\theta}} = \hat{\boldsymbol{\theta}}_o - \hat{\boldsymbol{\theta}}_u \sim \mathcal{N}(\delta\boldsymbol{\theta}, \delta\mathbf{P})$, with $\delta\boldsymbol{\theta} = \boldsymbol{\theta}_o - \boldsymbol{\theta}_u$ and $\delta\mathbf{P} = \mathbf{P}_o + \mathbf{P}_u$, where $\mathbf{P}_o, \mathbf{P}_u$ designate the corresponding covariance matrices. Under the null (H_o) hypothesis $\delta\hat{\boldsymbol{\theta}} = \hat{\boldsymbol{\theta}}_o - \hat{\boldsymbol{\theta}}_u \sim \mathcal{N}(\mathbf{0}, 2\mathbf{P}_o)$ and the quantity $\chi_{\boldsymbol{\theta}}^2 = \delta\hat{\boldsymbol{\theta}}^T \cdot \delta\mathbf{P}^{-1} \cdot \delta\hat{\boldsymbol{\theta}}$ (with $\delta\mathbf{P} = 2\mathbf{P}_o$) follows χ^2 distribution with d (parameter vector dimensionality) degrees of freedom (Fassois and Sakellariou 2007, Fassois and Sakellariou 2009),(Ljung 1999, p. 558).

As the covariance matrix \mathbf{P}_o corresponding to the healthy structure is unavailable, its estimated version $\hat{\mathbf{P}}_o$ is used. Then, the following test is constructed at the α (type I) risk level:

$$\begin{aligned} \chi_{\boldsymbol{\theta}}^2 \leq \chi_{1-\alpha}^2(d) & \implies H_o \text{ is accepted} && \text{(healthy structure)} \\ \text{Else} & \implies H_1 \text{ is accepted} && \text{(damaged structure),} \end{aligned} \quad (2.7)$$

with $\chi_{1-\alpha}^2(d)$ designating the χ^2 distribution's $1 - \alpha$ critical point.

Damage identification may be based on the multiple hypotheses testing problem of Table 2.2 comparing the parameter vector $\hat{\boldsymbol{\theta}}_u$ belonging to the current state of the structure to those corresponding to different damage types $\hat{\boldsymbol{\theta}}_A, \hat{\boldsymbol{\theta}}_B, \dots$

2.3.2.2 Residual based methods

These methods (Fassois and Sakellariou 2007, Fassois and Sakellariou 2009) attempt damage detection and identification using characteristic quantities that are functions of residual sequences obtained by driving the current signal(s) Z_u through suitable predetermined –in the baseline phase– models M_o, M_A, M_B, \dots , each one corresponding to a particular state of the structure (healthy and damaged structure under specific damage types). The general idea is that the residual sequence obtained by a model that truly reflects the actual (current) state of the structure will possess certain distinct properties, and will be thus possible to distinguish. An advantage of the methods is that model identification is not repeated in the inspection phase.

Let M_V designate the model representing the structure in its V state ($V = o$ or $V = A, B, \dots$). The residual series obtained by driving the current signals Z_u through each one of the aforementioned models are designated as $e_{ou}[t], e_{Au}[t], e_{Bu}[t], \dots$ and are characterized by respective variances $\sigma_{ou}^2, \sigma_{Au}^2, \sigma_{Bu}^2, \dots$ –notice that the first subscript designates the model employed and the second the

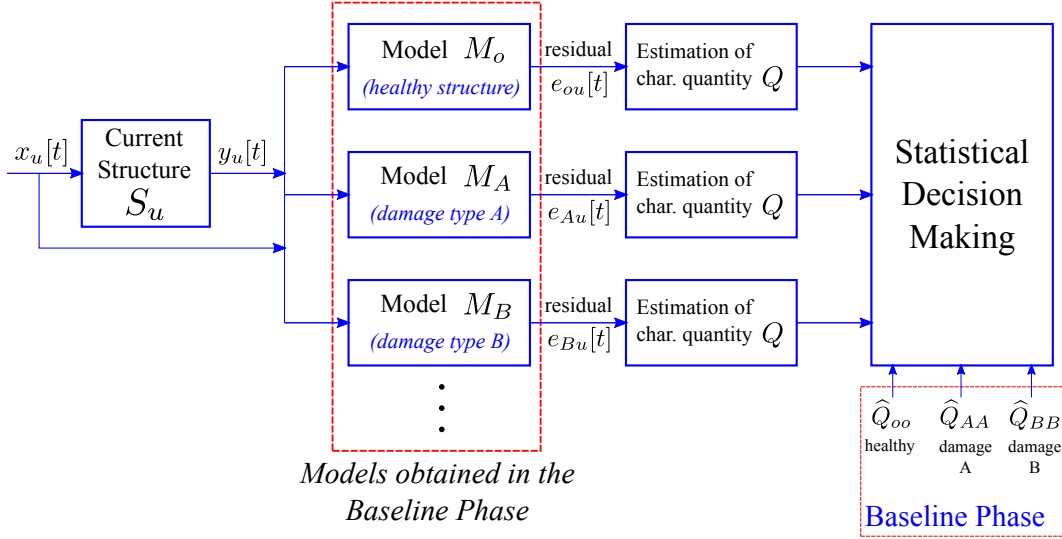


Figure 2.2: Schematic for residual based statistical time series methods for SHM (the inspection phase is depicted outside the dashed boxes).

structural state corresponding to the current excitation and/or response signal(s) used. The characteristic quantities obtained from the corresponding residual series are designated as $Q_{ou}, Q_{Au}, Q_{Bu}, \dots$. The characteristic quantities obtained using the baseline data records are designated as Q_{VV} ($V = o$ or $V = A, B, \dots$).

A schematic for the residual based statistical time series methods for SHM is illustrated in Figure 2.2.

Residual variance based method

In this method the characteristic quantity is the residual variance. Damage detection is based on the fact that the residual series $e_{ou}[t]$, obtained by driving the current signal(s) Z_u through the model M_o corresponding to the nominal (healthy) structure should be characterized by variance σ_{ou}^2 , which becomes minimal (specifically equal to σ_{oo}^2) if and only if the current structure is healthy. The following hypothesis testing problem is then set up:

$$\begin{aligned} H_o &: \sigma_{oo}^2 = \sigma_{ou}^2 && \text{(null hypothesis - healthy structure)} \\ H_1 &: \sigma_{oo}^2 < \sigma_{ou}^2 && \text{(alternative hypothesis - damaged structure).} \end{aligned} \quad (2.8)$$

Under the null (H_o) hypothesis the residuals $e_{ou}[t]$ are (just like the residuals $e_{oo}[t]$) iid zero mean Gaussian with variance σ_{oo}^2 (Fassois and Sakellariou 2007). Hence, the quantities $N_u \hat{\sigma}_{ou}^2 / \sigma_{oo}^2$ and $(N_o - d) \hat{\sigma}_{oo}^2 / \sigma_{oo}^2$ follow central χ^2 distributions with N_u and $N_o - d$ degrees of freedom, respectively. Note that N_o and N_u designate the number of samples used in estimating the residual variance in the healthy and current cases, respectively (typically $N_o = N_u = N$), and d designates the dimensionality of the model parameter vector. Consequently, the statistic $\hat{\sigma}_{ou}^2 / \hat{\sigma}_{oo}^2$ follows F distribution with $(N_u, N_o - d)$ degrees of freedom. The following test is then constructed at the α (type I) risk level:

$$\begin{aligned} F = \frac{\hat{\sigma}_{ou}^2}{\hat{\sigma}_{oo}^2} \leq f_{1-\alpha}(N_u, N_o - d) &\implies H_o \text{ is accepted (healthy structure)} \\ \text{Else} &\implies H_1 \text{ is accepted (damaged structure).} \end{aligned} \quad (2.9)$$

Damage identification may be achieved based on the multiple hypotheses testing problem of Table 2.2.

Residual likelihood function based method

In this method damage detection is based on the likelihood function under the null (H_o) hypothesis of a healthy structure (Fassois and Sakellariou 2007, Fassois and Sakellariou 2009),(Gertler 1998, pp. 119–120). The hypothesis testing problem considered is:

$$\begin{aligned} H_o & : \boldsymbol{\theta}_o = \boldsymbol{\theta}_u && \text{(null hypothesis – healthy structure)} \\ H_1 & : \boldsymbol{\theta}_o \neq \boldsymbol{\theta}_u && \text{(alternative hypothesis – damaged structure),} \end{aligned} \quad (2.10)$$

with $\boldsymbol{\theta}_o, \boldsymbol{\theta}_u$ designating the parameter vectors corresponding to the healthy and current structure, respectively. Assuming serial independence of the residual sequence, the Gaussian likelihood function $L_y(Y, \boldsymbol{\theta}/X)$ for the data Y given X is obtained (Fassois and Sakellariou 2007, Fassois and Sakellariou 2009)(Box *et al.* 1994, p. 226).

Under the null (H_o) hypothesis, the residual series $e_{ou}[t]$ generated by driving the current signal(s) through the nominal model is (just like $e_{oo}[t]$) iid Gaussian with zero mean and variance σ_{oo}^2 . Decision making may be then based on the likelihood function under H_o evaluated for the current data, by requiring it to be larger or equal to a threshold l (which is to be selected) in order for the null (H_o) hypothesis to be accepted:

$$\begin{aligned} L_y(Y, \boldsymbol{\theta}_o/X) \geq l & \implies H_o \text{ is accepted} && \text{(healthy structure)} \\ \text{Else} & \implies H_1 \text{ is accepted} && \text{(damaged structure).} \end{aligned} \quad (2.11)$$

Under the null (H_o) hypothesis, the statistic $N\widehat{\sigma}_{ou}^2/\widehat{\sigma}_{oo}^2$ follows χ^2 distribution with N degrees of freedom (Fassois and Sakellariou 2007, Fassois and Sakellariou 2009). This leads to the re-expression of the above decision making rule as follows:

$$\begin{aligned} \chi_N^2 = \frac{N\widehat{\sigma}_{ou}^2}{\widehat{\sigma}_{oo}^2} \leq \chi_{1-\alpha}^2(N) & \implies H_o \text{ is accepted} && \text{(healthy structure)} \\ \text{Else} & \implies H_1 \text{ is accepted} && \text{(damaged structure),} \end{aligned} \quad (2.12)$$

with $\chi_{1-\alpha}^2(N)$ designating the χ^2 distribution's $1 - \alpha$ critical point. Note that the above decision making is similar to that of the previous (residual based variance) method.

In the case of vector time series models the corresponding vector residual series $\mathbf{e}_{ou}[t]$ is iid Gaussian with zero mean and covariance matrix $\boldsymbol{\Sigma}_o$. Under the null (H_o) hypothesis the above decision making rule may be re-expressed as follows:

$$\begin{aligned} \sum_{t=1}^N (\mathbf{e}_{ou}^T[t, \boldsymbol{\theta}_o] \cdot \boldsymbol{\Sigma}_o \cdot \mathbf{e}_{ou}[t, \boldsymbol{\theta}_o]) \leq l & \implies H_o \text{ is accepted} && \text{(healthy structure)} \\ \text{Else} & \implies H_1 \text{ is accepted} && \text{(damaged structure).} \end{aligned} \quad (2.13)$$

Damage identification may be achieved by computing the likelihood function for the current signal(s) for the various values of $\boldsymbol{\theta}$ ($\boldsymbol{\theta}_A, \boldsymbol{\theta}_B, \dots$) and accepting the hypothesis that corresponds to the maximum value of the likelihood.

Residual uncorrelatedness based method

This method is based on the fact that the residual sequence $e_{ou}[t]$ obtained by driving the current signal(s) Z_u through the nominal model will be *uncorrelated* (white) if and only if the current structure is in its nominal (healthy) state (Fassois and Sakellariou 2007, Fassois and Sakellariou 2009). Damage detection may be then based on the hypothesis testing problem:

$$\begin{aligned} H_o & : \rho[\tau] = 0 \quad \tau = 1, 2, \dots, r && \text{(null hypothesis – healthy structure)} \\ H_1 & : \rho[\tau] \neq 0 \quad \text{for some } \tau && \text{(alternative hypothesis – damaged structure),} \end{aligned} \quad (2.14)$$

with $\rho[\tau]$ designating the normalized autocovariance function (see Table 2.3) of the $e_{ou}[t]$ residual sequence.

Under the null (H_o) hypothesis, $e_{ou}[t]$ is iid Gaussian with zero mean and the statistic $\chi_\rho^2 = N(N+2) \sum_{\tau=1}^r (N-\tau)^{-1} \hat{\rho}^2[\tau]$ follows χ^2 distribution with r degrees of freedom and $\hat{\rho}[t]$ designating the estimator of $\rho[t]$ (Box *et al.* 1994, p. 314). Decision making is then based on the following test at the α (type I) risk level:

$$\begin{aligned} \chi_\rho^2 = N(N+2) \sum_{\tau=1}^r (N-\tau)^{-1} \hat{\rho}^2[\tau] \leq \chi_{1-\alpha}^2(r) &\implies H_o \text{ is accepted} && \text{(healthy structure)} \\ \text{Else} &\implies H_1 \text{ is accepted} && \text{(damaged structure).} \end{aligned} \quad (2.15)$$

Damage identification may be achieved by similarly examining which one of the $e_{Vu}[t]$ ($V = A, B, \dots$) residual series is uncorrelated.

2.3.2.3 The Sequential Probability Ratio Test (SPRT) based method

This method employs the Sequential Probability Ratio Test (SPRT) (Wald 2004, Ghosh and Sen 1991) in order to detect a change in the standard deviation σ of the model scalar residual sequence ($e[t] \sim \mathcal{N}(0, \sigma^2)$, $t = 1, \dots, N$) (parametric method). An SPRT of strength (α, β) , with α, β designating the type I (false alarm) and II (missed damage) error probabilities, respectively, is used for the following hypothesis testing problem:

$$\begin{aligned} H_o &: \sigma_{ou} \leq \sigma_o && \text{(null hypothesis – healthy structure)} \\ H_1 &: \sigma_{ou} \geq \sigma_1 && \text{(alternative hypothesis – damaged structure)} \end{aligned} \quad (2.16)$$

with σ_{ou} designating the standard deviation of a scalar residual signal obtained by driving the current excitation and response signals through the healthy structural model, and σ_o, σ_1 user defined values. The basis of the SPRT is the logarithm of the likelihood ratio function based on n samples:

$$\mathcal{L}(n) = \log \frac{f(e[1], \dots, e[n]|H_1)}{f(e[1], \dots, e[n]|H_o)} = \sum_{t=1}^n \log \frac{f(e[t]|H_1)}{f(e[t]|H_o)} = n \cdot \log \frac{\sigma_o}{\sigma_1} + \frac{\sigma_1^2 - \sigma_o^2}{2\sigma_o^2\sigma_1^2} \cdot \sum_{t=1}^n e^2[t] \quad (2.17)$$

with $\mathcal{L}(n)$ designating the decision parameter of the method and $f(e[t]|H_i)$ the probability density function (normal distribution) of the residual sequence under hypothesis H_i ($i = 0, 1$).

The following test is then constructed at the (α, β) risk levels:

$$\begin{aligned} \mathcal{L}(n) \leq B &\implies H_o \text{ is accepted} && \text{(healthy structure)} \\ \mathcal{L}(n) \geq A &\implies H_1 \text{ is accepted} && \text{(damaged structure)} \\ B < \mathcal{L}(n) < A &\implies \text{no decision is made} && \text{(continue the test)} \end{aligned} \quad (2.18)$$

with $B = \log[\beta/(1-\alpha)]$ and $A = \log[(1-\beta)/\alpha]$. Following a decision, $\mathcal{L}(n)$ is reset to zero.

Damage identification may be achieved by performing SPRTs similar to the above separately for damages of each potential type.

2.4 Application on a lightweight truss structure

In this section the experimental comparison and assessment of several *univariate* (scalar) statistical time series methods on a lightweight laboratory aluminum truss structure is presented. The damage cases considered correspond to loosening of various bolts connecting certain of the truss elements. Random force excitation is provided via an electromechanical shaker, while the vibration responses are measured at various positions via dynamic strain gauges. Two non-parametric methods, namely a Power Spectral Density (PSD) and a Frequency Response Function (FRF) based method, as well as four parametric methods, namely a model parameter based, a residual variance, a residual likelihood function, and a residual uncorrelatedness based method, are briefly reviewed and experimentally assessed.

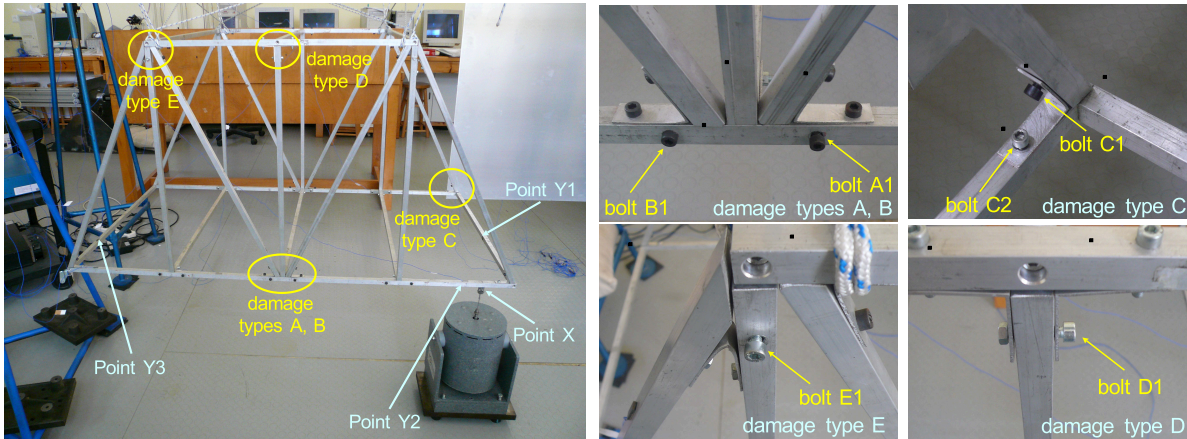


Figure 2.3: The aluminum truss structure and the experimental set-up: The force excitation (Point X), the vibration measurement positions (Points Y1 – Y3), and the considered damage types (A, B, C, D, and E).

2.4.1 The lightweight truss structure

The truss structure is depicted in Figure 2.3, suspended through a set of cords. It consists of twenty eight elements with rectangular cross sections (15×15 mm) jointed together via steel elbow plates and bolts. All parts are constructed from standard aluminum with the overall dimensions being $1400 \times 700 \times 800 \times 700$ mm.

2.4.2 The damage types and the experiments

The damages considered correspond to complete loosening of various bolts at different joints of the structure. Five distinct types are specifically considered (Figure 2.3): The first damage type, referred to as *damage type A*, corresponds to the loosening of bolt A1 joining together an horizontal with a vertical element. The second damage type, referred to as *damage type B*, corresponds to the loosening of bolts A1 and B1 joining together an horizontal with a vertical element. Damage type B affects the same elements as damage type A, but it is more severe, as loosening of two bolts is involved. The third damage type, referred to as *damage type C*, corresponds to the loosening of bolts C1 and C2 joining together an horizontal with a diagonal element. The fourth damage type, referred to as *damage type D*, corresponds to the loosening of bolt D1 joining together an horizontal with a vertical element. Finally, the fifth damage type, referred to as *damage type E*, corresponds to the loosening of bolt E1 joining together a vertical with a diagonal element. All damage types considered are summarized in Table 2.4.

The force excitation is a random Gaussian signal applied vertically at Point X (Figure 2.3) via an electromechanical shaker (MB Dynamics Modal 50A, max load 225 N) equipped with a stinger, and measured via an impedance head (PCB 288D01, sensitivity 98.41 mV/lb). The vibration responses are measured at different points via dynamic strain gauges (PCB ICP 740B02, 0.005 – 100 kHz, 50 mV/ $\mu\epsilon$; sampling frequency $f_s = 256$ Hz, signal bandwidth 0.5 – 100 Hz). The force and strain signals are driven through a signal conditioning device (PCB 481A02) into the data acquisition system (SigLab 20-42). In this study damage detection and identification results based on each one of the three vibration response signals (Points Y1, Y2 and Y3 – Figure 2.3) and obtained via *scalar* versions of the methods are presented. This allows examination of the potential of the methods to achieve damage detection and identification even through a single vibration signal measurement.

Structural State	Description	Total Number of Experiments
Healthy	—	40 (1 baseline)
Damage type A	loosening of bolt A1	32 (1 baseline)
Damage type B	loosening of bolts A1 and B1	32 (1 baseline)
Damage type C	loosening of bolts C1 and C2	32 (1 baseline)
Damage type D	loosening of bolt D1	32 (1 baseline)
Damage type E	loosening of bolt E1	32 (1 baseline)
Sampling frequency: $f_s = 256$ Hz, Signal bandwidth: [0.5 – 100] Hz		
Signal length N in samples (s): Non-parametric methods: $N = 30\,720$ (120 s)		
Parametric methods: $N = 10\,000$ (39 s)		

Table 2.4: The considered damage types, number of experiments, and vibration signal details.

A significant number of test cases is considered in the experimental assessment: In each test case a specific experiment (out of a total of 40 experiments for the healthy structure and 32 experiments for each damage state, with one from each category reserved for the baseline phase – Table 2.4) and vibration response measurement position (Points Y1 – Y3, Figure 2.3) are employed. Experimental details are presented in Table 2.4. Notice that the sample mean is subtracted from each signal and scaling by the signal’s sample standard deviation is implemented.

The experimental assessment of the univariate statistical time series methods is based on a number of test cases, each corresponding to a single (out of several possible) structural states (damage scenarios – see Table 2.4), a single experiment (Table 2.4), and a single vibration response measurement position (out of Points Y1, Y2, Y3 – Figure 2.3). Note that 40 experiments are run for the healthy structure and 32 for each considered damage state (damage types A, B, . . . , E).

In subsections 2.4.3 and 2.4.4 representative results for the first vibration measurement position (Point Y1, Figure 2.3) are presented, while in subsection 2.4.5 summary results for all three vibration measurement positions are presented.

2.4.3 Baseline phase: structural identification under various structural states (measurement position Y1)

2.4.3.1 Non-parametric methods

Non-parametric identification of the structure is based on $N = 30\,720$ (≈ 120 s) sample-long excitation-response signals. An $L = 2048$ sample-long Hamming data window with zero overlap is used (number of segments $K = 15$) for PSD (MATLAB function *pwelch.m*) and FRF (MATLAB function *tfestimate.m*) Welch based estimation (see Tables 2.3 and 2.5).

The obtained response PSD and FRF magnitude estimates for the healthy and damaged states of the structure (Point Y1) are depicted in Figure 2.4. As it may be observed, the healthy and damaged curves are rather similar in the 0.5 – 30 Hz range, where the first twelve modes are included. Significant differences between the healthy and damage types C, D and E curves are seen in the 30 – 58 Hz range, where the next three modes are included. Finally, discrepancies are more evident for damage types C and E in the 58 – 100 Hz range, where the next eight modes are included.

The data sets used for obtaining the above response PSD and FRF estimates for the healthy and damaged structural states are considered as the only baseline (reference) data sets throughout this work and are used for obtaining the nominal characteristic quantities Q_o for each time series method. The healthy baseline data set is used for the damage detection task, while the damaged baseline data

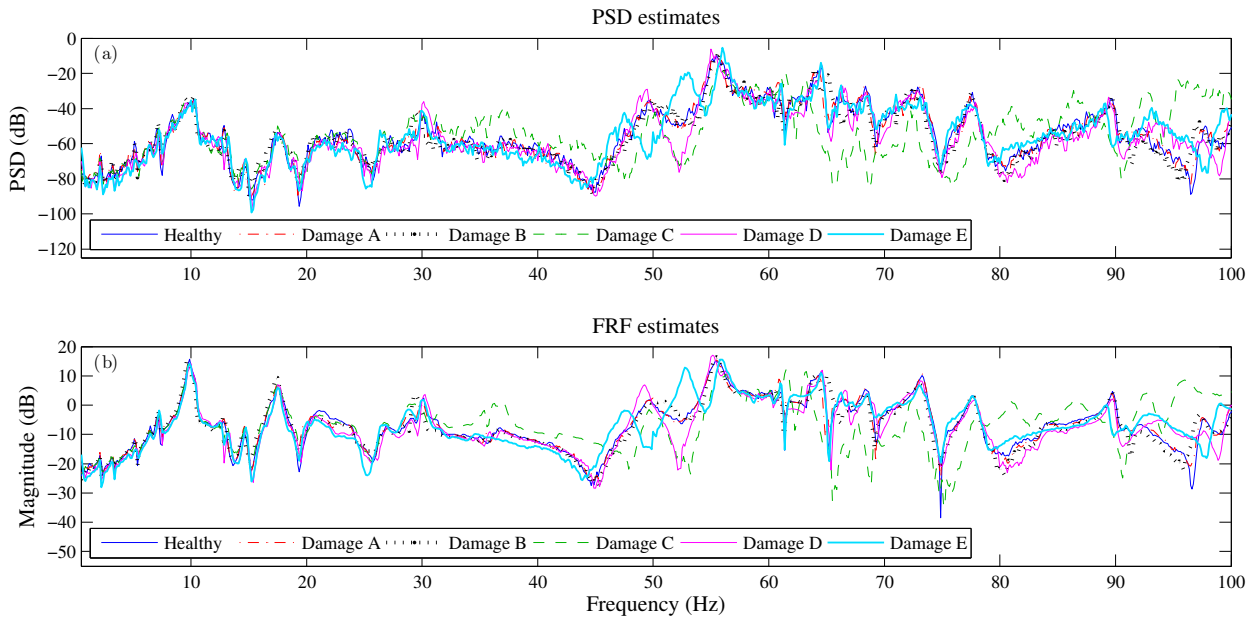


Figure 2.4: (a) Power Spectral Density (PSD) and (b) Frequency Response Function (FRF) magnitude estimates for the healthy and damaged structural states (response Y1).

sets are used for the damage identification task.

2.4.3.2 Parametric methods

Parametric identification of the structural dynamics is based on $N = 10\,000$ (≈ 39 s) sample-long excitation and single response signals which are used for estimating AutoRegressive with eXogenous excitation (ARX) models (MATLAB function *arx.m*). The modeling strategy consists of the successive fitting of ARX(na, nb) models (with na, nb designating the AR and X orders, respectively; in this study $na = nb = n$) until a suitable model is selected. Model parameter estimation is achieved by minimizing a quadratic Prediction Error (PE) criterion leading to a Least Squares (LS) estimator (Fassois 2001), (Ljung 1999, p. 206). Model order selection, which is crucial for successful identification, may be based on a combination of tools, including the Bayesian Information Criterion (BIC) (Figure 2.5a), which is a statistical criterion that penalizes model complexity (order) as a counteraction to a decreasing quality criterion (Fassois 2001), (Ljung 1999, pp. 505–507), monitoring of the RSS/SSS (Residual Sum of Squares / Signal Sum of Squares) criterion (Figure 2.5b), monitoring of the residual autocorrelation function (MATLAB function *autocorr.m*) (Ljung 1999, p. 512), and use of “stabilization diagrams” (Figure 2.6) which depict the estimated modal parameters (usually frequencies) as a function of increasing model order (Fassois 2001, Ljung 1999).

Data length	$N = 30\,720$ samples (≈ 120 s)
Method	Welch
Segment length	$L = 2048$ samples
No of non-overlapping segments	$K = 15$ segments
Window type	Hamming
Frequency resolution	$\Delta f = 0.125$ Hz

Table 2.5: Non-parametric estimation details.

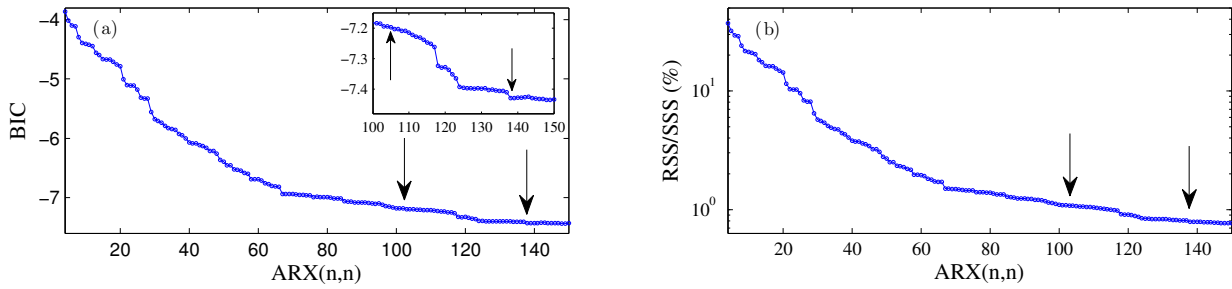


Figure 2.5: Order selection criteria for $ARX(n, n)$ type parametric models in the healthy case (response: (a) BIC and (b) RSS/SSS).

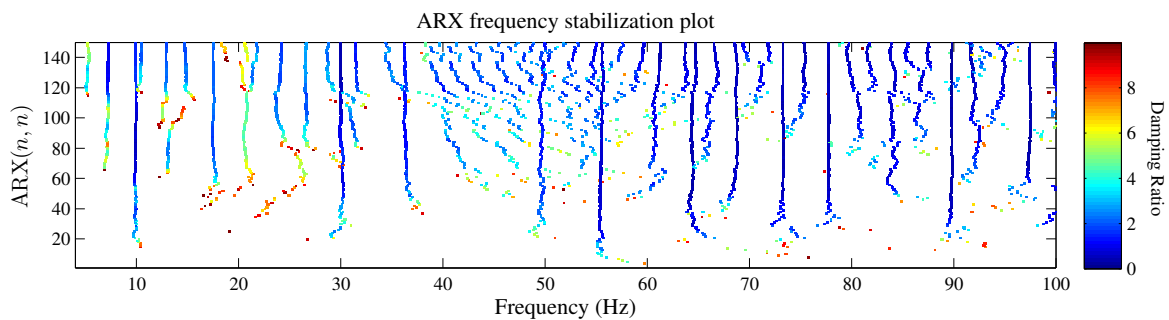


Figure 2.6: Frequency stabilization diagram for $ARX(n, n)$ type models in the healthy case (response Y1).

An approximate plateau in the BIC and RSS/SSS sequences is achieved for model order $n > 70$ (Figure 2.5). Furthermore, as indicated in the frequency stabilization diagram of Figure 2.6, model orders of $n > 90$ are adequate for most natural frequencies to get stabilized. Notice the color bar in Figure 2.6, which demonstrates the damping ratios for each frequency for increasing model order.

The above identification procedure leads to an $ARX(103, 103)$ model (vibration measurement position Y1), which is selected as adequate for the model parameter, residual variance, and likelihood function based methods. The identified $ARX(103, 103)$ representation has 207 parameters with the Sample Per Parameter (SPP) number being equal to 48.3. For the residual uncorrelatedness based method an $ARX(138, 138)$ model is selected, as the corresponding model residuals need to be as white as possible in order for the method to work effectively. The identified $ARX(138, 138)$ representation has 277 parameters ($SPP = 36.1$). The selected models and estimation details are summarized in Table 2.6. Note that the identification procedure generally leads to different ARX models (including somewhat different model orders) for each vibration measurement position.

2.4.4 Inspection phase (measurement position Y1)

2.4.4.1 PSD based method

Typical PSD based damage detection results are presented in Figure 2.7. Evidently, correct detection at the $\alpha = 10^{-4}$ risk level is obtained in each case, as the test statistic is shown not to exceed the critical points (dashed horizontal lines) in the healthy case, while it exceeds them in the damaged cases. Observe that damage types C (two bolts loosened) and D (one bolt loosened) are easiest to

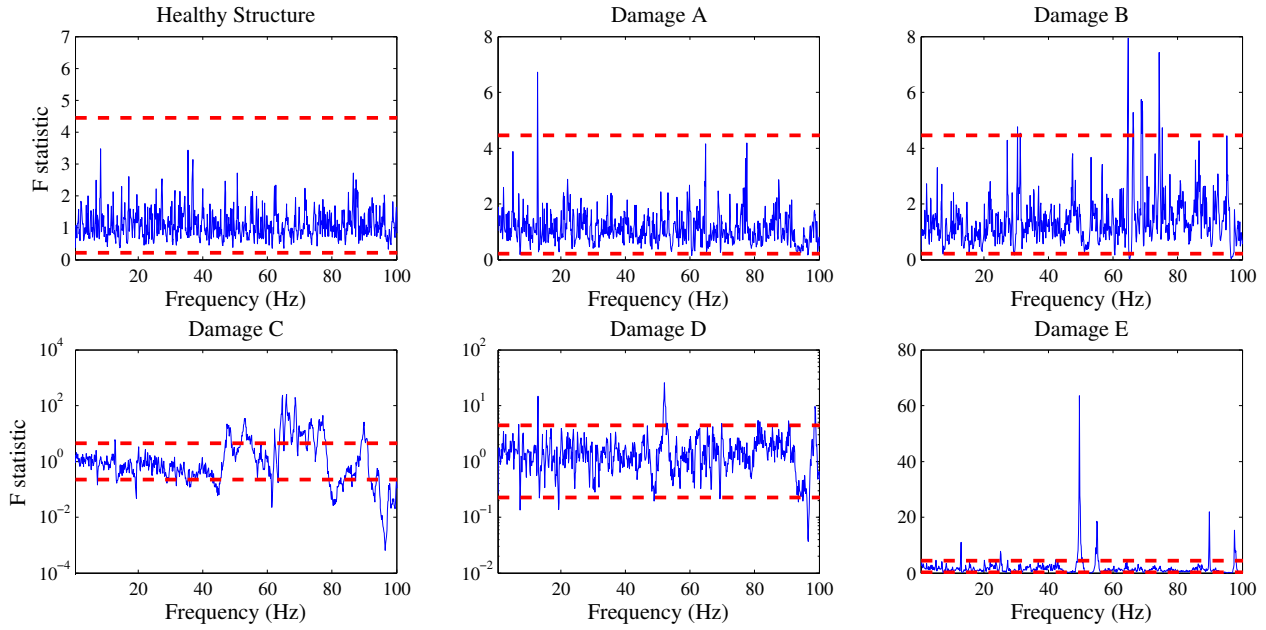


Figure 2.7: PSD based method (response Y1): Indicative damage detection results for six representative test cases (one healthy and five damaged) at the $\alpha = 10^{-4}$ risk level. The actual structural state is shown above each plot box. A damage is detected if the test statistic exceeds the critical points (dashed horizontal lines).

detect (note the logarithmic scale on the vertical axis of Figure 2.7), while damage type A (one bolt loosened) is hardest (the test statistic is within the critical points for most frequencies).

Representative damage identification results at the $\alpha = 10^{-4}$ risk level are presented in Figure 2.8, with the actual damage being of type A. When testing the hypothesis of damage type A, the test statistic does not exceed the critical points, while it clearly does so when testing the hypothesis of any other damage type.

2.4.4.2 FRF based method

Figure 2.9 presents typical FRF based damage detection results. Evidently, correct detection at the $\alpha = 10^{-5}$ risk level is achieved in each case, as the test statistic is shown not to exceed the critical points (dashed horizontal lines) in the healthy case, while it exceeds them in the damaged cases. Again, damage types C and D appear as easiest to detect, while damage types A and B are hardest.

Indicative damage identification results at the $\alpha = 10^{-5}$ risk level are presented in Figure 2.10, with the actual damage being of type C. When testing the hypothesis of damage type C, the test

Method	Selected Model	Number of estimated parameters	SPP
Model parameter	ARX(103, 103)	207 parameters	48.3
Residual variance	ARX(103, 103)	207 parameters	48.3
Residual likelihood	ARX(103, 103)	207 parameters	48.3
Residual uncorrelatedness	ARX(138, 138)	277 parameters	36.1

Parameter estimation method: Weighted Least Squares (WLS), QR implementation

Table 2.6: Selected models and estimation details (response Y1).

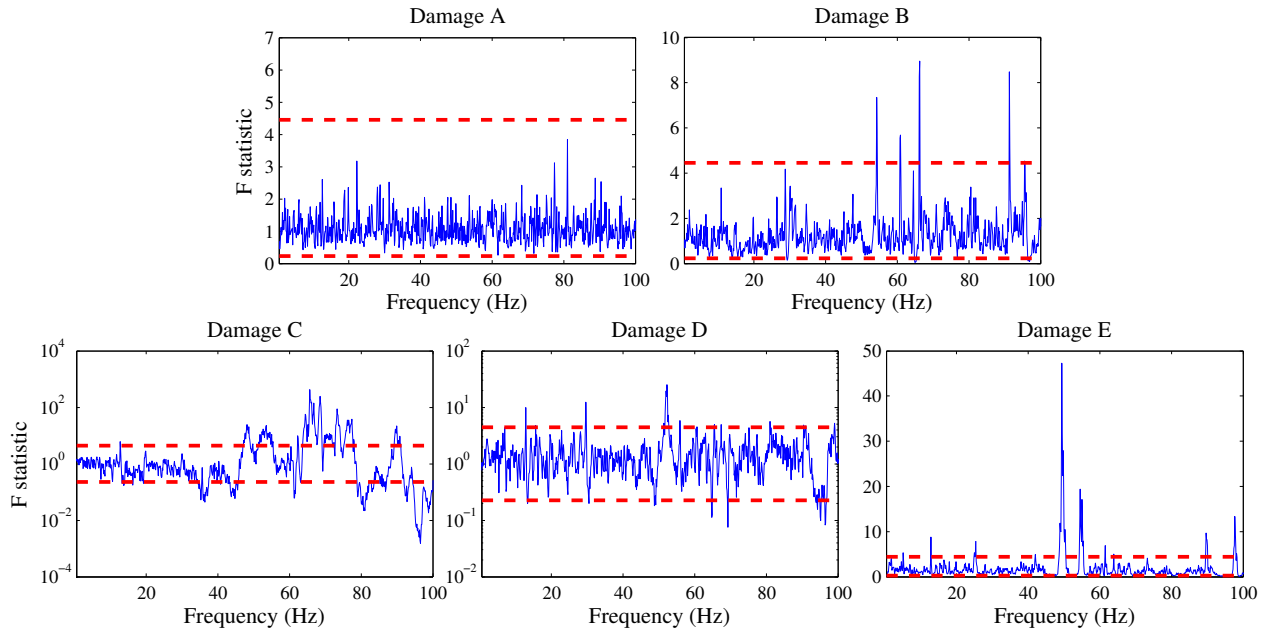


Figure 2.8: PSD based method (response Y1): Indicative damage identification results for five damage test cases at the $\alpha = 10^{-4}$ risk level, with the actual damage being of type A. Each considered test case is shown above each plot box. A damage type is identified as current when the test statistic does not exceed the critical points (dashed horizontal lines).

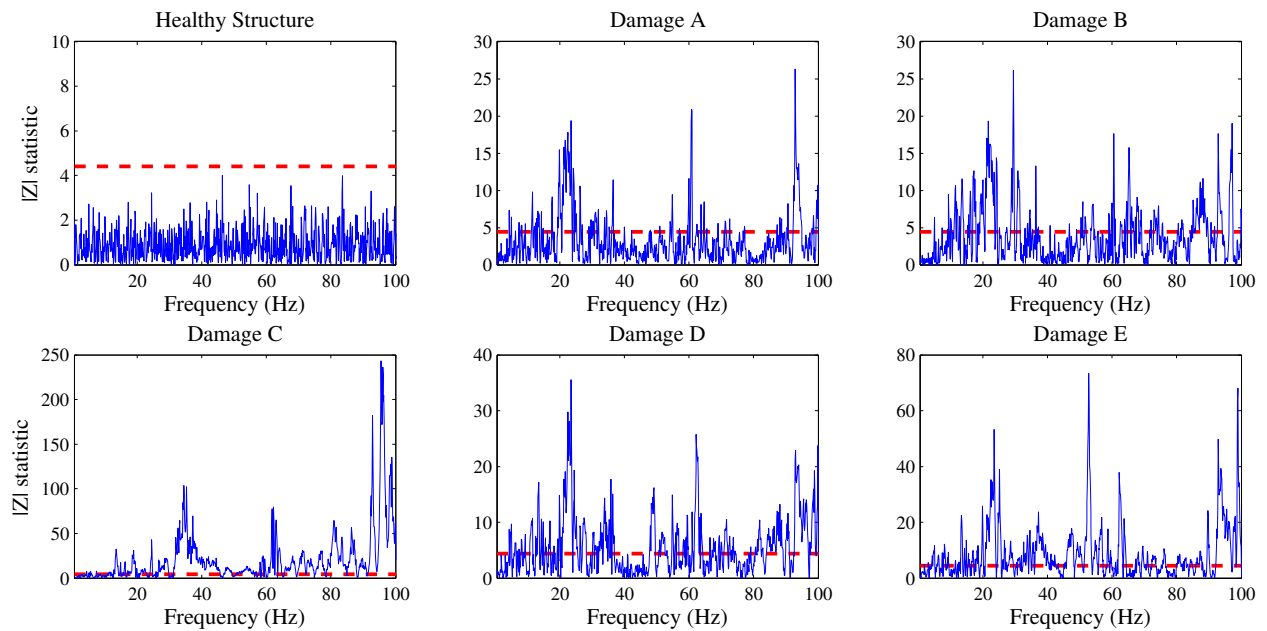


Figure 2.9: FRF magnitude based method (response Y1): Indicative damage detection results for six representative test cases (one healthy and five damaged) at the $\alpha = 10^{-5}$ risk level. The actual structural state is shown above each plot box. A damage is detected if the test statistic exceeds the critical points (dashed horizontal lines).

statistic does not exceed the critical points, while it clearly does so when testing the hypothesis of any other damage type.

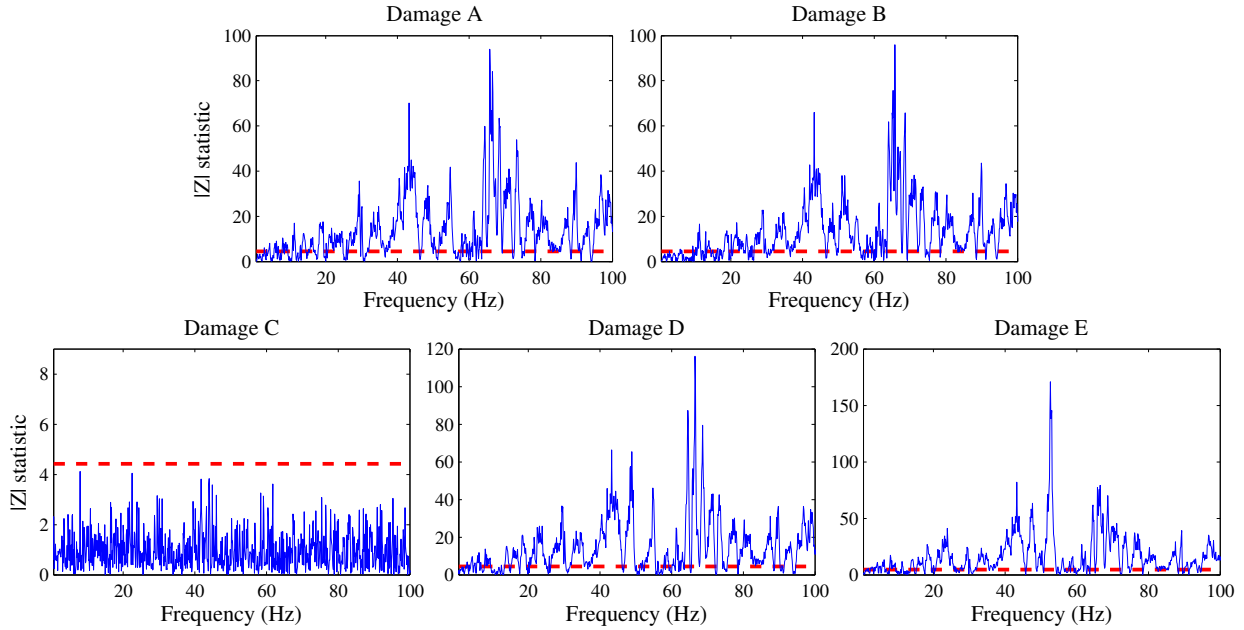


Figure 2.10: FRF magnitude based method (response Y1): Indicative damage identification results for five damage test cases at the $\alpha = 10^{-5}$ risk level, with the actual damage being of type C. Each considered test case is shown above each plot box. A damage type is identified as current when its test statistic does not exceed the critical points (dashed horizontal lines).

2.4.4.3 Model parameter based method

The model parameter based method (excitation-response case) is based on the identified ARX(103, 103) models from the baseline phase, as well as on identified ARX(103, 103) models from the current (unknown) data records Z_u (inspection phase).

Figure 2.11 depicts typical scalar model parameter estimates (a_1 and b_o) based on ARX(103, 103) models for two healthy and five damaged states of the structure. The dark lines represent the scalar parameter estimates for each test case, while the shaded boxes designate their corresponding ± 3 sample standard deviation confidence intervals. It may be observed that the parameter estimates obtained from models representing damaged structural states significantly differ from the parameter estimates obtained from healthy models. Moreover, the interval estimates obtained from the healthy models overlap, implying rather small changes.

Figures 2.12 and 2.13 present typical parametric damage detection and identification results, respectively, obtained by the model parameter based method at the $\alpha = 10^{-12}$ risk level. Evidently, correct detection (Figure 2.12) is obtained in each case, as the test statistic is shown not to exceed the critical point in the healthy case, while it exceeds it in the damaged cases; note the logarithmic scale on the vertical axis which indicates significant difference between the healthy and damaged test statistics. Moreover, Figure 2.13 demonstrates the ability of the method to accurately identify the actual damage type.

2.4.4.4 Residual based methods

Residual variance based method

This method tackles damage detection and identification based on the identified (in the baseline

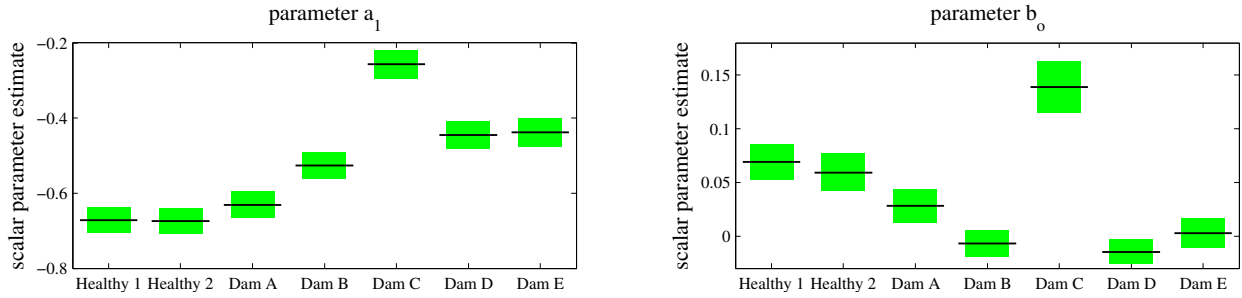


Figure 2.11: Model parameter based method (response Y1): Model parameter estimates for two healthy and five damage states (the dark lines represent point estimates and the shaded boxes ± 3 sample standard deviation confidence intervals).

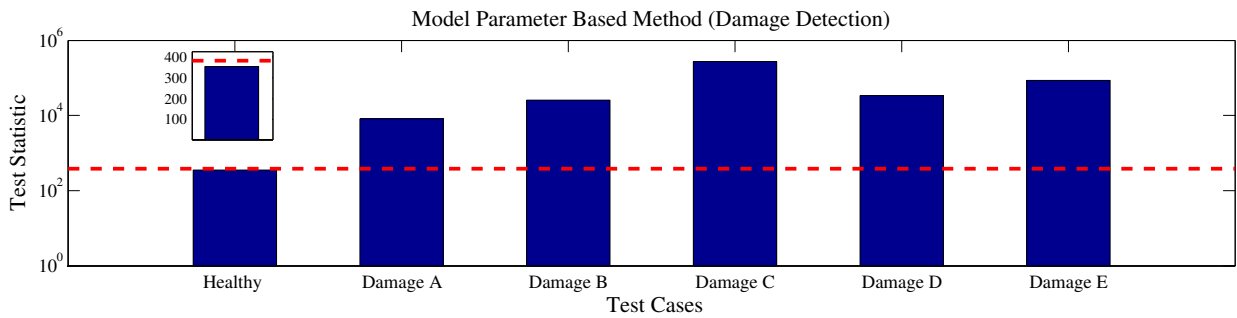


Figure 2.12: Model parameter based method (response Y1): Indicative damage detection results for six representative test cases (one healthy and five damaged) at the $\alpha = 10^{-12}$ risk level. A damage is detected if the test statistic (bar) exceeds the critical point (dashed horizontal line).

phase) ARX(103, 103) models – no model identification is involved in the inspection phase. Figure 2.14 depicts typical residual variance estimates based on ARX(103, 103) models for two healthy and five damaged states of the structure. The dark lines represent the scalar residual variance estimates for each test case, while the shaded boxes designate their corresponding ± 3 standard deviation confidence intervals. The residual variances $\hat{\sigma}_{ou}^2, \hat{\sigma}_{Au}^2, \dots, \hat{\sigma}_{Eu}^2$, corresponding to each test case, are estimated from the respective residual sequences $e_{ou}[t], e_{Au}[t], \dots, e_{Eu}[t]$ obtained by driving the current (unknown) signals Z_u through the models M_o, M_A, \dots, M_E , respectively.

As it may be observed, the residual variance interval estimates $\hat{\sigma}_{ou}^2$ obtained from the two healthy data sets are quite close and overlap. On the other hand, the variance estimates $\hat{\sigma}_{Au}^2, \dots, \hat{\sigma}_{Eu}^2$ obtained from representative damaged data sets are significantly greater than the healthy estimates (interval estimates are clearly separated). Notice that the more severe damage types (such as types C and E) yield greater residual variance estimates than the less severe ones (damage types A and B).

Typical damage detection and identification results are presented in Figures 2.15 and 2.16, respectively, at the $\alpha = 10^{-12}$ risk level. Evidently, correct detection (Figure 2.15) is obtained in each considered case, as the test statistic is shown not to exceed the critical point in the healthy case, while it exceeds it in the damaged test cases. Moreover, Figure 2.16 demonstrates the ability of the method to correctly identify the actual damage type (note the logarithmic scale on the vertical axes).

The residual variance and likelihood function based methods exhibit quite identical performance, as the data record length N is large. This is expected and rather obvious from the comparison of Equations (2.9) and (2.12). Hence, for the sake of brevity, the results for the likelihood function based method are omitted.

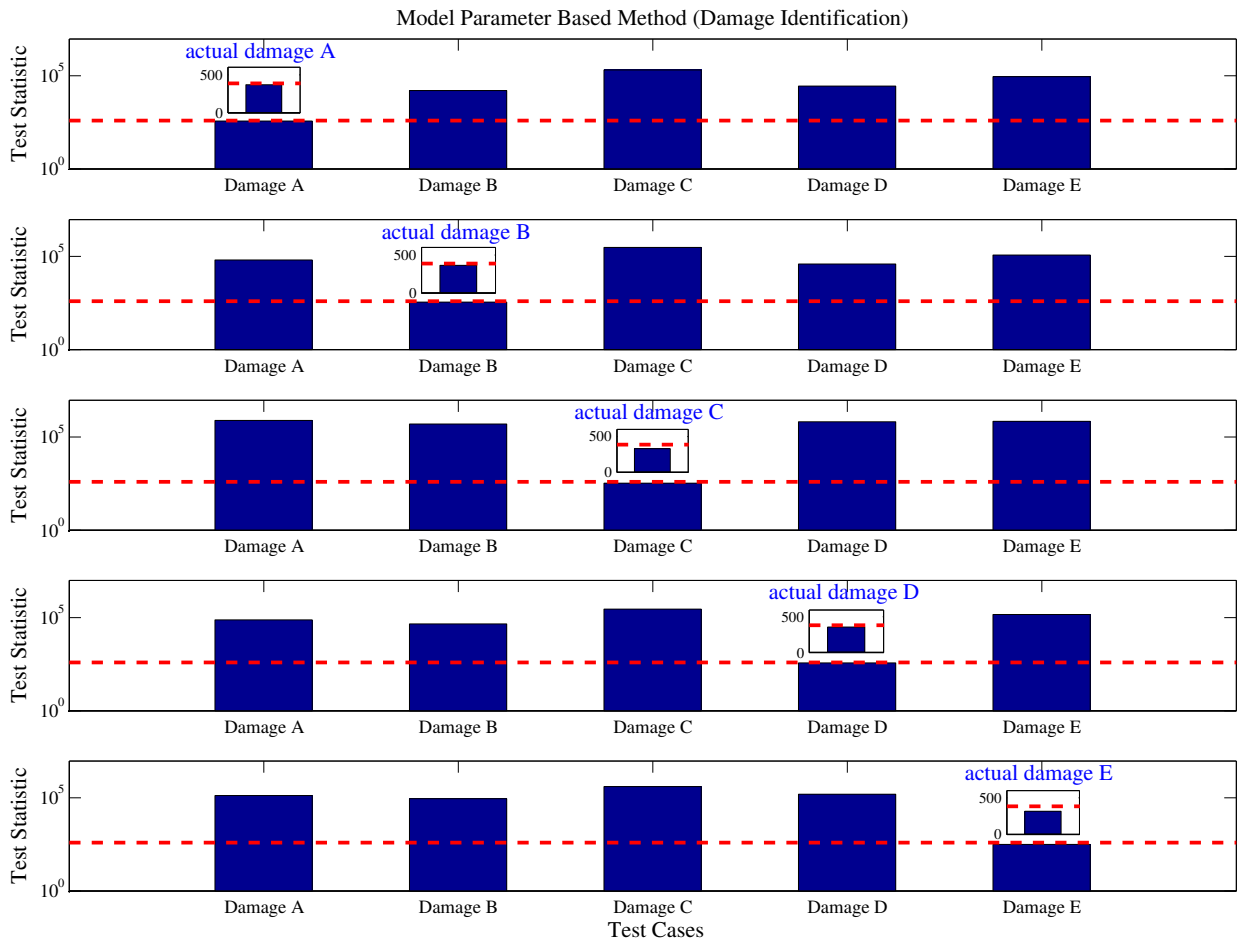


Figure 2.13: Model parameter based method (response Y1): Indicative damage identification results for five damage test cases at the $\alpha = 10^{-12}$ risk level. Each bar corresponds to each considered hypothesis test, with the actual damage indicated within each subplot. A damage type is identified as current if the test statistic (bar) does not exceed the critical point (dashed horizontal line).

Residual uncorrelatedness based method

This method tackles damage detection and identification based on the identified (in the baseline phase) ARX(138, 138) models. Figure 2.17 depicts typical residual normalized ACF estimates $\hat{\rho}[\tau]$ for the first four lags ($\tau = 1, \dots, 4$), based on ARX(138, 138) models for the healthy and five damaged structural states. The residuals for each considered state of the structure are obtained by driving the current data records Z_u through the models M_o, M_A, \dots, M_E . Under the null hypothesis of a healthy current structure, the first residual series (obtained by driving the signals through the model M_o) normalized ACF estimates should lie within the statistical insignificance zone of $\pm 1.96/\sqrt{N}$ with probability $p = 0.95$. This should not be the case for the other residual series (obtained by driving the signals through the each one of the M_A, \dots, M_E models).

Representative damage detection and identification results via the residual uncorrelatedness based method are, at the $\alpha = 10^{-12}$ risk level with $r = 25$ (see Equation 2.15), presented in Figures 2.18 and 2.19, respectively. Evidently, correct detection (Figure 2.18) is obtained in each case, as the test statistic is shown not to exceed the critical point in the healthy case, while it exceeds it in the damaged test cases. Moreover, Figure 2.19 demonstrates the ability of the method to accurately identify the actual damage type as the current one.

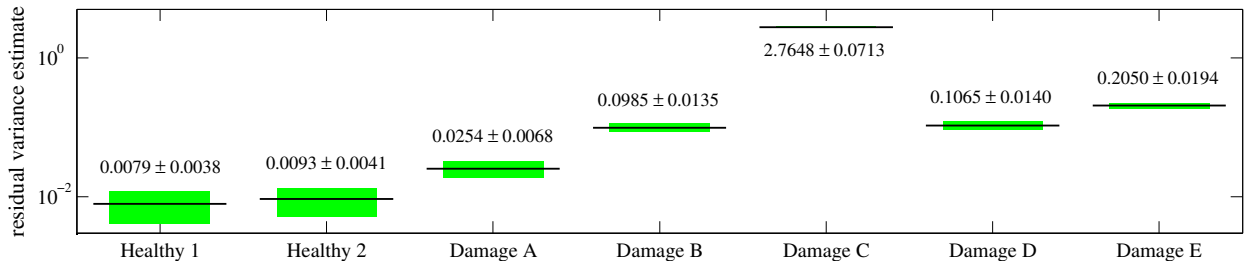


Figure 2.14: Residual variance based method (response Y1): Residual variance estimates based on ARX(103, 103) models for two healthy and five damaged states (the dark lines represent point variance estimates and the shaded boxes ± 3 sample standard deviation confidence intervals).

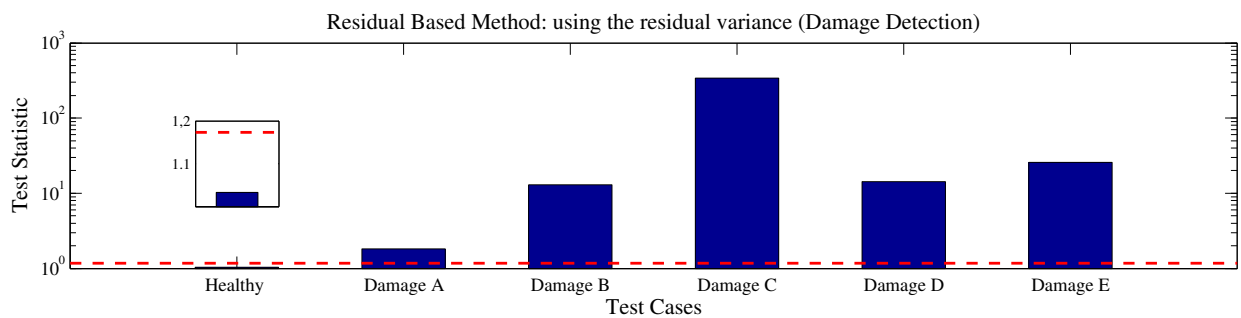


Figure 2.15: Residual variance based method (response Y1): Indicative damage detection results for six representative test cases (one healthy and five damaged) at the $\alpha = 10^{-12}$ risk level. A damage is detected if the test statistic (bar) exceeds the critical point (dashed horizontal line).

2.4.5 Summary results and discussion (all measurement positions)

Summary results for all test cases, which include all three measurement positions (Y1, Y2 and Y3), are presented in Table 2.7. Both non-parametric and parametric methods achieve accurate damage detection with almost always zero false alarms. In fact only the FRF based method exhibits one and two false alarms for vibration measurement positions Y1 and Y3, respectively. Moreover, the ability of the methods to effectively detect damage is demonstrated by the fact that no missed damage cases are observed. The damage identification results demonstrate the ability of the methods to accurately identify the actual damage type. No damage misclassification cases are observed, except for the FRF based method where misclassification errors occur for damage type A (Table 2.7).

It is also important to note that the methods are capable of detecting and identifying damage using a single response signal. This is true for the cases where the damage location is relatively close to the response sensor, but also to the cases where the damage location is far from that. Performance is of course, and expectedly, affected by this distance, and this is also shown in the damage type A case where the lowest misclassification rate occurs for sensor Y2 (Table 2.7) which is closest to the damage location.

Overall, both non-parametric and parametric statistical time series methods demonstrate high potential for effective damage detection and identification based even on a single vibration response signal. Between the two non-parametric methods, the FRF based one appears to achieve better damage detection and identification. Among the parametric methods, the residual based methods appear to achieve clearer damage detection and identification than the parameter based method.

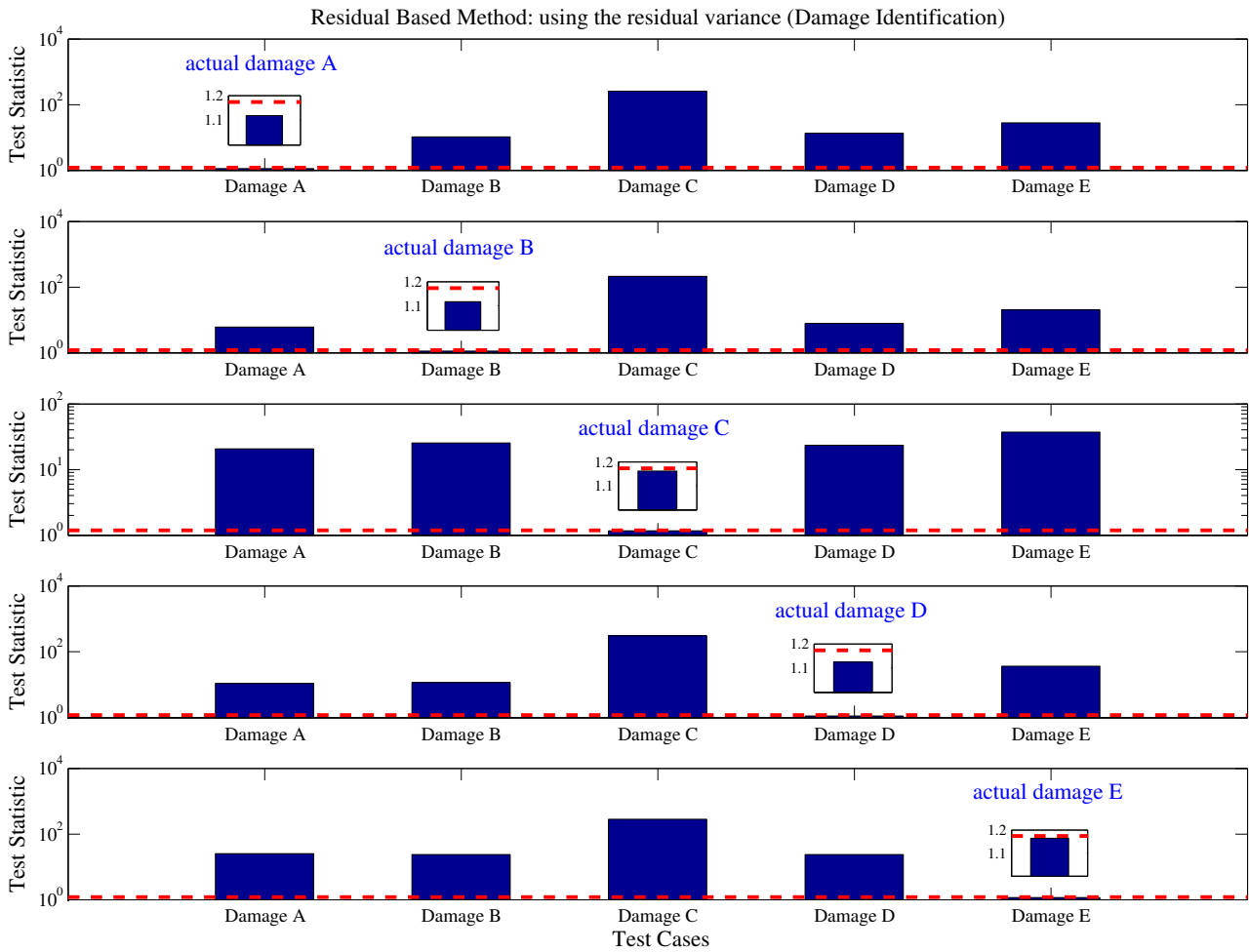


Figure 2.16: Residual variance based method (response Y1): Indicative damage identification results for five damage test cases at the $\alpha = 10^{-12}$ risk level. Each bar corresponds to each considered hypothesis test, with the actual damage indicated within each subplot. A damage type is identified as current if the test statistic (bar) does not exceed the critical point (dashed horizontal line).

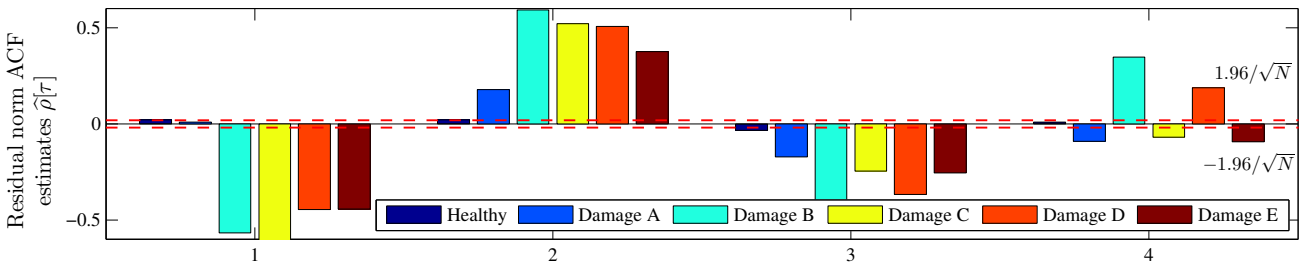


Figure 2.17: Residual uncorrelatedness based method (response Y1): Normalized residual ACF estimates $\hat{\rho}[\tau]$ based on ARX(138, 138) models for one healthy and five damaged states. The dashed horizontal lines designate the limits within which the ACF can be accepted as being zero at the $\alpha = 0.05$ risk level.

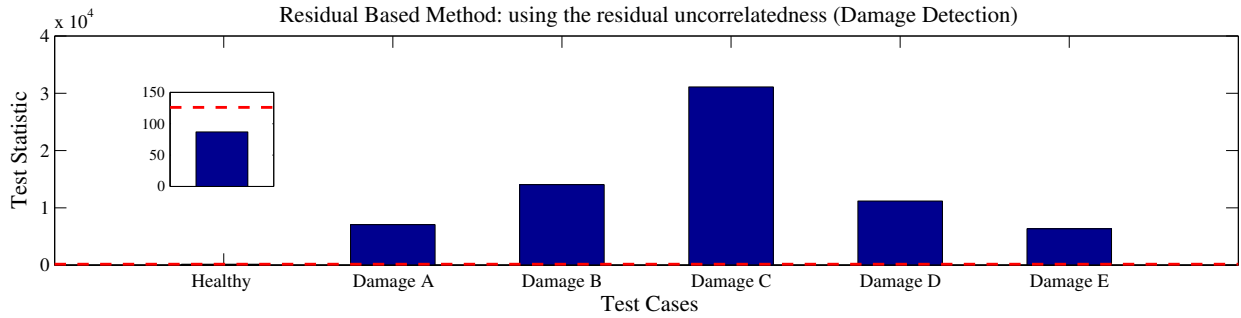


Figure 2.18: Residual uncorrelatedness based method (response Y1): Indicative damage detection results for six representative test cases (one healthy and five damaged) at the $\alpha = 10^{-12}$ risk level (max lag $r = 25$). A damage is detected if the test statistic (bar) exceeds the critical point (dashed horizontal line).

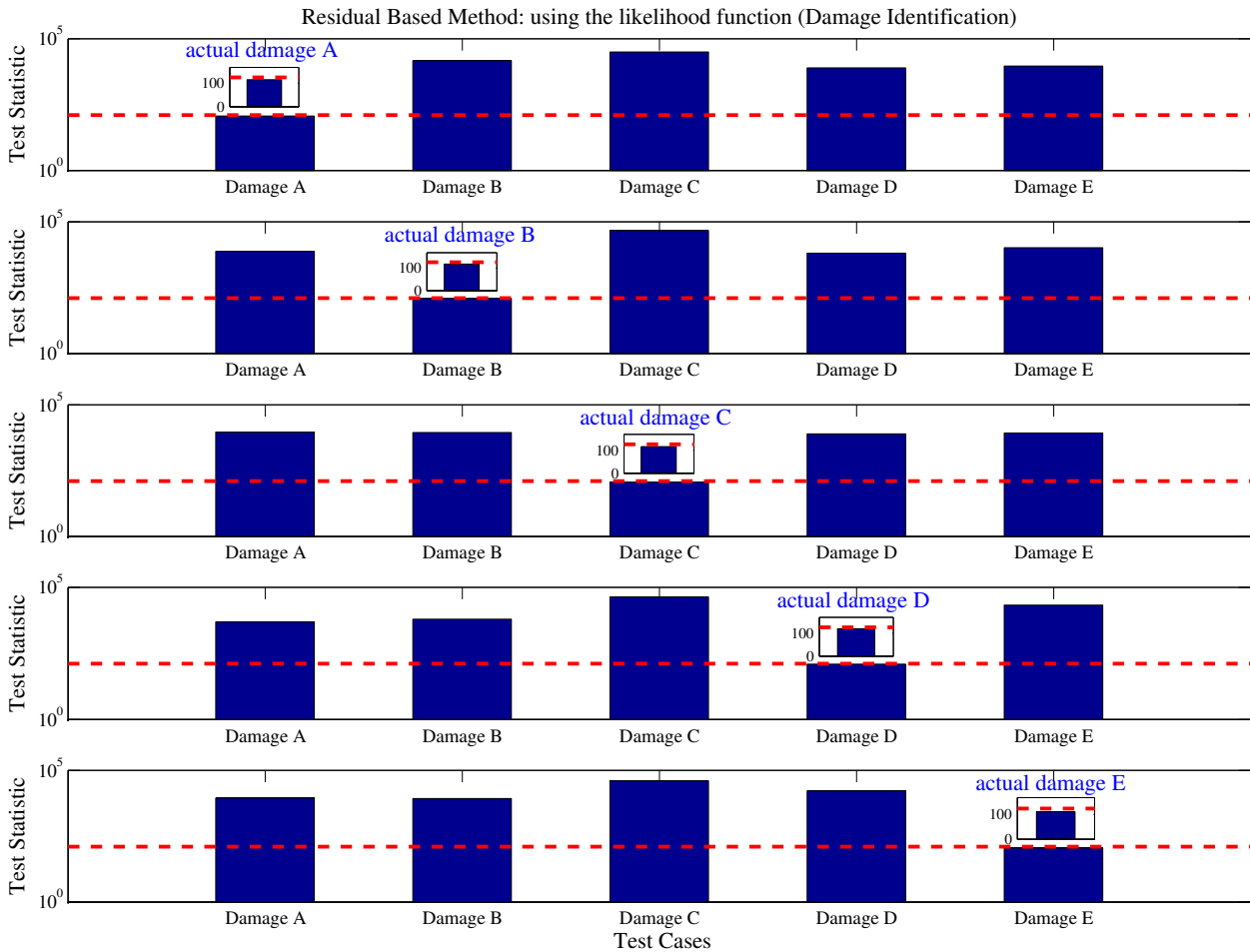


Figure 2.19: Residual uncorrelatedness based method (response Y1): Indicative damage identification results for five damage test cases at the $\alpha = 10^{-12}$ risk level (max lag $r = 25$). Each bar corresponds to each considered hypothesis test, with the actual damage indicated within each subplot. A damage type is identified as current if the test statistic (bar) does not exceed the critical point (dashed horizontal line).

Method	Damage Detection					
	False alarms	Missed damage				
		damage A	damage B	damage C	damage D	damage E
PSD based	0/0/0	0/0/0	0/0/0	0/0/0	0/0/0	0/0/0
FRF based	1/0/2	0/0/0	0/0/0	0/0/0	0/0/0	0/0/0
Mod. parameter [†]	0/0/0	0/0/0	0/0/0	0/0/0	0/0/0	0/0/0
Res. variance [†]	0/0/0	0/0/0	0/0/0	0/0/0	0/0/0	0/0/0
Res. likelihood [†]	0/0/0	0/0/0	0/0/0	0/0/0	0/0/0	0/0/0
Res. uncorrelatedness [†]	0/0/0	0/0/0	0/0/0	0/0/0	0/0/0	0/0/0

False alarms for points Y1/Y2/Y3 out of 39 test cases each.

Missed damages for points Y1/Y2/Y3 out of 31 test cases each; [†]adjusted α .

Method	Damage Identification				
	Damage misclassification				
	damage A	damage B	damage C	damage D	damage E
PSD based	0/0/0	0/0/0	0/0/0	0/0/0	0/0/0
FRF based	2/1/2	0/0/0	0/0/0	0/0/0	0/0/0
Mod. parameter [†]	0/0/0	0/0/0	0/0/0	0/0/0	0/0/0
Res. variance [†]	0/0/0	0/0/0	0/0/0	0/0/0	0/0/0
Res. likelihood [†]	0/0/0	0/0/0	0/0/0	0/0/0	0/0/0
Res. uncorrelatedness [†]	0/0/0	0/0/0	0/0/0	0/0/0	0/0/0

Damage misclassification for points Y1/Y2/Y3 out of 31 test cases each; [†]adjusted α .

Table 2.7: Damage detection and identification summary results for three responses (Y1, Y2 and Y3).

Nevertheless, a number of issues require some attention on part of the user. First, careful model identification – especially in the parametric case – is crucial for successful damage diagnosis. Parametric models require accurate parameter estimation and appropriate model structure (order) selection in order to properly represent the structural dynamics and be effectively used for damage detection and identification. Therefore, parametric methods require adequate user expertise and are somewhat more elaborate than their non-parametric counterparts. In particular, extra attention should be paid to successful model identification in conjunction with the model residual uncorrelatedness method, as the corresponding model residuals should be as close to whiteness as possible in order for the method to work effectively.

Another issue of primary importance is the proper selection of the risk level α (type I error), for reasons associated with the methods' robustness and effectiveness. If this is not properly adjusted, damage diagnosis will be ineffective, as false alarm, missed damage, and damage misclassification cases may occur. The user is advised to make an initial investigation of the false alarm rates for different α levels using several healthy data sets. Afterwards, potential missed damage cases may be checked with data corresponding to various damaged structural states. When applying the model residual uncorrelatedness based method, the user should be aware of the fact that the max lag r value may also affect performance. Thus, a tentative inquiry on the way max lag r value affects false alarm occurrence should be undertaken. Depending on the exact type and order of the parametric model used, max lag r values may range from a few to $N/4$ (N is the residual signal length in samples).

Moreover, in order for most parametric methods to work effectively, a very small value of type I risk level α is often needed. This is due to the fact that the current parametric time series models (ARMA, ARX, state space and so on) used for modeling the structural dynamics are incapable of fully capturing the experimental, operational and environmental uncertainties that the structure is subjected to – in this context see references Hios and Fassois (2009b) and Michaelides and Fassois (2008). For this reason, a very small α is often selected in order to compensate for the lack of effective

uncertainty modeling. This subject, along with more accurate modeling of uncertainties, is important for current and future research.

The selection of the number and position of measurement sensors is another important issue. Several vibration based damage diagnosis techniques that appear to work well in test cases may perform poorly when subjected to the measurement constraints imposed by actual testing (Doebbling *et al.* 1996, Doebbling *et al.* 1998). Techniques that are to be seriously considered for implementation in the field should demonstrate that they can perform well under limitations of a small number of measurement positions and under the constraint that these positions should be selected a priori, without a priori knowledge of the damage location. As already demonstrated, statistical time series methods are capable of treating damage diagnosis based on limited or even on a single pair of excitation-response measurements and may also achieve a certain level of automation, although their performance on large scale structures needs to be further investigated.

Finally, in the case of multiple damage scenarios, or even single damage cases not considered in the baseline (training) phase, statistical time series methods are capable of effectively treating the damage detection subproblem. The damage identification (classification) subproblem is clearly more difficult, and requires the use of advanced methods, such as those more recently developed by the author and co-workers (Sakellariou and Fassois 2008, Kopsaftopoulos and Fassois 2007). Work on these methods is still on-going, and experimental comparisons along with full assessments are to be made.

2.5 Application on a scale aircraft skeleton structure

The goal of the present section is the comparative assessment of several *scalar* (univariate) and *vector* (multivariate) methods for SHM via their application on an aircraft scale skeleton structure in which different damage scenarios correspond to the loosening of different bolts. The methods are further classified as non-parametric or parametric and response-only or excitation-response. Preliminary results by various methods may be found in the recent papers of Kopsaftopoulos *et al.* (2010) and Kopsaftopoulos and Fassois (2011*d*). It should be noted that the structure has been used in the past for the development of novel scalar (univariate) methods for precise damage localization and magnitude (size) estimation using different (simulated) damages consisting of small masses attached to the structure (Sakellariou and Fassois 2008, Kopsaftopoulos and Fassois 2007). Due to their ability to address the precise localization and magnitude estimation problems, these methods are generally more complex. As the focus of the present study is more on damage detection and identification (the latter in the sense of estimating the damage scenario from a given pool of potential scenarios), only simpler methods are utilized.

More specifically, four scalar methods, namely a Power Spectral Density (PSD), a Frequency Response Function (FRF), a model residual variance, and a Sequential Probability Ratio Test (SPRT) based method are employed, along with two vector methods, namely a model parameter based and a residual likelihood function based method.

2.5.1 The scale aircraft skeleton structure

The scale aircraft skeleton structure used in the experiments was designed by ONERA (France) in conjunction with the Structures and Materials Action Group SM-AG19 of the Group for Aeronautical Research and Technology in Europe (GARTEUR) (Degener and Hermes 1996, Balmes and Wright 1997) and manufactured at the University of Patras (Figure 2.20). It represents a typical aircraft skeleton design and consists of six solid beams with rectangular cross sections representing the fuselage ($1500 \times 150 \times 50$ mm), the wing ($2000 \times 100 \times 10$ mm), the horizontal ($300 \times 100 \times 10$ mm) and vertical stabilizers ($400 \times 100 \times 10$ mm), and the right and left wing-tips ($400 \times 100 \times 10$ mm). All parts are constructed from standard aluminum and are jointed together via steel plates and bolts. The total mass of the structure is approximately 50 kg.

2.5.2 The damage scenarios and the experiments

Damage detection and identification is based on vibration testing of the structure, which is suspended through a set of bungee cords and hooks from a long rigid beam sustained by two heavy-type stands (Figure 2.20). The suspension is designed in a way as to exhibit a pendulum rigid body mode below the frequency range of interest, as the boundary conditions are free-free.

The excitation is broadband random stationary Gaussian force applied vertically at the right wing-tip (Point X, Figure 2.20) through an electromechanical shaker (MB Dynamics Modal 50A, max load 225 N). The actual force exerted on the structure is measured via an impedance head (PCB M288D01, sensitivity 98.41 mV/lb), while the resulting vertical acceleration responses at Points Y1, Y2, Y3 and Y4 (Figure 2.20) are measured via lightweight accelerometers (PCB 352A10 miniature ICP accelerometers, 0.7 g, frequency range 0.003 – 10 kHz, sensitivity ~ 1.052 mV/m/s²). The force and acceleration signals are driven through a conditioning charge amplifier (PCB 481A02) into the data acquisition system based on two SigLab 20-42 measurement modules (each module featuring four 20-bit simultaneously sampled A/D channels, two 16-bit D/A channels, and analog anti-aliasing

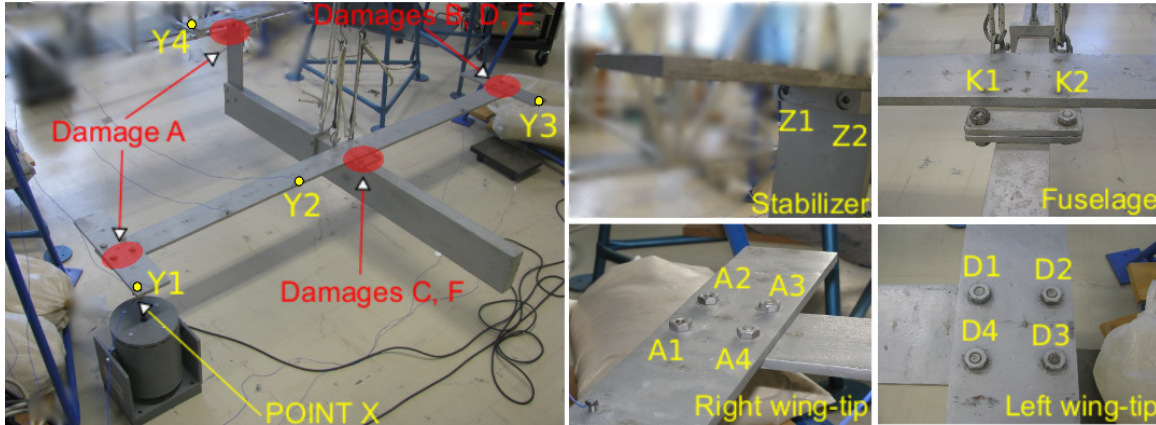


Figure 2.20: The scale aircraft skeleton structure and the experimental set-up: The force excitation (Point X), the vibration measurement locations (Points Y1 – Y4), and the bolts connecting the various elements of the structure.

filters).

The damage scenarios considered correspond to the loosening of various bolts at different joints of the structure (Figure 2.20). Six distinct scenarios (types) are considered and summarized in Table 2.5.2. The assessment of the presented statistical time series methods with respect to the damage detection and identification subproblems is based on 60 experiments for the healthy and 40 experiments for each considered damage state of the structure (damage types A, B, . . . , F – see Table 2.5.2) – each experiment corresponding to a single test case. Moreover, *four* vibration measurement locations (Figure 2.20, Points Y1 – Y4) are employed in order to determine the ability of the considered methods in treating damage diagnosis using single or multiple vibration response signals. The frequency range of interest is selected as 4 – 200 Hz, with the lower limit set in order to avoid instrument dynamics and rigid body modes. Each signal is digitized at $f_s = 512$ Hz and is subsequently sample mean corrected and normalized by its sample standard deviation (Table 2.5.2).

A single healthy data set is used for establishing the baseline (reference) set, while 60 healthy and 240 damage sets (six damage types with 40 experiments each) are used as inspection data sets. For damage identification, a single data set for each damage structural state (damage types A, B, . . . , F) is used for establishing the baseline (reference) set, while the same 240 sets are considered as inspection data sets (each corresponding to a test case in which the actual structural state is considered

Structural state	Description	No of inspection experiments (test cases)
Healthy	—	60
Damage A	loosening of bolts A1, A4, Z1, Z2	40
Damage B	loosening of bolts D1, D2, D3	40
Damage C	loosening of bolts K1	40
Damage D	loosening of bolts D2, D3	40
Damage E	loosening of bolts D3	40
Damage F	loosening of bolts K1, K2	40
Sampling frequency: $f_s = 512$ Hz, Signal bandwidth: 4 – 200 Hz		
Signal length in samples (s):		
Non-parametric methods: $N = 46\ 080$ (90 s); Parametric methods: $N = 15\ 000$ (29 s)		

Table 2.8: The damage scenarios and experimental details.

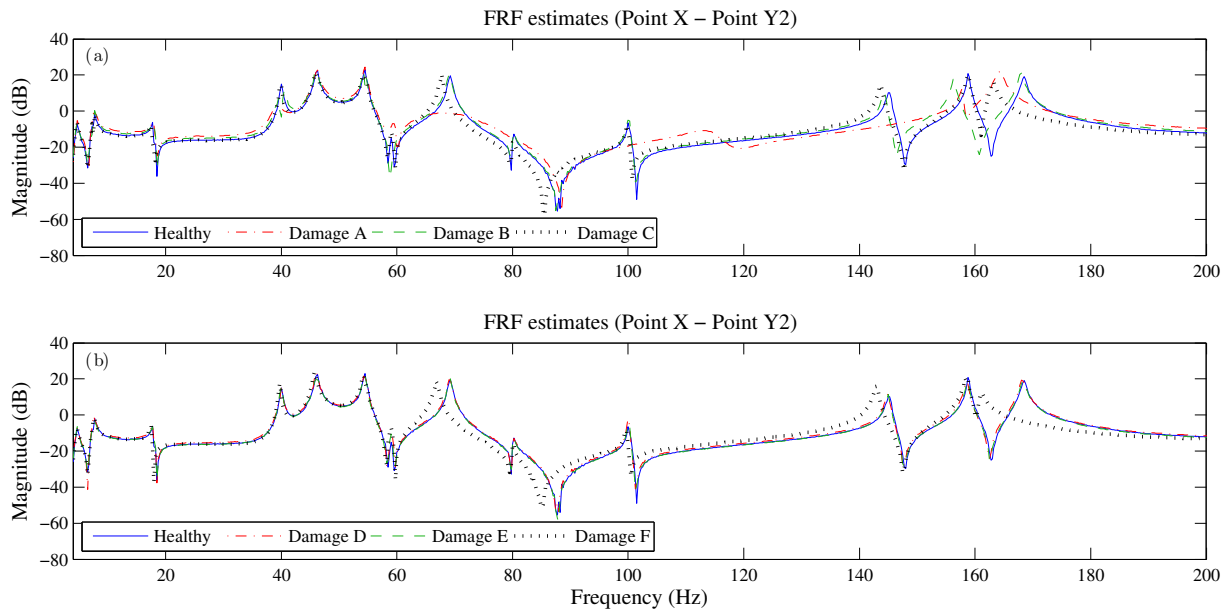


Figure 2.21: Non-parametric Welch-based Frequency Response Function (FRF) magnitude estimates for the healthy and damaged structural states (Point X – Point Y2 transfer function).

unknown). The time series models are estimated and the corresponding estimates of the characteristic quantity Q are extracted ($\hat{Q}_A, \hat{Q}_B, \dots, \hat{Q}_F$ in the baseline phase; \hat{Q}_u in the inspection phase). Damage identification is presently based on successive binary hypothesis tests – as opposed to multiple hypothesis tests – and should be thus considered as preliminary (Fassois and Sakellariou 2009).

2.5.3 Structural dynamics of the healthy structure

2.5.3.1 Non-parametric identification

Non-parametric identification of the structural dynamics is based on $N = 46\,080$ (≈ 90 s) sample-long excitation-response signals obtained from *four* vibration measurement locations on the structure (see Figure 2.20). An $L = 2\,048$ sample-long Hamming data window with zero overlap is used (number of segments $K = 22$) for PSD (MATLAB function *pwelch.m*) and FRF (MATLAB function *tfestimate.m*) Welch based estimation (see Table 2.9).

The obtained FRF magnitude estimates for the healthy and damage states of the structure for the Point X – Point Y2 transfer function are depicted in Figure 2.21. As it may be observed the FRF magnitude curves are quite similar in the 4 – 60 Hz range; notice that this range includes the first five modes of the structure. Significant differences between the healthy and damage type A, C

Data length	$N = 46\,080$ samples (≈ 90 s)
Method	Welch
Segment length	$L = 2\,048$ samples
Non-overlapping segments	$K = 22$ segments
Window type	Hamming
Frequency resolution	$\Delta f = 0.355$ Hz

Table 2.9: Non-parametric estimation details.

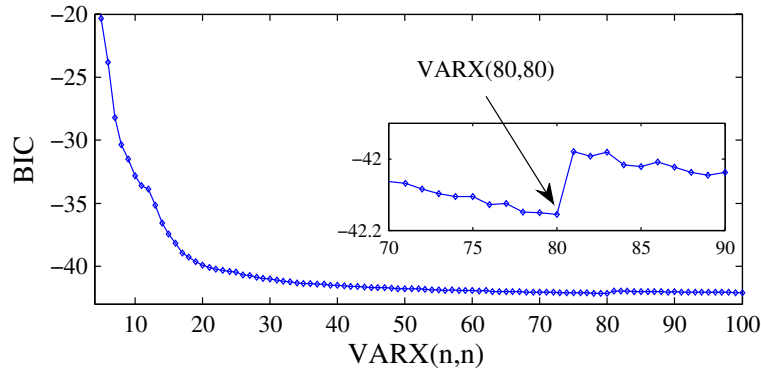


Figure 2.22: Bayesian Information Criterion (BIC) for $\text{VARX}(n,n)$ type parametric models in the healthy case.

and F magnitude curves are observed in the range of 60 – 150 Hz, where the next four modes are included. Finally, in the range of 150 – 200 Hz another two modes are present, and discrepancies are more evident for damage types A, B, C and F. Notice that the FRF magnitude curves for damage types D and E are very similar to those of the healthy structure.

2.5.3.2 Parametric identification

Parametric identification of the structural dynamics is based on $N = 15\,000$ (≈ 29 s) sample-long excitation and vibration response signals used in the estimation of Vector AutoRegressive with exogenous excitation (VARX) models (MATLAB function *arx.m*). The modeling strategy consists of the successive fitting of $\text{VARX}(na, nb)$ models (with na, nb designating the AR and X orders, respectively; $na = nb = n$ is currently used) until a candidate model is selected. Model parameter estimation is achieved by minimizing a quadratic Prediction Error (PE) criterion (trace of residual covariance matrix) leading to a Least Squares (LS) estimator (Fassois 2001), (Ljung 1999, p. 206). Model order selection, which is crucial for successful identification, may be based on a combination of tools, including the Bayesian Information Criterion (BIC) (Figure 2.22), which is a statistical criterion that penalizes model complexity (order) as a counteraction to a decreasing model fit criterion (Fassois 2001), (Ljung 1999, pp. 505–507) and the use of “stabilization diagrams” which depict the estimated modal parameters (usually frequencies) as a function of increasing model order (Fassois 2001). BIC minimization is achieved for model order $n = 80$ (Figure 2.22), thus a 4–variate $\text{VARX}(80, 80)$ model is selected as adequate for the residual variance, model parameter, and likelihood function based methods. The identified $\text{VARX}(80, 80)$ representation has $d = 1\,604$ parameters, yielding a Sample Per Parameter (SPP) ratio equal to 37.4 ($N \times (\text{no of outputs})/d$).

It should be noted that the complete 4–variate $\text{VARX}(80, 80)$ model is employed in conjunction with vector methods in Section 2.5.5. Yet, scalar parts of this model corresponding to excitation – single response are used in conjunction with scalar methods in Section 2.5.4. This is presently done for purposes of simplicity and it is facilitated by the fact that only a single (scalar) excitation is present.

Method	Principle	Test Statistic	Type
PSD based	$S_u(\omega) \stackrel{?}{=} S_o(\omega)$	$F = \widehat{S}_o(\omega)/\widehat{S}_u(\omega) \sim F(2K, 2K)$	<i>scalar</i>
FRF based	$\delta H(j\omega) = H_o(j\omega) - H_u(j\omega) \stackrel{?}{=} 0$	$Z = \delta \widehat{H}(j\omega) / \sqrt{2\widehat{\sigma}_H^2(\omega)} \sim N(0, 1)$	<i>scalar</i>
Residual variance	$\sigma_{ou}^2 \stackrel{?}{\leq} \sigma_{oo}^2$	$F = \widehat{\sigma}_{ou}^2/\widehat{\sigma}_{oo}^2 \sim F(N, N - d)$	<i>scalar</i>
SPRT based	$\sigma_{ou} \stackrel{?}{\leq} \sigma_o$ or $\sigma_{ou} \stackrel{?}{\geq} \sigma_1$	$\mathcal{L}(n) = n \cdot \log \frac{\sigma_o}{\sigma_1} + \frac{\sigma_1^2 - \sigma_o^2}{2\sigma_o^2\sigma_1^2} \cdot \sum_{t=1}^n e^2[t]$	<i>scalar</i>
Model parameter	$\delta\boldsymbol{\theta} = \boldsymbol{\theta}_o - \boldsymbol{\theta}_u \stackrel{?}{=} \mathbf{0}$	$\chi_\theta^2 = \delta\widehat{\boldsymbol{\theta}}^T (2\widehat{\mathbf{P}}_\theta)^{-1} \delta\widehat{\boldsymbol{\theta}} \sim \chi^2(d)$	<i>vector</i>
Residual likelihood	$\boldsymbol{\theta}_o \stackrel{?}{=} \boldsymbol{\theta}_u$	$\sum_{t=1}^N (\mathbf{e}_{ou}^T[t, \boldsymbol{\theta}_o] \cdot \boldsymbol{\Sigma}_o \cdot \mathbf{e}_{ou}[t, \boldsymbol{\theta}_o]) \leq l$	<i>vector</i>

Explanation of Symbols:

$S(\omega)$: Power Spectral Density (PSD) function; $|H(j\omega)|$: Frequency Response Function (FRF) magnitude

$\sigma_H^2(\omega) = \text{var} [|\widehat{H}_o(j\omega)|]$; $\boldsymbol{\theta}$: model parameter vector; d : parameter vector dimensionality; \mathbf{P}_θ : covariance of $\boldsymbol{\theta}$

σ_{oo}^2 : variance of residual signal obtained by driving the healthy structure signals through the healthy model

σ_{ou}^2 : variance of residual signal obtained by driving the current structure signals through the healthy model

$\mathbf{e}_{ou}[t, \boldsymbol{\theta}_o]$: vector residual sequence obtained by driving the current structure signals through the healthy model

σ_o, σ_1 : user defined values for the residual standard deviation under healthy and damage states, respectively

\mathbf{e} : k -variate residual sequence; $\boldsymbol{\Sigma}$: residual covariance matrix; l : user defined threshold

The subscripts “o” and “u” designate the healthy and current (unknown) structural states, respectively.

Table 2.10: Characteristics of the employed statistical time series methods for SHM

2.5.4 Application of scalar time series methods

Scalar statistical time series methods for SHM employ *scalar* (univariate) models and corresponding statistics. In this section two non-parametric scalar methods, namely a Power Spectral Density (PSD) based method and a Frequency Response Function (FRF) based method, and two parametric scalar methods, namely a residual variance based method and a Sequential Probability Ratio Test (SPRT) based method, are applied to the scale aircraft skeleton structure. The methods’ main characteristics are summarized in Table 2.10.

2.5.4.1 The Power Spectral Density (PSD) based method

Typical non-parametric damage detection results using the vibration measurement location of Point Y1 are presented in Figure 2.23. Evidently, correct detection at the $\alpha = 10^{-4}$ risk level is obtained in each case, as the test statistic is shown not to exceed the critical point (dashed horizontal lines) in the healthy test case, while it exceeds it in each damage test case. Observe that damage types A, B and C (see Figure 2.20 and Table 2.5.2) are more easily detectable (note the logarithmic scale on the vertical axis of Figure 2.23), while damage types D and E are harder to detect. This is in agreement with the remarks made in subsection 2.5.3.1. Furthermore, notice that the frequency bandwidth of [150 – 170] Hz is more sensitive to damage. This is also in agreement with the remarks made in subsection 2.5.3.1 and seems to be due to the fact that the two natural frequencies in this bandwidth are more sensitive to the considered damage scenarios (see Figure 2.21). Representative damage identification results at the $\alpha = 10^{-4}$ risk level and using (as an example) the vibration measurement location at Point Y3 are presented in Figure 2.24, with the actual damage being of type A. The test statistic does not exceed the critical point when the Damage A hypothesis is considered, while it exceeds it in all remaining cases. This correctly identifies damage type A as the current underlying damage.

Summary damage detection and identification results for each vibration measurement location (Figure 2.20) are presented in Table 2.11. The PSD based method achieves accurate damage detection as no false alarms are exhibited, while the number of missed damage cases is zero for all considered damaged structural states. The method is also capable of identifying the actual damage type, as zero

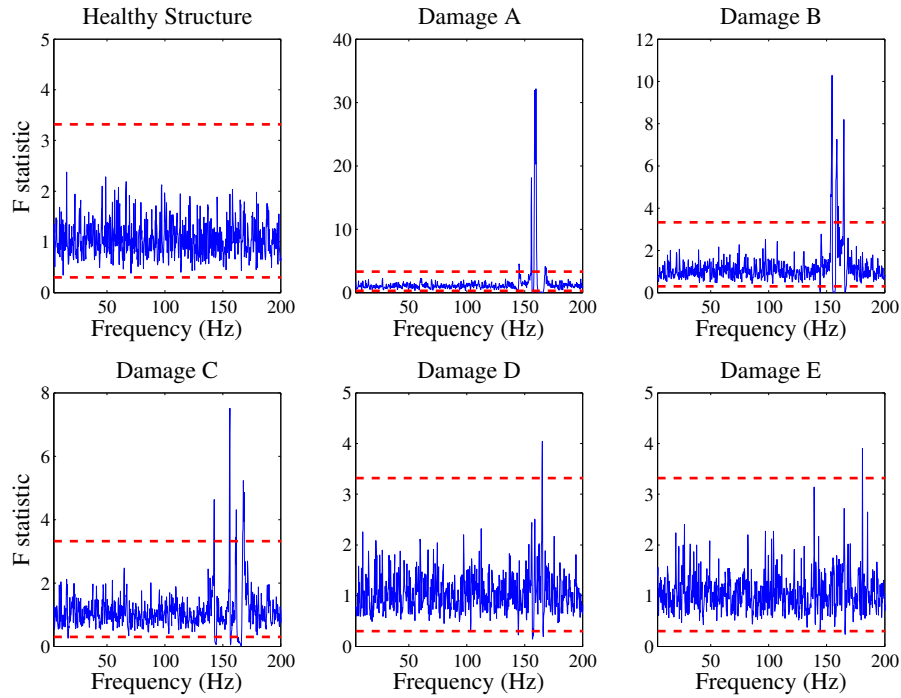


Figure 2.23: PSD based method: Representative damage detection results (sensor Y1) at the $\alpha = 10^{-4}$ risk level. The actual structural state is shown above each plot.

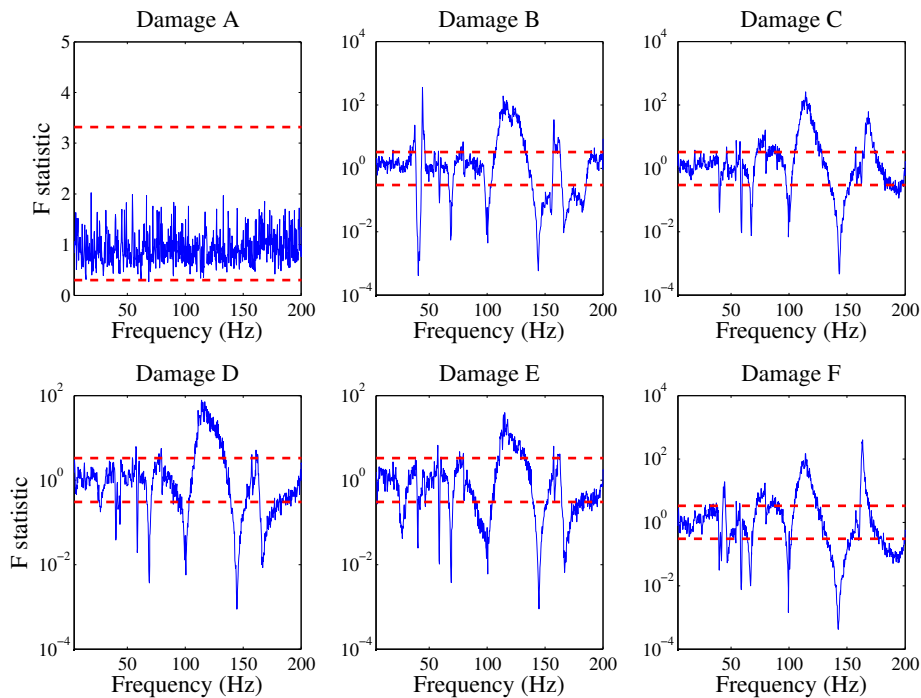


Figure 2.24: PSD based method: Representative damage identification results (sensor Y3) at the $\alpha = 10^{-4}$ risk level, with the actual damage being of type A. Each considered damage hypothesis is shown above each plot.

damage misclassification errors are reported for damage types A, C, D and F, while it exhibits some misclassification errors for damage type E. The misclassification problem is more intense for damage type B when either the Y3 or the Y4 vibration measurement location is used (Table 2.11).

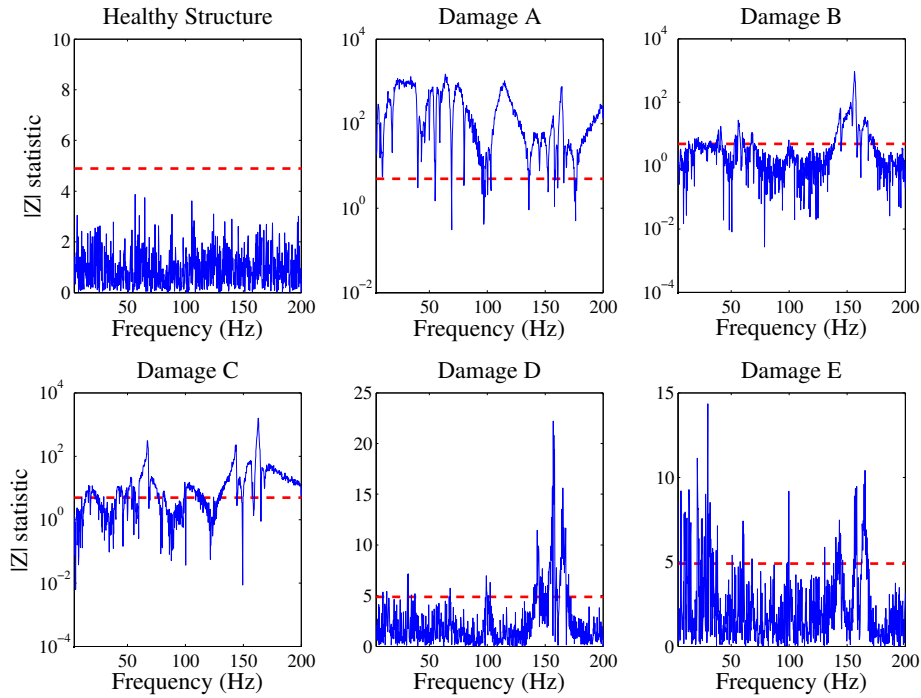


Figure 2.25: FRF based method: Representative damage detection results (sensor Y4) at the $\alpha = 10^{-6}$ risk level. The actual structural state is shown above each plot.

2.5.4.2 The Frequency Response Function (FRF) based method

Figure 2.25 presents typical non-parametric damage detection results via the FRF based method using the vibration measurement location of Point Y4. Evidently, correct detection at the $\alpha = 10^{-6}$ risk level is achieved in each case, as the test statistic is shown not to exceed the critical points (dashed horizontal lines) in the healthy case, while it exceeds them in all damage cases. Again, damage types A, B and C are more easily detectable (hence more severe), while damage types D and E are harder to detect. Representative damage identification results at the $\alpha = 10^{-6}$ risk level using (as an example) the vibration measurement location of Point Y2 are presented in Figure 2.26, with the actual damage being of type E. The test statistic does not exceed the critical point when the Damage E hypothesis is considered, while it exceeds it in all other cases. This correctly identifies damage type E as the current underlying damage.

Summary damage detection and identification results for each vibration measurement location (Figure 2.20) are presented in Table 2.11. The FRF based method achieves effective damage detection as no false alarms or missed damages are reported (Table 2.11). The method on the other hand, exhibits decreased accuracy in damage identification as significant numbers of damage misclassification errors are reported for damage types B and D (Table 2.11).

2.5.4.3 The residual variance based method

The residual variance based method employs an excitation – single response submodel obtained from the complete 4–variate VARX(80, 80) models identified in the baseline phase, as well as on a corresponding residual series obtained by driving the current (structure in unknown state) excitation and single response signals through the same submodel (inspection phase). Damage detection and identification is achieved via statistical comparison of the two residual variances. Representative damage

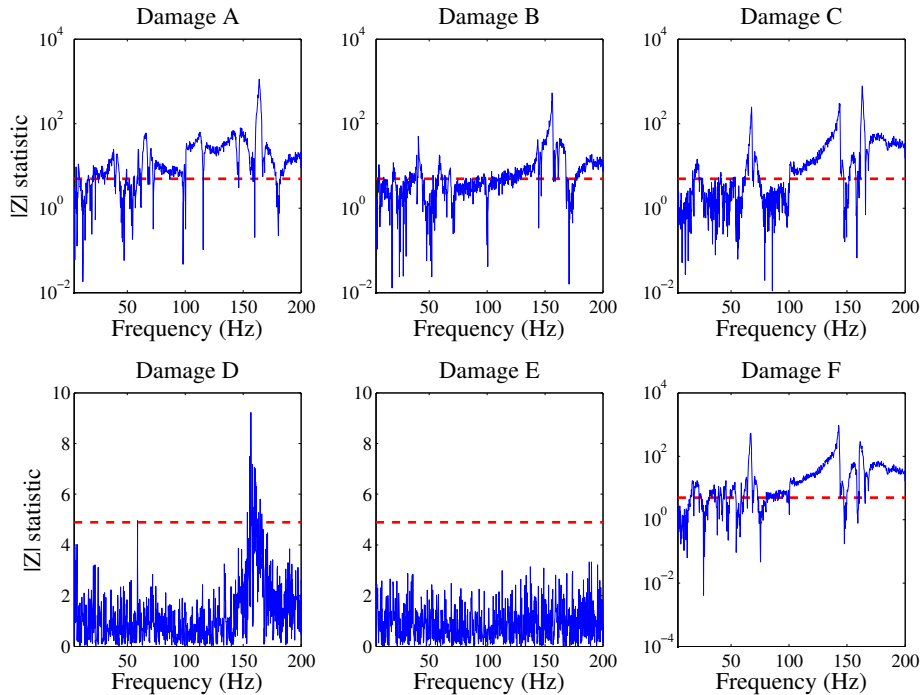


Figure 2.26: FRF based method: Representative damage identification results (sensor Y2) at the $\alpha = 10^{-6}$ risk level, with the actual damage being of type E. Each considered damage hypothesis is shown above each plot.

detection and identification results obtained via the residual variance based method (when the vibration measurement location of Point Y2 is used) are presented in Figures 2.27 and 2.28, respectively. Evidently, correct detection (Figure 2.27) is obtained in each considered case, as the test statistic is shown not to exceed the critical point in the healthy case, while it exceeds it in each damage test case. Moreover, Figure 2.28 demonstrates the ability of the method to correctly identify the actual damage type – in this case the vibration measurement location of Point Y3 is used.

Summary damage detection and identification results for each vibration measurement location (Figure 2.20) are presented in Table 2.11. The method achieves effective damage detection and identification as no false alarms, missed damage, or damage misclassification errors are observed.

2.5.4.4 The Sequential Probability Ratio Test (SPRT) based method

The SPRT based method employs an excitation – single response submodel obtained from the complete 4–variate VARX(80, 80) models identified in the baseline phase, as well as a corresponding residual series obtained by driving the current (structure in unknown state) excitation and single response signals through the same submodel (inspection phase). Damage detection and identification is achieved via statistical comparison of the two residual standard deviations using the SPRT. The nominal residual standard deviation σ_o is selected as the mean standard deviation of the residuals obtained from the 60 healthy data sets driven through the submodel (corresponding to the selected response) of the baseline healthy VARX(80, 80) model. The residual standard deviation ratio σ_1/σ_o is chosen equal to 1.1, designating a 10% increase in the nominal standard deviation (see equations 2.16 and 2.17).

Representative damage detection results at the $\alpha = \beta = 0.01$ risk levels obtained via the SPRT based method for the vibration response (sensor) of Point Y1 are shown in Figure 2.29. A damage is

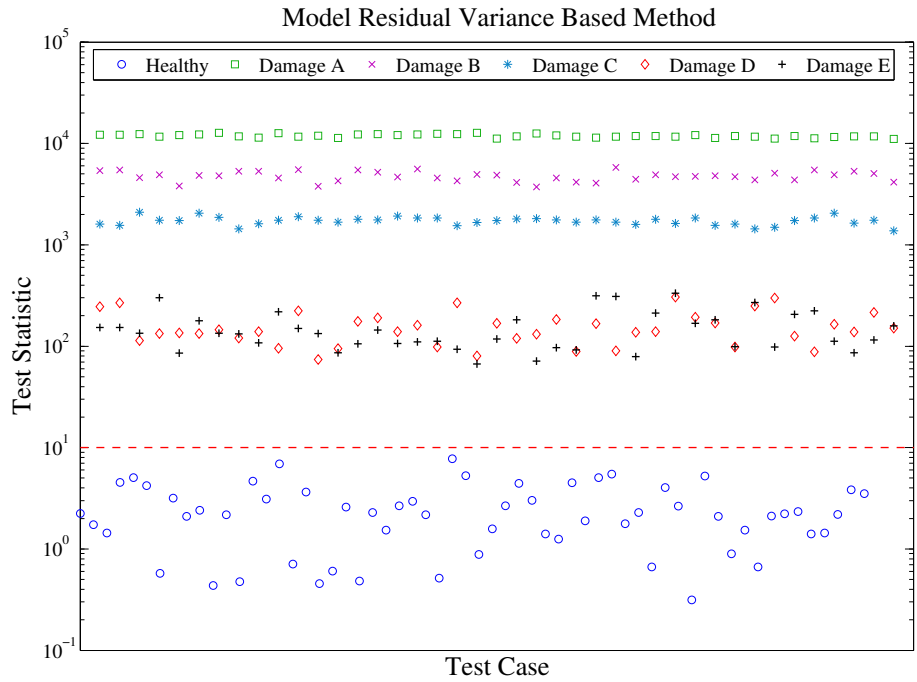


Figure 2.27: Residual variance based method: Representative damage detection results (sensor Y2; healthy – 60 experiments; damaged – 200 experiments). A damage is detected if the test statistic exceeds the critical point (dashed horizontal line).

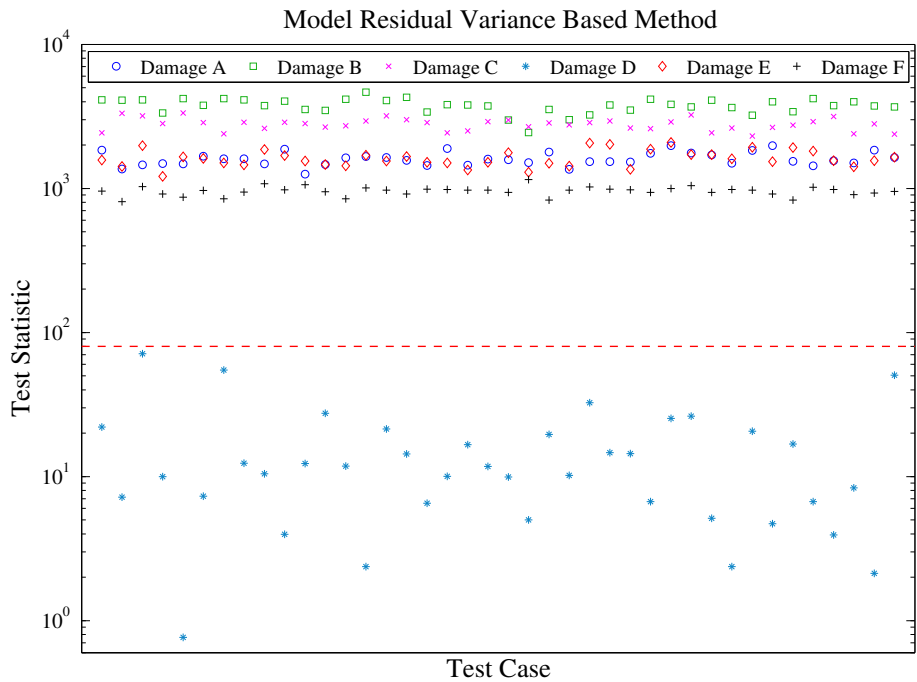


Figure 2.28: Residual variance based method: Representative damage identification results (sensor Y3; 240 experiments), with the actual damage being of type D. A damage is identified as type D if the test statistic is below the critical point (dashed horizontal line).

detected when the test statistic exceeds the upper critical point (dashed horizontal lines), while the structure is determined to be in its healthy state when the test statistic lies below the lower critical point. After a decision is made, the test statistic is reset to zero and the test continues, thus during

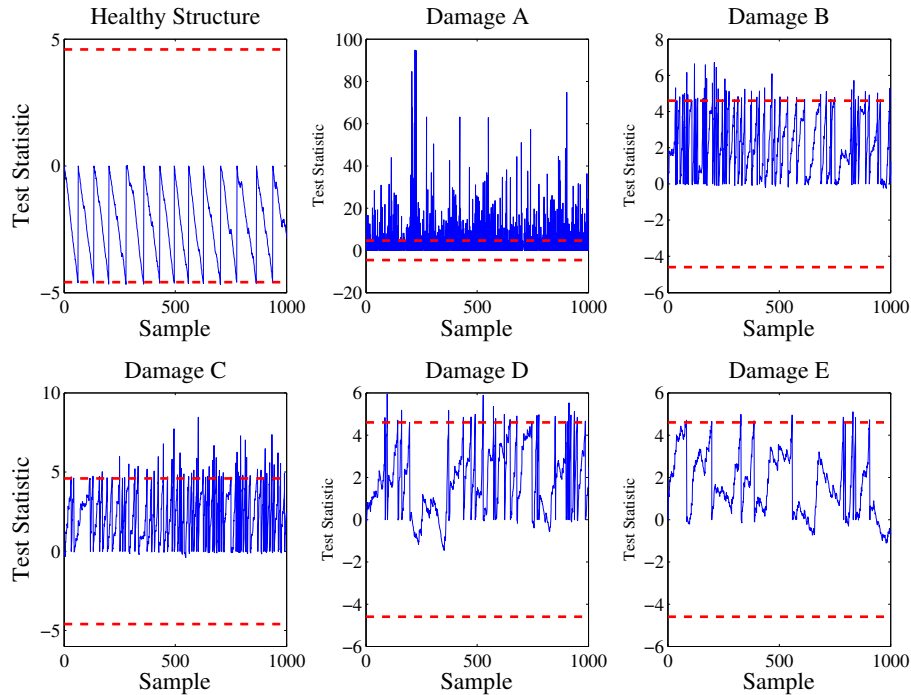


Figure 2.29: SPRT based method: Representative damage detection results (sensor Y1) at the $\alpha = \beta = 0.01$ risk levels ($\sigma_1/\sigma_o = 1.1$). The actual structural state is shown above each plot.

testing multiple decisions are made. Evidently, correct detection (Figure 2.29) is obtained in each test case, as the test statistic is shown to exceed multiple times (multiple correct decisions) the lower critical point in the healthy case, while it exceeds the upper critical point in the damage test cases. Observe that damage types A and C (Table 2.5.2) appear easier to detect, while damage types D and E appear harder to detect. This is in agreement with the remarks made in subsection 2.5.3.1 and Figure 2.21. Moreover, representative damage identification results at the $\alpha = \beta = 0.01$ risk levels ($\sigma_1/\sigma_o = 1.1$) for the vibration measurement location of Point Y4 are depicted in Figure 2.30, with the actual damage being of type B.

Summary damage detection and identification results for each vibration measurement location are presented in Table 2.11. The method exhibits excellent performance in damage detection and identification as no false alarms, missed damages, or damage misclassification errors are observed.

2.5.5 Application of vector time series methods

Vector statistical time series methods for SHM employ *vector* (multivariate) models and corresponding statistics (Lütkepohl 2005). Despite their phenomenal resemblance to their univariate counterparts, multivariate models generally have a much richer structure, while they typically require multivariate statistical decision making procedures (Fassois and Sakellariou 2009, Lütkepohl 2005). In this section two parametric methods, namely a model parameter based method and a residual likelihood function based method, are applied to the scale aircraft skeleton structure. The methods' main characteristics are summarized in Table 2.10.

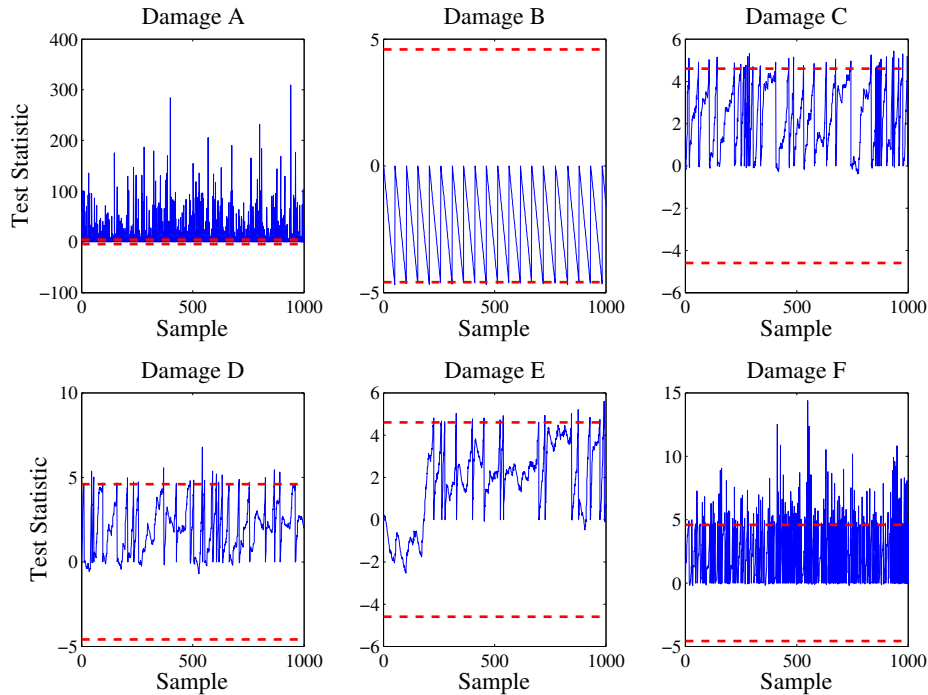


Figure 2.30: SPRT based method: Representative damage identification results (sensor Y4) at the $\alpha = \beta = 0.01$ risk levels ($\sigma_1/\sigma_o = 1.1$) with the actual damage being of type B. Each considered damage hypothesis is shown above each plot.

2.5.5.1 The model parameter based method

The model parameter based method employs the excitation and *all* response signals, along with the *complete* 4-variate VARX(80,80) model identified in the baseline phase. In addition, a corresponding 4-variate VARX(80,80) model is identified in each test case using the current signals (inspection phase).

Figure 2.31 presents representative damage detection results. The healthy test statistics are shown in circles (60 experiments), while the least severe damage types D and E are presented with asterisks and diamonds, respectively (one for each one of the 40 test cases). Evidently, correct detection is obtained in each test case, as the test statistic is shown not to exceed the critical point in the healthy cases, while it exceeds it in the damage cases. Representative damage identification results (240 test cases), with the actual damage being of type F, are presented in Figure 2.32. Evidently, correct identification is obtained in each considered test case, as the test statistics are shown not to exceed the critical point in the damage type F case, while the test cases corresponding to the other damage types exceed the critical point. Note the logarithmic scale on the vertical axis which indicates significant difference between the damage type F statistics and the rest damage types statistics for the considered test cases.

Summary damage detection and identification results are presented in Table 2.12. The method achieves accurate damage detection and identification, as no false alarm, missed damage, or damage misclassification errors are reported.

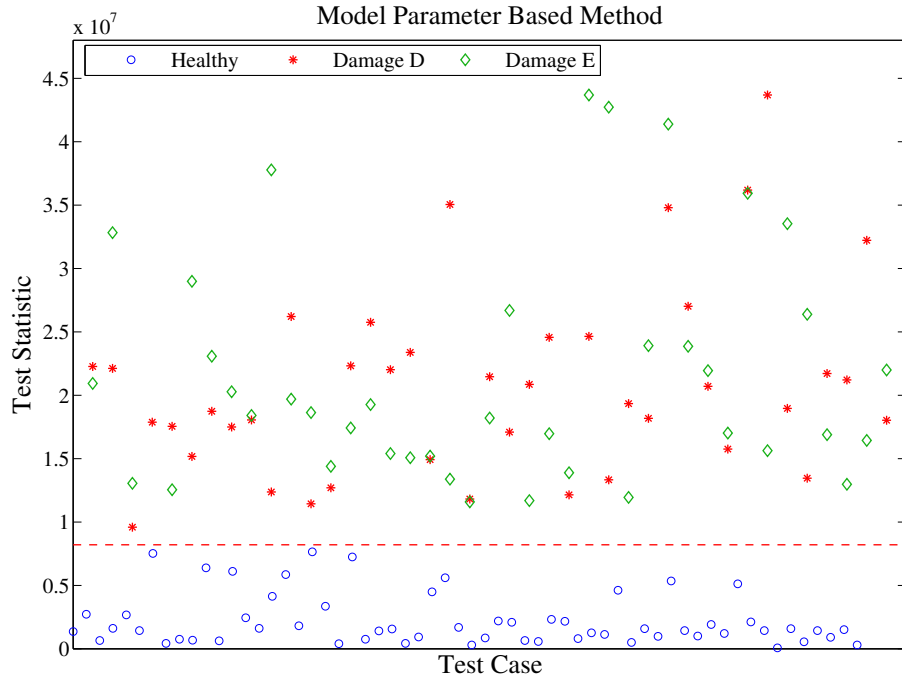


Figure 2.31: Model parameter based method: Representative damage detection results for three structural states (healthy – 60 experiments; damaged – 80 experiments). A damage is detected if the test statistic exceeds the critical point (dashed horizontal line).

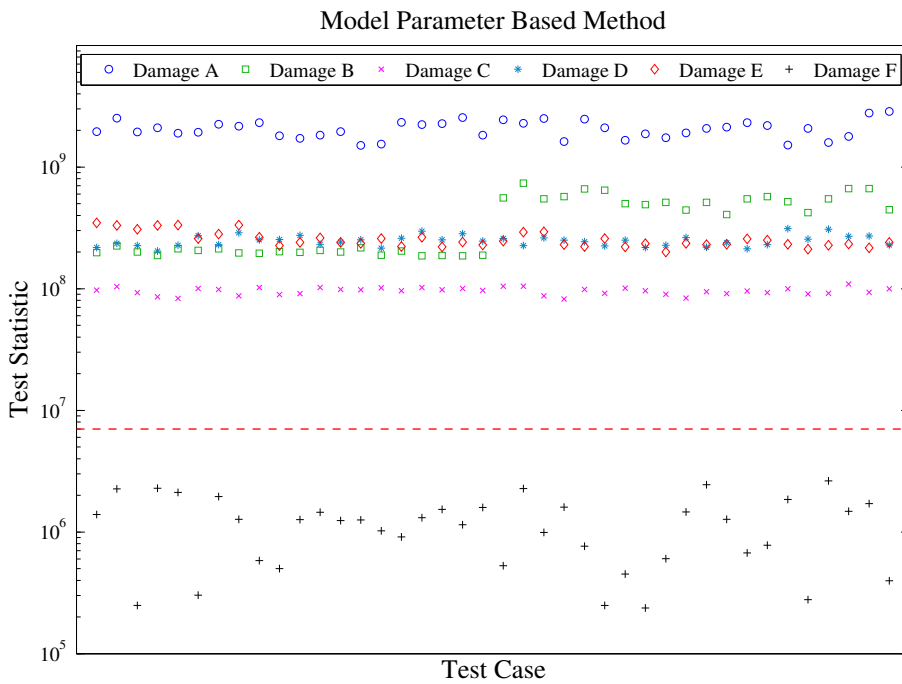


Figure 2.32: Model parameter based method: Representative damage identification results (240 experiments), with the actual damage being of type F. A damage is identified as type F if the test statistic is below the critical point (dashed horizontal line).

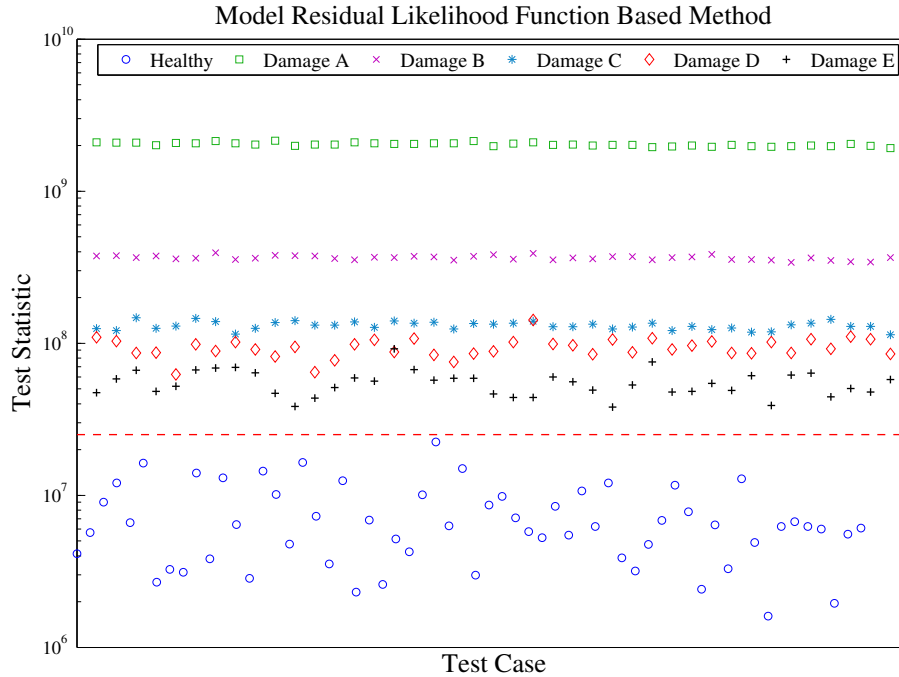


Figure 2.33: Residual likelihood function based method: Representative damage detection results (healthy – 60 experiments; damaged – 200 experiments). A damage is detected if the test statistic exceeds the critical point (dashed horizontal line).

2.5.5.2 The residual likelihood function based method

The residual likelihood function method employs the *complete* 4-variate VARX(80, 80) model identified in the baseline phase. Figure 2.33 presents representative damage detection results. Evidently, correct detection is obtained in each test case, as the test statistic is shown not to exceed the critical point in the healthy cases, while it exceeds it in each damage test case. Representative damage identification results, with the actual damage being of type A, are depicted in Figure 2.34. Evidently, correct identification is obtained in each considered test case, as the test statistics are shown not to exceed the critical point in the damage type A case, while the test cases corresponding to the other damage types exceed the critical point.

Summary damage detection and identification results are presented in Table 2.12. The method achieves accurate damage detection and identification, as no false alarm, missed damage, or damage misclassification cases are reported.

2.5.6 Discussion

Scalar time series methods for SHM are shown to achieve effective damage detection and identification, although *non-parametric* scalar methods do seem to encounter some difficulties. The PSD based method achieves excellent damage detection, although it exhibits some misclassification errors for damage type E. The misclassification problem is more intense for damage type B when the vibration measurement location Y3 or Y4 is used.

The FRF based method achieves accurate damage detection with no false alarms or missed damage errors, except for vibration measurement location Y4 for which it exhibits an increased number of false alarms. Moreover, it faces problems in correctly identifying damage types B and D, as the

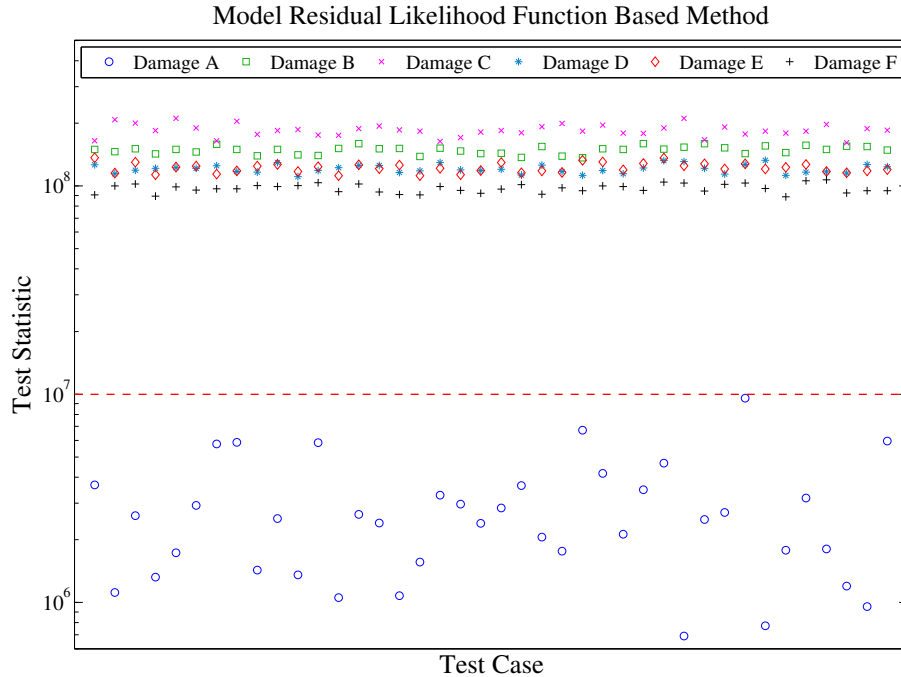


Figure 2.34: Residual likelihood function based method: Representative damage identification results (240 experiments), with the actual damage being of type A. A damage is identified as type A if the test statistic is below the critical point (dashed horizontal line).

number of damage misclassification errors is higher for these specific damage types. Both of these damage types involve loosening of bolts on the left wing-tip (Figure 2.20). The FRF based method yields results inferior to those obtained by the PSD based method even though it employs excitation-response signals (while the latter employs response-only signals). This is probably due to the larger PSD estimate uncertainty, which seems to better “accommodate” actual structural and experimental uncertainties.

The scalar parametric residual variance and SPRT based methods achieve excellent performance in accurately detecting and identifying damage employing any one of the vibration measurement locations (Table 2.11).

Vector time series methods for SHM achieve very accurate damage detection and identification, as with properly adjusted risk level α (type I error) no false alarm, missed damage, or damage misclassification errors are reported (Table 2.12). Moreover, the methods demonstrate better “global” damage detection capability. Nevertheless, parametric vector models require accurate parameter estimation and appropriate model structure (order) selection in order to accurately represent the structural dynamics and effectively tackle the damage detection and identification problems. Therefore, methods falling into this category require adequate user expertise and are somewhat more elaborate than their scalar or non-parametric counterparts.

2.6 Concluding remarks

A comparative experimental assessment of vibration based statistical time series methods for SHM was presented via their application to damage diagnosis on a lightweight aluminum truss structure and a scale aircraft skeleton structure. Some of the important conclusions drawn from this study may be summarized as follows:

Method	Damage Detection						
	False alarms	Missed damage					
		damage A	damage B	damage C	damage D	damage E	damage F
PSD based	0/0/0/0	0/0/0/0	0/0/0/0	0/0/0/0	0/0/0/0	0/0/0/0	0/0/0/0
FRF based	1/0/0/ 35	0/0/0/0	0/0/0/0	0/0/0/0	0/0/1/0	0/1/0/0	0/0/0/0
Res. variance [†]	0/0/0/0	0/0/0/0	0/0/0/0	0/0/0/0	0/0/0/0	0/0/0/0	0/0/0/0
SPRT based	0/0/0/0	0/0/0/0	0/0/0/0	0/0/0/0	0/0/0/0	0/0/0/0	0/0/0/0

False alarms for response points Y1/Y2/Y3/Y4 out of 60 test cases per point.
Missed damages for response points Y1/Y2/Y3/Y4 out of 40 test cases per point; [†]adjusted α .

Method	Damage Identification					
	Damage misclassification					
	damage A	damage B	damage C	damage D	damage E	damage F
PSD based	0/0/0/0	0/0/21/21	0/0/0/0	0/0/0/0	0/0/1/2	0/0/0/0
FRF based	0/0/0/0	10/4/7/8	6/10/2/0	5/22/9/8	2/9/5/2	0/3/1/0
Res. variance [†]	0/0/0/0	0/0/0/0	0/0/0/0	0/0/0/0	0/0/0/0	0/0/0/0
SPRT based	0/0/0/0	0/0/0/0	0/0/0/0	0/0/0/0	0/0/0/0	0/0/0/0

Damage misclassification for response points Y1/Y2/Y3/Y4 out of 40 test cases per point; [†]adjusted α .

Table 2.11: Scalar methods: damage detection and identification summary results.

Method	Damage Detection							Damage Identification					
	False alarms	Missed damage						Damage misclassification					
		dam A	dam B	dam C	dam D	dam E	dam F	dam A	dam B	dam C	dam D	dam E	dam F
Mod. par. [†]	0	0	0	0	0	0	0	0	0	0	0	0	0
Res. lik. [†]	0	0	0	0	0	0	0	0	0	0	0	0	0

False alarms out of 60 test cases. **Missed damages** out of 40 test cases.
Damage misclassification out of 40 test cases; [†]adjusted α .

Table 2.12: Vector methods: damage detection and identification summary results.

- Statistical time series methods for SHM achieve damage detection and identification based on (i) *scalar* or *vector* random excitation and/or vibration response signals, (ii) statistical model building, and (iii) statistical decision making under uncertainty.
- Both non-parametric and parametric, as well as scalar and vector methods were shown to effectively tackle damage detection and identification, with parametric methods achieving excellent performance with zero (in the present study) false alarm, missed damage, and damage misclassification rates.
- Both non-parametric and parametric methods of scalar and vector schemes were shown to have global damage detection capability, as they are able to detect “local” and “remote” damage with respect to the sensor position used.
- All methods were shown to be capable of correctly identifying the actual damage type, with the exception of the FRF based method which exhibited a small number of damage misclassification errors.
- Parametric time series methods are more elaborate and demand increased user expertise compared to their generally simpler non-parametric counterparts. Yet, they were shown to offer increased sensitivity and accuracy. Moreover, vector methods based on multivariate models are more elaborate, but offer the potential of further enhanced performance.
- The availability of data records corresponding to various potential damage scenarios is necessary in order to treat damage identification. This may not be possible with the actual structure itself,

but laboratory scale models or analytical (Finite Element) models may be used for this purpose.

- The extension of the methods to the more general *multivariate* case requires the use of corresponding vector models and multivariate statistical decision making procedures and needs to be fully investigated in the future.
- The need for methods capable of working under varying operational and environmental conditions and uncertainties is important and also the subject of current research (for instance Hios and Fassois 2009a, Michaelides and Fassois 2008).

Chapter 3

Identification of Stochastic Systems Under Multiple Operating Conditions: The Vector-dependent Functionally Pooled (VFP) Parametrization

In many applications a system operates under a variety of operating conditions which affect its dynamics, with each condition kept constant for a single commission cycle. The goal of this chapter is the identification of stochastic systems under multiple operating conditions via Vector-dependent Functionally Pooled (VFP) models. This chapter's work is based on the novel *Functional Pooling (FP) framework*, which has been recently introduced by the Stochastic Mechanical Systems & Automation group of the Mechanical Engineering & Aeronautics Department at University of Patras. The fourth chapter of the thesis addresses the problem of identifying a globally valid and parsimonious system model based on input-output data records obtained under a sample of operating conditions characterized by more than one parameters (for instance operating temperature and humidity or damage location and damage magnitude). Thus, models that include a *vector* characterization of the operating condition (referred to as *operating parameter vector*) are postulated. The problem is tackled within the novel Functional Pooling (FP) framework that postulates proper global models of the ARX and ARMAX types, data pooling techniques, and statistical parameter estimation. Corresponding Vector-dependent Functionally Pooled (VFP) ARX and ARMAX models are postulated, and proper estimators of the Least Squares (LS), Maximum Likelihood (ML), and Prediction Error (PE) types are developed. Model structure estimation is achieved via customary criteria, such as the Akaike and Bayesian information criteria (AIC and BIC, respectively), and a novel Genetic Algorithm (GA) based procedure. The strong consistency of the VFP-ARX least squares and maximum likelihood estimators is established, whereas the effectiveness of the complete estimation and identification method is demonstrated via two Monte Carlo studies.

3.1 Introduction

In many applications a system may operate under different operating conditions during different service intervals or commission cycles, while maintaining its condition within each cycle. As is often the case in practice, each operating condition may affect the system/structure and its dynamics. Typical examples include materials and mechanical structures under different environmental conditions such as temperature and humidity, rotating machinery operating at various speeds, hydraulic systems operating under different temperatures or fluid pressures, mechanical systems under different load or lubrication conditions, physiological systems under different conditions, and so on.

In such cases, it is important to identify a *global* and *parsimonious* (compact) model describing the system under *any* operating condition, based on input and noise-corrupted output data records corresponding to a *sample* of those conditions. It could be, perhaps, argued that the problem may be handled using a number of “pseudo-independent” conventional mathematical models and customary identification techniques that could artificially split the problem into a number of seemingly unrelated subproblems. Each model could be then obtained based on data records corresponding to each operating condition. Models corresponding to other (intermediate) operating conditions would not be readily available, but could be “interpolated” based on those identified. This approach would, nevertheless, suffer from a number of problems: First it would fail to provide a single global and parsimonious model valid under all admissible operating conditions. Second, it would be suboptimal, characterized by reduced statistical accuracy, as it would result in a large number of estimated parameters and ineffective use of the information available in the totality of the data records. For instance, the *interrelations* among the different data records would be ignored, as a result of separating the problem into seemingly unrelated subproblems.

In order to effectively handle such problems, a novel *Functional Pooling (FP) framework* has been introduced by the Stochastic Mechanical Systems & Automation group of the Mechanical Engineering & Aeronautics Department at University of Patras (Sakellariou and Fassois 2007, Sakellariou and Fassois 2007b, Kopsaftopoulos and Fassois 2006a). This framework circumvents the above difficulties and allows for effective and accurate (statistically efficient) identification of a global and parsimonious model describing the system under any admissible operating condition. It is based on the novel concept of functional pooling that introduces functional dependencies (in terms of the operating parameter) in the postulated model structure. It is this specific characteristic that, unlike in conventional pooling used in fields such as econometrics (Dielman 1989, Greene 2003) where the effects of “operating conditions” are “smoothed out”, allows for both precise and parsimonious modeling.

The proposed Functional Pooling (FP) framework is based on three important entities:

- (i) A *stochastic Functionally Pooled (FP)* model structure that explicitly allows for system modeling under *multiple* operating conditions via a single (“global”) mathematical representation. This representation is characterized by parameters that *functionally* (explicitly) depend on the operating condition (*quasi-static dependence*). It thus allows for the effective and compact modeling of the dynamics under all possible conditions, as well as for *optimal statistical accuracy*, due to its limited parametrization and the full accounting of the interrelations among the various data records.
- (ii) *Data pooling* techniques (see Dielman (1989) and Greene (2003)) for combining and optimally treating (as one entity) the data obtained from the various experiments.
- (iii) Statistical techniques for model estimation.

The resulting framework is referred to as a statistical *Functional Pooling framework*, and the corresponding models as stochastic *Functionally Pooled (FP) models*. It is worth noting that by considering a specific damage type as an operating condition, the approach is well suited for effectively tackling the damage detection, identification (localization) and magnitude estimation problems, and some versions have been used within this context (Sakellariou and Fassois 2008, Kopsaftopoulos and Fassois 2007, Kopsaftopoulos and Fassois 2011*e*). Nevertheless, the usefulness of the approach is far broader, and includes system analysis, characterization, prediction and automatic control.

A schematic representation of the FP framework is provided in Figure 3.1. The only essential practical condition for using this framework and identifying “global” system models is that each operating condition corresponds to a specific value of a measurable variable, henceforth referred to as the *operating parameter*. The case of a *scalar* operating parameter (for instance operating temperature) has been treated in a previous work (Sakellariou 2005, Sakellariou and Fassois 2007, Sakellariou and Fassois 2007*b*). This chapter focuses on the case of a *vector* operating parameter (consisting of two or more scalars, for instance operating temperature and humidity).

The class of FP models could be in the most general terms considered to belong to the broader family of Linear Parameter Varying (LPV) models (for details in LPV model identification see Toth (2010) and Bamieh and Giarre (2003), and the references therein). Nevertheless and despite their superficial resemblance, these two model classes address somewhat different identification issues with quite different perspectives. LPV identification is achieved via two major approaches: (i) the local approach and (ii) the global approach. In the local approach LTI models are identified in a number of (local) operating points corresponding to constant scheduling signals and the resulting local linear models are interpolated (possibly by using data from an additional global experiment) to an LPV model (Toth 2010). For the interpolation various techniques and approaches have been introduced, varying from interpolation on pole estimates to the technique where each local (LTI) model is converted to a state space model in canonical form, and subsequently the coefficients in this model are interpolated. The local approach would, nevertheless, suffer from a number of problems as it would fail to provide a single global and parsimonious model valid under all admissible operating conditions, while it would be suboptimal, characterized by reduced statistical accuracy, as it would result in a large number of estimated parameters and ineffective use of the information available in the totality of the data records. For instance, the *interrelations* among the different data records would be ignored, as a result of separating the problem into seemingly unrelated subproblems. In the global approach though one has to determine a global LPV model structure and an identification criterion and data from a *single global experiment* are employed in order to estimate an LPV model (Toth 2010).

In the FP framework the only essential practical condition for identifying parsimonious global system models is the availability of data records from each operating condition (point) with each such condition corresponding to a specific value of one (or more) measurable variable. Furthermore, this framework circumvents the aforementioned difficulties that the LPV local approach faces and allows for effective and accurate (statistically efficient) identification of a global and parsimonious model describing the system under any admissible operating condition. Moreover, the interrelations among the different data records belonging to the various operating conditions are fully taken into account, as the FP model structure employs appropriate data pooling techniques. Furthermore, an extremely important difference is that the LPV global approach employs data obtained from a single experiment, which is not the case in the FP framework, as it employs data records obtained under a sample of the operating conditions. From all the above it is obvious that, despite their phenomenal similarities, the FP and LPV model structures constitute distinct representations that have important differences and therefore should be clearly distinguished.

Thus, this chapter addresses the problem of identifying a globally valid and parsimonious system

model based on input-output data records obtained under a sample of operating conditions characterized by more than one parameters (for instance operating temperature and humidity). Thus, models that include a *vector* characterization of the operating condition (referred to as *operating parameter vector*) are postulated. The problem is tackled within the novel Functional Pooling (FP) framework that postulates proper global models of the ARX and ARMAX types, data pooling techniques, and statistical parameter estimation. Corresponding Vector-dependent Functionally Pooled (VFP) ARX and ARMAX models are postulated, and proper estimators of the Least Squares (LS), Maximum Likelihood (ML), and Prediction Error (PE) types are developed. Model structure estimation is achieved via customary criteria (Bayesian Information Criterion and Akaike Information Criterion) and a Genetic Algorithm (GA) based procedure. The strong consistency of the estimators is established, whereas the effectiveness of the complete estimation and identification method is demonstrated via Monte Carlo experiments.

The main contributions of the chapter are:

- Extension of the FP models employing a scalar operating parameter to the Vector-dependent FP models employing the *operating parameter vector*.
- Model structure estimation is achieved via customary criteria such as the BIC and the AIC, as well as via a Genetic Algorithm (GA) based procedure.
- A new VFP model form is introduced in which the innovations sequence variance is projected to a functional subspace, so now it may be available not only for the sample of operating conditions (available data records), but it may be efficiently estimated for all the potential admissible operating conditions, thus for all the potential operating parameter vectors \mathbf{k} .
- The strong consistency of the least squares and the maximum likelihood estimators is established, as well as the asymptotic distribution of the all the considered estimators.
- Assessment of the proposed estimators and structure selection procedures via two Monte Carlo studies, investigating both cases of complete and non-complete functional subspaces.

3.2 Vector-dependent Functionally Pooled (VFP) model structure

3.2.1 The data set

Model Identification is based on input and noise-corrupted output data records corresponding to a sample of the admissible operating conditions. The data records are of length N , each one corresponding to a specific value of the operating parameter vector \mathbf{k} , which, without loss of generality, is assumed to be two-dimensional. A sample of M_1 values is used for the first externally measurable variable k^1 (first element of vector \mathbf{k}), while a sample of M_2 values is used for the second externally measurable variable k^2 (second element of vector \mathbf{k}).

A total of $M_1 \times M_2$ experiments (one for each element of \mathbf{k}) are performed, with the complete series covering the required range of each scalar parameter, say $[k_{min}^1, k_{max}^1]$ and $[k_{min}^2, k_{max}^2]$, via the discretizations $k^1 = k_1^1, k_2^1, \dots, k_{M_1}^1$ and $k^2 = k_1^2, k_2^2, \dots, k_{M_2}^2$. Hence each experiment is characterized by a specific value of \mathbf{k} , say $\mathbf{k} = [k_i^1, k_j^2]$. This vector is, for simplicity of notation, also designated as the duplet $k_{i,j} = (k_i^1, k_j^2)$ (the first subscript of $k_{i,j}$ designating the value of k^1 and the second that of k^2).

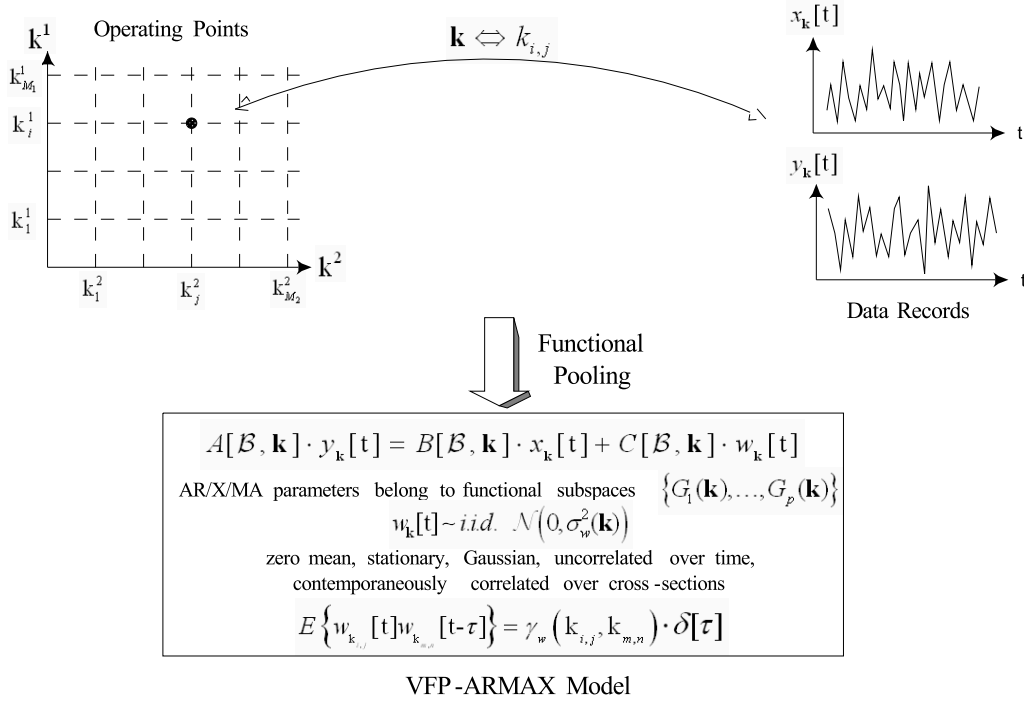


Figure 3.1: Schematic representation of the problem showing the operating points on the (k^1, k^2) plane, an excitation-response data set corresponding to a particular operating point, and the VFP-ARMAX model structure.

Input and noise-corrupted output data records from different operating points corresponding to various values of the operating parameter vector are used (Figure 3.1):

$$Z^{NM_1M_2} \triangleq \left\{ x_{\mathbf{k}}[t], y_{\mathbf{k}}[t] \mid \mathbf{k} \triangleq [k^1 \ k^2]^T, t = 1, \dots, N, k^1 \in \{k_1^1, \dots, k_{M_1}^1\}, k^2 \in \{k_1^2, \dots, k_{M_2}^2\} \right\}. \quad (3.1)$$

In this expression t designates normalized discrete time (the corresponding analog time being $t \cdot T$ with T standing for the sampling period), and $x_{\mathbf{k}}[t], y_{\mathbf{k}}[t]$ the input and noise-corrupted output signals corresponding to \mathbf{k} . N stands for the signal length (in samples) corresponding to each experiment (each \mathbf{k}).

3.2.2 The VFP-ARX model structure

Vector-dependent Functionally Pooled AutoRegressive with eXogenous input (VFP-ARX) models constitute conceptual extensions of their conventional ARX counterparts, with the important difference that the model parameters belong to functional subspaces spanned by specific functions of \mathbf{k} (basis functions). A VFP-ARX(na, nb)_[pa, pb] model, with na, nb designating its AR and X orders, and pa, pb its AR and X parameter subspace dimensionalities, respectively, is of the form:

$$y_{\mathbf{k}}[t] + \sum_{i=1}^{na} a_i(\mathbf{k}) \cdot y_{\mathbf{k}}[t-i] = \sum_{i=0}^{nb} b_i(\mathbf{k}) \cdot x_{\mathbf{k}}[t-i] + w_{\mathbf{k}}[t] \quad (3.2)$$

$$w_{\mathbf{k}}[t] \sim \text{iid} \mathcal{N}(0, \sigma_w^2(\mathbf{k})) \quad \mathbf{k} \in \mathbb{R}^2 \quad (3.3)$$

$$a_i(\mathbf{k}) \triangleq \sum_{j=1}^{pa} a_{i,j} \cdot G_{d_a(j)}(\mathbf{k}), \quad b_i(\mathbf{k}) \triangleq \sum_{j=1}^{pb} b_{i,j} \cdot G_{d_b(j)}(\mathbf{k}) \quad (3.4)$$

$$E\{w_{k_{i,j}}[t] \cdot w_{k_{m,n}}[t - \tau]\} = \gamma_w[k_{i,j}, k_{m,n}] \cdot \delta[\tau] \quad (3.5)$$

with $x_{\mathbf{k}}[t]$, $y_{\mathbf{k}}[t]$ the excitation and response signals, respectively, and $w_{\mathbf{k}}[t]$ the disturbance (innovations) signal that is a white (serially uncorrelated) zero-mean with variance $\sigma_w^2(\mathbf{k})$ and potentially cross-correlated with its counterparts corresponding to different experiments. The symbol $E\{\cdot\}$ designates statistical expectation, $\delta[\tau]$ the Kronecker delta (equal to unity for $\tau = 0$ and equal to zero for $\tau \neq 0$), $\mathcal{N}(\cdot, \cdot)$ Gaussian distribution with the indicated mean and variance, and iid stands for identically independently distributed.

As (3.4) indicates, the AR and X parameters $a_i(\mathbf{k})$, $b_i(\mathbf{k})$ are modelled as explicit functions of the operating parameter vector \mathbf{k} (\mathbf{k} -varying parameters) belonging to the functional subspaces:

$$\begin{aligned} \mathcal{F}\langle a_i(\mathbf{k}) \rangle &\triangleq \{G_{d_a(1)}(\mathbf{k}), G_{d_a(2)}(\mathbf{k}), \dots, G_{d_a(pa)}(\mathbf{k})\} \\ \mathcal{F}\langle b_i(\mathbf{k}) \rangle &\triangleq \{G_{d_b(1)}(\mathbf{k}), G_{d_b(2)}(\mathbf{k}), \dots, G_{d_b(pb)}(\mathbf{k})\} \end{aligned}$$

spanned by the (mutually independent) basis functions $G_{d_a(j)}(\mathbf{k})$, $G_{d_b(j)}(\mathbf{k})$ consisting of polynomials of two variables (vector polynomials) obtained as cross-products from the corresponding univariate polynomials (Chebyshev, Legendre, Jacobi and other families – for details see Appendix A). The indices $d_a(j)$ ($j = 1, \dots, pa$) and $d_b(j)$ ($j = 1, \dots, pb$) designate the specific basis functions that are included in each subspace. The constants $a_{i,j}$ and $b_{i,j}$ designate the AR and X coefficients of projection, respectively.

For convenience, the following notation for the complete, that is including consecutive basis functions equal to the subspace dimensionality, functional subspaces is introduced:

$$\mathcal{F}_p \triangleq \{G_0(\mathbf{k}), G_1(\mathbf{k}), \dots, G_p(\mathbf{k})\}. \quad (3.6)$$

The VFP-ARX model is thus parameterized in terms of the the model's projection coefficients $a_{i,j}$, $b_{i,j}$, the innovations covariance $\gamma_w[k_{i,j}, k_{m,n}]$ ($\gamma_w[k_{i,j}, k_{i,j}] = \sigma_w^2[k_{i,j}]$), and the model structure \mathcal{M} , defined by the model orders na , nb and the functional subspaces $\mathcal{F}\langle a_i(\mathbf{k}) \rangle$, $\mathcal{F}\langle b_i(\mathbf{k}) \rangle$.

Based on the backshift operator \mathcal{B} ($\mathcal{B}^i \cdot x[t] \triangleq x[t - i]$) the VFP-ARX model may be expressed as follows:

$$A[\mathcal{B}, \mathbf{k}] \cdot y_{\mathbf{k}}[t] = B[\mathcal{B}, \mathbf{k}] \cdot x_{\mathbf{k}}[t] + w_{\mathbf{k}}[t] \quad (3.7)$$

with $A[\mathcal{B}, \mathbf{k}]$, $B[\mathcal{B}, \mathbf{k}]$ designating the AR and X, respectively, \mathbf{k} -varying polynomial operators:

$$A[\mathcal{B}, \mathbf{k}] \triangleq 1 + \sum_{i=1}^{na} a_i(\mathbf{k})\mathcal{B}^i, \quad B[\mathcal{B}, \mathbf{k}] \triangleq \sum_{i=0}^{nb} b_i(\mathbf{k})\mathcal{B}^i. \quad (3.8)$$

The ARX signal flow can be depicted as in Figure 3.2.

As already mentioned, the innovations sequences $w_{\mathbf{k}}[t]$ corresponding to different operating conditions may be *contemporaneously correlated*, that is

$$E\{w_{k_{i,j}}[t]w_{k_{i,j}}[t]\} = \sigma_w^2([k_{i,j}]) \quad \text{and} \quad E\{w_{k_{i,j}}[t]w_{k_{m,n}}[t]\} = \gamma_w[k_{i,j}, k_{m,n}].$$

Defining the VFP model's *cross-section innovations vector* as:

$$\mathbf{w}[t] \triangleq \left[w_{k_{1,1}}[t] \ w_{k_{1,2}}[t] \ \dots \ w_{k_{1,M_2}}[t] \ \dots \ w_{k_{M_1,M_2}}[t] \right]^T \quad (3.9)$$

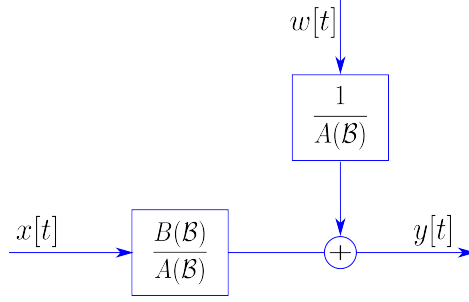


Figure 3.2: The ARX model structure.

with covariance matrix:

$$\mathbf{\Gamma}_{\mathbf{w}[t]} = E\{\mathbf{w}[t]\mathbf{w}^T[t]\} = \begin{bmatrix} \sigma_w^2[k_{1,1}] & \gamma_w[k_{1,1}, k_{1,2}] & \dots & \gamma_w[k_{1,1}, k_{M_1, M_2}] \\ \gamma_w[k_{1,2}, k_{1,1}] & \sigma_w^2[k_{1,2}] & \dots & \gamma_w[k_{1,2}, k_{M_1, M_2}] \\ \vdots & \vdots & \ddots & \vdots \\ \gamma_w[k_{M_1, M_2}, k_{1,1}] & \gamma_w[k_{M_1, M_2}, k_{1,2}] & \dots & \sigma_w^2[k_{M_1, M_2}] \end{bmatrix} \quad (3.10)$$

then the covariance matrix corresponding to the time instants $t = 1, \dots, N$ is given by:

$$\mathbf{\Gamma}_{\mathbf{w}} = \mathbf{\Gamma}_{\mathbf{w}[t]} \otimes \mathbf{I}_N \quad (3.11)$$

with \otimes designating Kronecker product (Bernstein 2005, chap. 7).

In the case of *cross-sectionally uncorrelated* innovations sequences with *different variances* ($\sigma_w^2[k_{1,1}] \neq \sigma_w^2[k_{1,2}] \neq \dots \neq \sigma_w^2[k_{M_1, M_2}]$, *groupwise heteroscedasticity*), the covariance matrix is given by:

$$\mathbf{\Gamma}_{\mathbf{w}} = \begin{bmatrix} \sigma_w^2[k_{1,1}]\mathbf{I}_N & 0 & \dots & 0 \\ 0 & \sigma_w^2[k_{2,2}]\mathbf{I}_N & \dots & 0 \\ \vdots & \vdots & \ddots & \vdots \\ 0 & 0 & \dots & \sigma_w^2[k_{M_1, M_2}]\mathbf{I}_N \end{bmatrix} \quad (3.12)$$

In the simpler case of *cross-sectionally uncorrelated* innovations sequences with *equal variances* ($\sigma_w^2[k_{1,1}] = \sigma_w^2[k_{1,2}] = \dots = \sigma_w^2[k_{M_1, M_2}] = \sigma_w^2$, *groupwise homoscedasticity*), the covariance matrix is given by $\mathbf{\Gamma}_{\mathbf{w}} = \sigma_w^2 \mathbf{I}_{NM_1 M_2}$ with $\mathbf{I}_{NM_1 M_2}$ indicating the unity matrix.

It is worth noting that:

1. All information in terms of interrelations among the data records in $Z^{NM_1 M_2}$ is reflected in the covariance matrix $\mathbf{\Gamma}_{\mathbf{w}[t]} = E\{\mathbf{w}[t]\mathbf{w}^T[t]\}$ with $\mathbf{w}[t] \triangleq [w_{k_{1,1}}[t] \dots w_{k_{M_1, M_2}}[t]]^T$. This knowledge is incorporated into the parameter estimation phase to obtain statistical models.
2. The projection of the parameters $a_i(\mathbf{k}), b_i(\mathbf{k})$ on the functional subspaces $\mathcal{F}\langle a_i(\mathbf{k}) \rangle, \mathcal{F}\langle b_i(\mathbf{k}) \rangle$ allows for models capable of representing the system dynamics everywhere within $[k_{min}^1, k_{max}^1] \times [k_{min}^2, k_{max}^2] \in \mathbb{R}^2$, and not only at the distinct values $\{k_1^1, k_2^1, \dots, k_{M_1}^1\} \times \{k_1^2, k_2^2, \dots, k_{M_2}^2\}$ involved in $Z^{NM_1 M_2}$.
3. The form of functional dependence is an important issue. Physical insight may be used, although experience has shown that orthogonal polynomials, or trigonometric functions are sufficient.

The representation of equations (3.2) – (3.5) is referred to as a VFP-ARX model of orders (n_a, n_b) and functional subspace dimensionalities pa, pb , or in short a VFP-ARX(n_a, n_b) $_{[pa, pb]}$ model.

It is parameterized in terms of the parameter vector:

$$\bar{\boldsymbol{\theta}} \triangleq [\alpha_{i,j} \ ; \ b_{i,j} \ ; \ \gamma_w[k_{i,j}, k_{m,n}]]^T \quad \forall i, j, m, n \quad (3.13)$$

with $\gamma_w[k_{i,j}, k_{i,j}] = \sigma_w^2[k_{i,j}]$.

The complete VFP-ARX model *estimation* and *identification* problem may be then stated as follows: “Given the input – output data records $\{x_{\mathbf{k}}[t]\}_{t=1}^N$, $\{y_{\mathbf{k}}[t]\}_{t=1}^N$ for $\mathbf{k} = k_{1,1}, k_{1,2}, \dots, k_{M_1, M_2}$ and the VFP-ARX model set:

$$\mathcal{G} \triangleq \left\{ \mathcal{M}(\bar{\boldsymbol{\theta}}) : \begin{aligned} A[\mathcal{B}, \mathbf{k}, \bar{\boldsymbol{\theta}}] \cdot y_{\mathbf{k}}[t] &= B[\mathcal{B}, \mathbf{k}, \bar{\boldsymbol{\theta}}] \cdot x_{\mathbf{k}}[t] + e_{\mathbf{k}}[t, \bar{\boldsymbol{\theta}}]; \\ \gamma_w[k_{i,j}, k_{m,n}] &= E\{e_{k_{i,j}}[t, \bar{\boldsymbol{\theta}}]e_{k_{m,n}}[t, \bar{\boldsymbol{\theta}}]\} \quad \forall i, j, m, n \end{aligned} \right\} \quad (3.14)$$

select an element of \mathcal{G} that best fits the measured data.”

In this expression $e_{\mathbf{k}}[t, \bar{\boldsymbol{\theta}}]$ stands for the model’s one-step-ahead prediction error (residual) sequence, which is designated as function of the parameters to be estimated. This signifies the fact that (just like the parameters) it is initially unknown, but may be obtained based on the current model parameters and the measured excitation-response vibration signals.

The VFP-ARX representation is assumed to satisfy the following conditions:

- CD1. *Stability condition.* The poles of the AR polynomials (see Equation (3.7)) should lie inside the unit circle $\forall \mathbf{k}$.
- CD2. *Irreducibility condition.* The polynomials $A[\mathcal{B}, \mathbf{k}]$ and $B[\mathcal{B}, \mathbf{k}]$ are coprime (have no common factors) $\forall \mathbf{k}$.
- CD3. The input signal $x_{\mathbf{k}}[t]$ is stationary, ergodic and persistently exciting with $E\{x_{k_{i,j}}[t]w_{k_{m,n}}[t]\} = 0$ $\forall i, j, m, n$.

3.2.3 The VFP-ARMAX model structure

Vector-dependent Functionally Pooled AutoRegressive Moving Average with eXogenous input (VFP-ARMAX) models constitute conceptual extensions of their conventional ARMAX counterparts, with the important difference that the model parameters belong to functional subspaces spanned by specific \mathbf{k} functions (basis functions). A VFP-ARMAX(na, nb, nc)_[pa, pb, pc] model, with na, nb, nc designating its AR, X, MA orders and pa, pb, pc its AR, X, MA parameter subspace dimensionalities, is of the form:

$$y_{\mathbf{k}}[t] + \sum_{i=1}^{na} a_i(\mathbf{k}) \cdot y_{\mathbf{k}}[t-i] = \sum_{i=0}^{nb} b_i(\mathbf{k}) \cdot x_{\mathbf{k}}[t-i] + w_{\mathbf{k}}[t] + \sum_{i=1}^{nc} c_i(\mathbf{k}) \cdot w_{\mathbf{k}}[t-i] \quad (3.15)$$

$$w_{\mathbf{k}}[t] \sim \text{iid } \mathcal{N}(0, \sigma_w^2(\mathbf{k})) \quad \mathbf{k} \in \mathbb{R}^2 \quad (3.16)$$

$$a_i(\mathbf{k}) \triangleq \sum_{j=1}^{pa} a_{i,j} \cdot G_{d_a(j)}(\mathbf{k}), \quad b_i(\mathbf{k}) \triangleq \sum_{j=1}^{pb} b_{i,j} \cdot G_{d_b(j)}(\mathbf{k}), \quad c_i(\mathbf{k}) \triangleq \sum_{j=1}^{pc} c_{i,j} \cdot G_{d_c(j)}(\mathbf{k}) \quad (3.17)$$

$$E\{w_{k_{i,j}}[t] \cdot w_{k_{m,n}}[t - \tau]\} = \gamma_w[k_{i,j}, k_{m,n}] \cdot \delta[\tau] \quad (3.18)$$

with $x_{\mathbf{k}}[t]$, $y_{\mathbf{k}}[t]$ the excitation and response signals, respectively, and $w_{\mathbf{k}}[t]$ the disturbance (innovations) signal that is a white (serially uncorrelated) zero-mean with variance $\sigma_w^2(\mathbf{k})$ and potentially cross-correlated with its counterparts corresponding to different experiments. The symbol $E\{\cdot\}$ designates statistical expectation, $\delta[\tau]$ the Kronecker delta (equal to unity for $\tau = 0$ and equal to zero for $\tau \neq 0$), $\mathcal{N}(\cdot, \cdot)$ Gaussian distribution with the indicated mean and variance, and iid stands for identically independently distributed.

As (3.17) indicates, the AR, X and MA parameters $a_i(\mathbf{k})$, $b_i(\mathbf{k})$, $c_i(\mathbf{k})$ are modelled as explicit functions of the operating parameter vector \mathbf{k} (\mathbf{k} -varying parameters) belonging to functional subspaces:

$$\begin{aligned} \mathcal{F}\langle a_i(\mathbf{k}) \rangle &\triangleq \{G_{d_a(1)}(\mathbf{k}), G_{d_a(2)}(\mathbf{k}), \dots, G_{d_a(pa)}(\mathbf{k})\} \\ \mathcal{F}\langle b_i(\mathbf{k}) \rangle &\triangleq \{G_{d_b(1)}(\mathbf{k}), G_{d_b(2)}(\mathbf{k}), \dots, G_{d_b(pb)}(\mathbf{k})\} \\ \mathcal{F}\langle c_i(\mathbf{k}) \rangle &\triangleq \{G_{d_c(1)}(\mathbf{k}), G_{d_c(2)}(\mathbf{k}), \dots, G_{d_c(pc)}(\mathbf{k})\} \end{aligned}$$

spanned by the (mutually independent) basis functions $G_{d_a(j)}(\mathbf{k})$, $G_{d_b(j)}(\mathbf{k})$, $G_{d_c(j)}(\mathbf{k})$ consisting of polynomials of two variables (vector polynomials) obtained as cross-products from univariate polynomials (Chebyshev, Legendre, Jacobi and other families – for details see Appendix A). The indices $d_a(j)$ ($j = 1, \dots, pa$), $d_b(j)$ ($j = 1, \dots, pb$) and $d_c(j)$ ($j = 1, \dots, pc$) designate the specific basis functions that are included in each subspace. The constants $a_{i,j}$, $b_{i,j}$ and $c_{i,j}$ designate the AR, X and MA coefficients of projection, respectively.

The VFP-ARMAX model is thus parameterized in terms of the the model's projection coefficients $a_{i,j}$, $b_{i,j}$, $c_{i,j}$, the innovations covariance $\gamma_w[k_{i,j}, k_{m,n}]$ ($\gamma_w[k_{i,j}, k_{i,j}] = \sigma_w^2[k_{i,j}]$) and the model structure \mathcal{M} , defined by the model orders na , nb , nc and the functional subspaces $\mathcal{F}\langle a_i(\mathbf{k}) \rangle$, $\mathcal{F}\langle b_i(\mathbf{k}) \rangle$, $\mathcal{F}\langle c_i(\mathbf{k}) \rangle$.

Based on the backshift operator \mathcal{B}^i ($\mathcal{B} \cdot x[t] \triangleq x[t-i]$) the VFP-ARMAX model may be expressed as follows:

$$A[\mathcal{B}, \mathbf{k}] \cdot y_{\mathbf{k}}[t] = B[\mathcal{B}, \mathbf{k}] \cdot x_{\mathbf{k}}[t] + C[\mathcal{B}, \mathbf{k}] \cdot w_{\mathbf{k}}[t] \quad (3.19)$$

with $A[\mathcal{B}, \mathbf{k}]$, $B[\mathcal{B}, \mathbf{k}]$, $C[\mathcal{B}, \mathbf{k}]$ designating the AR, X and MA, respectively, \mathbf{k} -varying polynomial operators:

$$A[\mathcal{B}, \mathbf{k}] \triangleq 1 + \sum_{i=1}^{na} a_i(\mathbf{k})\mathcal{B}^i, \quad B[\mathcal{B}, \mathbf{k}] \triangleq \sum_{i=0}^{nb} b_i(\mathbf{k})\mathcal{B}^i, \quad C[\mathcal{B}, \mathbf{k}] \triangleq 1 + \sum_{i=1}^{nc} c_i(\mathbf{k})\mathcal{B}^i. \quad (3.20)$$

The representation of equations (3.15) – (3.18) is referred to as a VFP-ARMAX model of orders (na, nb, nc) and functional subspace dimensionalities (pa, pb, pc) , or in short a

$$\bar{\theta} \triangleq [\alpha_{i,j} \vdots b_{i,j} \vdots c_{i,j} \vdots \gamma_w[k_{i,j}, k_{m,n}]]^T \quad \forall i, j, m, n \quad (3.21)$$

with $\gamma_w[k_{i,j}, k_{i,j}] = \sigma_w^2[k_{i,j}]$.

The complete VFP-ARMAX model *estimation* and *identification* problem may be then posted as follows: “Given the input – output data records $\{x_{\mathbf{k}}[t]\}_{t=1}^N$, $\{y_{\mathbf{k}}[t]\}_{t=1}^N$ for $\mathbf{k} = k_{1,1}, k_{1,2}, \dots, k_{M_1, M_2}$ and the VFP-ARMAX model set:

$$\begin{aligned} \mathcal{G} \triangleq \{ \mathcal{M}(\bar{\theta}) : A[\mathcal{B}, \mathbf{k}, \bar{\theta}] \cdot y_{\mathbf{k}}[t] &= B[\mathcal{B}, \mathbf{k}, \bar{\theta}] \cdot x_{\mathbf{k}}[t] + C[\mathcal{B}, \mathbf{k}, \bar{\theta}] \cdot e_{\mathbf{k}}[t, \bar{\theta}] \\ | \gamma_w[k_{i,j}, k_{m,n}] &= E\{e_{k_{i,j}}[t, \bar{\theta}]e_{k_{m,n}}[t, \bar{\theta}]\}, \forall i, j, m, n \} \end{aligned}$$

select an element of \mathcal{G} that best fits the measured data.”

In this expression $e_{\mathbf{k}}[t, \bar{\boldsymbol{\theta}}]$ stands for the model’s one-step-ahead prediction error (residual) sequence.

The VFP-ARMAX representation is assumed to satisfy the following conditions:

- CD4. *Stability condition.* The poles of the AR and MA polynomials should lie inside the unit circle $\forall \mathbf{k}$.
- CD5. *Irreducibility condition.* The polynomials $A[\mathcal{B}, \mathbf{k}]$, $B[\mathcal{B}, \mathbf{k}]$, $C[\mathcal{B}, \mathbf{k}]$ are coprime (have no common factors) $\forall \mathbf{k}$.
- CD6. The input signal $x_{\mathbf{k}}[t]$ is stationary, ergodic and persistently exciting with $E\{x_{k_i,j}[t]w_{k_m,n}[t]\} = 0 \forall i, j, m, n$.

The VFP-ARMAX representation of (3.19) may be equivalently expressed in terms of the inverse function operators (Söderström and Stoica 1989) in the following form:

$$\begin{aligned} C^{-1}[\mathcal{B}, \mathbf{k}] \cdot A[\mathcal{B}, \mathbf{k}] \cdot y_{\mathbf{k}}[t] &= C^{-1}[\mathcal{B}, \mathbf{k}] \cdot B[\mathcal{B}, \mathbf{k}] \cdot x_{\mathbf{k}}[t] + w_{\mathbf{k}}[t] \\ \iff I[\mathcal{B}, \mathbf{k}] \cdot y_{\mathbf{k}}[t] &= H[\mathcal{B}, \mathbf{k}] \cdot x_{\mathbf{k}}[t] + w_{\mathbf{k}}[t] \end{aligned} \quad (3.22)$$

with:

$$I[\mathcal{B}, \mathbf{k}] \triangleq 1 + \sum_{j=1}^{\infty} i_j(\mathbf{k})\mathcal{B}^j = C^{-1}[\mathcal{B}, \mathbf{k}] \cdot A[\mathcal{B}, \mathbf{k}] \quad (3.23)$$

$$H[\mathcal{B}, \mathbf{k}] \triangleq 1 + \sum_{j=1}^{\infty} h_j(\mathbf{k})\mathcal{B}^j = C^{-1}[\mathcal{B}, \mathbf{k}] \cdot B[\mathcal{B}, \mathbf{k}] \quad (3.24)$$

with $I[\mathcal{B}, \mathbf{k}]$, $H[\mathcal{B}, \mathbf{k}]$ designating the indicated infinite order inverse function polynomial operators and $\{i_j\}_{j=0}^{\infty}$, $\{h_j\}_{j=0}^{\infty}$ the corresponding \mathbf{k} -varying inverse functions.

3.2.4 The VFP model structure with innovations variance projection

The VFP model structures of the previous subsections model the AR, X and MA parameters $a_i(\mathbf{k})$, $b_i(\mathbf{k})$, $c_i(\mathbf{k})$ as explicit functions of the operating parameter vector \mathbf{k} as belonging to the functional subspaces:

$$\begin{aligned} \mathcal{F}\langle a_i(\mathbf{k}) \rangle &\triangleq \{G_{d_a(1)}(\mathbf{k}), G_{d_a(2)}(\mathbf{k}), \dots, G_{d_a(p_a)}(\mathbf{k})\} \\ \mathcal{F}\langle b_i(\mathbf{k}) \rangle &\triangleq \{G_{d_b(1)}(\mathbf{k}), G_{d_b(2)}(\mathbf{k}), \dots, G_{d_b(p_b)}(\mathbf{k})\} \\ \mathcal{F}\langle c_i(\mathbf{k}) \rangle &\triangleq \{G_{d_c(1)}(\mathbf{k}), G_{d_c(2)}(\mathbf{k}), \dots, G_{d_c(p_c)}(\mathbf{k})\} \end{aligned}$$

Nevertheless there is no explicit function for the innovations sequences (residual) variances $\sigma_w^2(\mathbf{k})$. Thus, the potential user may estimate only the residual variances that belong to the operating parameter vectors \mathbf{k} of the employed data set. Thus, in order to tackle the aforementioned drawback, the projection of the innovations sequences variance to functional subspaces, as in the case of the AR and X parameters, spanned by bivariate polynomial basis functions, is introduced.

By employing the innovations variance functional subspace:

$$\mathcal{F}\langle \sigma_w^2(\mathbf{k}) \rangle \triangleq \{G_{d_s(1)}(\mathbf{k}), G_{d_s(2)}(\mathbf{k}), \dots, G_{d_s(p_s)}(\mathbf{k})\} \quad (3.25)$$

the innovations sequences variances may be projected to the selected basis functions (see Appendix A) as follows:

$$\sigma_w^2(\mathbf{k}) \triangleq \sum_{j=1}^{ps} s_j \cdot G_j(\mathbf{k}) = \mathbf{g}_s^T(\mathbf{k}) \cdot \mathbf{s} \quad (3.26)$$

with \mathbf{s} designating the innovations variance projections coefficients.

3.3 Vector-dependent Functionally Pooled (VFP) model estimation

The model identification problem is usually distinguished into two subproblems: the parameter estimation subproblem (*estimation*) and the model structure selection subproblem (*identification*).

3.3.1 VFP-ARX model estimation

For model estimation the VFP-ARX model of (3.2) – (3.5) may be expressed as follows:

$$y_{\mathbf{k}}[t] + \sum_{i=1}^{na} a_i(\mathbf{k}) \cdot y_{\mathbf{k}}[t-i] = \sum_{i=0}^{nb} b_i(\mathbf{k}) \cdot x_{\mathbf{k}}[t-i] + e_{\mathbf{k}}[t] \quad (3.27)$$

$$e_{\mathbf{k}}[t] \sim \text{iid } \mathcal{N}(0, \sigma_e^2(\mathbf{k})) \quad \mathbf{k} \in \mathbb{R}^2 \quad (3.28)$$

$$a_i(\mathbf{k}) \triangleq \sum_{j=1}^{pa} a_{i,j} \cdot G_{da(j)}(\mathbf{k}), \quad b_i(\mathbf{k}) \triangleq \sum_{j=1}^{pb} b_{i,j} \cdot G_{db(j)}(\mathbf{k}) \quad (3.29)$$

$$E\{e_{k_{i,j}}[t] \cdot e_{k_{m,n}}[t-\tau]\} = \gamma_e[k_{i,j}, k_{m,n}] \cdot \delta[\tau] \quad (3.30)$$

with $e_{\mathbf{k}}[t]$ designating the model's one-step-ahead prediction error or residual (corresponding to $w_{\mathbf{k}}[t]$) with variance $\sigma_e^2(\mathbf{k})$.

In the general case the model's one-step-ahead prediction error (residual) sequences $e_{\mathbf{k}}[t]$ may be contemporaneously correlated, that is $E\{e_{k_{i,j}}[t]e_{k_{i,j}}[t]\} = \sigma_e^2[k_{i,j}]$ and $E\{e_{k_{i,j}}[t]e_{k_{m,n}}[t]\} = \gamma_e[k_{i,j}, k_{m,n}]$, with the model residual cross-section vector defined as $\mathbf{e}[t] \triangleq [e_{k_{1,1}}[t] \dots e_{k_{M_1, M_2}}[t]]^T$. The cross-section vector covariance then is:

$$\Gamma_{\mathbf{e}[t]} = E\{\mathbf{e}[t]\mathbf{e}^T[t]\} = \begin{bmatrix} \sigma_e^2[k_{1,1}] & \gamma_e[k_{1,1}, k_{1,2}] & \dots & \gamma_e[k_{1,1}, k_{M_1, M_2}] \\ \gamma_e[k_{1,2}, k_{1,1}] & \sigma_e^2[k_{1,2}] & \dots & \gamma_e[k_{1,2}, k_{M_1, M_2}] \\ \vdots & \vdots & \ddots & \vdots \\ \gamma_e[k_{M_1, M_2}, k_{1,1}] & \gamma_e[k_{M_1, M_2}, k_{1,2}] & \dots & \sigma_e^2[k_{M_1, M_2}] \end{bmatrix} \quad (3.31)$$

and the covariance matrix for the time instants $t = 1, \dots, N$ is given as:

$$\Gamma_{\mathbf{e}} = \Gamma_{\mathbf{e}[t]} \otimes \mathbf{I}_N.$$

3.3.1.1 A Functionally Pooled (FP) linear regression framework

Consider the general case of VFP-ARX models with “incomplete” (not necessary including consecutive basis functions) functional subspaces. The estimation of the VFP-ARX projection coefficients vector $\boldsymbol{\theta}$, consisting of the corresponding AR and X coefficient of projection vectors \mathbf{a} and \mathbf{b} respectively:

$$\boldsymbol{\theta} \triangleq [\mathbf{a}^T \ ; \ \mathbf{b}^T]^T \quad (3.32)$$

$$\mathbf{a} \triangleq [a_{1,1} \dots a_{1,pa} \dotscolor \dotscolor a_{na,1} \dots a_{na,pa}]^T, \quad \mathbf{b} \triangleq [b_{0,1} \dots b_{0,pb} \dotscolor \dotscolor b_{nb,1} \dots b_{nb,pb}]^T$$

is presently considered based on available signal samples $\{x_{\mathbf{k}}[t]\}_{t=1}^N$, $\{y_{\mathbf{k}}[t]\}_{t=1}^N$ and a selected model structure \mathcal{M} .

The VFP-ARX model of Equation (3.27) may be rewritten as:

$$y_{\mathbf{k}}[t] = \left[\varphi_{AR}^T[t] \otimes \mathbf{g}_{AR}^T(\mathbf{k}) \dotscolor \varphi_X^T[t] \otimes \mathbf{g}_X^T(\mathbf{k}) \right] \cdot \boldsymbol{\theta} + e_{\mathbf{k}}[t] = \boldsymbol{\phi}_{\mathbf{k}}^T[t] \cdot \boldsymbol{\theta} + e_{\mathbf{k}}[t] \quad (3.33)$$

with:

$$\begin{aligned} \varphi_{AR}[t] &\triangleq [-y_{\mathbf{k}}[t-1] \dots -y_{\mathbf{k}}[t-na]]^T \\ \varphi_X[t] &\triangleq [x_{\mathbf{k}}[t] \dots x_{\mathbf{k}}[t-nb]]^T \\ \mathbf{g}_{AR}(\mathbf{k}) &\triangleq [G_{d_a(1)}(\mathbf{k}) \ G_{d_a(2)}(\mathbf{k}) \dots G_{d_a(pa)}(\mathbf{k})]^T \\ \mathbf{g}_X(\mathbf{k}) &\triangleq [G_{d_b(1)}(\mathbf{k}) \ G_{d_b(2)}(\mathbf{k}) \dots G_{d_b(pb)}(\mathbf{k})]^T. \end{aligned}$$

Pooling together the expressions of the VFP-ARX model [Equation (3.33)] corresponding to all operating parameters \mathbf{k} ($k_{1,1}, k_{1,2}, \dots, k_{M_1, M_2}$) considered in the experiments (cross-sectional pooling) yields:

$$\begin{bmatrix} y_{k_{1,1}}[t] \\ y_{k_{1,2}}[t] \\ \vdots \\ y_{k_{1,M_2}}[t] \\ y_{k_{2,1}}[t] \\ \vdots \\ y_{k_{M_1, M_2}}[t] \end{bmatrix} = \begin{bmatrix} \boldsymbol{\phi}_{k_{1,1}}^T[t] \\ \boldsymbol{\phi}_{k_{1,2}}^T[t] \\ \vdots \\ \boldsymbol{\phi}_{k_{1,M_2}}^T[t] \\ \boldsymbol{\phi}_{k_{2,1}}^T[t] \\ \vdots \\ \boldsymbol{\phi}_{k_{M_1, M_2}}^T[t] \end{bmatrix} \cdot \boldsymbol{\theta} + \begin{bmatrix} e_{k_{1,1}}[t] \\ e_{k_{1,2}}[t] \\ \vdots \\ e_{k_{1,M_2}}[t] \\ e_{k_{2,1}}[t] \\ \vdots \\ e_{k_{M_1, M_2}}[t] \end{bmatrix} \implies \mathbf{y}[t] = \boldsymbol{\Phi}[t] \cdot \boldsymbol{\theta} + \mathbf{e}[t]. \quad (3.34)$$

Then, following substitution of the data for $t = 1, \dots, N$ the following expression is obtained:

$$\mathbf{y} = \boldsymbol{\Phi} \cdot \boldsymbol{\theta} + \mathbf{e} \quad (3.35)$$

with:

$$\mathbf{y} \triangleq \begin{bmatrix} \mathbf{y}[1] \\ \vdots \\ \mathbf{y}[N] \end{bmatrix}, \quad \boldsymbol{\Phi} \triangleq \begin{bmatrix} \boldsymbol{\Phi}[1] \\ \vdots \\ \boldsymbol{\Phi}[N] \end{bmatrix}, \quad \mathbf{e} \triangleq \begin{bmatrix} \mathbf{e}[1] \\ \vdots \\ \mathbf{e}[N] \end{bmatrix}.$$

3.3.1.2 Least Squares (LS) based estimation methods

Using the above linear regression framework the simplest possible approach for estimating the projection coefficient vector $\boldsymbol{\theta}$ is based on minimization of the Ordinary Least Squares (OLS) criterion:

$$J^{\text{OLS}}(\boldsymbol{\theta}, Z^{NM_1M_2}) \triangleq \frac{1}{N} \sum_{t=1}^N \mathbf{e}^T[t] \mathbf{e}[t]$$

which leads to the *Ordinary Least Squares (OLS)* estimator:

$$\hat{\boldsymbol{\theta}}^{\text{OLS}} = [\boldsymbol{\Phi}^T \boldsymbol{\Phi}]^{-1} [\boldsymbol{\Phi}^T \mathbf{y}]. \quad (3.36)$$

A more appropriate criterion for the *contemporaneously correlated residual* case is (in view of the Gauss-Markov theorem of Greene (2003)) the Weighted Least Squares (WLS) criterion:

$$J^{\text{WLS}}(\boldsymbol{\theta}, Z^{NM_1M_2}) \triangleq \frac{1}{N} \sum_{t=1}^N \mathbf{e}^T[t] \boldsymbol{\Gamma}_{\mathbf{w}[t]}^{-1} \mathbf{e}[t] = \frac{1}{N} \mathbf{e}^T \boldsymbol{\Gamma}_{\mathbf{w}}^{-1} \mathbf{e}$$

with $\boldsymbol{\Gamma}_{\mathbf{w}[t]}$, $\boldsymbol{\Gamma}_{\mathbf{w}}$ given by (3.10) and (3.11), respectively. This leads to the *Weighted Least Squares (WLS)* estimator:

$$\hat{\boldsymbol{\theta}}^{\text{WLS}} = [\boldsymbol{\Phi}^T \boldsymbol{\Gamma}_{\mathbf{w}}^{-1} \boldsymbol{\Phi}]^{-1} [\boldsymbol{\Phi}^T \boldsymbol{\Gamma}_{\mathbf{w}}^{-1} \mathbf{y}]. \quad (3.37)$$

As the covariance matrix $\boldsymbol{\Gamma}_{\mathbf{w}}$ is practically unavailable, it may be consistently estimated by using the Ordinary Least Squares (OLS) estimator, thus:

$$\hat{\boldsymbol{\Gamma}}_{\mathbf{w}[t]}^{\text{OLS}} = \frac{1}{N} \sum_{t=1}^N \mathbf{e}[t, \hat{\boldsymbol{\theta}}^{\text{OLS}}] \mathbf{e}^T[t, \hat{\boldsymbol{\theta}}^{\text{OLS}}] \quad (3.38)$$

with $\mathbf{e}[t, \hat{\boldsymbol{\theta}}^{\text{OLS}}]$ designating the residuals $\mathbf{e}[t]$ for $\boldsymbol{\theta} = \hat{\boldsymbol{\theta}}^{\text{OLS}}$.

Then:

$$\hat{\boldsymbol{\Gamma}}_{\mathbf{w}}^{\text{OLS}} = \hat{\boldsymbol{\Gamma}}_{\mathbf{w}[t]}^{\text{OLS}} \otimes \mathbf{I}_N. \quad (3.39)$$

The estimator in (3.37) is then expressed as:

$$\hat{\boldsymbol{\theta}}^{\text{WLS}} = [\boldsymbol{\Phi}^T (\hat{\boldsymbol{\Gamma}}_{\mathbf{w}}^{\text{OLS}})^{-1} \boldsymbol{\Phi}]^{-1} [\boldsymbol{\Phi}^T (\hat{\boldsymbol{\Gamma}}_{\mathbf{w}}^{\text{OLS}})^{-1} \mathbf{y}] \quad (3.40)$$

while the final residual covariance matrix is estimated as:

$$\hat{\boldsymbol{\Gamma}}_{\mathbf{w}[t]}^{\text{WLS}} = \frac{1}{N} \sum_{t=1}^N \mathbf{e}[t, \hat{\boldsymbol{\theta}}^{\text{WLS}}] \mathbf{e}^T[t, \hat{\boldsymbol{\theta}}^{\text{WLS}}]. \quad (3.41)$$

In the case of *cross-sectionally uncorrelated* residual sequences with *different variances* ($\sigma_e^2[k_{1,1}] \neq \sigma_e^2[k_{1,2}] \neq \dots \neq \sigma_e^2[k_{M_1, M_2}]$, *groupwise heteroscedasticity*) the residual covariance matrix $\boldsymbol{\Gamma}_{\mathbf{w}}$ for all \mathbf{k} has the same form as (3.12). As the variances are practically unavailable, they may be consistently estimated (White 2001):

$$\hat{\sigma}_e^2(\mathbf{k}, \hat{\boldsymbol{\theta}}^{\text{OLS}}) = \frac{1}{N} \sum_{t=1}^N e_{\mathbf{k}}^2[t, \hat{\boldsymbol{\theta}}^{\text{OLS}}] \quad (3.42)$$

for all \mathbf{k} , with $e_{\mathbf{k}}^2[t, \hat{\boldsymbol{\theta}}^{\text{OLS}}]$ designating the residual sequences obtained by applying OLS. The $\hat{\boldsymbol{\theta}}^{\text{WLS}}$ estimator is then given by (3.40). The final residual variance is estimated as:

$$\hat{\sigma}_w^2(\mathbf{k}) = \hat{\sigma}_e^2(\mathbf{k}, \hat{\boldsymbol{\theta}}^{\text{WLS}}) = \frac{1}{N} \sum_{t=1}^N e_{\mathbf{k}}^2[t, \hat{\boldsymbol{\theta}}^{\text{WLS}}]. \quad (3.43)$$

In the simpler case of *cross-sectionally uncorrelated* residual sequences with *equal variances* ($\sigma_e^2[k_{1,1}] = \sigma_e^2[k_{1,2}] = \dots = \sigma_e^2[k_{M_1, M_2}] = \sigma_e^2$, *groupwise homoscedasticity*) the covariance matrix is $\boldsymbol{\Gamma}_{\mathbf{w}} = \sigma_w^2 \mathbf{I}_{NM_1M_2}$ with $\mathbf{I}_{NM_1M_2}$ designating the unit matrix. In this case the WLS estimator coincides with its OLS counterpart. The residual variance is estimated by (3.43).

Variance projection model form

In the case where the innovations sequences variance is also projected to a functional subspace, an initial estimate of the innovations residual matrix $\mathbf{\Gamma}\mathbf{w}$ may be obtained by using OLS or WLS at a first stage. The coefficients of projection vector to be estimated is defined as:

$$\boldsymbol{\theta} \triangleq [\mathbf{a}^T : \mathbf{b}^T : \mathbf{s}^T]^T = [\boldsymbol{\vartheta}^T : \mathbf{s}^T]^T \quad (3.44)$$

with

$$\mathbf{a} \triangleq [a_{1,1} \dots a_{1,pa} : \dots : a_{na,1} \dots a_{na,pa}]^T, \quad \mathbf{b} \triangleq [b_{0,1} \dots b_{0,pb} : \dots : b_{nb,1} \dots b_{nb,pb}]^T$$

$$\mathbf{s} \triangleq [s_1 \ s_2 \ \dots \ s_{ps}]^T$$

and the basis functions vector defined as:

$$\mathbf{g}_s(\mathbf{k}) \triangleq [G_{d_s(1)}(\mathbf{k}) \ G_{d_s(2)}(\mathbf{k}) \ \dots \ G_{d_s(ps)}(\mathbf{k})]^T. \quad (3.45)$$

The estimation of $\boldsymbol{\theta}$ is achieved in two stages. In the first stage the estimation of $\boldsymbol{\vartheta}$ is achieved via the OLS or WLS as previously presented (see Equations (3.36) and (3.40)). Afterwards, an initial estimate of the innovations residual matrix $\mathbf{\Gamma}\mathbf{w}_{[t]}$ may be obtained via the Equations (3.39) and (3.41).

Then, by taking the diagonal elements of the covariance matrix $\widehat{\mathbf{\Gamma}}\mathbf{w}_{[t]}$, which belong to the cross-section residual variances, in a vector $\boldsymbol{\gamma}$ the following expression is obtained:

$$\boldsymbol{\gamma} = \mathbf{g}_s^T \cdot \mathbf{s} \quad (3.46)$$

which may be solved for the innovations projection coefficients vector \mathbf{s} in a least squares sense.

3.3.1.3 The Maximum Likelihood (ML) estimation method

The complete parameter vector $\bar{\boldsymbol{\theta}}$ is estimated as:

$$\widehat{\boldsymbol{\theta}}^{\text{ML}} \triangleq \arg \max_{\boldsymbol{\theta}} L(\boldsymbol{\theta}, \mathbf{\Gamma}\mathbf{w}_{[t]}/\mathbf{e}) \quad (3.47)$$

with $L(\cdot)$ the natural logarithm of the conditional likelihood function (Söderström and Stoica 1989, Mendel 1995). In the general case of *normally distributed* and *contemporaneously correlated* residuals $e_{\mathbf{k}}[t] \forall \mathbf{k}$ (Söderström and Stoica 1989, p. 198) we have:

$$L(\boldsymbol{\theta}, \mathbf{\Gamma}\mathbf{w}_{[t]}/\mathbf{e}[t_1], \dots, \mathbf{e}[t_N]) = \ln \prod_{t=1}^N p(\mathbf{e}[t]/\boldsymbol{\theta}, \mathbf{\Gamma}\mathbf{w}_{[t]})$$

$$= -\frac{1}{2} \sum_{t=1}^N \mathbf{e}^T[t] \mathbf{\Gamma}\mathbf{w}_{[t]}^{-1} \mathbf{e}[t] - \frac{NM_1M_2}{2} \ln 2\pi - \frac{N}{2} \ln \det\{\mathbf{\Gamma}\mathbf{w}_{[t]}\} \quad (3.48)$$

with $p(\cdot)$ designating the Gaussian probability density function. By setting:

$$\boldsymbol{\Lambda}(\boldsymbol{\theta}) \triangleq \frac{1}{N} \sum_{t=1}^N \mathbf{e}[t, \boldsymbol{\theta}] \mathbf{e}^T[t, \boldsymbol{\theta}] \quad (3.49)$$

(3.48) becomes:

$$L(\boldsymbol{\theta}, \mathbf{\Gamma}\mathbf{w}_{[t]}/\mathbf{e}) = -\frac{N}{2} \text{Tr} \boldsymbol{\Lambda}(\boldsymbol{\theta}) \mathbf{\Gamma}\mathbf{w}_{[t]}^{-1} - \frac{N}{2} \ln \det\{\mathbf{\Gamma}\mathbf{w}_{[t]}\} - \frac{NM_1M_2}{2} \ln 2\pi. \quad (3.50)$$

The first derivative of (3.50) with respect to $\mathbf{\Gamma}_{\mathbf{w}[t]}$ leads to:

$$\frac{\partial L(\boldsymbol{\theta}, \mathbf{\Gamma}_{\mathbf{w}[t]}/\mathbf{e})}{\partial \mathbf{\Gamma}_{\mathbf{w}[t]}} = \frac{N}{2} \mathbf{\Gamma}_{\mathbf{w}[t]}^{-1} \boldsymbol{\Lambda}(\boldsymbol{\theta}) \mathbf{\Gamma}_{\mathbf{w}[t]}^{-1} - \frac{N}{2} \mathbf{\Gamma}_{\mathbf{w}[t]}^{-1} \quad (3.51)$$

and equating it to zero yields $\mathbf{\Gamma}_{\mathbf{w}[t]} = \boldsymbol{\Lambda}(\boldsymbol{\theta})$.

As it may be shown, $L(\boldsymbol{\theta}, \mathbf{\Gamma}_{\mathbf{w}[t]}/\mathbf{e})$ is maximized with respect to $\mathbf{\Gamma}_{\mathbf{w}[t]}$ for $\mathbf{\Gamma}_{\mathbf{w}[t]} = \boldsymbol{\Lambda}(\boldsymbol{\theta})$ and the maximum likelihood estimate of $\boldsymbol{\Lambda}(\boldsymbol{\theta})$ is given by (3.49) for the optimum value of $\boldsymbol{\theta}$ that has to be determined. By replacing $\mathbf{\Gamma}_{\mathbf{w}[t]}$ with $\boldsymbol{\Lambda}(\boldsymbol{\theta})$ in (3.50) yields:

$$L(\boldsymbol{\theta}/\mathbf{e}) = -\frac{NM_1M_2}{2}(\ln 2\pi + 1) - \frac{N}{2} \ln \det\{\boldsymbol{\Lambda}(\boldsymbol{\theta})\}. \quad (3.52)$$

Maximizing equation (3.52) with respect to $\boldsymbol{\theta}$ leads to the *ML estimator*:

$$\hat{\boldsymbol{\theta}}^{\text{ML}} \triangleq \arg \min_{\boldsymbol{\theta}} \det\{\boldsymbol{\Lambda}(\boldsymbol{\theta})\} \quad (3.53)$$

and $\hat{\mathbf{\Gamma}}_{\mathbf{w}[t]} = \boldsymbol{\Lambda}(\hat{\boldsymbol{\theta}}^{\text{ML}}) = \frac{1}{N} \sum_{t=1}^N \mathbf{e}[t, \hat{\boldsymbol{\theta}}^{\text{ML}}] \mathbf{e}^T[t, \hat{\boldsymbol{\theta}}^{\text{ML}}]$. Notice that obtaining $\hat{\boldsymbol{\theta}}^{\text{ML}}$ requires the use of iterative optimization techniques (Söderström and Stoica 1989, Ljung 1999).

In the *heteroscedastic* case we have:

$$\begin{aligned} \ln \det\{\boldsymbol{\Lambda}(\boldsymbol{\theta})\} &= \ln(\sigma_e^2[k_{1,1}, \boldsymbol{\theta}] \cdot \dots \cdot \sigma_e^2[k_{M_1, M_2}, \boldsymbol{\theta}]) \\ &= \ln \sigma_e^2[k_{1,1}, \boldsymbol{\theta}] + \dots + \ln \sigma_e^2[k_{M_1, M_2}, \boldsymbol{\theta}] \\ &= \sum_{k^1=k_1^1}^{k_{M_1}^1} \sum_{k^2=k_1^2}^{k_{M_2}^2} \ln \sigma_e^2(\mathbf{k}, \boldsymbol{\theta}). \end{aligned} \quad (3.54)$$

Maximizing (3.52) with respect to $\boldsymbol{\theta}$ leads to the optimal value of $\boldsymbol{\theta}$ (as in (3.53)) and:

$$\hat{\sigma}_w^2(\mathbf{k}) = \hat{\sigma}_e^2(\mathbf{k}, \hat{\boldsymbol{\theta}}^{\text{ML}}) = \frac{1}{N} \sum_{t=1}^N e_{\mathbf{k}}^2[t, \hat{\boldsymbol{\theta}}^{\text{ML}}]. \quad (3.55)$$

In the *homoscedastic* case we have:

$$\ln \det\{\boldsymbol{\Lambda}(\boldsymbol{\theta})\} = \ln[\sigma_e^2(\boldsymbol{\theta})]^{M_1M_2} = M_1M_2 \ln \sigma_e^2(\boldsymbol{\theta}) \quad (3.56)$$

and the final residual variance is given by (3.55).

Variance projection model form

In this case the complete parameter vector $\bar{\boldsymbol{\theta}}$ defined in Equation (3.44) is estimated as:

$$\hat{\boldsymbol{\theta}}^{\text{ML}} \triangleq \arg \max_{\boldsymbol{\theta}} L(\boldsymbol{\theta}/\mathbf{e}). \quad (3.57)$$

In the general case of normally distributed and heteroscedastic residuals $e_{\mathbf{k}}[t] \forall \mathbf{k}$ we have:

$$\begin{aligned} L(\boldsymbol{\theta}/\mathbf{e}) &= \ln \prod_{t=1}^N p(\mathbf{e}[t]/\boldsymbol{\theta}) = \ln \prod_{k^1=k_1^1}^{k_{M_1}^1} \prod_{k^2=k_1^2}^{k_{M_2}^2} \prod_{t=1}^N p(e_{k_{i,j}}[t]/\boldsymbol{\theta}) \\ &= -\frac{NM_1M_2}{2} \ln 2\pi - \frac{N}{2} \sum_{k^1=k_1^1}^{M_1} \sum_{k^2=k_1^2}^{M_2} \ln(\mathbf{g}_s^T(\mathbf{k}) \cdot \mathbf{s}) - \frac{1}{2} \sum_{k^1=k_1^1}^{M_1} \sum_{k^2=k_1^2}^{M_2} \sum_{t=1}^N \frac{e_{\mathbf{k}}^2[t, \boldsymbol{\theta}]}{\mathbf{g}_s^T(\mathbf{k}) \cdot \mathbf{s}} \end{aligned} \quad (3.58)$$

with $e_{\mathbf{k}}^2[t, \boldsymbol{\vartheta}]$ designating the residual sequence corresponding to vector $\boldsymbol{\vartheta}$, which contains the AR and X coefficients of projection.

Maximization of the log-likelihood function of Equation (3.58) constitutes a non-linear optimization problem that has to be handled via iterative techniques (Söderström and Stoica 1989, Ljung 1999). As it may be observed, both the $\boldsymbol{\vartheta}$ and \mathbf{s} vectors that are to be estimated are included in Equation (3.58). Depending on the dimensions of these vectors, the above non-linear optimization problem may be difficult to handle. Thus, it may be convenient to be accordingly divided and hence, treated via appropriate multistage methods.

3.3.2 VFP-ARMAX model estimation

For model estimation the VFP-ARMAX model of (3.15) – (3.18) may be expressed as follows:

$$y_{\mathbf{k}}[t] + \sum_{i=1}^{na} a_i(\mathbf{k}) \cdot y_{\mathbf{k}}[t-i] = \sum_{i=0}^{nb} b_i(\mathbf{k}) \cdot x_{\mathbf{k}}[t-i] + e_{\mathbf{k}}[t] + \sum_{i=1}^{nc} c_i(\mathbf{k}) \cdot e_{\mathbf{k}}[t-i] \quad (3.59)$$

$$e_{\mathbf{k}}[t] \sim \text{iid } \mathcal{N}(0, \sigma_e^2(\mathbf{k})) \quad \mathbf{k} \in \mathbb{R}^2 \quad (3.60)$$

$$a_i(\mathbf{k}) \triangleq \sum_{j=1}^{pa} a_{i,j} \cdot G_{da(j)}(\mathbf{k}), \quad b_i(\mathbf{k}) \triangleq \sum_{j=1}^{pb} b_{i,j} \cdot G_{db(j)}(\mathbf{k}), \quad c_i(\mathbf{k}) \triangleq \sum_{j=1}^{pc} c_{i,j} \cdot G_{dc(j)}(\mathbf{k}) \quad (3.61)$$

$$E\{e_{k_{i,j}}[t] \cdot e_{k_{m,n}}[t-\tau]\} = \gamma_e[k_{i,j}, k_{m,n}] \cdot \delta[\tau] \quad (3.62)$$

with $e_{\mathbf{k}}[t]$ designating the model's one-step-ahead prediction error or residual (corresponding to $w_{\mathbf{k}}[t]$) with variance $\sigma_e^2(\mathbf{k})$.

In the general case the model's one-step-ahead prediction error (residual) sequences $e_{\mathbf{k}}[t]$ may be contemporaneously correlated, that is $E\{e_{k_{i,j}}[t]e_{k_{i,j}}[t]\} = \sigma_e^2[k_{i,j}]$ and $E\{e_{k_{i,j}}[t]e_{k_{m,n}}[t]\} = \gamma_e[k_{i,j}, k_{m,n}]$, with the model residual cross-section vector defined as $\mathbf{e}[t] \triangleq [e_{k_{1,1}}[t] \dots e_{k_{M_1, M_2}}[t]]^T$. The cross-section vector covariance then is:

$$\begin{aligned} \Gamma_{\mathbf{e}[t]} &= E\{\mathbf{e}[t]\mathbf{e}^T[t]\} \\ &= \begin{bmatrix} \sigma_e^2[k_{1,1}] & \dots & \gamma_e[k_{1,1}, k_{M_1, M_2}] \\ \vdots & \ddots & \vdots \\ \gamma_e[k_{M_1, M_2}, k_{1,1}] & \dots & \sigma_e^2[k_{M_1, M_2}] \end{bmatrix} \end{aligned}$$

and the covariance matrix for the time instants $t = 1, \dots, N$ is given as:

$$\Gamma_{\mathbf{e}} = \Gamma_{\mathbf{e}[t]} \otimes \mathbf{I}_N.$$

3.3.2.1 The Prediction Error (PE) method

Consider the general case of VFP-ARMAX models with “incomplete” (not necessarily including consecutive basis functions) functional subspaces. The estimation of the VFP-ARMAX projection coefficients vector $\boldsymbol{\theta}$, consisting of the corresponding AR, X and MA coefficient of projection vectors \mathbf{a} , \mathbf{b} and \mathbf{c} respectively:

$$\boldsymbol{\theta} \triangleq [\mathbf{a}^T : \mathbf{b}^T : \mathbf{c}^T]^T \quad (3.63)$$

is presently considered based on available signal samples $\{x_{\mathbf{k}}[t]\}_{t=1}^N$, $\{y_{\mathbf{k}}[t]\}_{t=1}^N$ and a selected model structure \mathcal{M} .

The estimation of $\boldsymbol{\theta}$ may be based on the Prediction Error (PE) principle, according to which a quadratic scalar function $f(\cdot)$ (typically positive) of the model's one-step-ahead prediction error $e_{\mathbf{k}}[t, \boldsymbol{\theta}]$ (residual) sequence is minimized with respect to vector $\boldsymbol{\theta}$:

$$\hat{\boldsymbol{\theta}} = \arg \min_{\boldsymbol{\theta}} f(e_{\mathbf{k}}[t, \boldsymbol{\theta}]) \quad (3.64)$$

with $\arg \min$ designating ‘‘argument minimizing’’ and $e_{\mathbf{k}}[t, \boldsymbol{\theta}]$ being provided by the model expression (Söderström and Stoica 1989):

$$\begin{aligned} C[\mathcal{B}, \mathbf{k}, \mathbf{c}]e_{\mathbf{k}}[t, \boldsymbol{\theta}] &= A[\mathcal{B}, \mathbf{k}, \mathbf{a}]y_{\mathbf{k}}[t] - B[\mathcal{B}, \mathbf{k}, \mathbf{b}]x_{\mathbf{k}}[t] \implies \\ \implies e_{\mathbf{k}}[t, \boldsymbol{\theta}] &= I[\mathcal{B}, \mathbf{k}, \mathbf{a}, \mathbf{c}]y_{\mathbf{k}}[t] - H[\mathcal{B}, \mathbf{k}, \mathbf{b}, \mathbf{c}]x_{\mathbf{k}}[t]. \end{aligned} \quad (3.65)$$

In the general case of contemporaneously correlated residuals the criterion to be minimized according to the Gauss-Markov theorem (Ljung 1999, p. 555) is:

$$J_1(\boldsymbol{\theta}, Z^{NM_1M_2}) \triangleq \frac{1}{N} \sum_{t=1}^N e^T[t] \boldsymbol{\Gamma}_{\mathbf{w}[t]}^{-1} e[t] = \frac{1}{N} e^T \boldsymbol{\Gamma}_{\mathbf{w}}^{-1} e \quad (3.66)$$

with $\boldsymbol{\Gamma}_{\mathbf{w}[t]}$ and $\boldsymbol{\Gamma}_{\mathbf{w}}$ the corresponding innovations covariance matrices given by (3.10) and (3.11), respectively. The residual covariance matrix may be estimated as:

$$\hat{\boldsymbol{\Gamma}}_{\mathbf{w}[t]} = \frac{1}{N} \sum_{t=1}^N e[t, \hat{\boldsymbol{\theta}}] e^T[t, \hat{\boldsymbol{\theta}}]. \quad (3.67)$$

In the case of groupwise heteroscedastic residuals, that is serially and cross-sectionally uncorrelated residuals with different variances ($\sigma_e^2[k_{1,1}] \neq \sigma_e^2[k_{1,2}] \neq \dots \neq \sigma_e^2[k_{M_1, M_2}]$), among the different groups of data for all operating conditions, the criterion to be minimized is given by (3.66), from which the best linear unbiased estimator (BLUE) is obtained when the innovations covariance matrix is used as a weighting matrix.

As the innovations covariance matrix $\boldsymbol{\Gamma}_{\mathbf{w}}$ is practically unavailable, it may be replaced by consistent estimates. It is noted that this weighted least squares estimation may be iterated until potential convergence in the projection coefficients vector is achieved.

In the simpler case of groupwise homoscedastic residuals, that is serially and cross-sectionally uncorrelated residuals with equal variances ($\sigma_e^2[k_{1,1}] = \sigma_e^2[k_{1,2}] = \dots = \sigma_e^2[k_{M_1, M_2}]$), the criterion to be minimized is:

$$J_2(\boldsymbol{\theta}, Z^{NM_1M_2}) \triangleq \frac{1}{N} \sum_{t=1}^N e^T[t] e[t]. \quad (3.68)$$

The final residual variance is then estimated as follows:

$$\hat{\sigma}_w^2(\mathbf{k}) = \frac{1}{N} \sum_{t=1}^N e_{\mathbf{k}}^2[t, \hat{\boldsymbol{\theta}}]. \quad (3.69)$$

In the above cases, as well as for ML estimation, the estimation of $\boldsymbol{\theta}$ constitutes a *non-linear* optimization problem as $e_{\mathbf{k}}[t, \boldsymbol{\theta}]$ is a *non-linear* function of the MA parameters. This non-linear problem has to be handled via iterative optimization techniques (Söderström and Stoica 1989, pp. 212–216), which are often amenable to wrong convergence problems due to the potential existence of several local minima in the PE criterion and require high computational burden.

Therefore, a Two Stage Least Squares (2SLS) method (see Fassois (2001), Petsounis and Fassois (2001) and the references therein) is formulated in order to overcome the problems associated with non-linear optimization by exclusively resorting on sequences of linear operations. The 2SLS method may be used as stand-alone or for the initialization of the Prediction Error (PE) and Maximum Likelihood (ML) methods.

3.3.2.2 The two Stage Least Squares (2SLS) method

Stage 1: Inverse function estimation

By replacing the theoretical inverse function operators $I[\mathcal{B}, \mathbf{k}]$ and $H[\mathcal{B}, \mathbf{k}]$ by truncated order versions of orders ni and nh , respectively, (3.65) is rewritten as:

$$I[\mathcal{B}, \mathbf{k}, \mathbf{i}] \cdot y_{\mathbf{k}}[t] = H[\mathcal{B}, \mathbf{k}, \mathbf{h}] \cdot x_{\mathbf{k}}[t] + e_{\mathbf{k}}[t, \mathbf{i}, \mathbf{h}] \quad (3.70)$$

with $e_{\mathbf{k}}[t, \mathbf{i}, \mathbf{h}]$ designating the model residual, \mathbf{i}, \mathbf{h} the vectors containing the projection coefficients of the truncated order operators $I[\mathcal{B}, \mathbf{k}, \mathbf{i}]$, $H[\mathcal{B}, \mathbf{k}, \mathbf{h}]$, respectively.

The estimation of vector $\boldsymbol{\vartheta} = [\mathbf{i}^T : \mathbf{h}^T]^T$ may be then achieved by an Ordinary Least Squares (OLS) estimator as in Equation (3.36), minimizing the model's Residual Sum of Squares (RSS), $e_{\mathbf{k}}^2[t, \mathbf{i}, \mathbf{h}]$, for all available operating parameters \mathbf{k} , by pooling together the data corresponding to the discrete values of \mathbf{k} considered in the experiments (see Equation (3.1)).

Stage 2: Projection Coefficient Estimation

Once the residual series $e_{\mathbf{k}}[t, \hat{\mathbf{i}}, \hat{\mathbf{h}}]$ has been obtained, the VFP-ARMAX model of (3.15), (3.17) is approximated by replacing the past, but not current, values of the prediction error $e_{\mathbf{k}}[t, \boldsymbol{\theta}]$ with the obtained $e_{\mathbf{k}}[t, \hat{\mathbf{i}}, \hat{\mathbf{h}}]$ via Equation (3.65).

Thus, the final projection coefficients vector $\boldsymbol{\theta}$ may be estimated as previously by minimizing the model's Residual Sum of Squares (RSS), $e_{\mathbf{k}}^2[t, \boldsymbol{\theta}]$, for all available operating parameters \mathbf{k} , through the OLS estimator (see Equation (3.36)). The final innovations covariance matrix is estimated using the currently estimated residuals $e_{\mathbf{k}}[t, \hat{\boldsymbol{\theta}}]$ in Equation (3.67).

3.3.2.3 The Maximum Likelihood (ML) estimation method

The complete parameter vector $\bar{\boldsymbol{\theta}}$ is estimated as:

$$\hat{\boldsymbol{\theta}}^{\text{ML}} \triangleq \arg \max_{\boldsymbol{\theta}} L(\boldsymbol{\theta}, \boldsymbol{\Gamma}_{\mathbf{w}[t]} / \mathbf{e})$$

with $L(\cdot)$ the natural logarithm of the conditional likelihood function (Söderström and Stoica 1989, Mendel 1995). In the general case of *normally distributed* and *contemporaneously correlated* residuals $e_{\mathbf{k}}[t] \forall \mathbf{k}$ (Söderström and Stoica 1989, p. 198) we have:

$$\begin{aligned} L(\boldsymbol{\theta}, \boldsymbol{\Gamma}_{\mathbf{w}[t]} / \mathbf{e}[t_1], \dots, \mathbf{e}[t_N]) &= \ln \prod_{t=1}^N p(\mathbf{e}[t] / \boldsymbol{\theta}, \boldsymbol{\Gamma}_{\mathbf{w}[t]}) \\ &= -\frac{1}{2} \sum_{t=1}^N \mathbf{e}^T[t] \boldsymbol{\Gamma}_{\mathbf{w}[t]}^{-1} \mathbf{e}[t] - \frac{NM_1 M_2}{2} \ln 2\pi - \frac{N}{2} \ln \det\{\boldsymbol{\Gamma}_{\mathbf{w}[t]}\} \end{aligned} \quad (3.71)$$

with $p(\cdot)$ designating the Gaussian probability density function. By setting:

$$\mathbf{\Lambda}(\boldsymbol{\theta}) \triangleq \frac{1}{N} \sum_{t=1}^N \mathbf{e}[t, \boldsymbol{\theta}] \mathbf{e}^T[t, \boldsymbol{\theta}] \quad (3.72)$$

it is proved (Söderström and Stoica 1989, p. 202), $L(\boldsymbol{\theta}, \mathbf{\Gamma}_{\mathbf{w}[t]}/e)$ is maximized with respect to $\mathbf{\Gamma}_{\mathbf{w}[t]}$ for $\mathbf{\Gamma}_{\mathbf{w}[t]} = \mathbf{\Lambda}(\boldsymbol{\theta})$ and the maximum likelihood estimate of $\mathbf{\Lambda}(\boldsymbol{\theta})$ is given by (3.72) for the optimum value of $\boldsymbol{\theta}$ that has to be determined.

The *ML estimator* finally is given by:

$$\hat{\boldsymbol{\theta}}^{\text{ML}} \triangleq \arg \min_{\boldsymbol{\theta}} \det\{\mathbf{\Lambda}(\boldsymbol{\theta})\} \quad (3.73)$$

with the final innovations (residual) covariance matrix estimated as:

$$\hat{\mathbf{\Gamma}}_{\mathbf{w}[t]} = \mathbf{\Lambda}(\hat{\boldsymbol{\theta}}^{\text{ML}}) = \frac{1}{N} \sum_{t=1}^N \mathbf{e}[t, \hat{\boldsymbol{\theta}}^{\text{ML}}] \mathbf{e}^T[t, \hat{\boldsymbol{\theta}}^{\text{ML}}].$$

Notice that obtaining $\hat{\boldsymbol{\theta}}^{\text{ML}}$ requires the use of iterative optimization techniques (Söderström and Stoica 1989, pp. 212–216).

In the *heteroscedastic* case we have:

$$\ln \det\{\mathbf{\Lambda}(\boldsymbol{\theta})\} = \sum_{k^1=k_1^1}^{k_{M_1}^1} \sum_{k^2=k_1^2}^{k_{M_2}^2} \ln \sigma_e^2(\mathbf{k}, \boldsymbol{\theta}), \quad (3.74)$$

while the final innovations variance is obtained by:

$$\hat{\sigma}_w^2(\mathbf{k}) = \hat{\sigma}_e^2(\mathbf{k}, \hat{\boldsymbol{\theta}}^{\text{ML}}) = \frac{1}{N} \sum_{t=1}^N e_{\mathbf{k}}^2[t, \hat{\boldsymbol{\theta}}^{\text{ML}}]. \quad (3.75)$$

In the *homoscedastic* case we have:

$$\ln \det\{\mathbf{\Lambda}(\boldsymbol{\theta})\} = \ln[\sigma_e^2(\boldsymbol{\theta})]^{M_1 M_2} = M_1 M_2 \ln \sigma_e^2(\boldsymbol{\theta}) \quad (3.76)$$

and the final residual variance is given by Equation (3.75).

3.4 Vector-dependent Functionally Pooled (VFP) model structure selection and validation

The problem of the VFP model structure selection (structure estimation) for a given basis function family (such as Chebyshev, Legendre and so on), that is model order determination for the AR, X, MA polynomials and determination of their corresponding functional subspaces, is referred to as the model identification problem. For purposes of conceptual simplicity it is presently assumed that $\mathcal{F}\langle a_i(\mathbf{k}) \rangle \triangleq \mathcal{F}\langle AR \rangle$, $\mathcal{F}\langle b_i(\mathbf{k}) \rangle \triangleq \mathcal{F}\langle X \rangle$ and $\mathcal{F}\langle c_i(\mathbf{k}) \rangle \triangleq \mathcal{F}\langle MA \rangle$, while the innovations variance projection is not presently considered.

Model structure selection may be based on customary statistical criteria, such as the Akaike Information Criterion (AIC) and Bayesian Information Criterion (BIC) (Schwarz 1978, Sakellariou 2005, Sakellariou and Fassois 2007, Akaike 1971, Reinsel 1993), that are adapted for the VFP model

structure and penalize model complexity as a counteraction to decreasing quality of fit criterion. Nevertheless, the present work proposes an additional Genetic Algorithm (GA) procedure based on Poulimenos (2007), which may be automated, while it is extremely useful in the case of functional basis dimensionality determination that involves incomplete (that is not necessarily including consecutive basis functions) functional subspaces (see Section 3.6.2).

3.4.1 Model structure selection (identification)

3.4.1.1 Structure selection based on customary criteria

Let $\mathcal{M}(\boldsymbol{\theta})$ be a general VFP-AR(MA)X model describing a given pool of N sample-long excitation-response signals $z^N = (x_{\mathbf{k}}^N, y_{\mathbf{k}}^N)$. Structure estimation for $\mathcal{M}(\boldsymbol{\theta})$ may be based on minimization of the Bayesian Information Criterion (BIC) (Schwarz 1978, Sakellariou 2005, Sakellariou and Fassois 2007),(Ljung 1999, pp. 505–507):

$$\widehat{\mathcal{M}}(\widehat{\boldsymbol{\theta}}) = \arg \min_{\mathcal{M}(\boldsymbol{\theta})} \text{BIC}, \quad \text{BIC} = \frac{1}{NM_1M_2} \left\{ -L(\boldsymbol{\theta}/z^N) + \dim(\boldsymbol{\theta}) \cdot \frac{\ln(NM_1M_2)}{2} \right\} \quad (3.77)$$

with $L(\cdot)$ designating the natural logarithm of the conditional likelihood of the indicated quantity. The Gaussian log-likelihood function of a VFP-ARMAX model $\mathcal{M}(\boldsymbol{\theta})$ given the signal samples z^N may be shown to be:

$$L(\boldsymbol{\theta}/z^N) = -\frac{NM_1M_2}{2}(\ln 2\pi + 1) - \frac{N}{2} \ln \det\{\boldsymbol{\Gamma} \mathbf{e}_{[t]}\}. \quad (3.78)$$

Hence, structure estimation for a VFP-AR(MA)X model $\mathcal{M}(\boldsymbol{\theta})$ based on BIC minimization may be obtained as:

$$\begin{aligned} \widehat{\mathcal{M}}(\widehat{\boldsymbol{\theta}}) &= \arg \min_{\mathcal{M}(\boldsymbol{\theta})} \frac{1}{NM_1M_2} \left\{ \frac{N}{2} \ln \det\{\boldsymbol{\Gamma} \mathbf{e}_{[t]}\} + \dim(\boldsymbol{\theta}) \cdot \frac{\ln(NM_1M_2)}{2} \right\} = \\ &= \arg \min_{\mathcal{M}(\boldsymbol{\theta})} \left\{ \ln \det\{\boldsymbol{\Gamma} \mathbf{e}_{[t]}\} + \dim(\boldsymbol{\theta}) \cdot \frac{\ln(NM_1M_2)}{N} \right\}. \end{aligned} \quad (3.79)$$

Similarly, the Akaike Information Criterion (AIC) (Ljung 1999, pp. 505–507),(Akaike 1971) is defined as follows:

$$\widehat{\mathcal{M}}(\widehat{\boldsymbol{\theta}}) = \arg \min_{\mathcal{M}(\boldsymbol{\theta})} \left\{ NM_1M_2 \ln \det\{\boldsymbol{\Gamma} \mathbf{e}_{[t]}\} + 2 \cdot \dim(\boldsymbol{\theta}) \right\}. \quad (3.80)$$

3.4.1.2 Genetic Algorithm (GA) based structure selection

Given a basis function family, selection of the VFP-AR(MA)X model structure \mathcal{M} refers to the estimation of the set of integers:

$$\mathcal{M} \triangleq \{na, nb, nc, pa, pb, pc, d_a(1), \dots, d_a(pa), d_b(1), \dots, d_b(pb), d_c(1), \dots, d_c(pc)\} \quad (3.81)$$

with na, nb, nc designating the AR, X and MA model orders, pa, pb, pc the dimensionalities of the functional subspaces $\mathcal{F}\langle AR \rangle, \mathcal{F}\langle X \rangle, \mathcal{F}\langle MA \rangle$, respectively, and $d_a(j)$ ($j = 1, \dots, pa$), $d_b(j)$ ($j = 1, \dots, pb$), $d_c(j)$ ($j = 1, \dots, pc$) the basis function indices of the respective subspaces.

Model structure estimation may then be seen as the estimation of the integer-valued model structure vector \mathbf{m} :

$$\mathbf{m} \triangleq \left[na \ nb \ nc \ : \ pa \ pb \ pc \ : \ d_a(1) \ \dots \ d_a(pa) \ : \ d_b(1) \ \dots \ d_b(pb) \ : \ d_c(1) \ \dots \ d_c(pc) \right]_{[6+pa+pb+pc]}^T \quad (3.82)$$

$$na, nb, nc \in \{1, \dots, \bar{n}\}, \quad pa, pb, pc \in \{1, \dots, \bar{p}\} \quad d_a(j), d_b(j), d_c(j) \in \{1, \dots, \bar{d}\} \quad (3.83)$$

with \bar{n} , \bar{p} and \bar{d} designating the maximum considered orders, subspace dimensionalities and basis function indices, respectively, which define the search space of the model structure estimation subproblem.

The estimation of \mathbf{m} may be based on minimization of the Bayesian Information Criterion (BIC – see Section 3.4.1.1):

$$\widehat{\mathbf{m}} = \arg \min_{\mathbf{m}} \text{BIC}(\mathbf{m}). \quad (3.84)$$

However, the model structure \mathcal{M} is not uniquely defined in terms of the model structure vector \mathbf{m} as defined in equation (3.82). As the sub-vectors $[d_a(1) \dots d_a(pa)]$, $[d_b(1) \dots d_b(pb)]$ and $[d_c(1) \dots d_c(pc)]$ correspond to ordered sets of integers, any recombination of them produces equivalent model structures (for example the vectors $[d_a(1) \ d_a(2) \ d_a(3)]$ and $[d_a(1) \ d_a(3) \ d_a(2)]$ correspond to the same model structure). Thus, the model structure \mathcal{M} is *not uniquely defined*, which implies that several global minima with respect to \mathbf{m} exist in the BIC criterion. Moreover, during the optimization procedure the dimension of the model structure vector \mathbf{m} varies, as the subspace dimensionalities pa, pb and pc change. Thus, it is obvious that the definition of the model structure vector \mathbf{m} of equation (3.82), although it seems to be a “natural” choice, is inappropriate for the actual optimization procedure.

In order for the model structure \mathcal{M} to be uniquely defined in terms of vector \mathbf{m} the problem is transformed into a binary variable optimization problem as follows:

$$\mathbf{m}_{bin} \triangleq \left[na \ nb \ nc \ : \ z_{a,1} \ \dots \ z_{a,pa} \ : \ z_{b,1} \ \dots \ z_{b,pb} \ : \ z_{c,1} \ \dots \ z_{c,pc} \right]_{[3+pa+pb+pc]} \quad (3.85)$$

with $z_{a,j}, z_{b,j}$ and $z_{c,j}$ designating binary variables indicating whether the basis function $G_j(\mathbf{k})$ is included in the functional subspace $\mathcal{F}\langle AR \rangle$, $\mathcal{F}\langle X \rangle$ and $\mathcal{F}\langle MA \rangle$, respectively. Thus:

$$z_{a,j} = 1 \iff G_j(\mathbf{k}) \in \mathcal{F}\langle AR \rangle, \quad z_{a,j} = 0 \iff G_j(\mathbf{k}) \notin \mathcal{F}\langle AR \rangle \quad (3.86)$$

and similarly for the variables $z_{b,j}$ and $z_{c,j}$.

By the above procedure the model structure \mathcal{M} is uniquely defined by the fixed-dimension vector \mathbf{m}_{bin} of equation (3.85). Hence, the estimation of \mathbf{m}_{bin} is achieved as:

$$\widehat{\mathbf{m}}_{bin} = \arg \min_{\mathbf{m}_{bin}} \text{BIC}(\mathbf{m}_{bin}). \quad (3.87)$$

The minimization of \mathbf{m}_{bin} constitutes a discrete variable optimization problem, which may be tackled via the use of Genetic Algorithms (GA) (Chipperfield *et al.* n.d.). In order to reduce the dimension of the optimization problem, usually the AR, X and MA model orders are initially selected via customary model order selection techniques (BIC, AIC, RSS/SSS) (Ljung 1999, Fassois 2001, Söderström and Stoica 1989), whereas the functional subspace dimensionalities and indices are selected via the use of GAs.

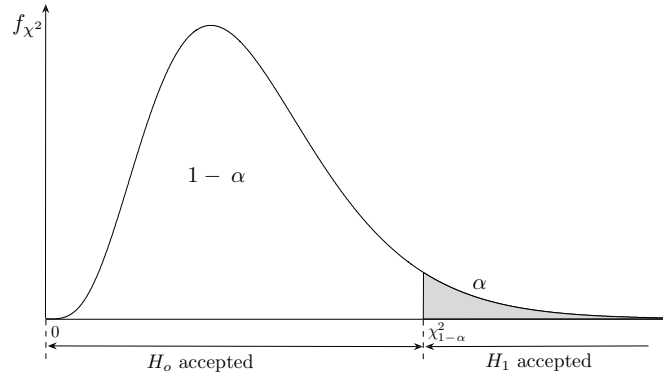


Figure 3.3: Statistical hypothesis testing based on a χ^2 distributed statistic (one-tail test).

3.4.2 Model validation

Once the model estimation and structure selection procedures have been completed, model validation is based on the assumptions concerning the residual sequences $\hat{e}_{\mathbf{k}}[t]$, which, for an accurate model, should be serially uncorrelated (over time), uncorrelated with the input $\forall \mathbf{k}$ (Assumptions CD3 and CD6) and cross-sectionally uncorrelated (over the different operating conditions) in the homoscedastic and heteroscedastic cases.

Testing the hypothesis of residual uncorrelatedness for each \mathbf{k} may be based on the following statistical hypothesis testing procedure:

$$\begin{aligned} H_o &: \rho[\tau] = 0 \quad \tau = 1, 2, \dots, r \quad (\text{white residuals}) \\ H_1 &: \rho[\tau] \neq 0 \quad \text{for some } \tau \quad (\text{not white residuals}) \end{aligned} \quad (3.88)$$

in which $\rho_V[\tau]$ ($\tau = 1, 2, \dots, r$) designates the residual series normalized autocorrelation at lag τ . Under the null hypothesis the following Q statistic follows a chi-square (χ^2) distribution with r degrees of freedom (Box *et al.* 1994, p. 314):

$$Q = N(N+2) \cdot \sum_{\tau=1}^r (N-\tau)^{-1} \hat{\rho}^2[\tau] \sim \chi^2(r) \quad (3.89)$$

in which N designates the residual signal length (in number of samples), $\hat{\rho}[\tau]$ the estimated (sample) normalized autocorrelation at lag τ , and r the maximum lag. This leads to the following test at the α risk level (see Figure 3.3):

$$\begin{aligned} Q < \chi_{1-\alpha}^2(r) &\implies H_o \text{ is accepted} \quad (\text{white residuals}) \\ \text{Else} &\implies H_1 \text{ is accepted} \quad (\text{not white residual}) \end{aligned} \quad (3.90)$$

with $\chi_{1-\alpha}^2(r)$ designating the distribution's $(1-\alpha)$ critical point.

The independence between the inputs and the residuals, and among the residuals of all operating conditions may be based on typical statistical tests using the sample cross-correlation function (Söderström and Stoica 1989, pp. 426–429), (Ljung 1999, p. 531–514), (Reinsel 1993, p. 132–133).

3.5 Asymptotic properties

3.5.1 Consistency analysis

The consistency of the OLS, WLS, ML and PE estimators presented in Section 3.3 is presently investigated. For simplicity, the case of cross-sectionally uncorrelated innovations sequences with different variances (*heteroscedastic case*) is considered. The estimated model is assumed to have the exact structure of the true system, with the latter and the excitation signals satisfying the assumptions CD1 – CD6 of Section 3.2.

For the Least Squares (LS) estimators of Section 3.3.1.2 we have proved the following theorem:

Theorem 3.5.1 (LS estimator consistency) *Let θ_o be the true projection coefficient vector, $w_{\mathbf{k}}[t]$ a white zero mean process with $E\{w_{\mathbf{k}}^2[t]\} = \sigma_w^2(\mathbf{k})$ for every operating point, and $E\{\phi_{\mathbf{k}}[t]\phi_{\mathbf{k}}^T[t]\}$ a nonsingular matrix. Then:*

$$\hat{\theta}_N^{LS} \xrightarrow{a.s.} \theta_o \quad (N \rightarrow \infty)$$

with *a.s.* designating convergence in the almost sure sense (White 2001, pp. 18–19). □

For the proof of Theorem 3.5.1 see Appendix B.

For the Maximum Likelihood (ML) estimators of Sections 3.3.1.3 and 3.3.2.3 we have the following theorem:

Theorem 3.5.2 (ML estimator consistency) *Let $\bar{\theta}_o = [\theta_o^T : \gamma_w[k_{i,j}, k_{m,n}]]$ be the true parameter vector, $w_{\mathbf{k}}[t]$ a normally distributed zero mean white process with $E\{w_{\mathbf{k}}^2[t]\} = \sigma_w^2(\mathbf{k})$ for every operating point, and $E\{\phi_{\mathbf{k}}[t]\phi_{\mathbf{k}}^T[t]\}$ a nonsingular matrix. Then:*

$$\hat{\theta}_N^{ML} \xrightarrow{a.s.} \bar{\theta}_o \quad (N \rightarrow \infty).$$

□

The interested reader may find the proof of Theorem 3.5.2 in Appendix B. This proof is direct extension of the corresponding proof found in Sakellariou (2005, pp. 70–72).

For the Prediction Error (PE) estimator of Section 3.3.2.1 we have the following theorem:

Theorem 3.5.3 (PE estimator consistency) *Let θ_o be the true projection coefficient vector, $e_{\mathbf{k}}[t]$ a white zero mean process with $E\{e_{\mathbf{k}}^2[t]\} = \sigma_e^2(\mathbf{k})$ for every operating point, and $E\{\psi_{\mathbf{k}}[t, \theta_o]\psi_{\mathbf{k}}^T[t, \theta_o]\}$, with $\psi_{\mathbf{k}}[t, \theta_o] = \partial e_{\mathbf{k}}[t, \theta_o]/\partial \theta_o$ a nonsingular matrix. Then:*

$$\hat{\theta}_N^{PE} \xrightarrow{p} \theta_o \quad (N \rightarrow \infty)$$

with *p* designating convergence in probability (White 2001, p. 24). □

The proof of Theorem 3.5.3 is direct extension of the corresponding proof found in Sakellariou (2005, pp. 145–147).

3.5.2 Asymptotic distribution

The asymptotic distribution theorems for the OLS, WLS, ML and PE estimators are presented in the following. For simplicity, the case of cross-sectionally uncorrelated innovations sequences with different variances (*heteroscedastic case*) is considered.

For the Least Squares (LS) estimators of Section 3.3.1.2 we have the following theorem:

Theorem 3.5.4 (LS estimator asymptotic distribution) *Let θ_o be the true projection coefficient vector, $w_{\mathbf{k}}[t]$ a white zero mean process with $E\{w_{\mathbf{k}}^2[t]\} = \sigma_w^2(\mathbf{k})$ for every operating point, and $E\{\phi_{\mathbf{k}}[t]\phi_{\mathbf{k}}^T[t]\}$ a nonsingular matrix. Then:*

$$\sqrt{NM_1M_2}(\hat{\theta} - \theta_o) \xrightarrow{d} \mathcal{N}(\mathbf{0}, \mathbf{P}) \quad (N \rightarrow \infty)$$

with

$$\mathbf{P} = \left[\frac{1}{M_1M_2} \sum_{k^1=k_i^1}^{M_1} \sum_{k^2=k_j^2}^{M_2} \frac{1}{\sigma_w^2(k_{i,j})} E\{\varphi_{k_{i,j}}[t, \theta_o] \varphi_{k_{i,j}}^T[t, \theta_o]\} \otimes \mathbf{G}_{k_{i,j}} \right]^{-1} \quad (3.91)$$

$$= \left[\frac{1}{M_1M_2} \sum_{k^1=k_i^1}^{M_1} \sum_{k^2=k_j^2}^{M_2} \frac{1}{\sigma_w^2(k_{i,j})} E\{\phi_{k_{i,j}}[t, \theta_o] \phi_{k_{i,j}}^T[t, \theta_o]\} \right]^{-1} = [\Phi^T \Gamma_w^{-1} \Phi]^{-1} \quad (3.92)$$

with d designating convergence in distribution (White 2001, pp. 65–66) and $\mathbf{G}_{k_{i,j}} = \mathbf{g}_{k_{i,j}} \mathbf{g}_{k_{i,j}}^T$. \square

The proof of Theorem 3.5.4 is direct extension of the corresponding proof found in Sakellariou (2005, pp. 73–76).

As the covariance matrix \mathbf{P} is unknown, it may be estimated using the available input-output data records of length N via the following estimator:

$$\hat{\mathbf{P}} = \left[\frac{1}{NM_1M_2} \sum_{k^1=k_i^1}^{M_1} \sum_{k^2=k_j^2}^{M_2} \frac{1}{\hat{\sigma}_w^2(k_{i,j})} \sum_{t=1}^N \phi_{k_{i,j}}[t] \phi_{k_{i,j}}^T[t] \right]^{-1} = [\Phi^T \hat{\Gamma}_w^{-1} \Phi]^{-1} \quad (3.93)$$

and

$$\hat{\sigma}_w^2(k_{i,j}) = \frac{1}{N} \sum_{t=1}^N e_{k_{i,j}}^2[t, \hat{\theta}] \quad (3.94)$$

Theorem 3.5.5 (ML estimator asymptotic distribution) *Let $\bar{\theta}_o = [\theta_o^T : \gamma_w[k_{i,j}, k_{m,n}]]$ be the true parameter vector, $w_{\mathbf{k}}[t]$ a normally distributed zero mean white process with $E\{w_{\mathbf{k}}^2[t]\} = \sigma_w^2(\mathbf{k})$ for every operating point, and $E\{\phi_{\mathbf{k}}[t]\phi_{\mathbf{k}}^T[t]\}$ a nonsingular matrix.*

Then the estimate $\hat{\theta}$ follows asymptotically Gaussian distribution with mean $\bar{\theta}_o$ and covariance matrix equal to the Cramer-Rao lower bound (Söderström and Stoica 1989, pp. 560–562):

$$\hat{\theta}_N^{ML} \sim \mathcal{N}(\bar{\theta}, \mathbf{P}^{ML}) \quad (N \rightarrow \infty).$$

\square

The proof of Theorem 3.5.5 is direct extension of the corresponding proof found in Sakellariou (2005, pp. 76–79).

The part of \mathbf{P}^{ML} that corresponds to the coefficients of projection vector $\boldsymbol{\theta}_o$ coincides with the covariance matrix of Equation (3.92) (Söderström and Stoica 1989, p. 562), (Sakellariou 2005, p. 78). Hence, the WLS estimator of Section 3.3.1.2 achieves efficient estimation of the coefficients of projection vector $\boldsymbol{\theta}$ reaching the Cramer-Rao lower bound, when consistent estimates of the true variances $\sigma_w^2(k_{i,j})$ are employed.

Theorem 3.5.6 (PE estimator asymptotic distribution) *Let $\boldsymbol{\theta}_o$ be the true projection coefficient vector, $e_{\mathbf{k}}[t]$ a white zero mean process with $E\{e_{\mathbf{k}}^2[t]\} = \sigma_e^2(\mathbf{k})$ for every operating point, and $E\{\boldsymbol{\psi}_{\mathbf{k}}[t, \boldsymbol{\theta}_o]\boldsymbol{\psi}_{\mathbf{k}}^T[t, \boldsymbol{\theta}_o]\}$, with $\boldsymbol{\psi}_{\mathbf{k}}[t, \boldsymbol{\theta}_o] = \partial e_{\mathbf{k}}[t, \boldsymbol{\theta}_o]/\partial \boldsymbol{\theta}_o$ a nonsingular matrix. Then:*

$$\sqrt{NM_1M_2}(\hat{\boldsymbol{\theta}} - \boldsymbol{\theta}_o) \xrightarrow{d} \mathcal{N}(\mathbf{0}, \mathbf{P}) \quad (N \rightarrow \infty)$$

with

$$\mathbf{P} = \left[\frac{1}{M_1M_2} \sum_{k^1=k_i^1}^{M_1} \sum_{k^2=k_j^2}^{M_2} \frac{1}{\sigma_w^2(k_{i,j})} E\{\boldsymbol{\psi}_{k_{i,j}}[t, \boldsymbol{\theta}_o]\boldsymbol{\psi}_{k_{i,j}}^T[t, \boldsymbol{\theta}_o]\} \right]^{-1} \quad (3.95)$$

with d designating convergence in distribution (White 2001, pp. 65–66). □

The proof of Theorem 3.5.6 is direct extension of the corresponding proof found in Sakellariou (2005, pp. 147–149).

3.6 Monte Carlo Studies

The effectiveness of the VFP model estimation based on the OLS, WLS and ML estimators, along with the model functional subspace selection and model validation is presently examined via two Monte Carlo studies. The first study explores the case of complete functional subspaces, that is subspaces consisting of consecutive basis functions, whereas the second study explores the case of non-complete functional subspaces, that is subspaces not necessarily including consecutive basis functions (see Appendix A).

The first Monte Carlo study, presented in Section 3.6.1, is based on a VFP-ARX(4,1)₆ model with its functional subspace consisting of the first 6 basis functions of Table 3.1 for both the AR and X parameters, thus a complete functional subspace of maximum polynomial degree 2 (quadratic). The second Monte Carlo study, presented in Section 3.6.2, is based on a VFP-ARX(4,1)₉ model with its functional subspace consisting of 9 basis functions for both the AR and X parameters. The first 6 basis are consecutive, thus up to degree 2, while the next three basis functions are the eighth ($P_{2,1}$), ninth ($P_{1,2}$), and thirteenth ($P_{2,2}$) of Table 3.1. Hence, a non-complete functional subspace of maximum polynomial degree 4 is considered.

In both Monte Carlo studies the maximum functional subspace from which the “actual” basis functions are selected is the complete subspace spanned by consecutive basis functions up to fourth degree. Thus, the maximum subspace considered includes all fifteen basis functions of Table 3.1, from which the structure selection algorithms presented in Section 3.4 should choose the true ones.

3.6.1 Test Case I: Complete parameter functional subspace

The first study is based on a VFP-ARX(4,1)₆ model ($na = 4, nb = 1$) with zero delay ($b_0 \neq 0$ in the eXogenous polynomial) and AR, X subspaces consisting of the first 6 basis functions of Table 3.1 for both the AR and X parameters (hence functional dimensionality $pa = pb = 6$). Thus a complete functional subspace of maximum polynomial degree 2 (quadratic) consisting of shifted Chebyshev polynomials of the second kind is employed (Dunkl and Xu 2001). The VFP-ARX(4,1)₆ model employed is presented in the following equation:

$$\left[1 + \sum_{i=1}^4 \sum_{j=1}^6 a_{i,j} G_j(\mathbf{k}) \cdot \mathcal{B}^i \right] \cdot y_{\mathbf{k}}[t] = \left[\sum_{i=0}^1 \sum_{j=1}^6 b_{i,j} G_j(\mathbf{k}) \cdot \mathcal{B}^i \right] x_{\mathbf{k}}[t] + w_{\mathbf{k}}[t] \quad (3.96)$$

with

$$\mathbf{g}_{AR}(\mathbf{k}) = \mathbf{g}_X(\mathbf{k}) = G(\mathbf{k}) = [G_1(\mathbf{k}) \dots G_6(\mathbf{k})]. \quad (3.97)$$

The study consists of 500 runs, in each one of which the first scalar operating parameter takes 20 values ($k_i^1 \in [1, 20]$) and the second scalar operating parameter takes 16 values ($k_j^2 \in [1, 16]$). Thus, each run includes excitation-response signals (of length equal to $N = 1024$ samples) from $M_1 \times M_2 = 320$ operating conditions. Each response is corrupted by random noise at the 10% standard deviation level in accordance with the ARX structure expression (innovations standard deviation over the noise-free response standard deviation equal to 0.1). The innovations sequences corresponding to different operating conditions are cross-sectionally uncorrelated, but characterized by different variances (groupwise heteroscedasticity). Some of the true system coefficients of projection (out of a total of 36) are indicated in Table 3.2. The innovations sequences (residuals) $w_{\mathbf{k}}[t]$ among the different operating conditions are considered cross-sectionally uncorrelated with different variances $\sigma_w^2(\mathbf{k})$ (groupwise heteroscedasticity). In all cases the system output(s) were generated by using a number of mutually independent, random sequences with zero mean and approximately flat spectra acting as system input(s) and random noise.

Model structure estimation consists of the selection of the functional subspace dimensionality p , as well as the specific basis functions (second kind shifted Chebyshev polynomials) that includes. In the case of complete functional subspaces, the problems of functional subspace dimensionality and specific basis function determination coincide. Thus, model structure estimation is achieved via the BIC criterion of Section 3.4.1.1, the Genetic Algorithm (GA) procedure of Section 3.4.1.2, as well as the Residual Sum of Squares normalized by the Series Sum of Squares (RSS/SSS) function:

$$RSS/SSS = \frac{1}{M_1 M_2} \sum_{k^1=k_1^1}^{k_{M_1}^1} \sum_{k^2=k_1^2}^{k_{M_2}^2} \frac{\sum_{t=1}^N e_{k_{i,j}}^2[t]}{\sum_{t=1}^N y_{k_{i,j}}^2[t]} \times 100\%. \quad (3.98)$$

- | | |
|----------------------------------|---|
| 1. constant basis function | $P_{0,0}$ |
| 2. linear basis functions | $P_{1,0}, P_{0,1}$ |
| 3. quadratic basis functions | $P_{2,0}, P_{1,1}, P_{0,2}$ |
| 4. cubic basis functions | $P_{3,0}, P_{2,1}, P_{1,2}, P_{0,3}$ |
| 5. fourth degree basis functions | $P_{4,0}, P_{3,1}, P_{2,2}, P_{1,3}, P_{0,4}$ |

Table 3.1: Functional subspaces of bivariate polynomials up to fourth degree (see Appendix A).

Projection Coefficient	True value	OLS estimate	WLS estimate	ML estimate
$a_{1,1}$	-0.01706	-0.01708 ± 0.00035	-0.01712 ± 0.00023	-0.01711 ± 0.00023
$a_{1,4}$	0.12289	0.12295 ± 0.00025	0.12294 ± 0.00016	0.12294 ± 0.00016
$a_{2,3}$	-0.03889	-0.03896 ± 0.00021	-0.38692 ± 0.00017	-0.38693 ± 0.00017
$a_{2,6}$	-0.00178	-0.00182 ± 0.00019	-0.00178 ± 0.00013	0.00178 ± 0.00013
$a_{3,2}$	-0.02903	-0.02905 ± 0.00021	-0.02903 ± 0.00017	-0.02903 ± 0.00017
$a_{4,1}$	0.59618	0.59622 ± 0.00031	0.59625 ± 0.00021	0.59625 ± 0.00021
$a_{4,4}$	-0.01629	-0.01630 ± 0.00022	-0.01630 ± 0.00014	-0.01630 ± 0.00014
$a_{4,5}$	-0.00605	-0.00600 ± 0.00016	-0.00601 ± 0.00013	-0.00602 ± 0.00013
$b_{0,1}$	0.74531	0.74526 ± 0.00045	0.74527 ± 0.00037	0.74527 ± 0.00038
$b_{0,3}$	0.46714	0.46714 ± 0.00051	0.46711 ± 0.00037	0.46712 ± 0.00037
$b_{1,2}$	0.63756	0.63768 ± 0.00054	0.63760 ± 0.00036	0.63760 ± 0.00035
$b_{1,6}$	0.16828	0.16841 ± 0.00062	0.16830 ± 0.00037	0.16831 ± 0.00037
$E_{AR}(\%)$		0.04066	0.03756	0.03720
$E_X(\%)$		0.01505	0.00451	0.00478
$\left(\frac{RSS}{SSS}\right)\%$		0.30579 ± 0.00036	0.30582 ± 0.00036	0.30582 ± 0.00036

mean estimate ±1 standard deviation

Table 3.2: Indicative Monte Carlo estimation results for the VFP-ARX(4, 1)₆ model (selected coefficients of projection; 500 runs per method; mean estimate ±1 standard deviation).

Model validation is based on the whiteness examination of the residuals for each \mathbf{k} as indicated in Section 3.4.2, as well as on the normalized cross correlation function (MATLAB function *crosscorr.m*) between the inputs and the residuals for all \mathbf{k} and among the residuals of the different operating conditions.

Figure 3.4 depicts the model structure selection criteria of BIC (Figure 3.4a) and RSS/SSS (Figure 3.4b) based on the WLS estimator of Equation (3.40). Both these criteria reach an approximate plateau for $p = 6$, nevertheless the BIC criterion, which penalizes the functional basis overdetermination, attains its minimum value for $p = 6$, while the RSS/SSS criterion keeps decreasing (see Figure 3.4a and Figure 3.4b close-ups, respectively). Moreover, Table 3.3 presents the GA details for the functional subspace selection task (see Equation (3.87)). The GA achieved excellent results, as it was able to select the correct functional subspace with 100% success based on 500 Monte Carlo runs (500 correct selections out of 500 Monte Carlo runs).

Figure 3.5 presents indicative model validation results based on the Q test of Section 3.4.2. The Q statistics estimated from the model residuals of each cross-section for one Monte Carlo run are depicted versus the $M_1 \times M_2 = 20 \times 16 = 320$ cross-sections. The dashed red line represents the critical point at the $\alpha = 0.01$ (99%) confidence level. The model is valid when the test statistics lie below the critical point (dashed red line) with respect to the selected confidence level. It is evident from Figure 3.5 that the VFP-ARX(4, 1)₆ is valid, as the Q statistic of all the model residual sequences, except three, lie below the critical point.

Population size	Elite count	Crossover fraction	Fitness function tolerance
30	3	0.7	10^{-4}

Table 3.3: Genetic Algorithm (GA) details for functional subspace determination of Test Case I.

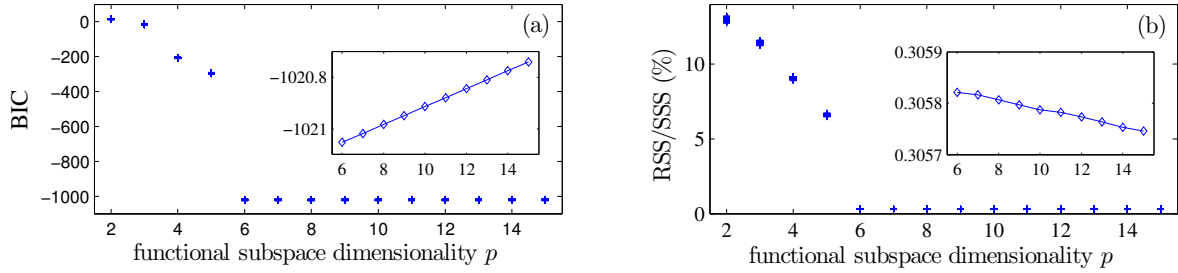


Figure 3.4: Functional basis dimensionality selection criteria for VFP-ARX(4,1)₆ models: (a) BIC and (b) RSS/SSS versus functional subspace dimensionality p (each cross (+) designates the value from one simulation run; 500 runs for each p). In the close-ups inside each plot the mean values for each p are depicted (\diamond).

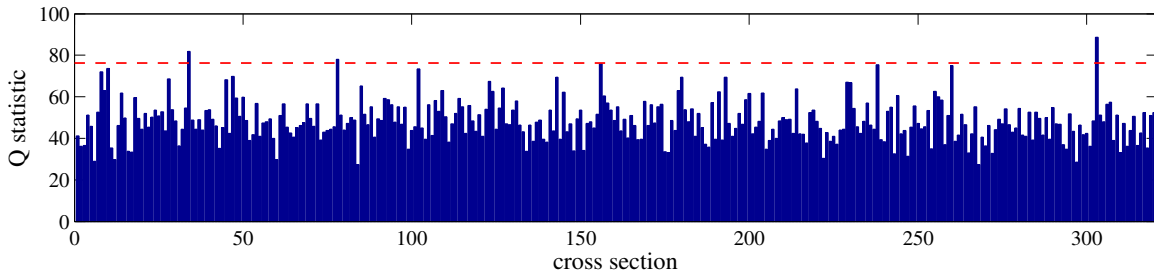


Figure 3.5: Indicative VFP-ARX(4,1)₆ model validation results: Q statistic versus the 320 cross-section at the $\alpha = 0.01$ (99%) confidence level (maxlag = 50). The model is valid when the test statistics lie below the critical point (dashed red line) for the selected confidence level.

Indicative VFP-ARX(4,1)₆ model validation results are shown in Figure 3.6. The top line plots depict the cross correlation function between various model residual series $e_{\mathbf{k}}[t]$ pairs at the $\alpha = 0.01$ (99%) confidence level, while the bottom line plots depict the cross correlation function between various input $x_{\mathbf{k}}$ and residual series $e_{\mathbf{k}}[t]$ pairs at the $\alpha = 0.01$ (99%) confidence level (maxlag = 50). In all cases it is evident that both the residual series pairs (top line plots), as well as the input-residual pairs (bottom line plots) are uncorrelated, a fact that proves the validity of the model. In all cases the residuals are found serially uncorrelated, cross-sectionally uncorrelated and uncorrelated with the inputs. Thus, model identification (in terms of functional subspace selection) is accurately achieved, as the true number of functional basis, as well as the specific basis functions in the case of the GA based method, is correctly estimated in all 500 runs.

Next, interval parameter estimates are constructed for the OLS, WLS and ML estimators, along with normalized (percentage) aggregate AR and X errors corresponding to the mean estimated values:

$$E_{AR} \triangleq \frac{\|\hat{\mathbf{a}} - \mathbf{a}^o\|}{\|\mathbf{a}^o\|} \%, \quad E_X \triangleq \frac{\|\hat{\mathbf{b}} - \mathbf{b}^o\|}{\|\mathbf{b}^o\|} \% \quad (3.99)$$

with \mathbf{a} and \mathbf{b} designating the AR and X coefficient of projection vectors, respectively, the superscript “ o ” designating the true value of these vectors, and $\|\mathbf{a}\| = \sum_i |a_i|$, $\|\mathbf{b}\| = \sum_i |b_i|$.

The Monte Carlo estimation summarized results for all the considered estimators are presented in Table 3.2 (mean estimates \pm standard deviations). All three estimators achieve excellent agreement between the true values of the projection coefficients (theoretical values) and the corresponding OLS, WLS and ML estimates. Moreover, the standard deviations of the estimated projection coefficients are extremely low with those belonging to the WLS and ML estimators giving even better results, as it was expected. Notice though that the WLS is initialized by the OLS variances (QR decomposition), while

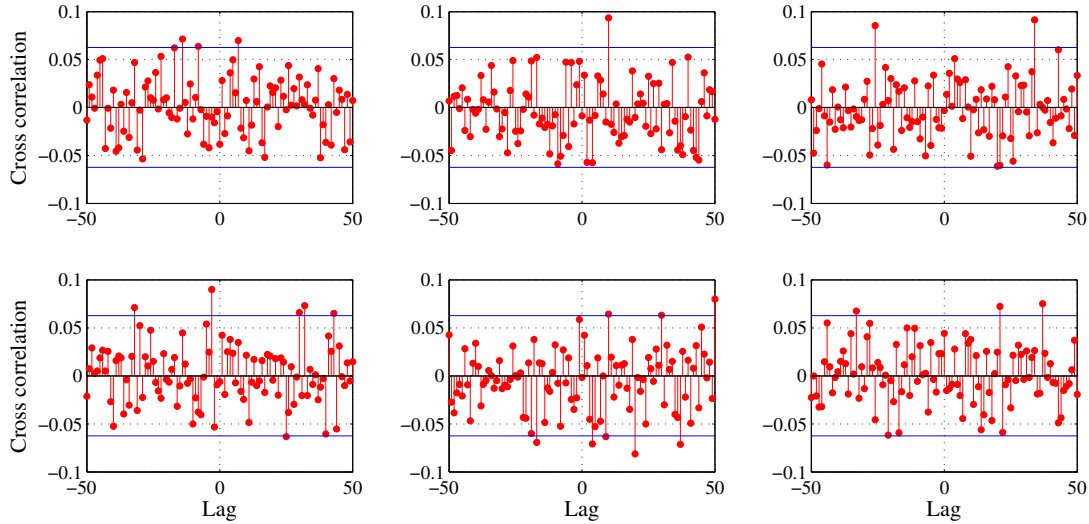


Figure 3.6: Indicative VFP-ARX(4,1)₆ model validation results: (a) top line plots: cross correlation function between various model residual series $e_{\mathbf{k}}[t]$ pairs at the $\alpha = 0.01$ (99%) confidence level, and (b) bottom line plots: cross correlation function between various input $x_{\mathbf{k}}$ and residual series $e_{\mathbf{k}}[t]$ pairs at the $\alpha = 0.01$ (99%) confidence level (max lag = 50).

the ML estimator is initialized by the WLS estimates, and makes use of the Gauss-Newton non-linear optimization scheme (Söderström and Stoica 1989) (maximum number of iterations 100; maximum number of function evaluations 5000; termination tolerance of the loss function 10^{-2} ; termination tolerance of the estimated parameters 10^{-8}). Furthermore, the extremely low AR and X aggregate errors and the low values of the RSS/SSS over the 500 runs constitute further indications for the excellent performance of the estimators.

Indicative parameter estimation results are pictorially depicted in Figure 3.7. The true values of the coefficient of projection are shown in dashed red lines, while the sample mean estimates (blue lines) from the 500 runs along with their 95% confidence intervals (± 1.96 sample standard deviations) are shown in shaded boxes. The dashed blue lines correspond to the theoretical WLS ± 1.96 standard deviations based the asymptotic distribution analysis of Section 3.5.2 as estimated via Equation (3.93). As it may be readily observed, all the results are very accurate. All three methods provide essentially unbiased estimates, with the WLS and ML methods expectedly providing better accuracy for the coefficients of projection (smaller standard deviations, thus narrower confidence intervals). Moreover, notice the excellent agreement between the theoretical and estimated WLS standard deviations of the projection coefficients, which demonstrates the validity of the asymptotic distribution analysis.

Figure 3.8 presents indicative VFP-ARX(4,1)₆ model residual sequence variance results by the OLS, WLS and ML estimators. The sample mean estimates and the ± 1.96 sample standard deviations (shaded boxes), along with the corresponding residual true values (dashed red lines) are presented. Again there is excellent agreement between the true and the estimated residual variances.

Figure 3.9 depicts the a_1 model parameter (first parameter of the AR polynomial) surface versus the k^1 and k^2 series of the operating parameters for the true (theoretical) system, as well as for the mean OLS, WLS, and ML estimates over the 500 runs. Furthermore, Figure 3.10 depicts the b_0 model parameter (first parameter of the X polynomial) surface versus the k^1 and k^2 series for the true (theoretical) system and the mean OLS, WLS, and ML estimates. In both cases the agreement of the true parameter surfaces with the corresponding estimated is evident.

The VFP-ARX(4,1)₆ second natural frequency ω_2 and first damping ratio ζ_1 surfaces versus

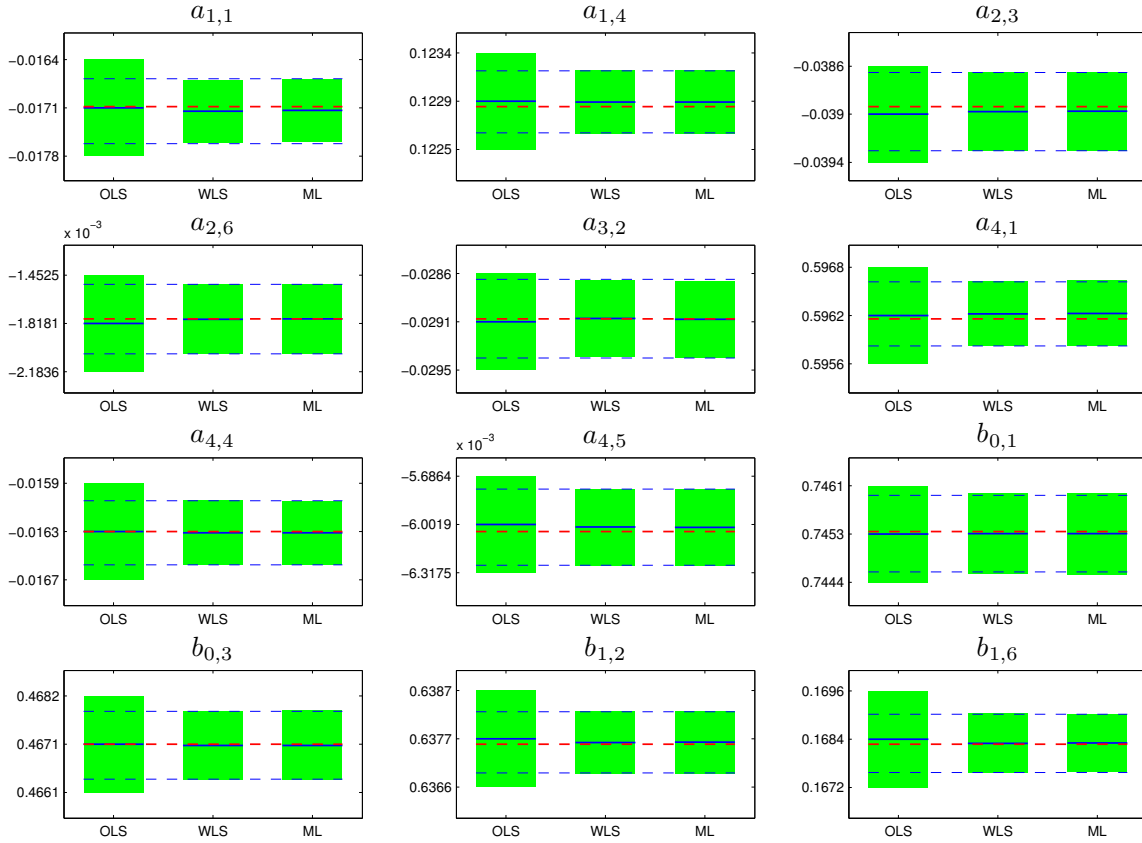


Figure 3.7: Indicative VFP-ARX(4,1)₆ projection coefficient estimation results by the OLS, WLS and ML methods (Monte Carlo results based on 500 runs per method): sample mean estimates ± 1.96 sample standard deviations (shaded boxes), along with the corresponding true values (dashed red lines - - -) and the theoretical asymptotic WLS standard deviations (dashed blue lines - - -), which coincide with the Cramer-Rao lower bound.

the k^1 and k^2 series are shown in Figures 3.11 and 3.12, respectively, for the true (theoretical) system and the mean OLS, WLS, and ML estimates over 500 runs. Notice the excellent agreement between the true and the estimated quantities in all cases. Moreover, Figure 3.13 depicts the VFP-ARX(4,1)₆ based frequency response magnitude surfaces versus frequency and k^1 operating parameter, with the k^2 operating parameter set to k_3^2 , for the true system, as well as for those estimated based on the mean projection coefficient vectors of the considered estimators. Again, the excellent agreement between the true and the estimated quantities is evident.

The complexity of each estimation method is assessed based on the CPU (Central Processing Unit) time required by a typical computer (Intel Core 2 Duo P8400 @ 2.26 GHz, 4 GB RAM, Linux Operating System) for achieving a single Monte Carlo run. The obtained relative times are presented in Table 3.4. Thus, indicative results for the required CPU times for the OLS, WLS, and ML estimation methods are 5.63, 11.85 and 54.13 seconds, respectively (also see Table 3.4), in order to obtain the final estimates of the same coefficients of projection vector for a single run of this test case. Notice, that the ML estimation method requires, as expected, the greatest amount of CPU time, while the OLS method the least. Nevertheless, the WLS method achieves an acceptable CPU time while it yields the most accurate estimation results.

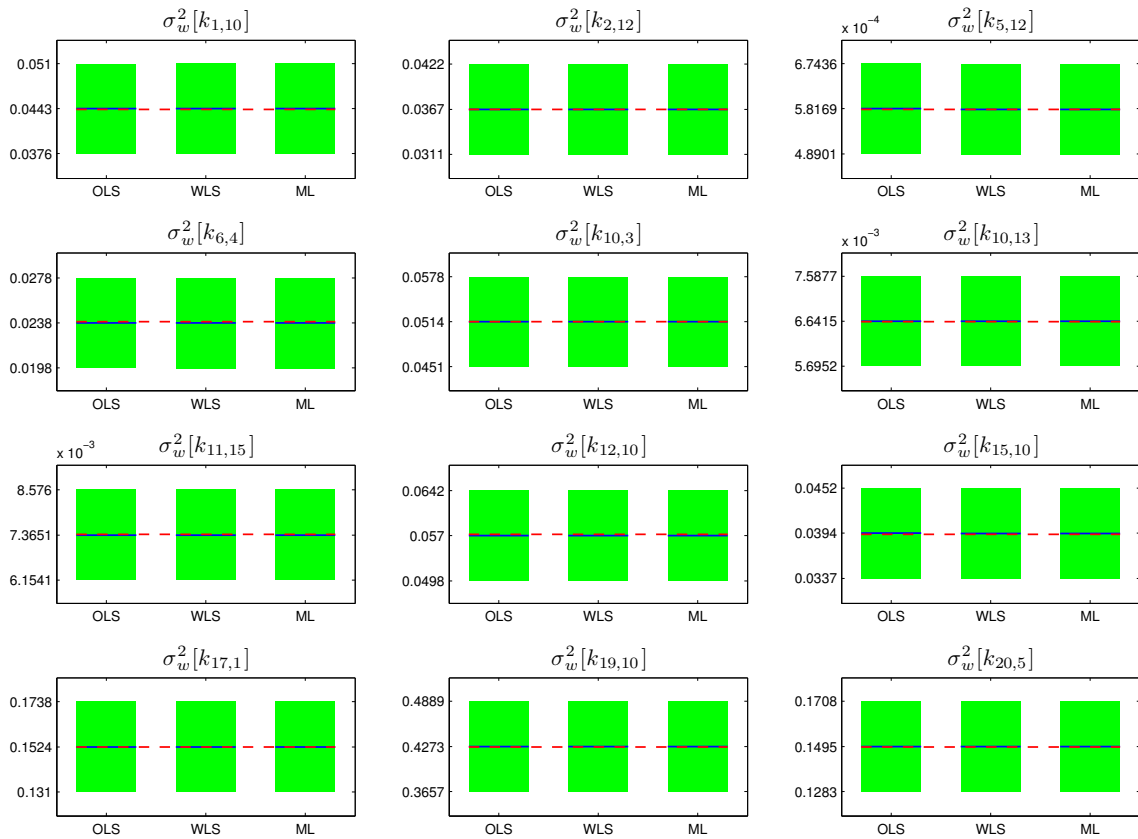


Figure 3.8: Indicative VFP-ARX(4, 1)₆ residual variance results by the OLS, WLS and ML methods (Monte Carlo results based on 500 runs per method): sample mean estimates ± 1.96 sample standard deviations (shaded boxes), along with the corresponding residual true values (dashed red lines - - -).

3.6.2 Test Case II: Non-complete parameter functional subspace

The second study is based on a VFP-ARX(4, 1)₉ model ($na = 4, nb = 1$) with zero delay ($b_0 \neq 0$ in the eXogenous polynomial) and AR, X subspaces consisting of 9 basis functions (hence functional dimensionality $pa = pb = 9$). The first 6 basis are consecutive, thus up to polynomial degree 2, while the next three basis functions are the eighth ($P_{2,1}$), ninth ($P_{1,2}$), and thirteenth ($P_{2,2}$) (see Table 3.1). Hence, a non-complete functional subspace of maximum polynomial degree 4 (quadratic) consisting of shifted Chebyshev polynomials of the second kind is considered. The VFP-ARX(4, 1)₉ model employed is presented in the following equation:

CPU time (%)			
Test Case	OLS	WLS	ML
I	10.41	21.89	100
II	12.93	17.55	100
Relative CPU time (%)			
I/II	51.32	79.50	63.73

Table 3.4: CPU and relative (test case I/test case II) CPU times for the OLS, WLS and ML estimation methods as percentage of the total ML time (single run).

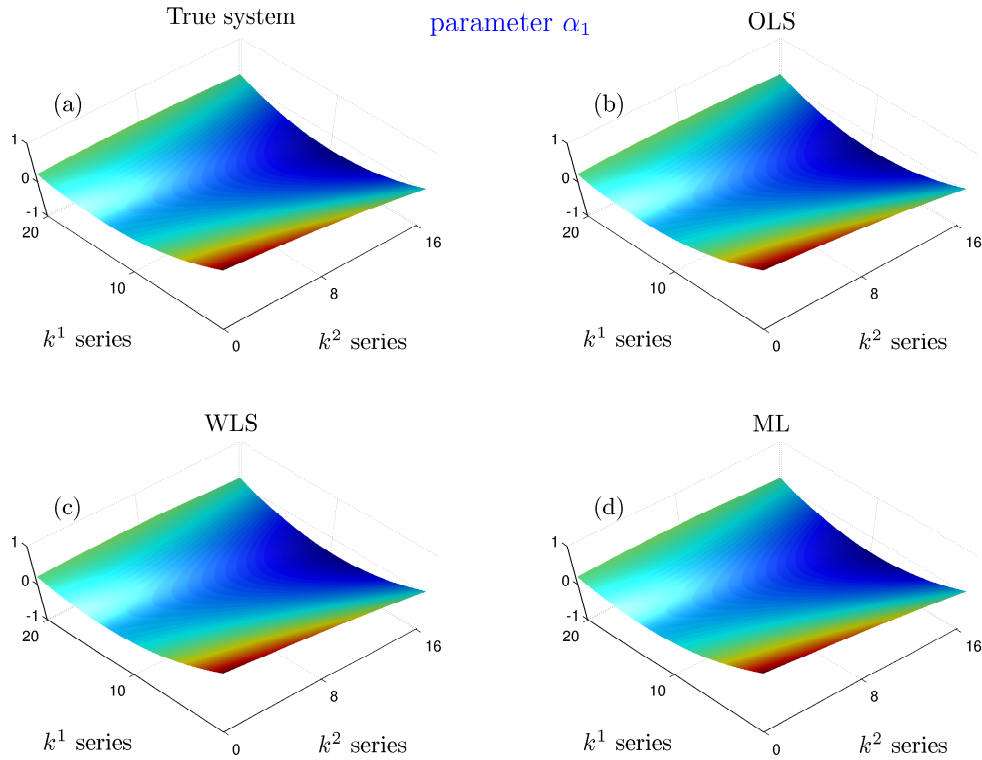


Figure 3.9: VFP-ARX(4,1)₆ model parameter a_1 estimates versus k^1 and k^2 series: (a) true system, (b) mean OLS estimate, (c) mean WLS estimate and (d) mean ML estimate (mean parameters over 500 runs).

Projection Coefficient	True value	OLS estimate	WLS estimate	ML estimate
$a_{1,1}$	-0.07969	-0.07971 ± 0.00036	-0.07974 ± 0.00023	-0.07973 ± 0.00023
$a_{1,4}$	0.10437	0.10436 ± 0.00024	0.10440 ± 0.00017	0.10441 ± 0.00017
$a_{1,9}$	-0.00474	-0.00475 ± 0.00015	-0.00476 ± 0.00011	-0.00476 ± 0.00011
$a_{2,3}$	-0.01176	-0.01176 ± 0.00023	-0.01178 ± 0.00014	-0.01178 ± 0.00014
$a_{2,5}$	0.01810	0.01811 ± 0.00020	0.01810 ± 0.00013	0.01810 ± 0.00013
$a_{3,1}$	-0.08097	-0.08089 ± 0.00028	-0.08088 ± 0.00021	-0.08087 ± 0.00021
$a_{3,4}$	0.06493	0.06490 ± 0.00021	0.06491 ± 0.00016	0.06491 ± 0.00016
$a_{3,9}$	-0.00922	-0.00922 ± 0.00015	-0.00922 ± 0.00011	-0.00922 ± 0.00011
$a_{4,5}$	-0.00511	-0.00508 ± 0.00018	-0.00509 ± 0.00013	-0.00509 ± 0.00013
$b_{0,1}$	0.74531	0.74526 ± 0.00063	0.74527 ± 0.00044	0.74526 ± 0.00044
$b_{0,7}$	0.71846	0.71844 ± 0.00069	0.71847 ± 0.00039	0.71848 ± 0.00039
$b_{1,2}$	0.63756	0.63756 ± 0.00077	0.63761 ± 0.00046	0.63761 ± 0.00044
E_{AR} (%)		0.04680	0.04094	0.04073
E_X (%)		0.00773	0.00367	0.00402
$\left(\frac{RSS}{SSS}\right)$ (%)		0.30665 ± 0.00041	0.30673 ± 0.00041	0.30673 ± 0.00041

mean estimate ±1 standard deviation

Table 3.5: Indicative Monte Carlo estimation results for the VFP-ARX(4,1)₉ model (selected coefficients of projection; 500 runs per method; mean estimate ±1 standard deviation).

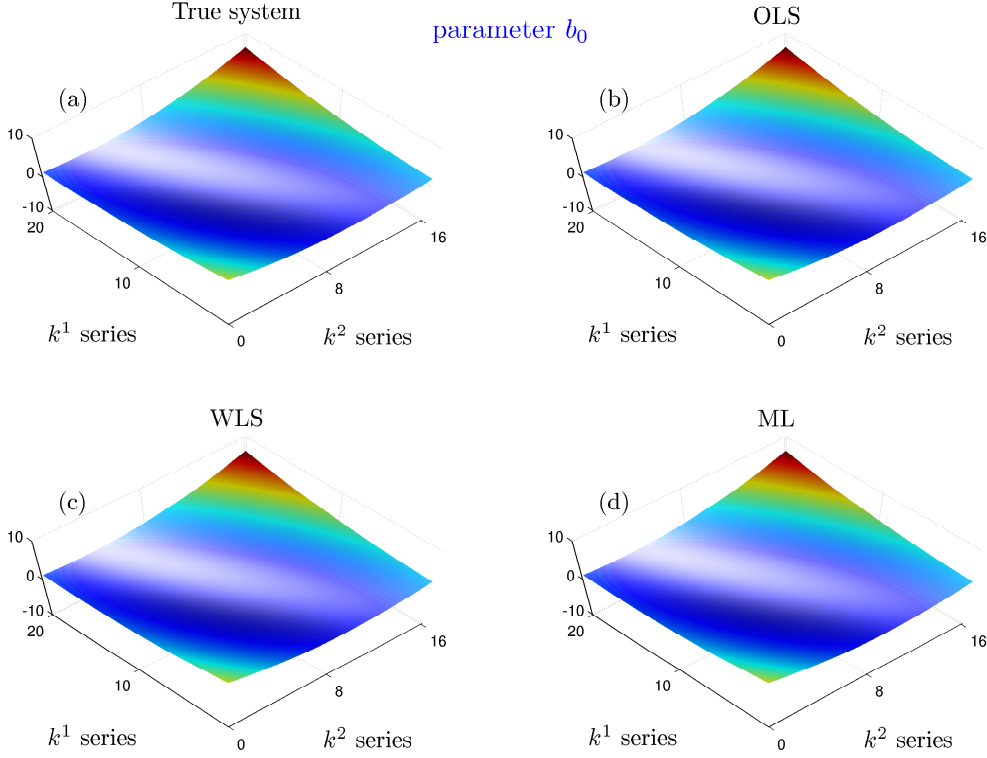


Figure 3.10: VFP-ARX(4, 1)₆ model parameter b_0 estimates versus k^1 and k^2 series: (a) true system, (b) mean OLS estimate, (c) mean WLS estimate and (d) mean ML estimate (mean parameters over 500 runs).

$$\left[1 + \sum_{i=1}^4 \sum_{j=1}^9 a_{i,j} G_j(\mathbf{k}) \cdot \mathcal{B}^i \right] \cdot y_{\mathbf{k}}[t] = \left[\sum_{i=0}^1 \sum_{j=1}^9 b_{i,j} G_j(\mathbf{k}) \cdot \mathcal{B}^i \right] x_{\mathbf{k}}[t] + w_{\mathbf{k}}[t] \quad (3.100)$$

with

$$\mathbf{g}_{AR}(\mathbf{k}) = \mathbf{g}_X(\mathbf{k}) = G(\mathbf{k}) = [G_1(\mathbf{k}) \dots G_6(\mathbf{k}) G_8(\mathbf{k}) G_9(\mathbf{k}) G_{13}(\mathbf{k})]. \quad (3.101)$$

The study consists of 500 runs, in each one of which the first scalar operating parameter takes 20 values ($k_i^1 \in [1, 20]$) and the second scalar operating parameter takes 16 values ($k_j^2 \in [1, 16]$). Thus, each run includes excitation-response signals (of length equal to $N = 1024$ samples) from $M_1 \times M_2 = 320$ operating conditions. Each response is corrupted by random noise at the 10% standard deviation level in accordance with the ARX structure expression (innovations standard deviation over the noise-free response standard deviation equal to 0.1). The innovations sequences (residuals) $w_{\mathbf{k}}[t]$ corresponding to different operating conditions are cross-sectionally uncorrelated, but characterized by different variances (groupwise heteroscedasticity). Some of the true system coefficients of projection (out of a total of 36) are indicated in Table 3.5. In all cases the system output(s) were generated by using a number of mutually independent, random sequences with zero mean and approximately flat spectra acting as system input(s) and random noise.

Model structure estimation consists of the selection of the functional subspace dimensionality p , as well as the specific basis functions (second kind shifted Chebyshev polynomials) that includes. In the case of complete functional subspaces, the problems of functional subspace dimensionality and specific basis function determination coincide, nevertheless this is not the case for this test case. As the functional subspace is non-complete, model structure estimation may not be achieved via the BIC criterion, as in this case it would require the estimation of a huge number of models, covering all

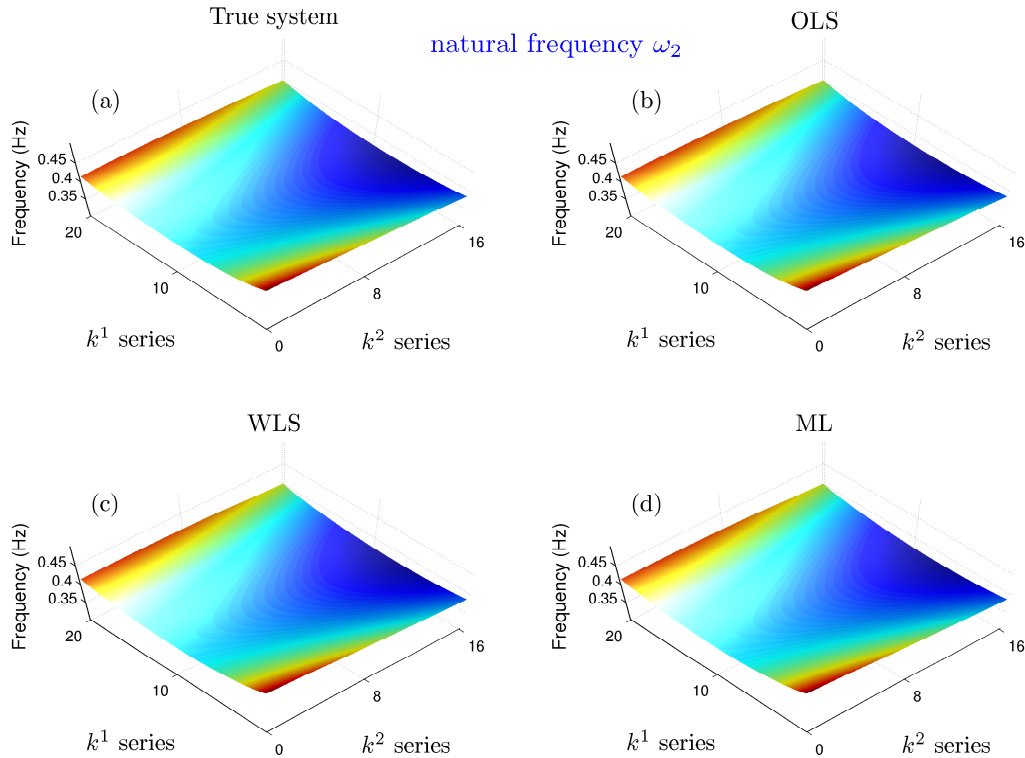


Figure 3.11: VFP-ARX(4,1)₆ second natural frequency ω_2 versus k^1 and k^2 series: (a) true system, (b) mean OLS estimate, (c) mean WLS estimate and (d) mean ML estimate (mean parameters over 500 runs).

the possible subspace dimensionalities, as well as the potential specific basis functions. Hence, the Genetic Algorithm (GA) procedure of Section 3.4.1.2 is necessary in this case in order to tackle the model structure estimation task.

Model validation is based on the whiteness examination of the residuals for each \mathbf{k} as indicated in Section 3.4.2, as well as on the normalized cross correlation function (MATLAB function *crosscorr.m*) between the inputs and the residuals for all \mathbf{k} and among the residuals of the different operating conditions.

Table 3.3 presents the GA details for the functional subspace selection task (see Equation (3.87)). The GA achieved very good results, as it was able to select the correct functional subspace dimensionality ($p = 9$) along with the correct specific basis functions (see Equation (3.101)) with 89% success based on 500 Monte Carlo runs (446 correct selections out of 500 Monte Carlo runs). These results could be improved if the population size is increased. Nevertheless, this would cause an increase in CPU time, thus the potential user should decide on the exact GA optimization parameters based on the available time, computational cost and desired estimation accuracy. For instance, the GA of test case I whose optimization details are presented in Table 3.3 needs about 100 seconds for a single run with a population size of 30, while the GA of this test case (see Table 3.6) with a population size of 140 needs about 600 seconds, hence 600% more CPU time.

Population size	Elite count	Crossover fraction	Fitness function tolerance
140	10	0.7	10^{-4}

Table 3.6: Genetic Algorithm (GA) details for functional subspace determination of Test Case II.

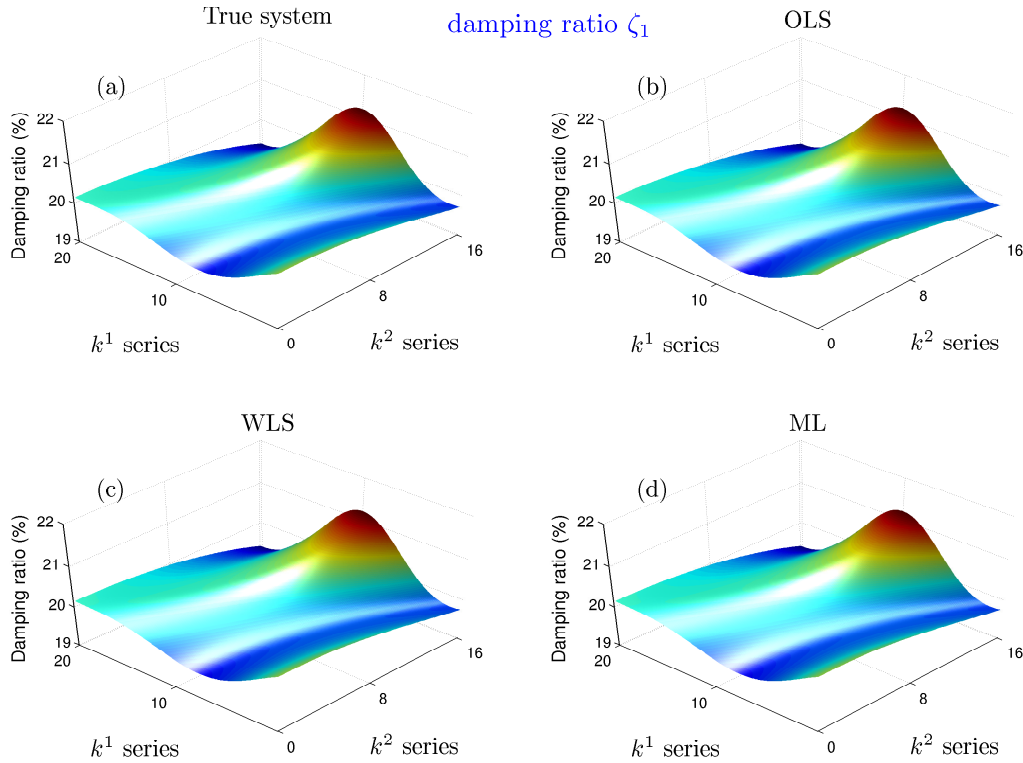


Figure 3.12: VFP-ARX(4, 1)₆ first damping ratio ζ_1 versus k^1 and k^2 series: (a) true system, (b) mean OLS estimate, (c) mean WLS estimate and (d) mean ML estimate (mean parameters over 500 runs).

Indicative VFP-ARX(4, 1)₉ model validation results are shown in Figure 3.14. The top line plots depict the cross correlation function between various model residual series $e_{\mathbf{k}}[t]$ pairs at the $\alpha = 0.01$ (99%) confidence level, while the bottom line plots depict the cross correlation function between various input $x_{\mathbf{k}}$ and residual series $e_{\mathbf{k}}[t]$ pairs at the $\alpha = 0.01$ (99%) confidence level (max lag = 50). In all cases it is evident that both the residual series pairs (top line plots), as well as the input-residual pairs (bottom line plots) are uncorrelated, a fact that proves the validity of the model. In all cases the residuals are found serially uncorrelated, cross-sectionally uncorrelated and uncorrelated with the inputs. Thus, model identification (in terms of functional subspace selection) is accurately achieved, as the true number of functional basis, as well as the specific basis functions in the case of the GA based method, is correctly estimated in all 500 runs.

The Monte Carlo estimation summarized results for the considered estimators are presented in Table 3.5 (mean estimates \pm standard deviations). All three estimators achieve excellent agreement between the true values of the projection coefficients (theoretical values) and the corresponding OLS, WLS and ML estimates. Moreover, the standard deviations of the estimated projection coefficients are extremely low with those belonging to the WLS and ML estimators giving even better results, as it was expected. Notice though that the WLS is initialized by the OLS variances (QR decomposition), while the ML estimator is initialized by the WLS estimates, and makes use of the Gauss-Newton non-linear optimization scheme (Söderström and Stoica 1989) (maximum number of iterations 100; maximum number of function evaluations 5000; termination tolerance of the loss function 10^{-2} ; termination tolerance of the estimated parameters 10^{-8}). Furthermore, the extremely low AR and X aggregate errors and the low values of the RSS/SSS over the 500 runs constitute further indications for the excellent performance of the estimators.

Indicative parameter estimation results are pictorially depicted in Figure 3.15. The true values

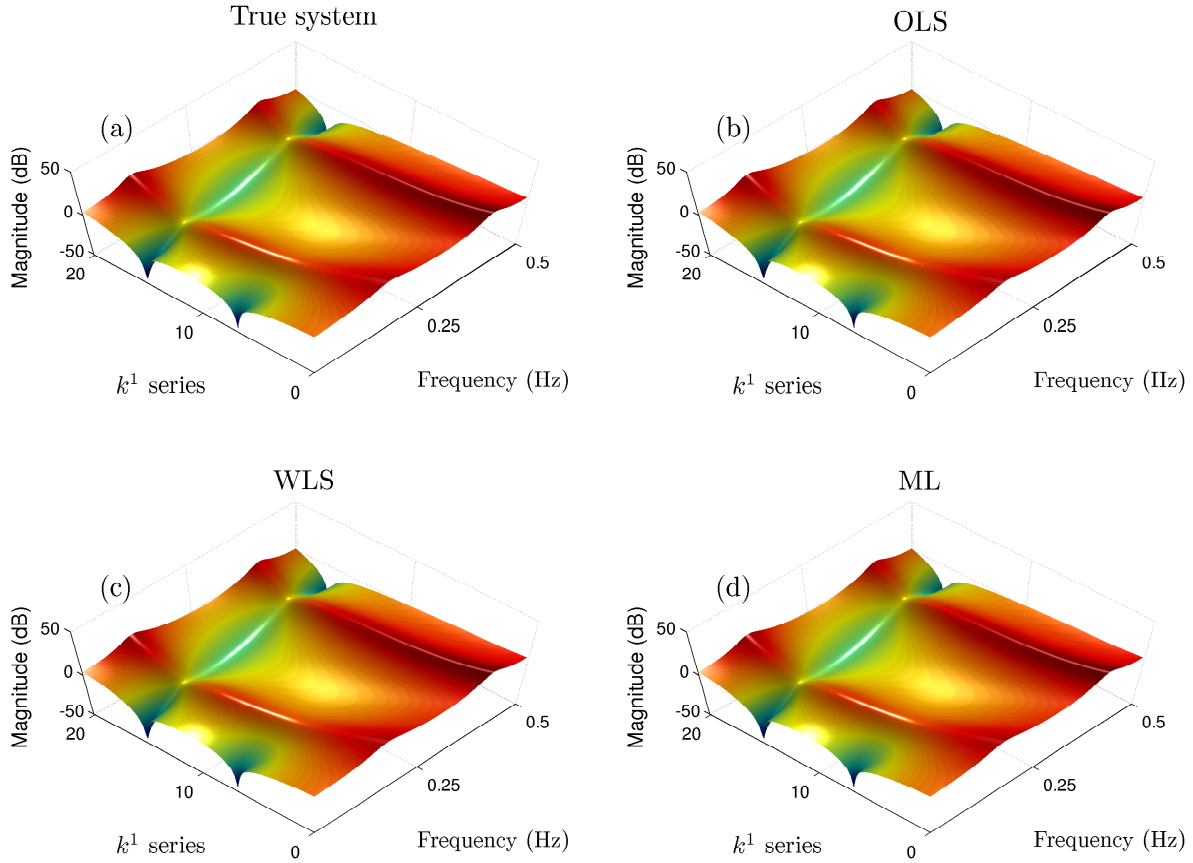


Figure 3.13: VFP-ARX(4, 1)₆ based frequency response magnitude versus frequency and k^1 series (k^2 is set to k_3^2): (a) true system, (b) mean OLS estimate, (c) mean WLS estimate and (d) mean ML estimate (mean parameters over 500 runs).

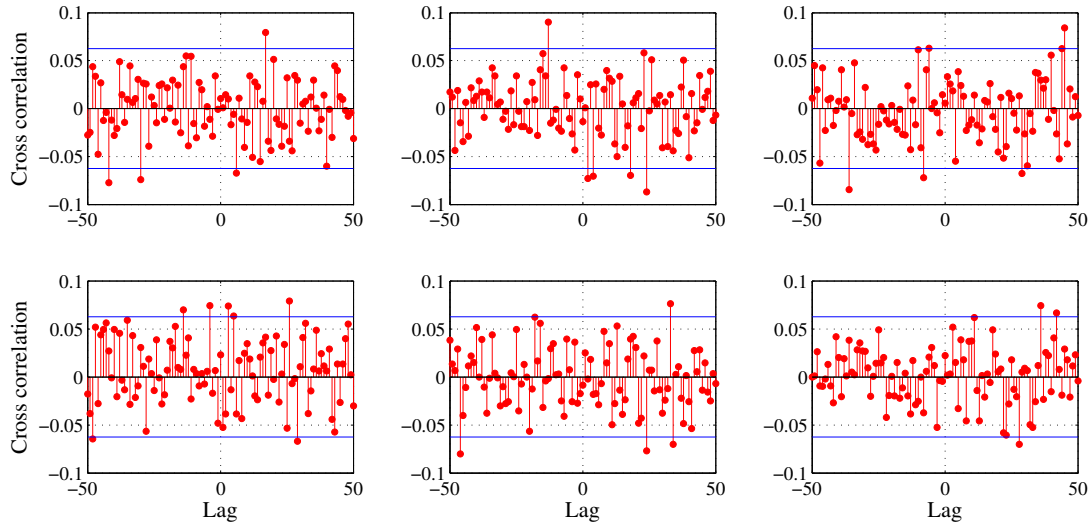


Figure 3.14: Indicative VFP-ARX(4, 1)₉ model validation results: (a) top line plots: cross correlation function between various model residual series $e_{\mathbf{k}}[t]$ pairs at the $\alpha = 0.01$ (99%) confidence level, and (b) bottom line plots: cross correlation function between various input $x_{\mathbf{k}}$ and residual series $e_{\mathbf{k}}[t]$ pairs at the $\alpha = 0.01$ (99%) confidence level (max lag = 50).

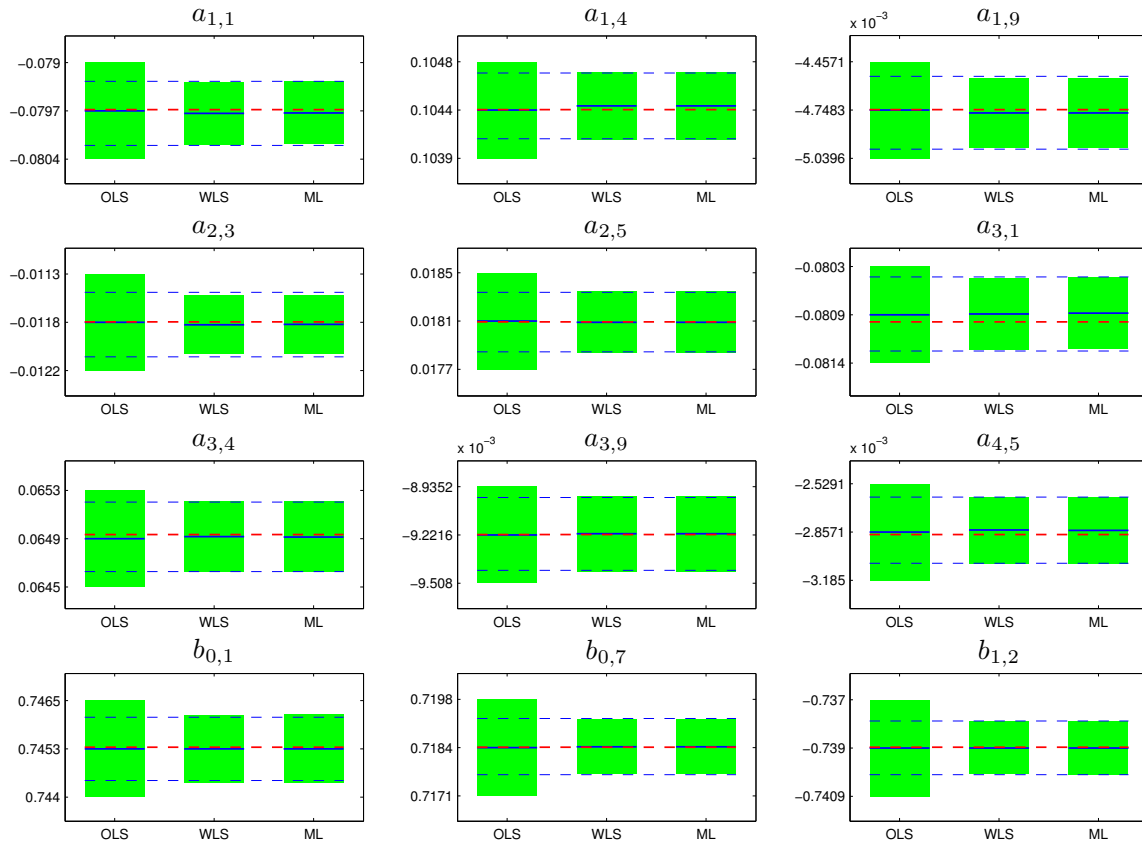


Figure 3.15: Indicative VFP-ARX(4,1)₉ projection coefficient estimation results by the OLS, WLS and ML methods (Monte Carlo results based on 500 runs per method): sample mean estimates ± 1.96 sample standard deviations (shaded boxes), along with the corresponding true values (dashed red lines - - -) and the theoretical asymptotic WLS standard deviations (dashed blue lines - - -), which coincide with the Cramer-Rao lower bound.

of the coefficient of projection are shown in dashed red lines, while the sample mean estimates (blue lines) from the 500 runs along with their 95% confidence intervals (± 1.96 sample standard deviations) are shown in shaded boxes. The dashed blue lines correspond to the theoretical WLS ± 1.96 standard deviations based the asymptotic distribution analysis of Section 3.5.2 as estimated via Equation (3.93). As it may be readily observed, all the results are very accurate. All three methods provide essentially unbiased estimates, with the WLS and ML methods expectedly providing better accuracy for the coefficients of projection (smaller standard deviations, thus narrower confidence intervals). Moreover, notice the excellent agreement between the theoretical and estimated WLS standard deviations of the projection coefficients, which demonstrates the validity of the asymptotic distribution analysis.

Figure 3.16 presents indicative VFP-ARX(4,1)₉ model residual sequence variance results by the OLS, WLS and ML estimators. The sample mean estimates and the ± 1.96 sample standard deviations (shaded boxes), along with the corresponding residual true values (dashed red lines) are presented. Again there is excellent agreement between the true and the estimated residual variances.

Figure 3.17 depicts the a_4 model parameter (fourth parameter of the AR polynomial) surface versus the k^1 and k^2 series of the operating parameters for the true (theoretical) system, as well as for the mean OLS, WLS, and ML estimates over the 500 runs. Furthermore, Figure 3.18 depicts the b_0 model parameter (first parameter of the X polynomial) surface versus the k^1 and k^2 series for the true (theoretical) system and the mean OLS, WLS, and ML estimates. In both cases the agreement of the true parameter surfaces with the corresponding estimated is evident.

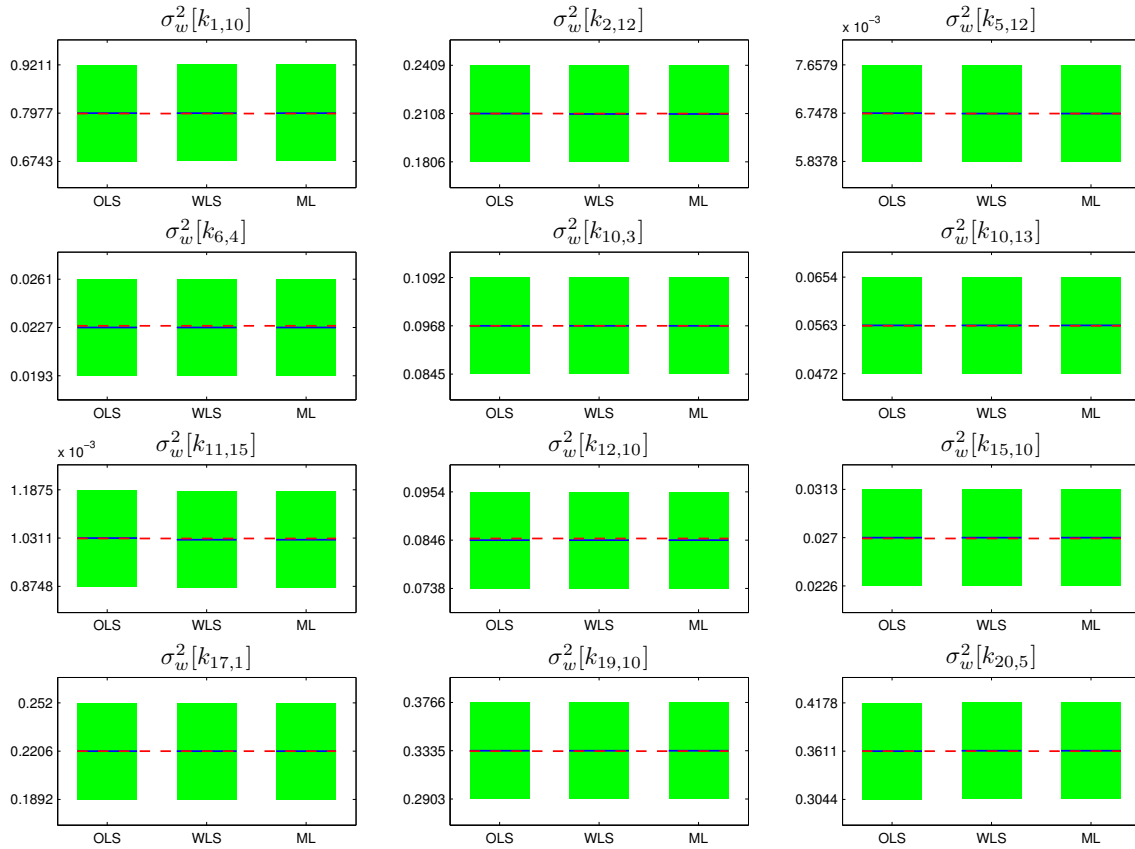


Figure 3.16: Indicative VFP-ARX(4, 1)₉ residual variance results by the OLS, WLS and ML methods (Monte Carlo results based on 500 runs per method): sample mean estimates ± 1.96 sample standard deviations (shaded boxes), along with the corresponding residual true values (dashed red lines - - -).

The VFP-ARX(4, 1)₉ second natural frequency ω_2 and first damping ratio ζ_1 surfaces versus the k^1 and k^2 series are shown in Figures 3.19 and 3.20, respectively, for the true (theoretical) system and the mean OLS, WLS, and ML estimates over 500 runs. Notice the excellent agreement between the true and the estimated quantities in all cases. Moreover, Figure 3.21 depicts the VFP-ARX(4, 1)₉ based frequency response magnitude surfaces versus frequency and k^2 operating parameter, with the k^1 operating parameter set to k_8^1 , for the true system, as well as for those estimated based on the mean projection coefficient vectors of the considered estimators. Again, the excellent agreement between the true and the estimated quantities is evident.

The complexity of each estimation method is assessed based on the CPU time required by a typical computer (Intel Core 2 Duo P8400 @ 2.26 GHz, 4 GB RAM, Linux Operating System) for achieving a single Monte Carlo run. The obtained relative times are presented in Table 3.4. Notice, that the ML estimation method requires, as expected, the greatest amount of CPU time, while the OLS method the least. Nevertheless, the WLS method achieves an acceptable CPU time while it yields the most accurate estimation results. The relative CPU time needed for the estimation of the VFP-ARX(4, 1)₆ and VFP-ARX(4, 1)₉ models with six and nine basis functions, respectively, for the considered parameter estimation methods are presented in Table 3.4. Notice that the greatest increase in CPU time is obtained for the WLS method, while the OLS method exhibits the smallest increase.

Additional results for both Monte Carlo studies may be found in Appendix C.

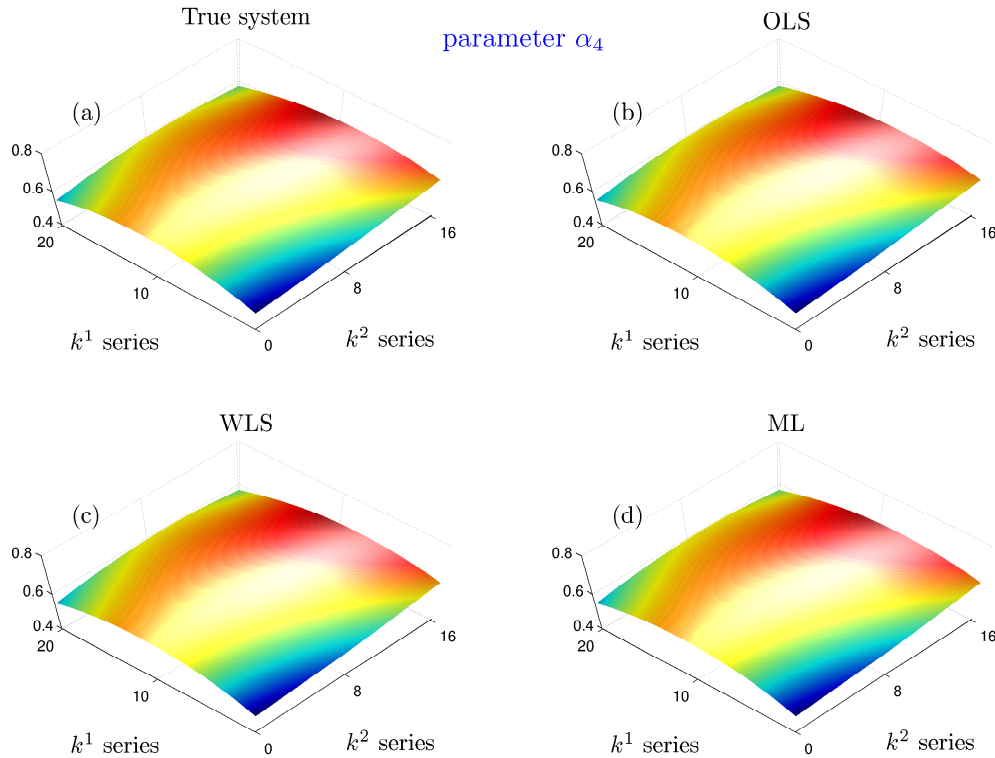


Figure 3.17: VFP-ARX(4, 1)₉ model parameter a_4 estimates versus k^1 and k^2 series: (a) true system, (b) mean OLS estimate, (c) mean WLS estimate and (d) mean ML estimate (mean parameters over 500 runs).

3.7 Concluding Remarks

In many applications a system operates under a variety of operating conditions which affect its dynamics, with each condition kept constant for a single commission cycle. The goal of this chapter was the identification of stochastic systems under multiple operating conditions via Vector-dependent Functionally Pooled (FP) models. This chapter's work is based on the novel *Functional Pooling (FP) framework*, which has been recently introduced by the Stochastic Mechanical Systems & Automation group of the Mechanical Engineering & Aeronautics Department at the University of Patras (Sakellariou 2005, Kopsaftopoulos and Fassois 2006a, Sakellariou and Fassois 2007, Sakellariou and Fassois 2007b).

Thus, the third chapter of the thesis addressed the problem of identifying a globally valid and parsimonious system model based on input-output data records obtained under a sample of operating conditions characterized by more than one parameters (for instance operating temperature and humidity). The problem was tackled within the novel Functional Pooling (FP) framework that postulates proper global models of the ARX and ARMAX types, data pooling techniques, and statistical parameter estimation. Corresponding Vector-dependent Functionally Pooled (VFP) ARX and ARMAX models were postulated, and proper estimators of the Least Squares (LS), Maximum Likelihood (ML), and Prediction Error (PE) types were developed. Model structure estimation was achieved via customary criteria (Bayesian Information Criterion) and a novel Genetic Algorithm (GA) based procedure. The strong consistency of the VFP-ARX least squares and maximum likelihood estimators is established, whereas the effectiveness of the complete estimation and identification method is demonstrated via two Monte Carlo studies.

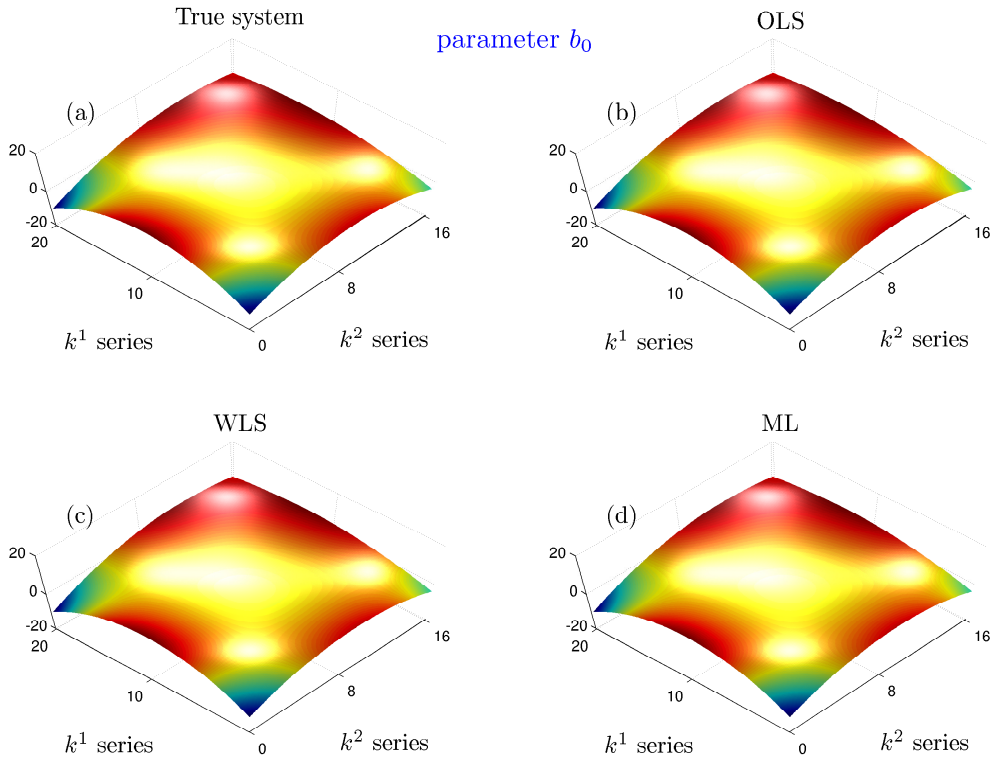


Figure 3.18: VFP-ARX(4, 1)₉ model parameter b_0 estimates versus k^1 and k^2 series: (a) true system, (b) mean OLS estimate, (c) mean WLS estimate and (d) mean ML estimate (mean parameters over 500 runs).

The main issues addressed in this chapter are the following:

- Extension of the FP models employing a scalar operating parameter to the Vector-dependent FP models employing the *operating parameter vector*.
- Model structure estimation was achieved via customary criteria such as the BIC and the AIC, as well as via a Genetic Algorithm (GA) based procedure.
- A new VFP model form was introduced in which the innovations sequence variance is projected to a functional subspace, so now it may be available not only for the sample of operating conditions (available data records), but it may be efficiently estimated for all the potential admissible operating conditions, thus for all the potential operating parameter vectors \mathbf{k} .
- The strong consistency of the least squares and the maximum likelihood estimators was established, as well as the asymptotic distribution of the all the considered estimators.
- Assessment of the proposed estimators and structure selection procedures via two Monte Carlo studies, investigating both the cases of complete and non-complete functional subspaces.
- Discussion of the estimators main features, as well as their corresponding computational times.

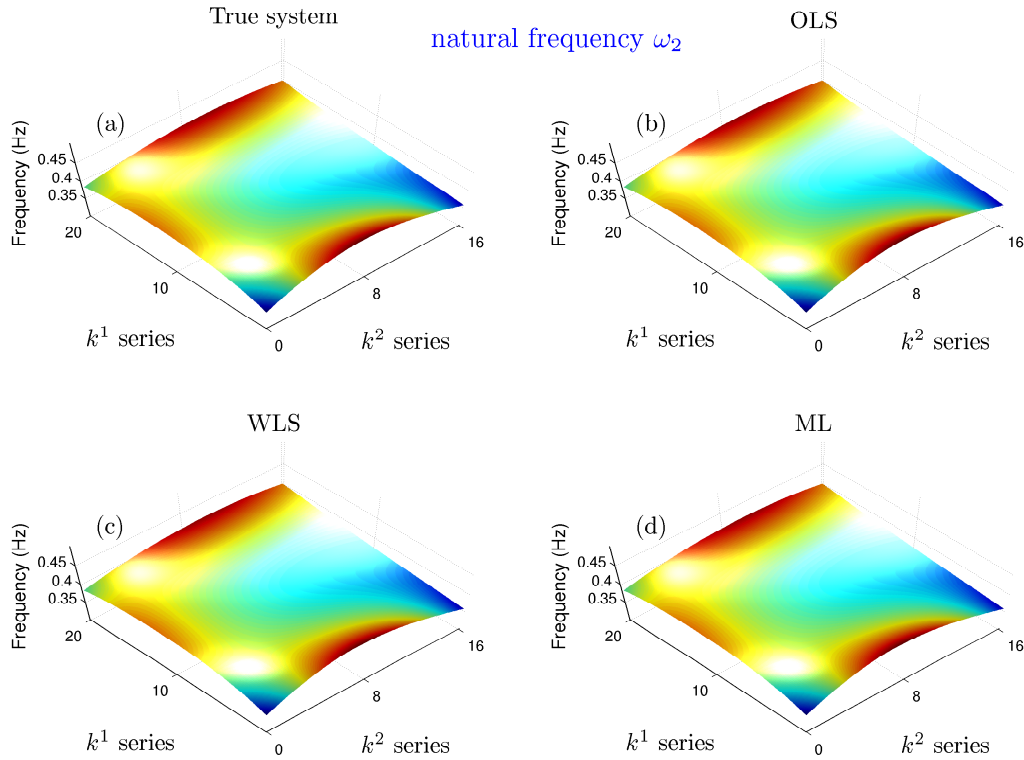


Figure 3.19: VFP-ARX(4, 1)₉ second natural frequency ω_2 versus k^1 and k^2 series: (a) true system, (b) mean OLS estimate, (c) mean WLS estimate and (d) mean ML estimate (mean parameters over 500 runs).

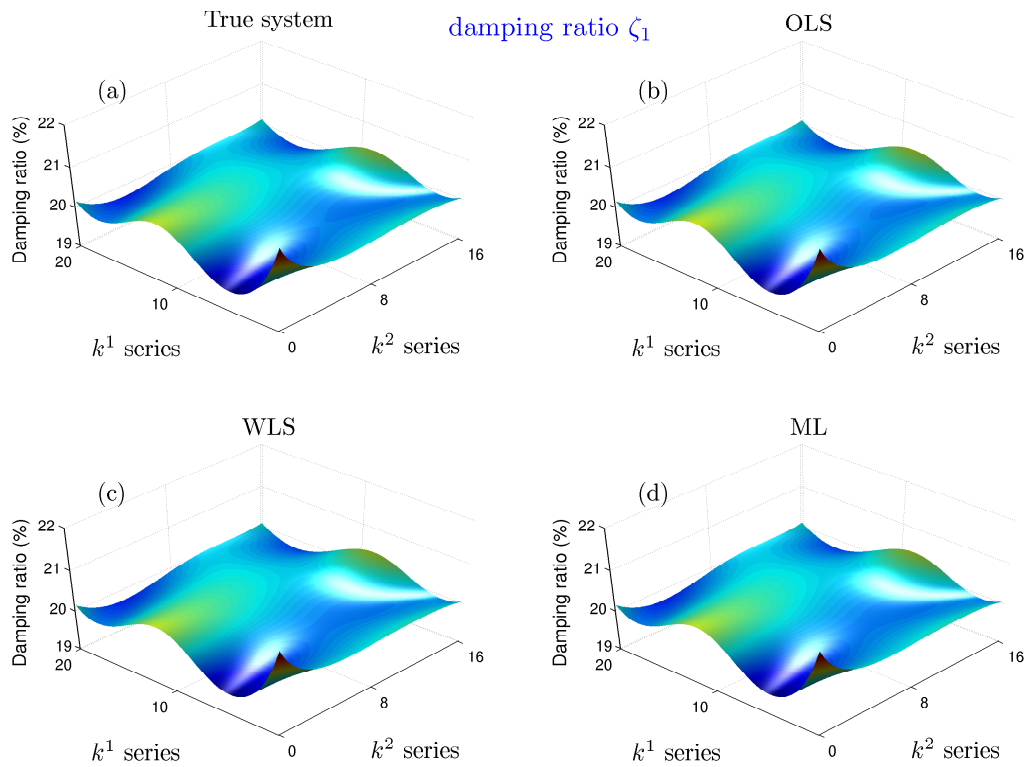


Figure 3.20: VFP-ARX(4, 1)₉ first damping ratio ζ_1 versus k^1 and k^2 series: (a) true system, (b) mean OLS estimate, (c) mean WLS estimate and (d) mean ML estimate (mean parameters over 500 runs).

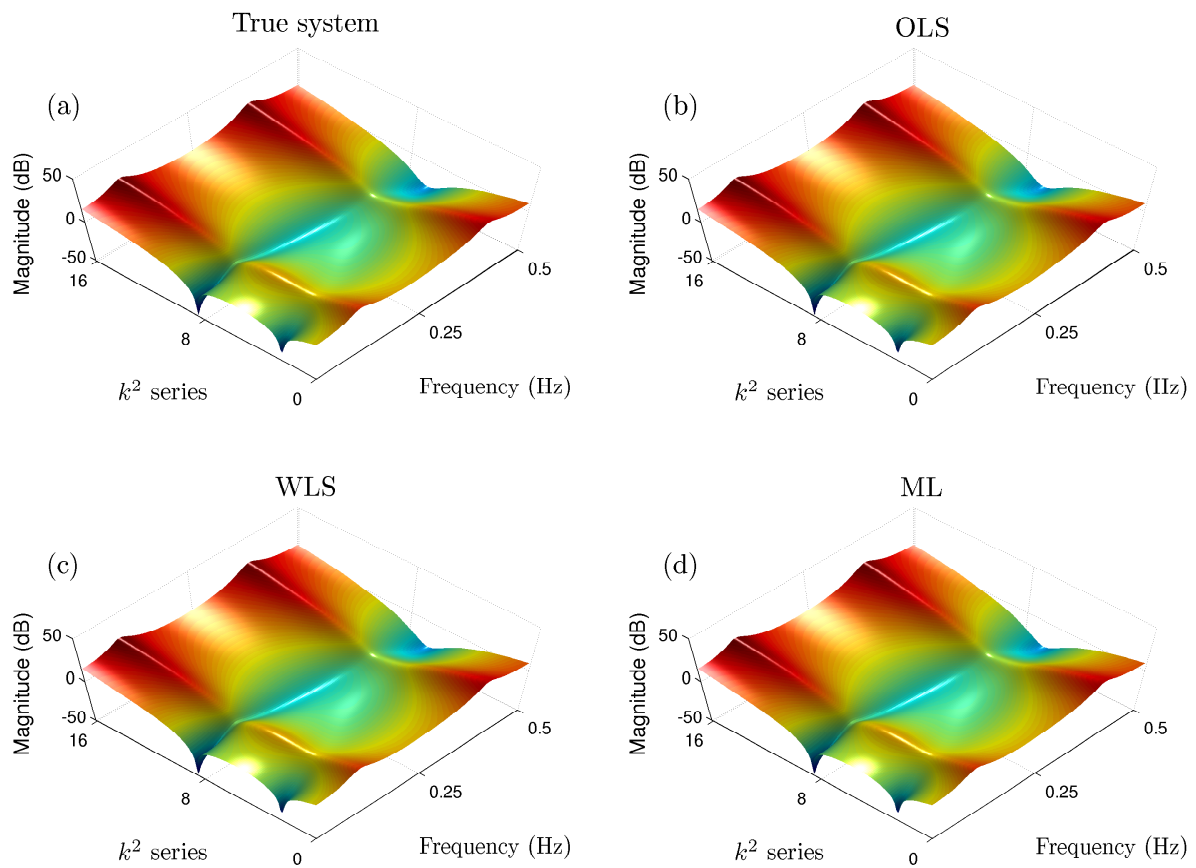


Figure 3.21: VFP-ARX(4,1)₉ based frequency response magnitude versus frequency and k^2 series (k^1 is set to k_8^1): (a) true system, (b) mean OLS estimate, (c) mean WLS estimate and (d) mean ML estimate (mean parameters over 500 runs).

Appendix A

Bivariate Polynomials

Bivariate (two-dimensional) orthogonal polynomials may be obtained as *tensor products* from their corresponding (Chebyshev, Legendre, Jacobi, or other (Dunkl and Xu 2001, Krall and Scheffer 1967, Kowalski 1982)) univariate counterparts. For example, the bivariate Chebyshev orthogonal polynomials have the following form:

$$P_{mn}(x, y) = P_m(x) \cdot P_n(y) \quad (x, y) \in [-1, 1] \times [-1, 1] \subset \mathbb{R}^2 \quad (\text{A.1})$$

with P_{mn} the bivariate Chebyshev polynomial of total degree mn and $P_m(x), P_n(y)$ the univariate Chebyshev polynomials of degrees m, n , respectively.

Theorem A.1 (construction of bivariate polynomial orthogonal basis (Krall and Scheffer 1967, Kowalski 1982)) *A polynomial orthogonal basis of maximum degree mn contains a total of $\frac{1}{2}(mn + 1)(mn + 2)$ basis functions obtained as follows:*

1.	constant basis function	$P_{0,0}$
2.	linear basis functions	$P_{1,0}, P_{0,1}$
3.	quadratic basis functions	$P_{2,0}, P_{1,1}, P_{0,2}$
4.	cubic basis functions	$P_{3,0}, P_{2,1}, P_{1,2}, P_{0,3}$
5.	fourth degree basis functions	$P_{4,0}, P_{3,1}, P_{2,2}, P_{1,3}, P_{0,4}$
⋮		
$mn + 1.$	degree mn basis functions	$P_{mn,0}, P_{mn-1,1}, P_{mn-2,2}, \dots, P_{1,mn-1}, P_{0,mn}$.

□

The univariate polynomials used in this study in order to obtain their bivariate counterparts are the shifted Chebyshev polynomials of the second kind (Type II Chebyshev polynomials), which belong to the broader family of Chebyshev orthogonal polynomials. These polynomials obey the following recurrence relation:

$$a_{1,n}G_{n+1}(x) = (a_{2,n} + a_{3,n}x)G_n(x) - a_{4,n}G_{n-1}(x) \quad x \in [0, 1] \subset \mathbb{R} \quad (\text{A.2})$$

with $a_{1,n} = a_{4,n} = 1$, $a_{2,n} = -2$, $a_{3,n} = 4$, and $G_0(x) = 0$, $G_1(x) = 1$.

Hence, the first five shifted Chebyshev polynomials of the second kind are:

$$\begin{aligned}P_0 &= 1 \\P_1 &= -1 + 2x \\P_2 &= 1 - 8x + 8x^2 \\P_3 &= -1 + 18x - 48x^2 + 32x^3 \\P_4 &= 1 - 32x + 160x^2 - 256x^3 + 128x^4\end{aligned}$$

In the present framework, where the two variables are damage magnitude (k^1) and damage location (k^2), the following variable selections are made:

$$x \in [0, 1] \subset \mathbb{R}, \quad x = k^1/k_{max}^1 \quad y \in [0, 1] \subset \mathbb{R}, \quad y = k^2/k_{max}^2. \quad (\text{A.3})$$

Appendix B

Proofs of Theorems

Proof of Theorem 3.5.1:

The true system can be written in linear regression form as follows:

$$y_{\mathbf{k}}[t] = \left[\boldsymbol{\varphi}_{AR}^T[t] \otimes \mathbf{g}_{AR}^T(\mathbf{k}) : \boldsymbol{\varphi}_X^T[t] \otimes \mathbf{g}_X^T(\mathbf{k}) \right] \cdot \boldsymbol{\theta} + w_{\mathbf{k}}[t] = \boldsymbol{\phi}_{\mathbf{k}}^T[t] \cdot \boldsymbol{\theta} + w_{\mathbf{k}}[t] \quad (\text{B.1})$$

with:

$$\begin{aligned} \boldsymbol{\varphi}_{AR}[t] &\triangleq [-y_{\mathbf{k}}[t-1] \dots -y_{\mathbf{k}}[t-na]]^T \\ \boldsymbol{\varphi}_X[t] &\triangleq [x_{\mathbf{k}}[t] \dots x_{\mathbf{k}}[t-nb]]^T \\ \mathbf{g}_{AR}(\mathbf{k}) &\triangleq [G_{d_a(1)}(\mathbf{k}) G_{d_a(2)}(\mathbf{k}) \dots G_{d_a(pa)}(\mathbf{k})]^T \\ \mathbf{g}_X(\mathbf{k}) &\triangleq [G_{d_b(1)}(\mathbf{k}) G_{d_b(2)}(\mathbf{k}) \dots G_{d_b(pb)}(\mathbf{k})]^T. \end{aligned}$$

The WLS estimator is rewritten as:

$$\begin{aligned} \widehat{\boldsymbol{\theta}}_N^{WLS} &= \left[\frac{1}{NM_1M_2} \sum_{k^1=k_i^1}^{M_1} \sum_{k^2=k_j^2}^{M_2} \frac{1}{\sigma_w^2(k_{i,j})} \sum_{t=1}^N \boldsymbol{\phi}_{k_{i,j}}[t] \boldsymbol{\phi}_{k_{i,j}}^T[t] \right]^{-1} \\ &\quad \left[\frac{1}{NM_1M_2} \sum_{k^1=k_i^1}^{M_1} \sum_{k^2=k_j^2}^{M_2} \frac{1}{\sigma_w^2(k_{i,j})} \sum_{t=1}^N \boldsymbol{\phi}_{k_{i,j}}[t] (\boldsymbol{\phi}_{k_{i,j}}^T[t] \boldsymbol{\theta}_o + w_{k_{i,j}}[t]) \right] \quad (\text{B.2}) \end{aligned}$$

$$\begin{aligned} &= \boldsymbol{\theta}_o + \underbrace{\left[\frac{1}{NM_1M_2} \sum_{k^1=k_i^1}^{M_1} \sum_{k^2=k_j^2}^{M_2} \frac{1}{\sigma_w^2(k_{i,j})} \sum_{t=1}^N \boldsymbol{\phi}_{k_{i,j}}[t] \boldsymbol{\phi}_{k_{i,j}}^T[t] \right]^{-1}}_{\mathbf{A}_N} \\ &\quad \underbrace{\left[\frac{1}{NM_1M_2} \sum_{k^1=k_i^1}^{M_1} \sum_{k^2=k_j^2}^{M_2} \frac{1}{\sigma_w^2(k_{i,j})} \sum_{t=1}^N \boldsymbol{\phi}_{k_{i,j}}[t] w_{k_{i,j}}[t] \right]}_{\mathbf{b}_N} \quad (\text{B.3}) \end{aligned}$$

Let:

$$\mathbf{A}_N = \frac{1}{NM_1M_2} \sum_{k^1=k_i^1}^{M_1} \sum_{k^2=k_j^2}^{M_2} \frac{1}{\sigma_w^2(k_{i,j})} \sum_{t=1}^N \boldsymbol{\phi}_{k_{i,j}}[t] \boldsymbol{\phi}_{k_{i,j}}^T[t] \quad (\text{B.4})$$

and

$$\mathbf{b}_N = \frac{1}{NM_1M_2} \sum_{k^1=k_i^1}^{M_1} \sum_{k^2=k_j^2}^{M_2} \frac{1}{\sigma_w^2(k_{i,j})} \sum_{t=1}^N \phi_{k_{i,j}}[t] w_{k_{i,j}}[t] \quad (\text{B.5})$$

Then from Söderström and Stoica (1989, pp. 547–548) and by using the algebraic definitions of Liu (1999) and Liu and Trenkler (2008)¹ it is proved that:

$$\begin{aligned} \sum_{t=1}^N \phi_{k_{i,j}}[t] \phi_{k_{i,j}}^T[t] &= \sum_{t=1}^N [\varphi_{AR_{k_{i,j}}}[t] \otimes \mathbf{g}_{AR}(k_{i,j}) \vdots \varphi_{X_{k_{i,j}}}[t] \otimes \mathbf{g}_X(k_{i,j})] \cdot \\ &\quad [\varphi_{AR_{k_{i,j}}}[t] \otimes \mathbf{g}_{AR}(k_{i,j}) \vdots \varphi_{X_{k_{i,j}}}[t] \otimes \mathbf{g}_X(k_{i,j})]^T \end{aligned} \quad (\text{B.6})$$

$$\begin{aligned} &= \left[\underbrace{[\varphi_{AR_{k_{i,j}}}[t] \vdots \varphi_{X_{k_{i,j}}}[t]]}_{\varphi_{k_{i,j}}[t]} * \underbrace{[\mathbf{g}_{AR}(k_{i,j}) \vdots \mathbf{g}_X(k_{i,j})]}_{\mathbf{g}(k_{i,j})} \right] \cdot \\ &\quad \left[\underbrace{[\varphi_{AR_{k_{i,j}}}[t] \vdots \varphi_{X_{k_{i,j}}}[t]]}_{\varphi_{k_{i,j}}[t]} * \underbrace{[\mathbf{g}_{AR}(k_{i,j}) \vdots \mathbf{g}_X(k_{i,j})]}_{\mathbf{g}(k_{i,j})} \right]^T \end{aligned} \quad (\text{B.7})$$

$$= \sum_{t=1}^N [\varphi_{k_{i,j}}[t] * \mathbf{g}(k_{i,j})] \cdot [\varphi_{k_{i,j}}[t] * \mathbf{g}(k_{i,j})]^T \quad (\text{B.8})$$

$$= \sum_{t=1}^N \varphi_{k_{i,j}}[t] \varphi_{k_{i,j}}^T[t] * \underbrace{\mathbf{g}(k_{i,j}) \mathbf{g}^T(k_{i,j})}_{\mathbf{G}_{k_{i,j}}} \quad (\text{B.9})$$

$$= \sum_{t=1}^N \varphi_{k_{i,j}}[t] \varphi_{k_{i,j}}^T[t] * \mathbf{G}_{k_{i,j}} \xrightarrow{a.s.} E\{\varphi_{k_{i,j}}[t] \varphi_{k_{i,j}}^T[t]\} * \mathbf{G}_{k_{i,j}} \quad (\text{B.10})$$

By Kolmogorov's theorem (White 2001, p. 19) is proved that:

$$\hat{\sigma}_w^2(k_{i,j}) \xrightarrow{a.s.} \sigma_w^2(k_{i,j}) \quad (\text{B.11})$$

By proposition 2.11 of White (2001, p. 19) and Equations (B.4), (B.10), and (B.11) we have the following result:

$$\mathbf{A}_N \xrightarrow{a.s.} \mathbf{Q}, \quad \mathbf{Q} : \text{a positive definite matrix} \quad (\text{B.12})$$

and \mathbf{b}_N can be expressed as:

$$\mathbf{b}_N = \frac{1}{M_1M_2} \sum_{k^1=k_i^1}^{M_1} \sum_{k^2=k_j^2}^{M_2} \frac{1}{\sigma_w^2(k_{i,j})} \mathbf{p}_{k_{i,j}} \quad (\text{B.13})$$

with:

$$\mathbf{p}_{k_{i,j}} = \frac{1}{N} \sum_{t=1}^N \phi_{k_{i,j}}[t] w_{k_{i,j}}[t] = \frac{1}{N} \sum_{t=1}^N \varphi_{k_{i,j}}[t] * \mathbf{g}(k_{i,j}) w_{k_{i,j}}[t] = \frac{1}{N} \sum_{t=1}^N \varphi_{k_{i,j}}[t] w_{k_{i,j}}[t] * \mathbf{g}(k_{i,j}) \quad (\text{B.14})$$

In Ljung (1999, p. 553) it is proved that:

$$\frac{1}{N} \sum_{t=1}^N \varphi_{k_{i,j}}[t] w_{k_{i,j}}[t] \xrightarrow{a.s.} 0 \quad (\text{B.15})$$

¹Kronecker product: $\mathbf{A} \otimes \mathbf{B} = (a_{ij} \mathbf{B}_{ij})_{ij}$. Khatri-Rao product: $\mathbf{A} * \mathbf{B} = (\mathbf{A}_{ij} \otimes \mathbf{B}_{ij})_{ij}$, where \mathbf{A}_{ij} is the ij -submatrix of \mathbf{A} and \mathbf{B}_{ij} is the ij -submatrix of \mathbf{B} .

Thus, from Equations (B.13) and (B.15) it follows that:

$$\mathbf{b}_N \xrightarrow{a.s.} 0 \quad (\text{B.16})$$

Hence, as $\hat{\boldsymbol{\theta}}_N^{WLS} = \boldsymbol{\theta}_o + \mathbf{A}_N^{-1} \mathbf{b}_N$, from (B.12) and (B.16) it is proved that:

$$\hat{\boldsymbol{\theta}}_N^{WLS} \xrightarrow{a.s.} \boldsymbol{\theta}_o. \quad (\text{B.17})$$

□

Proof of Theorem 3.5.2:

The first derivative of $L(\bar{\boldsymbol{\theta}}/e)$ at $\hat{\boldsymbol{\theta}}_{ML}$ can be expressed in Taylor series form around $\bar{\boldsymbol{\theta}}_o$ as follows (Sorenson 1980, p. 188):

$$\left[\frac{\partial L(\bar{\boldsymbol{\theta}}/e)}{\partial \bar{\boldsymbol{\theta}}} \right]_{\bar{\boldsymbol{\theta}}=\hat{\boldsymbol{\theta}}_{ML}} = \left[\frac{\partial L(\bar{\boldsymbol{\theta}}/e)}{\partial \bar{\boldsymbol{\theta}}} \right]_{\bar{\boldsymbol{\theta}}=\bar{\boldsymbol{\theta}}_o} + \left[\frac{\partial^2 L(\bar{\boldsymbol{\theta}}/e)}{\partial \bar{\boldsymbol{\theta}} \partial \bar{\boldsymbol{\theta}}^T} \right]_{\bar{\boldsymbol{\theta}}=\bar{\boldsymbol{\theta}}^*} (\hat{\boldsymbol{\theta}}_{ML} - \bar{\boldsymbol{\theta}}_o) \quad (\text{B.18})$$

where $\bar{\boldsymbol{\theta}}^*$ a vector near $\bar{\boldsymbol{\theta}}_o$ with $\bar{\boldsymbol{\theta}}^* = \lambda \bar{\boldsymbol{\theta}}_o + (1 - \lambda) \hat{\boldsymbol{\theta}}_{ML}$ and $0 \leq \lambda \leq 1$. Because $\hat{\boldsymbol{\theta}}_{ML}$ maximizes $L(\bar{\boldsymbol{\theta}}/e)$, the left term of (B.18) equals to zero, so we have:

$$\frac{1}{NM_1 M_2} \left[\frac{\partial L(\bar{\boldsymbol{\theta}}/e)}{\partial \bar{\boldsymbol{\theta}}} \right]_{\bar{\boldsymbol{\theta}}=\bar{\boldsymbol{\theta}}_o} = -\frac{1}{NM_1 M_2} \left[\frac{\partial^2 L(\bar{\boldsymbol{\theta}}/e)}{\partial \bar{\boldsymbol{\theta}} \partial \bar{\boldsymbol{\theta}}^T} \right]_{\bar{\boldsymbol{\theta}}=\bar{\boldsymbol{\theta}}^*} (\hat{\boldsymbol{\theta}}_{ML} - \bar{\boldsymbol{\theta}}_o) \quad (\text{B.19})$$

The left term of equation (B.19) can be written as follows:

$$\frac{1}{NM_1 M_2} \left[\frac{\partial L(\bar{\boldsymbol{\theta}}/e)}{\partial \bar{\boldsymbol{\theta}}} \right]_{\bar{\boldsymbol{\theta}}=\bar{\boldsymbol{\theta}}_o} = \frac{1}{NM_1 M_2} \sum_{k^1=k_i^1}^{M_1} \sum_{k^2=k_j^2}^{M_2} \left[\frac{\partial \ln p(e_{k_{i,j}}[t]/\bar{\boldsymbol{\theta}})}{\partial \bar{\boldsymbol{\theta}}} \right]_{\bar{\boldsymbol{\theta}}=\bar{\boldsymbol{\theta}}_o} \quad (\text{B.20})$$

Taking the derivative $\ln p(e_{k_{i,j}}[t]/\bar{\boldsymbol{\theta}})$ with respect to $\sigma_w^2(k_{i,j})$ and $\boldsymbol{\theta}$, for $\bar{\boldsymbol{\theta}} = \bar{\boldsymbol{\theta}}_o$ leads to:

$$\begin{aligned} \left. \frac{\partial \ln p(e_{k_{i,j}}[t]/\bar{\boldsymbol{\theta}})}{\partial \sigma_w^2(k_{i,j})} \right|_{\bar{\boldsymbol{\theta}}=\bar{\boldsymbol{\theta}}_o} &= \left. \frac{\partial}{\partial \sigma_w^2(k_{i,j})} \left\{ -\frac{1}{2} \ln 2\pi - \frac{1}{2} \ln \sigma_w^2(k_{i,j}) - \frac{1}{2} \frac{e_{k_{i,j}}[t, \boldsymbol{\theta}]}{\sigma_w^2(k_{i,j})} \right\} \right|_{\bar{\boldsymbol{\theta}}=\bar{\boldsymbol{\theta}}_o} \\ &= \underbrace{-\frac{1}{2\sigma_w^2(k_{i,j})} + \frac{w_{k_{i,j}}^2[t]}{2\sigma_w^4(k_{i,j})}}_{d_1(k_{i,j}, k_{i,j})} \end{aligned} \quad (\text{B.21})$$

$$\left. \frac{\partial \ln p(e_{k_{i,j}}[t]/\bar{\boldsymbol{\theta}})}{\partial \boldsymbol{\theta}} \right|_{\bar{\boldsymbol{\theta}}=\bar{\boldsymbol{\theta}}_o} = \underbrace{-\frac{1}{\sigma_w^2(k_{i,j})} w_{k_{i,j}}[t] \boldsymbol{\psi}_{k_{i,j}}[t, \boldsymbol{\theta}_o]}_{\mathbf{d}_2(k_{i,j}) \quad (na+nb+1) \times 1} \quad (\text{B.22})$$

with $\boldsymbol{\psi}_{k_{i,j}}[t, \boldsymbol{\theta}_o] = \left. \frac{\partial e_{k_{i,j}}[t]}{\partial \boldsymbol{\theta}} \right|_{\boldsymbol{\theta}=\boldsymbol{\theta}_o}$. It has to be noticed that $\left. \frac{\partial \ln p(e_{k_{i,j}}[t]/\bar{\boldsymbol{\theta}})}{\partial \sigma_w^2(k_{m,n})} \right|_{\bar{\boldsymbol{\theta}}=\bar{\boldsymbol{\theta}}_o} = 0$ for $(i, j) \neq (m, n)$, which means $d_1(k_{i,j}, k_{m,n}) = 0$.

Using the *ergodicity theorem* (Söderström and Stoica 1989, pp. 547–548) of the disturbance sequences (*white noise with zero mean*) and while $\boldsymbol{\psi}_{k_{i,j}}[t, \boldsymbol{\theta}_o] = \boldsymbol{\phi}_{k_{i,j}}^T[t, \boldsymbol{\theta}_o]$ includes input values and past output values independent of $w_{k_{i,j}}[t]$ we have:

$$\frac{1}{NM_1 M_2} \sum_{k^1=k_i^1}^{M_1} \sum_{k^2=k_j^2}^{M_2} \sum_{t=1}^N \overbrace{[\mathbf{d}_2^T d_1(k_{1,1}, k_{i,j}) \dots d_1(k_{M_1, M_2}, k_{i,j})]}^{\mathbf{d}_{kt}}]^T \xrightarrow{a.s.} 0 \quad (\text{B.23})$$

as

$$\begin{aligned} \frac{1}{NM_1M_2} \sum_{k^1=k_i^1}^{M_1} \sum_{k^2=k_j^2}^{M_2} \sum_{t=1}^N d_1(k_{i,j}, k_{m,n}) &= \frac{1}{NM_1M_2} \sum_{t=1}^N \left\{ -\frac{1}{2\sigma_w^2(k_{i,j})} + \frac{w_{k_{i,j}}^2[t]}{2\sigma_w^4(k_{i,j})} \right\} \\ \xrightarrow{a.s.} \frac{1}{M_1M_2} \left\{ -\frac{1}{2\sigma_w^2(k_{i,j})} + \frac{E\{w_{k_{i,j}}^2[t]\}}{2\sigma_w^4(k_{i,j})} \right\} &= \frac{1}{M_1M_2} \left\{ -\frac{1}{2\sigma_w^2(k_{i,j})} + \frac{\sigma_w^2(k_{i,j})}{2\sigma_w^4(k_{i,j})} \right\} = 0 \end{aligned} \quad (\text{B.24})$$

and

$$\begin{aligned} \frac{1}{NM_1M_2} \sum_{k^1=k_i^1}^{M_1} \sum_{k^2=k_j^2}^{M_2} \sum_{t=1}^N \mathbf{d}_2(k_{i,j}) &= \frac{1}{NM_1M_2} \sum_{k^1=k_i^1}^{M_1} \sum_{k^2=k_j^2}^{M_2} \sum_{t=1}^N \left\{ -\frac{1}{\sigma_w^2(k_{i,j})} w_{k_{i,j}}[t] \boldsymbol{\psi}_{k_{i,j}}[t, \boldsymbol{\theta}_o] \right\} \\ \xrightarrow{a.s.} \frac{1}{M_1M_2} \sum_{k^1=k_i^1}^{M_1} \sum_{k^2=k_j^2}^{M_2} \frac{1}{\sigma_w^2(k_{i,j})} E\{w_{k_{i,j}}[t]\} E\{\boldsymbol{\psi}_{k_{i,j}}[t, \boldsymbol{\theta}_o]\} &= 0 \end{aligned} \quad (\text{B.25})$$

For the expression of the second derivative the following property is used Söderström and Stoica (1989, pp. 560–562):

$$E \left\{ \frac{\partial \ln p(e_{k_{i,j}}[t]/\bar{\boldsymbol{\theta}})}{\partial \boldsymbol{\theta}} \bigg|_{\bar{\boldsymbol{\theta}}=\bar{\boldsymbol{\theta}}_o} \left[\frac{\partial \ln p(e_{k_{i,j}}[t]/\bar{\boldsymbol{\theta}})}{\partial \boldsymbol{\theta}} \bigg|_{\bar{\boldsymbol{\theta}}=\bar{\boldsymbol{\theta}}_o} \right]^T \right\} = -E \left\{ \frac{\partial^2 \ln p(e_{k_{i,j}}[t]/\bar{\boldsymbol{\theta}})}{\partial \bar{\boldsymbol{\theta}} \partial \bar{\boldsymbol{\theta}}^T} \bigg|_{\bar{\boldsymbol{\theta}}=\bar{\boldsymbol{\theta}}_o} \right\} \quad (\text{B.26})$$

Hence, the second derivative of $L(\bar{\boldsymbol{\theta}}/e)$ with respect to $\bar{\boldsymbol{\theta}}$ can be written using (B.26):

$$\begin{aligned} \frac{1}{NM_1M_2} \left[\frac{\partial^2 L(\bar{\boldsymbol{\theta}}/e)}{\partial \bar{\boldsymbol{\theta}} \partial \bar{\boldsymbol{\theta}}^T} \right]_{\bar{\boldsymbol{\theta}}=\bar{\boldsymbol{\theta}}_o} &= \frac{1}{NM_1M_2} \sum_{k^1=k_i^1}^{M_1} \sum_{k^2=k_j^2}^{M_2} \sum_{t=1}^N \left[\frac{\partial^2 \ln p(e_{k_{i,j}}[t]/\bar{\boldsymbol{\theta}})}{\partial \bar{\boldsymbol{\theta}} \partial \bar{\boldsymbol{\theta}}^T} \right]_{\bar{\boldsymbol{\theta}}=\bar{\boldsymbol{\theta}}_o} \\ \xrightarrow{a.s.} -\frac{1}{M_1M_2} \sum_{k^1=k_i^1}^{M_1} \sum_{k^2=k_j^2}^{M_2} E \left\{ \frac{\partial \ln p(e_{k_{i,j}}[t]/\bar{\boldsymbol{\theta}})}{\partial \boldsymbol{\theta}} \bigg|_{\bar{\boldsymbol{\theta}}=\bar{\boldsymbol{\theta}}_o} \left[\frac{\partial \ln p(e_{k_{i,j}}[t]/\bar{\boldsymbol{\theta}})}{\partial \boldsymbol{\theta}} \bigg|_{\bar{\boldsymbol{\theta}}=\bar{\boldsymbol{\theta}}_o} \right]^T \right\} & \end{aligned} \quad (\text{B.27})$$

Using $\mathbf{d}_{kt} = [\partial \ln p(e_{k_{i,j}}[t]/\bar{\boldsymbol{\theta}})/\partial \bar{\boldsymbol{\theta}}]_{\bar{\boldsymbol{\theta}}=\bar{\boldsymbol{\theta}}_o}$ the above equation becomes:

$$\begin{aligned} & -\frac{1}{M_1M_2} \sum_{k^1=k_i^1}^{M_1} \sum_{k^2=k_j^2}^{M_2} E \left\{ \frac{\partial \ln p(e_{k_{i,j}}[t]/\bar{\boldsymbol{\theta}})}{\partial \bar{\boldsymbol{\theta}}} \bigg|_{\bar{\boldsymbol{\theta}}=\bar{\boldsymbol{\theta}}_o} \left[\frac{\partial \ln p(e_{k_{i,j}}[t]/\bar{\boldsymbol{\theta}})}{\partial \bar{\boldsymbol{\theta}}} \bigg|_{\bar{\boldsymbol{\theta}}=\bar{\boldsymbol{\theta}}_o} \right]^T \right\} \\ &= -\frac{1}{M_1M_2} \sum_{k^1=k_i^1}^{M_1} \sum_{k^2=k_j^2}^{M_2} E\{\mathbf{d}_{kt} \mathbf{d}_{kt}^T\} = -\frac{1}{M_1M_2} \sum_{k^1=k_i^1}^{M_1} \sum_{k^2=k_j^2}^{M_2} \\ & E \left\{ \begin{bmatrix} \mathbf{d}_2(k_{i,j}) \mathbf{d}_2^T(k_{i,j}) & \mathbf{d}_2(k_{i,j}) d_1(k_{1,1}, k_{i,j}) & \dots & \mathbf{d}_2(k_{i,j}) d_1(k_{M_1, M_2}, k_{i,j}) \\ d_1(k_{1,1}, k_{i,j}) \mathbf{d}_2(k_{i,j}) & d_1(k_{1,1}, k_{i,j}) d_1(k_{1,1}, k_{i,j}) & \dots & d_1(k_{1,1}, k_{i,j}) d_1(k_{M_1, M_2}, k_{i,j}) \\ \vdots & \vdots & \ddots & \vdots \\ d_1(k_{M_1, M_2}, k_{i,j}) \mathbf{d}_2(k_{i,j}) & d_1(k_{M_1, M_2}, k_{i,j}) d_1(k_{1,1}, k_{i,j}) & \dots & d_1(k_{M_1, M_2}, k_{i,j}) d_1(k_{M_1, M_2}, k_{i,j}) \end{bmatrix} \right\} \end{aligned} \quad (\text{B.28})$$

It is noted that $d_1(k_{i,j}, k_{m,n}) = 0, \forall (i,j) \neq (m,n)$. The expected value of (B.28) is estimated as follows:

$$E\{\mathbf{d}_2(k_{i,j}) \mathbf{d}_2^T(k_{i,j})\} = E \left\{ \frac{1}{\sigma_w^4(k_{i,j})} w_{k_{i,j}}^2[t] \boldsymbol{\phi}_{k_{i,j}}[t, \boldsymbol{\theta}_o] \boldsymbol{\phi}_{k_{i,j}}^T[t, \boldsymbol{\theta}_o] \right\} = \frac{1}{\sigma_w^2(k_{i,j})} \underbrace{E\{\boldsymbol{\phi}_{k_{i,j}}[t, \boldsymbol{\theta}_o] \boldsymbol{\phi}_{k_{i,j}}^T[t, \boldsymbol{\theta}_o]\}}_{\mathbf{D}^{k_{i,j}}} \quad (\text{B.29})$$

$$\begin{aligned}
E\{\mathbf{d}_2(k_{i,j})d_1(k_{i,j}, k_{i,j})\} &= E\left\{\frac{1}{\sigma_w^2(k_{i,j})}w_{k_{i,j}}[t]\phi_{k_{i,j}}[t, \boldsymbol{\theta}_o]\left(-\frac{1}{2\sigma_w^2(k_{i,j})} + \frac{w_{k_{i,j}}^2[t]}{2\sigma_w^4(k_{i,j})}\right)\right\} \\
&= E\left\{-\frac{1}{2\sigma_w^4(k_{i,j})}w_{k_{i,j}}[t]\phi_{k_{i,j}}[t, \boldsymbol{\theta}_o] + \frac{w_{k_{i,j}}^3[t]}{2\sigma_w^4(k_{i,j})}\phi_{k_{i,j}}[t, \boldsymbol{\theta}_o]\right\} \\
&= -\frac{1}{2\sigma_w^4(k_{i,j})}E\{w_{k_{i,j}}[t]\}E\{\phi_{k_{i,j}}[t, \boldsymbol{\theta}_o]\} + \\
&\quad \frac{1}{2\sigma_w^6(k_{i,j})}E\{w_{k_{i,j}}^3[t]\}E\{\phi_{k_{i,j}}[t, \boldsymbol{\theta}_o]\} = 0
\end{aligned} \tag{B.30}$$

$$\begin{aligned}
E\{d_1(k_{i,j}, k_{i,j})d_1(k_{i,j}, k_{i,j})\} &= E\left\{\left(-\frac{1}{2\sigma_w^2(k_{i,j})} + \frac{w_{k_{i,j}}^2[t]}{2\sigma_w^4(k_{i,j})}\right)\left(-\frac{1}{2\sigma_w^2(k_{i,j})} + \frac{w_{k_{i,j}}^2[t]}{2\sigma_w^4(k_{i,j})}\right)\right\} \\
&= E\left\{\frac{1}{4\sigma_w^4(k_{i,j})} - \frac{2w_{k_{i,j}}^2[t]}{4\sigma_w^6(k_{i,j})} + \frac{w_{k_{i,j}}^4[t]}{4\sigma_w^8(k_{i,j})}\right\} \\
&= \frac{1}{4\sigma_w^4(k_{i,j})} - \frac{2\sigma_w^2(k_{i,j})}{4\sigma_w^6(k_{i,j})} + \frac{3\sigma_w^4(k_{i,j})}{4\sigma_w^8(k_{i,j})} = \frac{1}{2\sigma_w^4(k_{i,j})} = d_3(k_{i,j})
\end{aligned} \tag{B.31}$$

Hence, (B.27) is written as:

$$\begin{aligned}
&\frac{1}{NM_1M_2} \left[\frac{\partial^2 L(\bar{\boldsymbol{\theta}}/e)}{\partial \bar{\boldsymbol{\theta}} \partial \bar{\boldsymbol{\theta}}^T} \right]_{\bar{\boldsymbol{\theta}} = \bar{\boldsymbol{\theta}}_o} \xrightarrow{a.s.} \\
&\left[\begin{array}{cccccc}
-\frac{1}{M_1M_2} \sum_{k^1=k_i^1}^{M_1} \sum_{k^2=k_j^2}^{M_2} \mathbf{D}^{k_{i,j}} & 0 & 0 & \dots & 0 \\
0 & -\frac{1}{M_1M_2} d_3(k_{1,1}) & 0 & \dots & 0 \\
0 & 0 & -\frac{1}{M_1M_2} d_3(k_{1,2}) & \dots & 0 \\
\vdots & \vdots & \vdots & \ddots & \vdots \\
0 & 0 & 0 & \dots & \frac{1}{M_1M_2} d_3(k_{M_1, M_2})
\end{array} \right] = \mathcal{F}_{\bar{\boldsymbol{\theta}}_o}
\end{aligned} \tag{B.32}$$

Let $\mathcal{F}_{\bar{\boldsymbol{\theta}}_o}$ a non-singular matrix and $\mathcal{F}_{\hat{\boldsymbol{\theta}}^*} \approx \mathcal{F}_{\bar{\boldsymbol{\theta}}_o}$, then from Equations (B.19), (B.23) and (B.32) we have:

$$\hat{\boldsymbol{\theta}}_N^{ML} \xrightarrow{a.s.} \bar{\boldsymbol{\theta}}_o. \tag{B.33}$$

□

Appendix C

Additional Monte Carlo Results

C.1 Test Case I: Complete parameter functional subspace

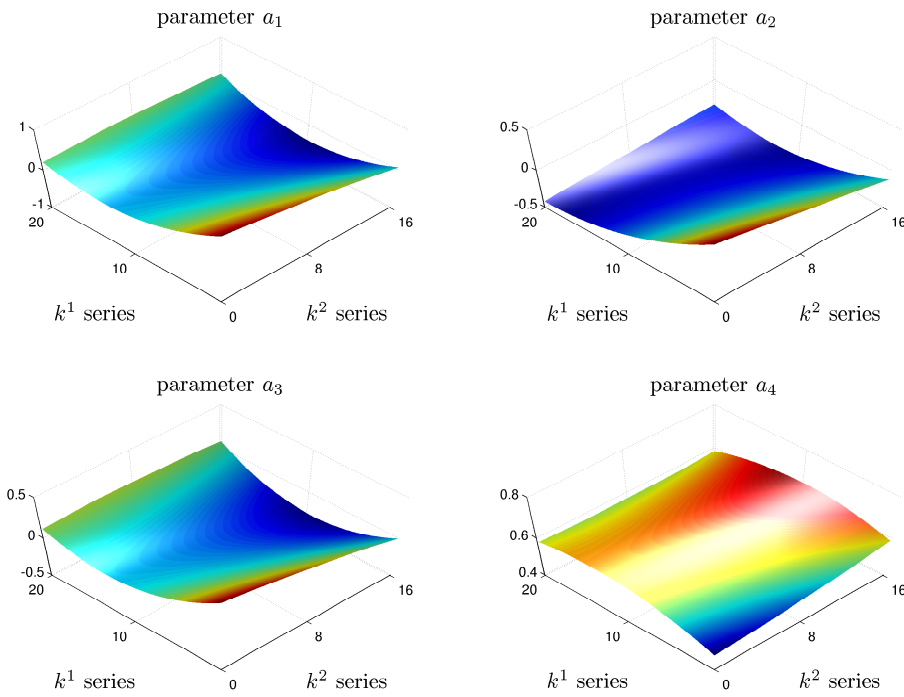


Figure C.1: AutoRegressive (AR) VFP-ARX(4,1)₆ true model parameters versus k^1 and k^2 series.

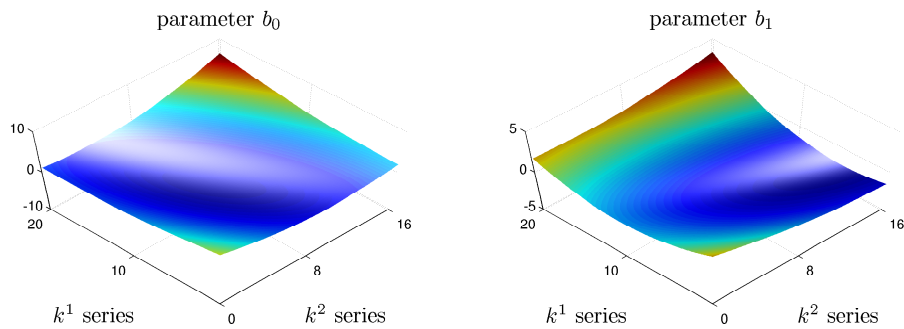


Figure C.2: Exogenous (X) VFP-ARX(4,1)₆ true model parameters versus k^1 and k^2 series.

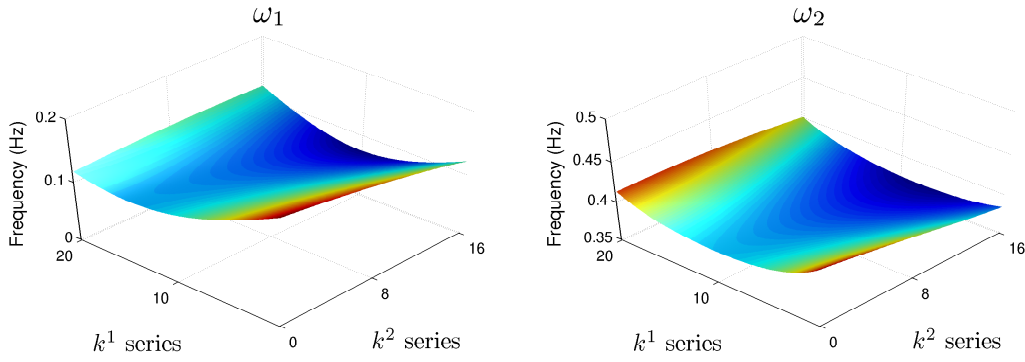


Figure C.3: The two VFP-ARX(4, 1)₆ true model natural frequencies ω versus k^1 and k^2 series.

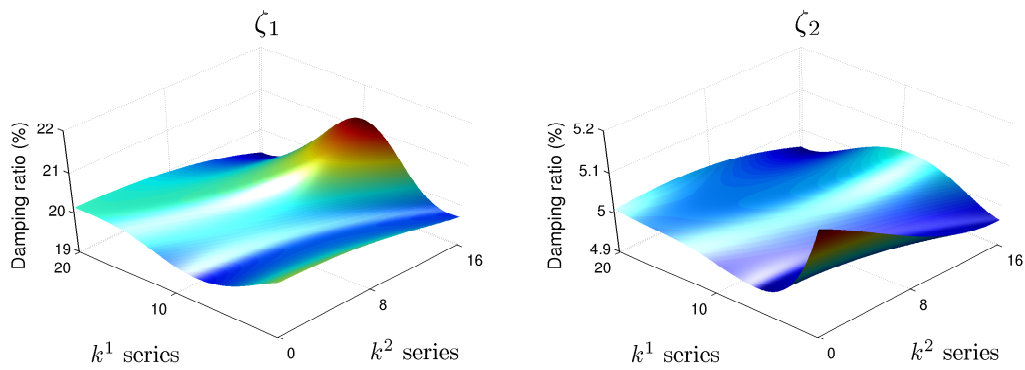


Figure C.4: The two VFP-ARX(4, 1)₆ true model damping ratios ζ versus k^1 and k^2 series.

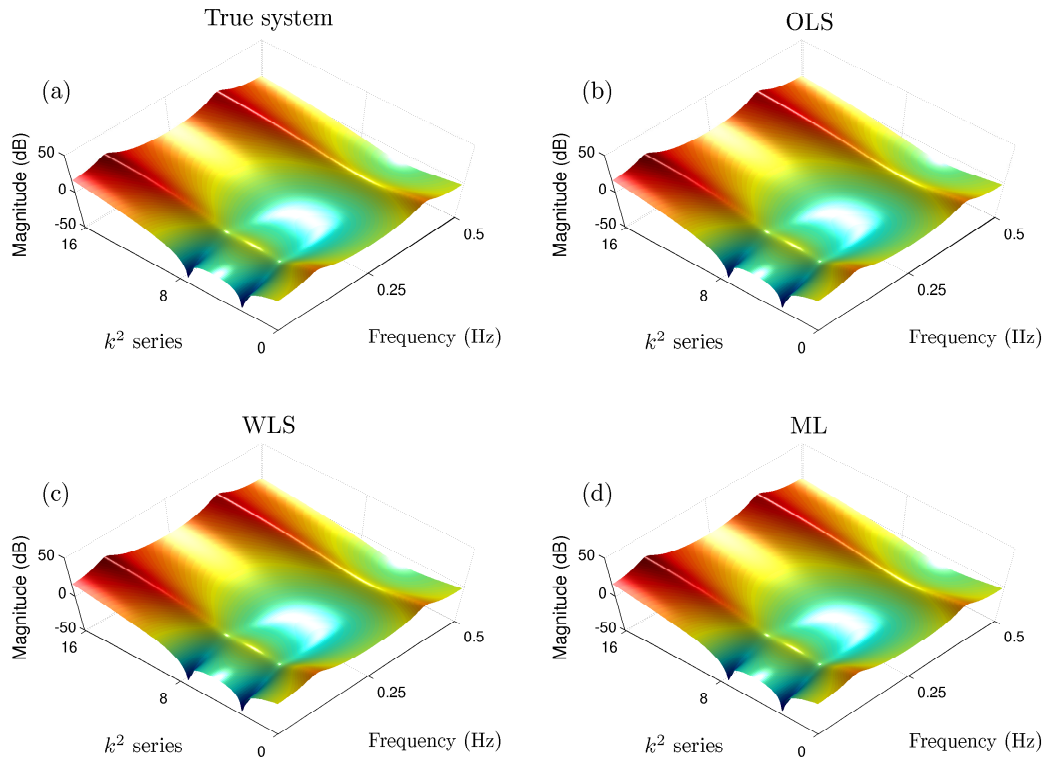


Figure C.5: VFP-ARX(4, 1)₆ based frequency response magnitude versus frequency and k^2 series (k^1 is set to k_8^1): (a) true system, (b) mean OLS estimate, (c) mean WLS estimate and (d) mean ML estimate (mean parameters over 500 runs).

C.2 Test Case II: Non-complete parameter functional subspace

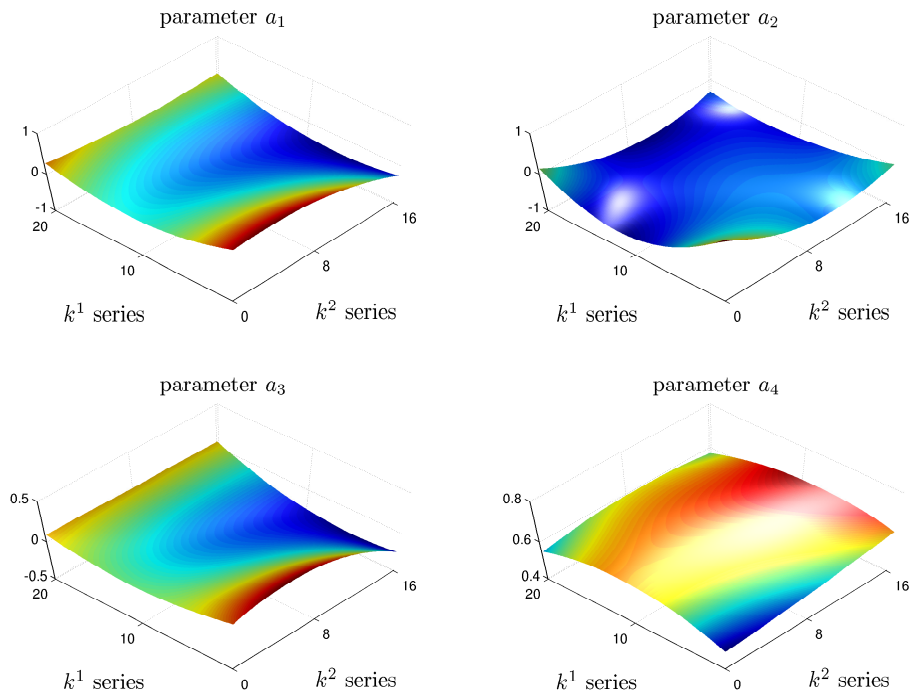


Figure C.6: AutoRegressive (AR) VFP-ARX(4, 1)₉ true model parameters versus k^1 and k^2 series.

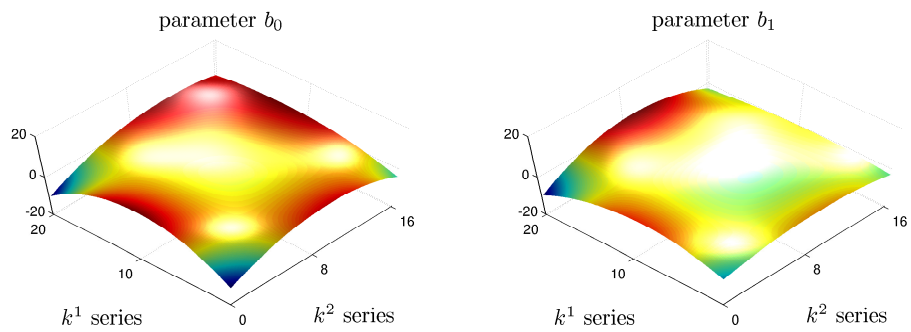


Figure C.7: Exogenous (X) VFP-ARX(4, 1)₉ true model parameters versus k^1 and k^2 series.

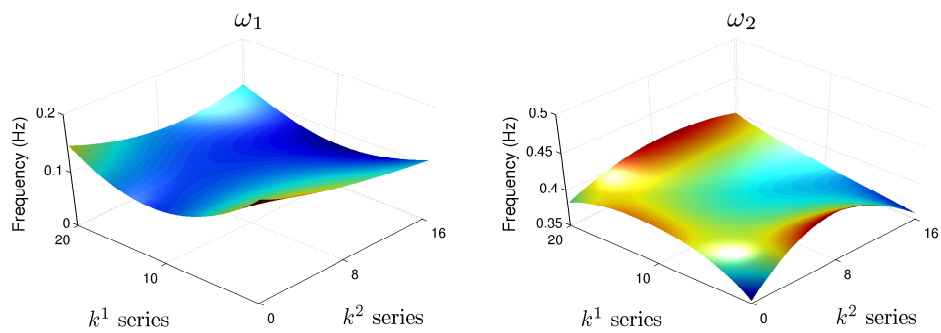


Figure C.8: The two VFP-ARX(4, 1)₉ true model natural frequencies ω versus k^1 and k^2 series.

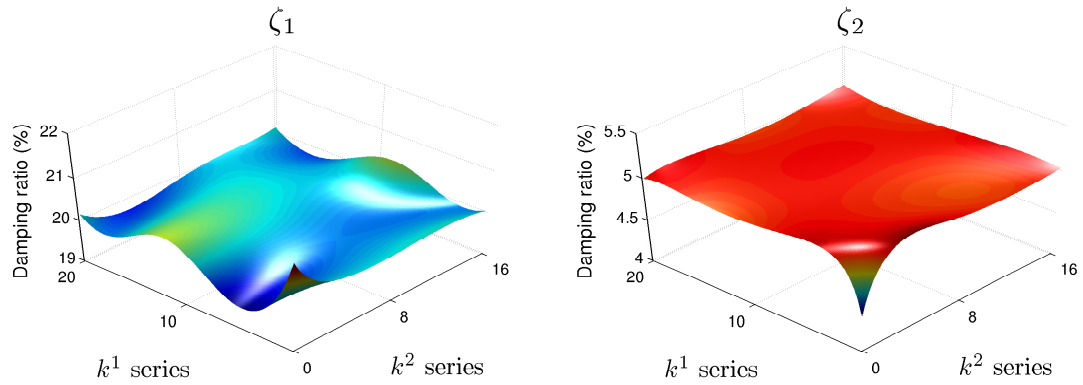


Figure C.9: The two VFP-ARX(4, 1)₉ true model damping ratios ζ versus k^1 and k^2 series.

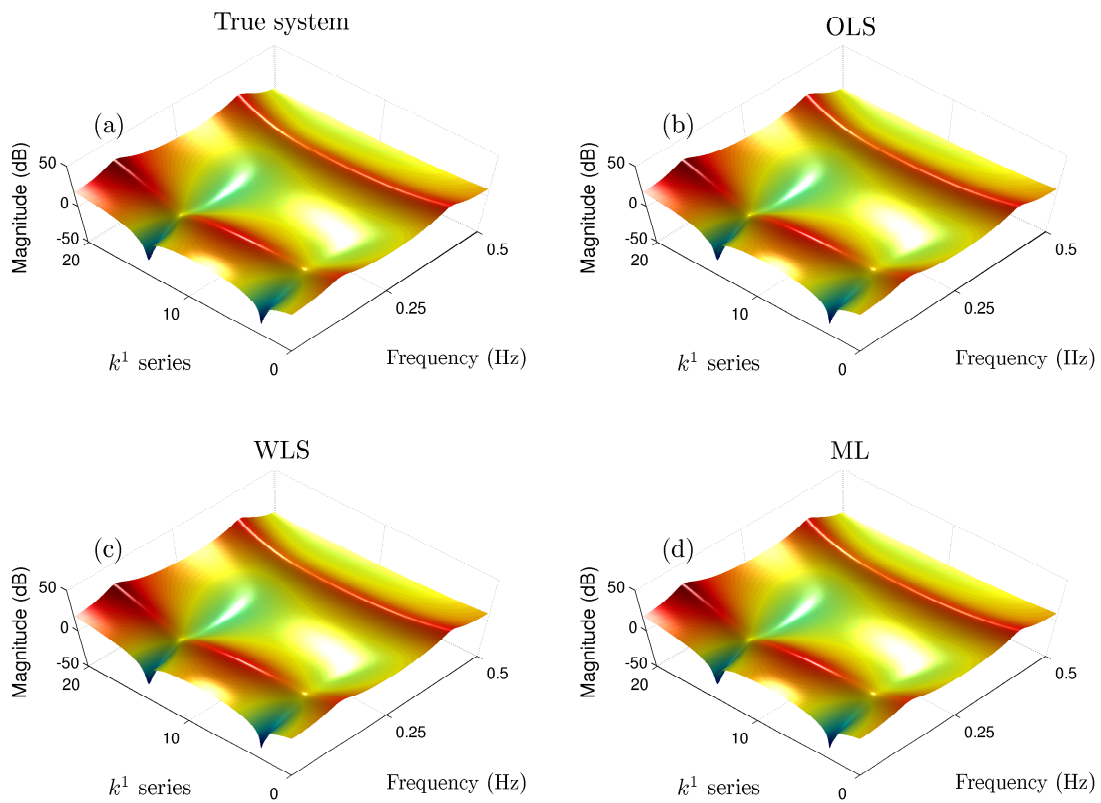


Figure C.10: VFP-ARX(4, 1)₉ based frequency response magnitude versus frequency and k^1 series (k^2 is set to k_5^2): (a) true system, (b) mean OLS estimate, (c) mean WLS estimate and (d) mean ML estimate (mean parameters over 500 runs).

Chapter 4

A Stochastic Functional Model Based Method for Vibration Based Damage Detection, Localization and Magnitude Estimation

A vibration based statistical time series method that is capable of effective damage detection, precise localization, and magnitude estimation within a unified stochastic framework is introduced. The method constitutes an important generalization of the recently introduced Functional Model Based Method (FMBM) in that it allows, for the first time in the statistical time series methods context, for complete and precise damage localization. More precisely, the proposed method can accurately localize damage anywhere on properly defined continuous topologies on the structure, instead of pre-defined specific locations. Estimator uncertainties are taken into account, and uncertainty ellipsoids are provided for the damage location and magnitude. To achieve its goal, the method is based on the extended class of Vector-dependent Functionally Pooled (VFP) models, which are characterized by parameters that depend on both damage magnitude and location, as well as on proper statistical estimation and decision making schemes. The method is validated and its effectiveness is experimentally assessed via its application to damage detection, precise localization, and magnitude estimation on a prototype GARTEUR-type laboratory scale aircraft skeleton structure. The damage scenarios considered consist of varying size small masses attached to various continuous topologies on the structure. The method is shown to achieve effective damage detection, precise localization, and magnitude estimation based on even a single pair of measured excitation-response signals.

4.1 Introduction

Damage detection, localization, and magnitude estimation (collectively referred to as damage diagnosis, or damage detection and identification) in vibrating structures, including aerospace, mechanical, civil, and marine structures, are of paramount importance for reasons associated with improved dynamic performance, proper operation, increased safety, and reduced maintenance costs (Doebling *et al.* 1996, Doebling *et al.* 1998, Farrar *et al.* 2001, Montalvão *et al.* 2006).

The need for global damage diagnosis methods that can be applied to realistic structures has led to the development of methods that examine changes in the structures' vibration characteristics. Vibration based methods for damage diagnosis thus form a technologically important and continuously evolving family, and are among the most accurate and effective (Doebling *et al.* 1998, Farrar *et al.* 2001, Montalvão *et al.* 2006, Fassois and Sakellariou 2007, Fassois and Sakellariou 2009, Fan and Qiao 2011). They offer a number of potential advantages, such as no requirement for visual inspection, "automation" capability, "global" coverage (in the sense of covering large areas of the structure), and the ability to work at a "system level". Nevertheless, and despite the fact that they generally tend to treat damage detection effectively, problems are frequently encountered when it comes to damage localization and magnitude estimation (damage quantification).

While damage detection has received considerable attention, no mature solutions yet exist for the damage localization and magnitude estimation (quantification) subproblems. To date, vibration based damage diagnosis methods that have shown promise to detect, locate (identify), and quantify damage are based on the basic idea that modal parameters (natural frequencies, mode shapes and modal damping) are functions of the physical properties of the structure (mass, damping and stiffness) (Doebling *et al.* 1998, Farrar *et al.* 2001, Montalvão *et al.* 2006, Farrar and Jauregui 1998*a*, Farrar and Jauregui 1998*b*). Therefore, changes in the physical properties will cause detectable changes in the modal properties. The majority of these methods is established on, or presumes, access to detailed and large size Finite Element (FE) models and utilize intensive model updating techniques (for tuning the model to the obtained data records) and pre- and post-damage data records (Farrar *et al.* 2001, Zimmerman *et al.* 2001, Nauerz and Fritzen 2001, Liberatore and Carman 2004, Perera *et al.* 2007). Furthermore, as complete FE models are utilized, these techniques require a significant number of measurement sensors and thus tend to be computationally and experimentally elaborate, while problems may be introduced by the measurement constraints imposed by actual testing conditions (Farrar *et al.* 2001, Farrar and Jauregui 1998*a*, Farrar and Jauregui 1998*b*, Zimmerman *et al.* 2001). Moreover, some of these methods appear to be inconsistent and unable to clearly identify the damage location when they are applied to less severe damage cases, while it may be ambiguous at times to determine whether they indicate damage at more than one location (Montalvão *et al.* 2006, Farrar and Jauregui 1998*a*).

On the other hand, recent studies embed the problem of vibration based damage detection, localization, and magnitude estimation in the alternative context of statistical pattern recognition (Sohn *et al.* 2001, Mattson and Pandit 2006*a*, Manson *et al.* 2003, Lee *et al.* 2006, Xi *et al.* 2000, Jung and Koh 2009). Statistical pattern recognition methods are based on signal analysis of the measured data aiming at the extraction of damage sensitive features. They utilize techniques related to time series and outlier analysis (Sohn *et al.* 2001, Mattson and Pandit 2006*a*, Manson *et al.* 2003), neural network analysis (Manson *et al.* 2003, Lee *et al.* 2006), and analysis of statistical parameters (Xi *et al.* 2000, Jung and Koh 2009). Neither sophisticated FE models nor modal parameters are employed in the implementation of these methods, while they are reportedly capable of achieving effective damage detection. Nevertheless, they often face difficulties when it comes to the more complicated tasks of damage localization and magnitude estimation, with the main drawbacks being the conversion

of the localization problem into a discrete classification problem (implying that only a finite number of specific potential damage locations is considered), the exhaustive search for appropriate damage sensitive features, the training necessary for damage localization, and the frequent need for sensor networks and sensor location optimization.

Statistical time series methods for Structural Health Monitoring (SHM) form a closely related category within the broader vibration based family of methods – see the survey articles of Fassois and Sakellariou (2007) and Fassois and Sakellariou (2009). These methods use random excitation and/or response signals from the structure in its healthy state and a number of potential damage states, along with statistical model building (identification) and statistical decision making for inferring the health state of the structure. They feature a number of potential advantages, such as accounting for measurement errors and uncertainties, allowing the use of normal operating data records, utilizing only *partial* identified structural models (as opposed to complete models required by most alternatives) and a very limited number of sensors (even a single sensor may be used in certain cases in conjunction with small structures). On the other hand, as complete structural models are not employed, time series methods may be limited to identifying (locating) damage only to the extent allowed by the type of model used.

In Sohn and Farrar (2001) a time series method based on AR-ARX models is used to locate damage sources in an eight degree-of-freedom mechanical system, whereas a subspace based method for damage localization within a FE model of the monitored structure is presented in Basseville *et al.* (2004). A statistical damage classification algorithm based on ARMA model parameters and assessed via experimental data obtained from the IASC-ASCE four-storey frame structure, the Z24 bridge, and the Malaysia-Singapore Second Link bridge is presented in Carden and Brownjohn (2008). The ARMA model parameters are used in Nair *et al.* (2006) to establish a damage detection and localization method with application to the ASCE benchmark structure, while in a follow up study Nair and Kiremidjian (2007), the ARMA parameters along with a Gaussian Mixture Model are employed to locate damage on the same structure. A two-stage damage diagnosis method based on the distance between ARMA models and pre-whitening filters is presented in Zheng and Mita (2007) and is tested using simulated and experimental data obtained from a building model. A damage identification procedure for bridge health monitoring based on features obtained from AR and ARX models is used and assessed via numerical simulations in Zhang (2007), while an ARX model and the standard deviation of its residuals are employed in Lu and Gao (2005) for damage detection and localization in a two and an eight degree-of-freedom simulated mass-spring system. Both non-parametric and parametric statistical time series methods are employed in Rizos *et al.* (2008) for skin damage detection and restoration assessment in a stiffened aircraft panel, while comparative assessment studies of the main non-parametric, parametric, scalar and vector statistical time series methods are provided in recent papers by the author (Kopsaftopoulos and Fassois 2010a, Kopsaftopoulos and Fassois 2011b).

Although statistical time series methods effectively tackle damage detection, they also face difficulties in achieving damage localization and magnitude estimation. Damage localization is usually achieved with respect to the available sensor positions on the structure, and thus effective localization depends on the exact number and location of the sensors. Furthermore, the large majority of the methods do not deal with damage quantification (damage severity estimation). In an effort to overcome these limitations, a novel Functional Model Based Method (FMBM) has been recently introduced by the Stochastic Mechanical Systems & Automation group of the Mechanical Engineering & Aeronautics Department at University of Patras (Sakellariou 2005, Sakellariou and Fassois 2008, Sakellariou *et al.* 2002). The FMBM is indeed capable of accurately representing the (typically partial) structural dynamics for a damage state for its *continuum* of damage magnitudes, as well as operating even on a single pair of excitation-response signals. Nevertheless, the method is limited in localizing damage at a *finite* number of specific *pre-determined* locations, instead of continuous topologies on the structure

– that is *any* point on a structural area or substructure. In this sense the FMBM does *not* allow for precise damage localization on a structure.

The *aim* of the present chapter is the introduction and experimental validation and assessment of a generalized version of the FMBM which is – for the first time within the context of statistical time series type methods – achieving complete and precise damage *localization* over *continuous topologies* on a structure, combined with damage magnitude estimation. Furthermore, estimator uncertainties are fully taken into account in all phases of the diagnostic procedure, and uncertainty ellipsoids are provided for combined damage location and magnitude. Like the original FMBM, the method utilizes a partial and reduced size identified model, and is capable of operating on a “low” number of measurement sensors – even on a single pair for “small” structures – and any type of vibration response signals (acceleration, velocity, displacement).

The method’s cornerstone is the new extended class of *Vector-dependent Functionally Pooled (VFP)* models (see Chapter 3 and Kopsaftopoulos and Fassois (2006a). These are generalizations of the Functional Pooled (FP) models of Sakellariou and Fassois (Sakellariou 2005, Sakellariou and Fassois 2008, Sakellariou and Fassois 2007), which now allow for the analytical inclusion of *both* damage location and magnitude on the dynamics. VFP models thus allow for the extension of the notion of *damage mode/fault mode* to include damage not only of all possible magnitudes, but also of all possible *locations* on a specific continuous topology on a structure. As VFP models have a richer structure than their FP counterparts and use bivariate (two-dimensional) functional subspaces for parameter projection, functional subspace dimensionality estimation is a more complicated task which is accomplished through a suitable Genetic Algorithm (GA) based procedure.

The method is validated and its effectiveness is experimentally assessed via a proof-of-concept application to damage detection, precise localization, and magnitude estimation on a prototype GARTEUR-type laboratory scale aircraft skeleton structure (Degener and Hermes 1996, Balmes and Wright 1997). The damage scenarios considered include the attachment of varying size small masses to various continuous topologies on the structure. The novelties of this experimental study include:

- (a) The feasibility of achieving *precise* damage localization and magnitude estimation based on only a *single* excitation-response signal pair is, for the first time, investigated and demonstrated.
- (b) Localization and damage magnitude *uncertainties* are explicitly considered and estimated, with *uncertainty ellipsoids* corresponding to specified probability levels being constructed.
- (c) The method’s operation and effectiveness is examined for *both* “local” and “remote” (with respect to the sensor location) damage. This is critical in view of the need for effective diagnosis with the smallest possible number of available sensors.
- (d) The effectiveness of the method in properly detecting and “negatively” localizing (that is excluding all considered structural topologies) damage that does *not* belong to any of the modelled types/topologies (referred to as *unmodelled damage*) is examined.

The rest of the chapter is organized as follows: The proposed VFP-ARX model based method is presented in Section 4.2, and the experimental set-up used for validation and assessment in Section 4.3. Experimental results are provided in Section 4.4, while the conclusions of the study are summarized in Section 4.5.

4.2 The VFP-ARX model based method

Like all statistical time series methods for SHM, the stochastic functional model, or more precisely the Vector-dependent Functionally Pooled AutoRegressive with eXogenous excitation (VFP-ARX) model, based method for combined damage detection, localization, and magnitude estimation consists of two phases: (a) A *baseline (training) phase*, which includes modelling of the considered damage topologies (modes), for the continuum of damage locations and magnitudes on a structural topology, via the novel class of stochastic VFP-ARX models, and (b) the *inspection phase*, which is performed whenever necessary or continuously during the structure's service cycle, and includes the functions of damage detection, localization, and magnitude estimation.

4.2.1 Baseline phase

4.2.1.1 Baseline modelling of the healthy structure

Although not strictly required, the modelling of the healthy (nominal) structure is an initial step performed in order to facilitate (in the sense of providing approximate model orders) the subsequent step of damage topology (mode) modelling.

A single experiment is performed, based on which an interval estimate of a discrete-time model (or a vector model or an array of models in the case of several vibration response measurement locations) representing the healthy structural dynamics is obtained via standard identification procedures (Fassois 2001, Ljung 1999). In this study an array of two single excitation and single response AutoRegressive with eXogenous excitation (ARX) models is used.

An ARX(na, nb) model is of the form¹ (Fassois 2001, Ljung 1999, Söderström and Stoica 1989):

$$y[t] + \sum_{i=1}^{na} a_i \cdot y[t-i] = \sum_{i=0}^{nb} b_i \cdot x[t-i] + e[t] \quad e[t] \sim \text{iid} \mathcal{N}(0, \sigma_e^2) \quad (4.1)$$

with t designating the normalized discrete time ($t = 1, 2, 3, \dots$ with absolute time being $(t-1)T_s$, where T_s stands for the sampling period), $x[t]$, $y[t]$ the measured excitation and vibration response signals, respectively, na , nb the AutoRegressive (AR) and eXogenous (X) orders, respectively, and $e[t]$ the stochastic model residual (one-step-ahead prediction error) sequence, that is a white (serially uncorrelated), Gaussian, zero mean with variance σ_e^2 sequence, uncorrelated with the excitation $x[t]$. The symbol $\mathcal{N}(\cdot, \cdot)$ designates Gaussian distribution with the indicated mean and variance, and iid stands for identically independently distributed.

The model is parameterized in terms of the parameter vector $\bar{\theta} = [a_i : b_i : \sigma_e^2]^T$ to be estimated from the measured signals (Fassois 2001, Ljung 1999). Model estimation may be achieved based on minimization of the Ordinary Least Squares (OLS) or the Weighted Least Squares (WLS) criteria (Fassois 2001, Ljung 1999). The modelling procedure involves the successive fitting of ARX(na, nb) models for increasing orders na and nb , until an adequate model is selected (Fassois 2001). Model order selection is based on the Bayesian Information Criterion (BIC) and the residual sum of squares normalized by the series sum of squares (RSS/SSS). Final model validation is based on formal verification of the residual (one-step-ahead prediction error) sequence uncorrelatedness (whiteness) hypothesis (Ljung 1999, pp. 512–513).

¹Lower case/capital bold face symbols designate vector/matrix quantities, respectively.

4.2.1.2 The notion of damage topology (mode)

The notion of *damage topology (mode)* refers to the union of all admissible damage magnitudes on a particular topology (section or component) of the structure (damage of all possible magnitudes at all possible locations along a topology). Hence, a damage topology is defined via two variables: (a) damage magnitude and (b) damage location. For this purpose, the novel stochastic Vector-dependent Functionally Pooled AutoRegressive with eXogenous excitation (VFP-ARX) models of Chapter 3 are used. The VFP-ARX representation allows for complete and precise damage topology description, as the model parameters and residual series covariance depend functionally on damage magnitude and damage location, while the corresponding interrelations and statistical dependencies between the different damage magnitudes and locations are taken into account.

The VFP-ARX representation belongs to the recently introduced broader class of stochastic FP models, which make use of data pooling techniques for combining and optimally treating (as one entity) the data obtained from various experiments corresponding to different structural states and statistical techniques for model estimation (Kopsaftopoulos and Fassois 2006a, Sakellariou and Fassois 2007, Hios and Fassois 2009b).

4.2.1.3 Damage topology (mode) modelling

The modelling of a specific damage topology (mode) via a VFP-ARX model involves consideration of all admissible damage magnitudes occurring at predetermined locations on a specific section/component of the structure (right/left wing, horizontal stabilizer, and so on). For this reason a total of $M_1 \times M_2$ experiments is performed (physically or via analytical models and simulation), with M_1 and M_2 designating the number of experiments under the various damage magnitudes and locations, respectively. Each experiment is characterized by a specific damage magnitude k^1 and a specific damage location k^2 , with the complete series covering the required range of each variable, say $[k_{min}^1, k_{max}^1]$ and $[k_{min}^2, k_{max}^2]$, via the discretizations $\{k_1^1, k_2^1, \dots, k_{M_1}^1\}$ and $\{k_1^2, k_2^2, \dots, k_{M_2}^2\}$ (it is tacitly assumed, without loss of generality, that the healthy structure corresponds to $k^1 = 0$). For the identification of a model corresponding to a specific damage topology the vector operating parameter \mathbf{k} containing the damage magnitude and damage location components, is defined as:

$$\mathbf{k} \triangleq [k_i^1 \ k_j^2]^T \iff k_{i,j}, \quad i = 1, \dots, M_1, \quad j = 1, \dots, M_2 \quad (4.2)$$

with $k_{i,j}$ designating the state of the structure corresponding to the i -th damage magnitude and the j -th damage location. This procedure yields a pool of excitation-response signal pairs (each of length N):

$$x_{\mathbf{k}}[t], y_{\mathbf{k}}[t] \quad \text{with } t = 1, \dots, N, \quad k^1 \in \{k_1^1, \dots, k_{M_1}^1\}, \quad k^2 \in \{k_1^2, \dots, k_{M_2}^2\}. \quad (4.3)$$

A proper mathematical description of the structure for the considered damage topology may be then obtained in the form of a VFP-ARX model. In the case of several vibration measurement locations an array of such models (or else a vector model) may be obtained, with each scalar model corresponding to each measurement location and being designated as $\mathcal{M}_{\mathbf{k}}^{XY}$ (with X indicating the damage topology and Y the vibration measurement location).

The VFP-ARX model structure postulated is of the following form (Chapter 3):

$$y_{\mathbf{k}}[t] + \sum_{i=1}^{na} a_i(\mathbf{k}) \cdot y_{\mathbf{k}}[t-i] = \sum_{i=0}^{nb} b_i(\mathbf{k}) \cdot x_{\mathbf{k}}[t-i] + e_{\mathbf{k}}[t] \quad (4.4a)$$

$$e_{\mathbf{k}}[t] \sim \text{iid } \mathcal{N}(0, \sigma_e^2(\mathbf{k})) \quad \mathbf{k} \in \mathbb{R}^2 \quad (4.4b)$$

$$a_i(\mathbf{k}) \triangleq \sum_{j=1}^p a_{i,j} \cdot G_j(\mathbf{k}), \quad b_i(\mathbf{k}) \triangleq \sum_{j=1}^p b_{i,j} \cdot G_j(\mathbf{k}) \quad (4.4c)$$

$$E\{e_{k_{i,j}}[t] \cdot e_{k_{m,n}}[t - \tau]\} = \gamma_e[k_{i,j}, k_{m,n}] \cdot \delta[\tau] \quad (4.4d)$$

with na , nb designating the AutoRegressive (AR) and eXogenous (X) orders, respectively, $x_{\mathbf{k}}[t]$, $y_{\mathbf{k}}[t]$ the excitation and response signals, respectively, and $e_{\mathbf{k}}[t]$ the model's residual (one-step-ahead prediction error) sequence, that is a white (serially uncorrelated) zero mean sequence with variance $\sigma_e^2(\mathbf{k})$. This sequence should be uncorrelated with the excitation $x_{\mathbf{k}}[t]$ but potentially cross-correlated with its counterparts corresponding to different experiments (different \mathbf{k} 's). The symbol $E\{\cdot\}$ designates statistical expectation, $\delta[\tau]$ the Kronecker delta (equal to unity for $\tau = 0$ and equal to zero for $\tau \neq 0$), $\mathcal{N}(\cdot, \cdot)$ Gaussian distribution with the indicated mean and variance, and iid stands for identically independently distributed.

As (4.4c) indicates, the AR and X parameters $a_i(\mathbf{k})$, $b_i(\mathbf{k})$ are modeled as explicit functions of the vector \mathbf{k} (which contains the damage magnitude and damage location components) by belonging to p -dimensional functional subspace spanned by the mutually independent basis functions $G_1(\mathbf{k}), G_2(\mathbf{k}), \dots, G_p(\mathbf{k})$ (*functional basis*). The functional basis consists of polynomials of two variables (bivariate) obtained as tensor products from their corresponding univariate polynomials (Chebyshev, Legendre, Jacobi, and other families (Dunkl and Xu 2001)), while the whole procedure of the subspace creation is described in detail in Appendix A of Chapter 3. The constants $a_{i,j}$ and $b_{i,j}$ designate the AR and X, respectively, coefficients of projection.

The VFP-ARX model of (4.4a)–(4.4d) is parameterized in terms of the parameter vector to be estimated from the measured signals:

$$\bar{\boldsymbol{\theta}} \triangleq [\alpha_{i,j} : b_{i,j} : \sigma_e^2(\mathbf{k})]^T \quad \forall \mathbf{k} \quad (4.5)$$

and may be written in linear regression form as:

$$y_{\mathbf{k}}[t] = [\boldsymbol{\varphi}_{\mathbf{k}}^T[t] \otimes \mathbf{g}^T(\mathbf{k})] \cdot \boldsymbol{\theta} + e_{\mathbf{k}}[t] = \boldsymbol{\phi}_{\mathbf{k}}^T[t] \cdot \boldsymbol{\theta} + e_{\mathbf{k}}[t] \quad (4.6)$$

with:

$$\boldsymbol{\varphi}_{\mathbf{k}}[t] \triangleq \left[-y_{\mathbf{k}}[t-1] \dots -y_{\mathbf{k}}[t-na] : x_{\mathbf{k}}[t] \dots x_{\mathbf{k}}[t-nb] \right]_{[(na+nb+1) \times 1]}^T \quad (4.7a)$$

$$\mathbf{g}(\mathbf{k}) \triangleq \left[G_1(\mathbf{k}) \dots G_p(\mathbf{k}) \right]_{[p \times 1]}^T \quad (4.7b)$$

$$\boldsymbol{\theta} \triangleq \left[a_{1,1} \dots a_{na,p} : b_{0,1} \dots b_{nb,p} \right]_{[(na+nb+1)p \times 1]}^T \quad (4.7c)$$

and T designating transposition and \otimes Kronecker product (Bernstein 2005, chap. 7).

Pooling together the expressions (4.6) of the VFP-ARX model corresponding to all vector operating parameters \mathbf{k} ($k_{1,1}, k_{1,2}, \dots, k_{M_1, M_2}$) considered in the experiments (cross-sectional pooling) yields:

$$\begin{bmatrix} y_{k_{1,1}}[t] \\ \vdots \\ y_{k_{M_1, M_2}}[t] \end{bmatrix} = \begin{bmatrix} \phi_{k_{1,1}}^T[t] \\ \vdots \\ \phi_{k_{M_1, M_2}}^T[t] \end{bmatrix} \cdot \boldsymbol{\theta} + \begin{bmatrix} e_{k_{1,1}}[t] \\ \vdots \\ e_{k_{M_1, M_2}}[t] \end{bmatrix} \implies \mathbf{y}[t] = \boldsymbol{\Phi}[t] \cdot \boldsymbol{\theta} + \mathbf{e}[t]. \quad (4.8)$$

Then, following substitution of the data for $t = 1, \dots, N$ the following expression is obtained:

$$\mathbf{y} = \boldsymbol{\Phi} \cdot \boldsymbol{\theta} + \mathbf{e} \quad (4.9)$$

with

$$\mathbf{y} \triangleq \begin{bmatrix} \mathbf{y}[1] \\ \vdots \\ \mathbf{y}[N] \end{bmatrix}, \quad \boldsymbol{\Phi} \triangleq \begin{bmatrix} \boldsymbol{\Phi}[1] \\ \vdots \\ \boldsymbol{\Phi}[N] \end{bmatrix}, \quad \mathbf{e} \triangleq \begin{bmatrix} \mathbf{e}[1] \\ \vdots \\ \mathbf{e}[N] \end{bmatrix}. \quad (4.10)$$

Using the above linear regression framework the simplest approach for estimating the projection coefficient vector $\boldsymbol{\theta}$ is based on minimization of the Ordinary Least Squares (OLS) criterion $J^{\text{OLS}} \triangleq \frac{1}{N} \sum_{t=1}^N \mathbf{e}^T[t] \mathbf{e}[t]$.

A more appropriate criterion is (in view of the Gauss-Markov theorem (Greene 2003)) the Weighted Least Squares (WLS) criterion:

$$J^{\text{WLS}} \triangleq \frac{1}{N} \sum_{t=1}^N \mathbf{e}^T[t] \boldsymbol{\Gamma}_{\mathbf{e}[t]}^{-1} \mathbf{e}[t] = \frac{1}{N} \mathbf{e}^T \boldsymbol{\Gamma}_{\mathbf{e}}^{-1} \mathbf{e} \quad (4.11)$$

which leads to the *Weighted Least Squares (WLS)* estimator:

$$\hat{\boldsymbol{\theta}}^{\text{WLS}} = [\boldsymbol{\Phi}^T \boldsymbol{\Gamma}_{\mathbf{e}}^{-1} \boldsymbol{\Phi}]^{-1} [\boldsymbol{\Phi}^T \boldsymbol{\Gamma}_{\mathbf{e}}^{-1} \mathbf{y}]. \quad (4.12)$$

In these expressions $\boldsymbol{\Gamma}_{\mathbf{e}} = E\{\mathbf{e}\mathbf{e}^T\}$ ($\boldsymbol{\Gamma}_{\mathbf{e}} = \boldsymbol{\Gamma}_{\mathbf{e}[t]} \otimes \mathbf{I}_N$, with \mathbf{I}_N designating the $N \times N$ unity matrix) designates the residual covariance matrix, which is practically unavailable. Nevertheless, it may be consistently estimated by applying (in an initial step) Ordinary Least Squares (details in Chapter 3). Once $\hat{\boldsymbol{\theta}}^{\text{WLS}}$ has been obtained, the final residual variance and residual covariance matrix estimates are obtained as:

$$\hat{\sigma}_{\mathbf{e}}^2(\mathbf{k}, \hat{\boldsymbol{\theta}}^{\text{WLS}}) = \frac{1}{N} \sum_{t=1}^N e_{\mathbf{k}}^2[t, \hat{\boldsymbol{\theta}}^{\text{WLS}}], \quad \hat{\boldsymbol{\Gamma}}_{\mathbf{e}[t]} = \frac{1}{N} \sum_{t=1}^N \mathbf{e}[t, \hat{\boldsymbol{\theta}}^{\text{WLS}}] \mathbf{e}^T[t, \hat{\boldsymbol{\theta}}^{\text{WLS}}]. \quad (4.13)$$

The estimator $\hat{\boldsymbol{\theta}}^{\text{WLS}}$ may, under mild conditions, be shown to be asymptotically Gaussian distributed with mean coinciding with the true parameter vector $\boldsymbol{\theta}^o$ and covariance matrix $\mathbf{P}_{\boldsymbol{\theta}}$:

$$\sqrt{N}(\hat{\boldsymbol{\theta}}_N - \boldsymbol{\theta}^o) \sim \mathcal{N}(\mathbf{0}, \mathbf{P}_{\boldsymbol{\theta}}) \quad (N \longrightarrow \infty) \quad (4.14)$$

based on which interval estimates of the true parameter vector may be constructed (for details see Chapter 3).

The problem of VFP-ARX model structure selection (structure estimation) for a given basis function family (such as Chebyshev, Legendre, and so on), that is model order determination for the AR and X polynomials and determination of their corresponding functional subspaces, is referred

to as the model identification problem. Usually, the AR and X model orders are initially selected via customary model order selection techniques (BIC, RSS, stabilization diagrams) (Ljung 1999), whereas the functional subspace dimensionalities are selected via a Genetic Algorithm (GA) procedure (Chipperfield *et al.* n.d.). Initially, maximum functional subspace dimensionalities are selected, which define the search space of the functional subspace estimation subproblem. The determination of the exact subspace dimensionalities is achieved via the use of GAs based on minimization of the BIC with respect to the candidate basis functions (see Section 3.4 for details).

4.2.2 Inspection phase

Let $x[t]$, $y[t]$ ($t = 1, 2, \dots, N$) represent the current excitation and response signals, respectively, obtained from the structure in an *unknown* (to be classified) state. Damage detection, localization, and magnitude estimation are based on the pre-determined in the baseline phase VFP-ARX models, with each model corresponding to a specific damage topology (mode). The current excitation and response signals are driven through these models and estimates of the current values of the operating vector \mathbf{k} and residual series $e_{\mathbf{k}}[t]$ are obtained from each one. Subsequently, these estimates are used for tackling the damage detection, localization, and magnitude estimation tasks within a statistical decision making framework.

4.2.2.1 Step I: Damage detection

Damage detection is based on the re-parameterized, in terms of \mathbf{k} and $\sigma_e^2(\mathbf{k})$ VFP-ARX model of *any* damage topology (e.g. V). Thus, the projection coefficients are replaced by the corresponding estimates available from the baseline phase, while the vector \mathbf{k} containing the damage magnitude and location, and the residual series variance $\sigma_e^2(\mathbf{k})$ are the current unknown parameters to be estimated:

$$\mathcal{M}^V(\mathbf{k}, \sigma_e^2(\mathbf{k})) : \quad y[t] + \sum_{i=1}^{na} a_i(\mathbf{k}) \cdot y[t-i] = \sum_{i=0}^{nb} b_i(\mathbf{k}) \cdot x[t-i] + e[t]. \quad (4.15)$$

The estimation of the currently unknown parameters \mathbf{k} and $\sigma_e^2(\mathbf{k})$ based on the current excitation and response signals, may be achieved via the following Nonlinear Least Squares (NLS) and variance estimators (refer to Ljung (1999, pp. 327–329) for details on NLS estimation):

$$\hat{\mathbf{k}} = \arg \min_{\mathbf{k}} \sum_{t=1}^N e^2[t], \quad \sigma_e^2(\hat{\mathbf{k}}) = \frac{1}{N} \sum_{t=1}^N e^2[t, \hat{\mathbf{k}}] \quad (4.16)$$

the first one realized via a hybrid optimization scheme based on Genetic Algorithms (GA) (Chipperfield *et al.* n.d.) and constrained nonlinear optimization (Sequential Quadratic Programming – SQP) (Gill *et al.* 1981, Coleman and Zhang n.d.).

The GA aims at exploring the complete search space ((k^1, k^2) plane) with the objective of locating promising regions within which the “true” \mathbf{k} might be located. Despite the GA’s inherent ability for effective global optimization, they often suffer in terms of exact global optimum localization. Hence, a constrained nonlinear optimization scheme is employed in a suitably defined neighborhood of the GA result in order to find the exact global optimum $\hat{\mathbf{k}}$.

Assuming that the structure is indeed under a damage belonging to damage topology V (or healthy) the first estimator may be shown to be asymptotically ($N \rightarrow \infty$) Gaussian distributed,

with mean equal to the true \mathbf{k} value and covariance matrix $\Sigma_{\mathbf{k}}$ ($\hat{\mathbf{k}} \sim \mathcal{N}(\mathbf{k}, \Sigma_{\mathbf{k}})$) coinciding with the Cramer-Rao lower bound, which may be obtained as:

$$\hat{\Sigma}_{\mathbf{k}} = \frac{\hat{\sigma}_e^2(\hat{\mathbf{k}})}{N} \left[\frac{1}{N} \sum_{t=1}^N \left[\boldsymbol{\varphi}^T[t] \otimes \frac{\partial \mathbf{g}^T(\mathbf{k})}{\partial \mathbf{k}} \Big|_{\mathbf{k}=\hat{\mathbf{k}}} \cdot \hat{\boldsymbol{\theta}} \right] \cdot \left[\boldsymbol{\varphi}^T[t] \otimes \frac{\partial \mathbf{g}^T(\mathbf{k})}{\partial \mathbf{k}} \Big|_{\mathbf{k}=\hat{\mathbf{k}}} \cdot \hat{\boldsymbol{\theta}} \right]^T \right]^{-1}. \quad (4.17)$$

In this expression $\boldsymbol{\varphi}[t]$ is defined as in (4.7a), while $\hat{\boldsymbol{\theta}}$ designates the available from the baseline phase estimate of projection coefficients vector corresponding to the selected damage topology model.

Since the healthy structure corresponds to $k^1 = 0$ (zero damage magnitude) for any damage topology model, damage detection may be based on the following hypothesis testing problem:

$$\begin{aligned} H_o & : k^1 = 0 \quad (\text{null hypothesis - healthy structure}) \\ H_1 & : k^1 \neq 0 \quad (\text{alternative hypothesis - damaged structure}). \end{aligned} \quad (4.18)$$

Under the null (H_o) hypothesis, the following statistic follows t -distribution with $N - 1$ degrees of freedom (which should be adjusted to $N - 2$ in case the estimated mean is subtracted from the residual series in the computation of $\hat{\Sigma}_{\mathbf{k}}$):

$$t = \frac{\hat{k}^1}{\hat{\sigma}_{k^1}} \sim t(N - 1) \quad (4.19)$$

with $\hat{\sigma}_{k^1}$ being the positive square root of the first diagonal element of $\hat{\Sigma}_{\mathbf{k}}$ (estimated standard deviation of k^1). This leads to the following test at the α risk level (probability of false alarm, or type I error, that is accepting H_1 although H_o is true, being equal to α):

$$\begin{aligned} t_{\frac{\alpha}{2}}(N - 1) \leq t \leq t_{1-\frac{\alpha}{2}}(N - 1) & \implies H_o \text{ is accepted (healthy structure)} \\ \text{Else} & \implies H_1 \text{ is accepted (damaged structure)} \end{aligned} \quad (4.20)$$

with t_α designating the t distribution's (with the indicated degrees of freedom) α critical point [defined such that $\text{Prob}(t \leq t_\alpha) = \alpha$].

4.2.2.2 Step II: Damage topology (mode) identification

Damage topology (mode) identification corresponds to the examination of which one of the available damage topology VFP-ARX models provides, for its estimated $\hat{\mathbf{k}}$, a valid representation of the *current* structural dynamics based on residual uncorrelatedness (whiteness) hypothesis testing. The current damage topology is that corresponding to the valid model, which will exhibit an uncorrelated (white) residual sequence for the corresponding $\hat{\mathbf{k}}$.

Once damage occurrence has been detected, current damage topology determination is based on the successive estimation (using the current data) and validation of the re-parameterized $\mathcal{M}^V(\mathbf{k}, \sigma_e^2(\mathbf{k}))$ VFP-ARX models (Equation 4.15) for $V = A, B, \dots$ corresponding to the various damage modes. The procedure stops as soon as a particular model is successfully validated, with the corresponding damage topology identified as current. Model validation may be based on a statistical test examining the residual uncorrelatedness (whiteness) via the statistical hypothesis testing problem:

$$\begin{aligned} H_o & : \rho_V[\tau] = 0 \quad \tau = 1, 2, \dots, r \quad (\text{damage is of type } V) \\ H_1 & : \rho_V[\tau] \neq 0 \quad \text{for some } \tau \quad (\text{damage is not of type } V) \end{aligned} \quad (4.21)$$

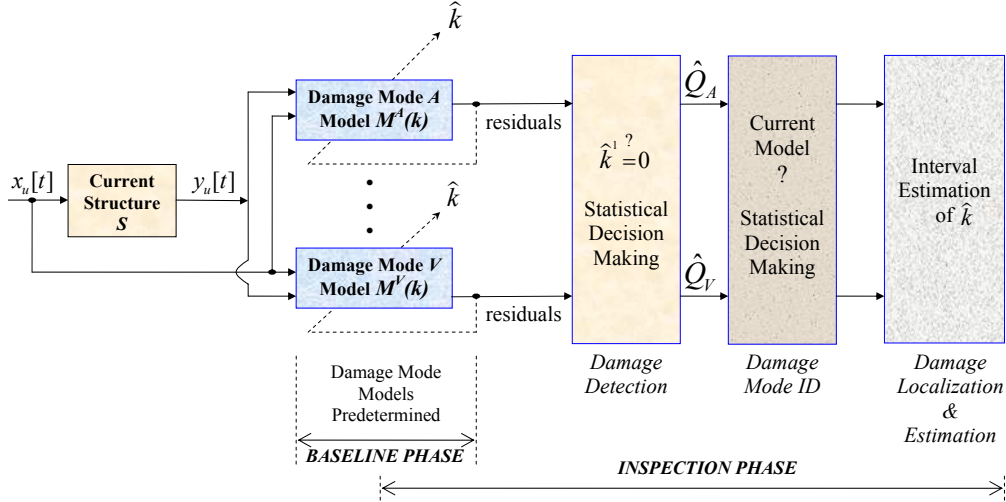


Figure 4.1: Flowchart representation of the VFP-ARX model based method.

in which $\rho_V[\tau]$ ($\tau = 1, 2, \dots, r$) designates the residual series normalized autocorrelation at lag τ . Under the null hypothesis the following Q statistic follows a chi-square (χ^2) distribution with r degrees of freedom (Box *et al.* 1994, p. 314):

$$Q = N(N + 2) \cdot \sum_{\tau=1}^r (N - \tau)^{-1} \hat{\rho}_V^2[\tau] \sim \chi^2(r) \quad (4.22)$$

in which N designates the residual signal length (in number of samples), $\hat{\rho}_V[\tau]$ the estimated (sample) normalized autocorrelation at lag τ , and r the maximum lag. This leads to the following test at the α risk level:

$$\begin{aligned} Q < \chi_{1-\alpha}^2(r) &\implies H_0 \text{ is accepted (damage is of type } V) \\ \text{Else} &\implies H_1 \text{ is accepted (damage is not of type } V) \end{aligned} \quad (4.23)$$

with $\chi_{1-\alpha}^2(r)$ designating the distribution's $(1 - \alpha)$ critical point.

It should be noticed that inability to identify a particular damage topology (obviously as not previously modeled) indirectly implies damage detection.

4.2.2.3 Step III: Damage localization and magnitude estimation

Damage localization and magnitude estimation are then based on the interval estimates of k^2 and k^1 , respectively, which are constructed based on the $\hat{\mathbf{k}}, \hat{\Sigma}_{\mathbf{k}}$ estimates obtained from the corresponding re-parameterized VFP-ARX model (of the form (4.15)) of the *current* valid damage topology. Thus, using Equation (4.19), the interval estimates of k^1 (damage magnitude) and k^2 (damage location) at the α risk level are:

$$k^i \text{ interval estimate: } \quad \left[\hat{k}^i + t_{\frac{\alpha}{2}}(N - 1) \cdot \hat{\sigma}_{k^i}, \hat{k}^i + t_{1-\frac{\alpha}{2}}(N - 1) \cdot \hat{\sigma}_{k^i} \right] \quad (4.24)$$

with $i = 1$ for damage magnitude and $i = 2$ for damage location, while $\hat{\sigma}_{k^i}$ is the positive square root of the i -th diagonal element of $\hat{\Sigma}_{\mathbf{k}}$.

Bivariate confidence bounds for $\mathbf{k} = [k^1 \ k^2]^T$ may be also obtained by observing that the quantity follows chi-square distribution with two degrees of freedom (Ljung 1999, p. 558):

$$(\hat{\mathbf{k}} - \mathbf{k})^T \boldsymbol{\Sigma}_{\mathbf{k}}^{-1} (\hat{\mathbf{k}} - \mathbf{k}) \sim \chi_{1-\alpha}^2(2). \quad (4.25)$$

Thus the probability that:

$$(\hat{\mathbf{k}} - \mathbf{k})^T \boldsymbol{\Sigma}_{\mathbf{k}}^{-1} (\hat{\mathbf{k}} - \mathbf{k}) \leq \chi_{1-\alpha}^2(2) \quad (4.26)$$

is equal to $1 - \alpha$ ($\chi_{1-\alpha}^2(2)$ designating the χ^2 distribution's with two degrees of freedom $1 - \alpha$ critical point). This expression defines an ellipsoid on the (k^1, k^2) plane within which the true (k^1, k^2) point should lie with probability $(1 - \alpha)$, or equivalently, with risk α (*bivariate confidence bounds*). The shape of the ellipsoid is determined by $\boldsymbol{\Sigma}_{\mathbf{k}}$. Notice that in practice $\boldsymbol{\Sigma}_{\mathbf{k}}$ is replaced by its estimate, which is assumed to be of negligible variability.

Figure 4.1 presents a flowchart representation of the VFP-ARX model based method for damage detection, identification and magnitude estimation.

4.3 The experimental set-up

4.3.1 The structure

The scale aircraft skeleton structure used in the experiments was designed by ONERA (France) in conjunction with the Structures and Materials Action Group SM-AG19 of the Group for Aeronautical Research and Technology in Europe (GARTEUR) (Degener and Hermes 1996, Balmes and Wright 1997). The currently used structure was manufactured at the University of Patras (Figure 4.2a). This testbed represents a typical aircraft skeleton design and consists of six solid beams with rectangular cross sections representing the fuselage, the wing, the horizontal and vertical stabilizers, and the right and left wing tips. All parts of the structure are constructed from standard aluminum and are jointed together via steel plates and screws. The total mass of the structure is approximately 50 kg and its dimensions are indicated in Table 4.1.

4.3.2 The damage topologies and scenarios

The damage scenarios considered correspond to the attachment of a variable number of unit masses, simulating local elasticity reductions, at three different topologies (presently geometrical axes) on the structure. Each unit mass approximately is 8.132 g and is attached to the structure using adhesive wax. Small masses are frequently used as a non-destructive way to simulate local stiffness reduction (for instance see Sakellariou and Fassois 2008, Kopsaftopoulos and Fassois 2007, Zepico-Valle *et al.* 2011, Panopoulou *et al.* 2011), while other types of damages, such as the loosening of bolts, have been also effectively considered in other recent studies (Kopsaftopoulos and Fassois 2011*b*, Kopsaftopoulos and Fassois 2011*d*). In the present study each damage belongs to one of three distinct *damage topologies* (modes) (see Figure 4.2 and Table 4.2):

- (a) The first (*damage topology (mode) A*) corresponds to the attachment of up to 10 unit masses at a single location, representing different damage magnitudes in the range of $[0, 81.32]$ g, at any point on the aa' axis (Figure 4.2b), starting from a and moving to the left along the right wing of the aircraft in the range $0 - 80$ cm – Figure 4.2.
- (b) The second (*damage topology (mode) B*) corresponds to the attachment of up to 10 unit masses at a single location, representing different damage magnitudes in the range of $[0, 81.32]$ g, at

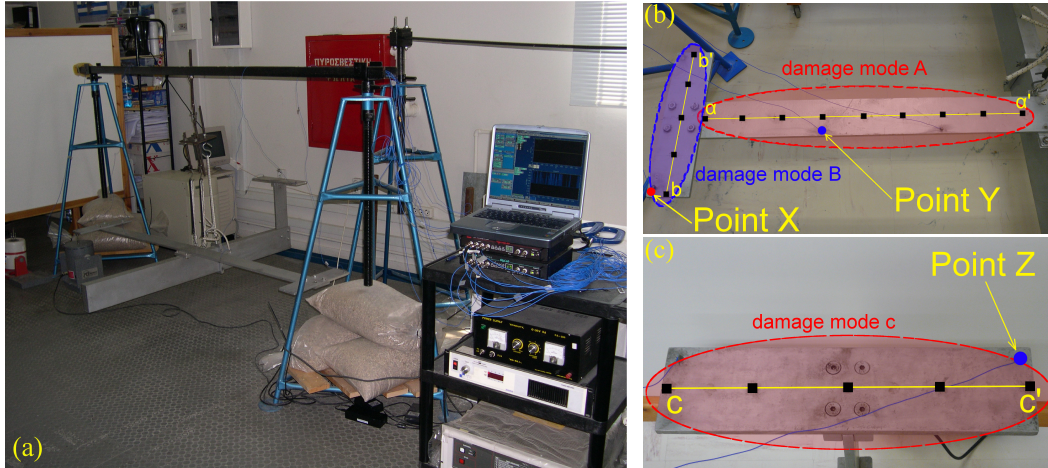


Figure 4.2: (a) The scale aircraft skeleton structure and the experimental set-up; (b) the right wing-tip with the force excitation (Point X), the first vibration measurement position (Point Y), and the aa' and bb' axes that define the A and B damage topologies, respectively; (c) the horizontal stabilizer with the second vibration measurement position (Point Z) and the cc' axis that defines the C damage topology.

any point on the bb' axis (Figure 4.2b), starting from b and moving backwards along the right wing-tip in the range 0 – 40 cm.

- (c) The third (*damage topology (mode) C*) corresponds to the attachment of up to 10 unit masses at a single location, representing different damage magnitudes in the range of [0, 81.32] g, at any point on the cc' axis (Figure 4.2c), starting from c and moving to the left along the horizontal stabilizer in the range 0 – 40 cm.

Each damage – belonging to any one of the above topologies or, perhaps, to an “unmodelled” topology – is designated as F_{k^1, k^2}^X , with $X = A, B, C$ indicating a particular damage topology, k^1 the damage magnitude (g of added mass) and k^2 the precise damage location (distance in cm along the pertinent axis). The healthy structure corresponds to $k^1 = 0$ (0 g of added mass) and is designated as F_o .

4.3.3 The experimental procedure

Damage detection, localization, and magnitude estimation are based on vibration testing of the structure, which is suspended through a set of bungee cords and hooks from a long rigid beam sustained by four heavy-type stands (Figure 4.2a). The suspension is designed in a way as to exhibit a pendulum

Component	Length (mm)	Width (mm)	Thickness (mm)
Fuselage	1500	150	50
Wings	2000	100	10
Horizontal Stabilizer	300	100	10
Vertical Stabilizer	400	100	10
Wing-tips	400	100	10

Table 4.1: Dimensions of the scale aircraft skeleton structure.

Damage Topology (Mode)	Description
A	any mass anywhere on the right wing ($k^1 \in [0, 81.32]$ g with $\delta k^1 = 8.132$ g, $k^2 \in [0, 80]$ cm)
B	any mass anywhere on the right wing-tip ($k^1 \in [0, 81.32]$ g with $\delta k^1 = 8.132$ g, $k^2 \in [0, 40]$ cm)
C	any mass anywhere on the hor. stab. ($k^1 \in [0, 81.32]$ g with $\delta k^1 = 8.132$ g, $k^2 \in [0, 40]$ cm)

Table 4.2: The considered damage topologies (modes) – see Figure 4.2b-c.

rigid body mode below the frequency range of interest, as the boundary conditions are free-free.

The excitation is broadband random stationary Gaussian applied vertically at the right wing-tip (Point X, Figure 4.2b) through an electromechanical modal shaker (MB Dynamics Modal 50A, max load 225 N) equipped with a stinger. The actual force exerted on the structure is measured via an impedance head (PCB M288D01, sensitivity 98.41 mV/lb), while the resulting vertical acceleration responses at Points Y and Z (Figure 4.2b-c) are measured via lightweight accelerometers (PCB 352A10 miniature ICP accelerometers, 0.7 g, frequency range 0.003 – 10 kHz, sensitivity ~ 1.052 mV/m/s²). The force and acceleration signals are driven through a conditioning charge amplifier (PCB 481A02) into the data acquisition system based on SigLab 20-42 measurement modules (each module featuring four 20-bit simultaneously sampled A/D channels, two 16-bit D/A channels, and analog anti-aliasing filters).

4.3.4 The signals

The excitation and response signal bandwidth is selected as 4 – 90 Hz, with the lower limit set in order to avoid instrument dynamics and rigid body modes. Each signal is digitized at $f_s = 256$ Hz, resulting in a length of $N = 1500$ samples, and is subsequently sample mean corrected and normalized by its sample standard deviation (Table 4.3).

4.4 Damage detection, localization, and magnitude estimation results

Damage detection, localization, and magnitude estimation results for damage of any magnitude occurring anywhere in one of the three specified *topologies* (modes) is now considered.

The considered damage test cases are summarized in Table 4.4 – each test case is considered twice, first via the Point Y and then via the Point Z sensor. Notice that Test Case I corresponds to the healthy structure, Test Cases II – IV to damage in topology A (right wing), Test Cases V – VI to damage in topology B (right wing-tip), Test Cases VII – VIII to damage in topology C (horizontal stabilizer), while Test Case IX does *not* belong to any of the considered topologies and for this reason it is referred to as “unmodelled” (it corresponds to damage on the left wing-tip). The challenging issue with this last Test Case is whether or not it will be possible to detect it and “negatively” localize it as not belonging to any one of the A – C topologies. It should be further emphasized that none of the

Sampling frequency: $f_s = 256$ Hz	Bandwidth: [4 – 90] Hz
Signal length: $N = 1500$ samples (5.85 s)	

Table 4.3: Signal pre-processing and details.

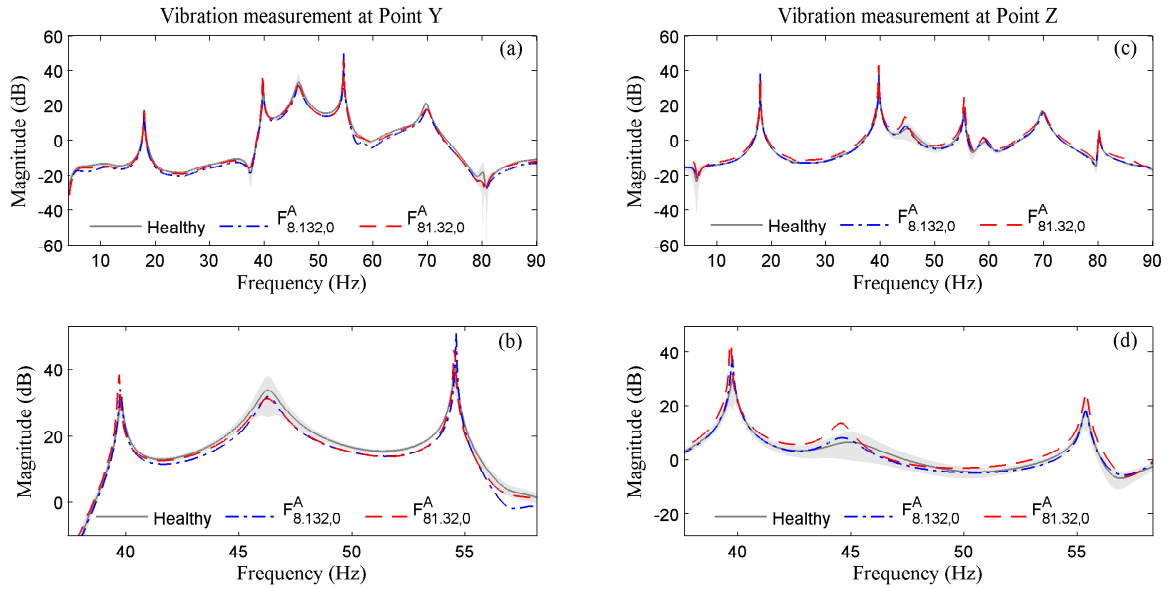


Figure 4.3: The effects of two topology A damages on parametrically obtained FRF magnitude curves corresponding to each one of the Point X – Point Y (a – b) and Point X – Point Z (c – d) transfer functions. The gray zones depict 95% confidence intervals (uncertainty zones) for the healthy FRF magnitudes. The (b) and (d) subplots are blow ups of (a) and (c), respectively.

damages considered in the Test Cases is used in the baseline (training) phase of the next subsection.

The damage diagnosis method operates on a single pair of excitation – response signals, namely the excitation force that is always applied at Point X, and a vibration acceleration response measured either at Points Y or at Point Z (Figure 4.2b-c). Depending on the distance of the employed accelerometer sensor from the damage occurrence location, the damage is labeled as being “local” or “remote” to the response sensor used.

The effects of the considered damage cases to the structural dynamics are depicted in Figure 4.3, which presents parametric (ARX(48, 48) model based) Frequency Response Function (FRF) magnitude estimates (Matlab function *ffplot.m*) for the Point X–Point Y and Point X–Point Z transfer functions for the healthy and two damage cases belonging to topology (mode) A (notice that 95% confidence

Test Case	Damage	Damage Topology (mode)	Description
I	F_o	–	Healthy structure
II	$F_{8.132,80}^A$	A	Mass of 8.132 g at 80 cm (right wing)
III	$F_{32.528,0}^A$	A	Mass of 32.528 g at 0 cm (right wing)
IV	$F_{40.66,75}^A$	A	Mass of 40.66 g at 75 cm (right wing)
V	$F_{8.132,0}^B$	B	Mass of 8.132 g at 0 cm (right wing-tip)
VI	$F_{16.26,5}^B$	B	Mass of 16.26 g at 5 cm (right wing-tip)
VII	$F_{12.19,10}^C$	C	Mass of 12.19 g at 10 cm (horizontal stab.)
VIII	$F_{81.32,30}^C$	C	Mass of 81.32 g at 30 cm (horizontal stab.)
IX	$F_{40.66,10}$	Unmodelled	Mass of 40.66 g at 10 cm (left wing-tip)

† Each case is considered separately via Point Y or Point Z measurements.

Table 4.4: The considered test cases†.

intervals are also depicted for the healthy FRFs). Evidently, the effects of damage are rather small, which underscores the challenges underlying the damage diagnosis problem.

4.4.1 Baseline phase

4.4.1.1 Baseline modelling of the healthy structure

Conventional ARX models representing the healthy structure are obtained through standard identification procedures (Fassois 2001, Ljung 1999) based on obtained excitation-response signals (5.85 s, $N = 1500$ sample long, Matlab function *arx.m*). This leads to an ARX(48, 48) model characterized by zero delay ($b_o \neq 0$ in the exogenous polynomial) for the Point X–Point Y transfer function. Similarly, an ARX(51, 51) model ($b_o \neq 0$) is obtained for the Point X–Point Z transfer function. These models are used as reference and for providing approximate orders for the corresponding damage topology (mode) models of the next paragraph. The global modal characteristics (natural frequencies and damping ratios) of the structure based on the identified ARX(48, 48) model of the healthy structure are presented in Table 4.5.

4.4.1.2 Modelling of the dynamics for damage topologies (modes) A, B, C

Damage mode modelling for damage topology (mode) A (right wing – refer to Table 4.2) is based on signals obtained from a total of $M_1 \times M_2 = 99$ experiments. 9 experiments correspond to the healthy structure ($k^1 = 0$ g) and 90 to the damaged structure (1 – 10 unit masses being placed at each one of 9 locations on the right wing – Figure 4.2b). The mass and location increments used are $\delta k^1 = 8.132$ g and $\delta k^2 = 10$ cm, covering the intervals $[0, 81.32]$ g and $[0, 80]$ cm.

Damage mode modelling for damage topologies (modes) B (right wing-tip) and C (horizontal stabilizer) (refer to Table 4.2) is based on signals obtained from a total of $M_1 \times M_2 = 55$ experiments. 5 experiments correspond to the healthy structure ($k^1 = 0$ g) and 50 to the damaged structure (1 – 10 unit masses being placed at each one of 5 locations on the right wing-tip for damage mode B or on the horizontal stabilizer for damage mode C – Figure 4.2b-c). The mass and location increments used are $\delta k^1 = 8.132$ g and $\delta k^2 = 10$ cm, covering the intervals $[0, 81.32]$ g and $[0, 40]$ cm.

Based on the signals collected from the aforementioned experiments, two models are identified for each one of the A, B, C damage topologies: The first model describes the Point X – Point Y dynamics (transfer function) and the second the Point X – Point Z dynamics (transfer function).

Mode	Natural Frequency (Hz)	Damping Ratio (%)
1	6.21	8.70
2	17.95	0.33
3	39.80	0.26
4	46.11	0.75
5	54.51	0.04
6	55.37	0.24
8	59.60	3.29
9	69.74	0.78
10	80.11	0.14

Table 4.5: Global modal characteristics (natural frequencies and damping ratios) of the structure based on the identified ARX(48, 48) model of the healthy structure.

Damage Topology (mode)	Vibration measurement at Point Y	Vibration measurement at Point Z
A	$\mathcal{M}_{\mathbf{k}}^{AY} : \text{VFP-ARX}(48, 48)_{30}$	$\mathcal{M}_{\mathbf{k}}^{AZ} : \text{VFP-ARX}(51, 51)_{30}$
B	$\mathcal{M}_{\mathbf{k}}^{BY} : \text{VFP-ARX}(57, 57)_{30}$	$\mathcal{M}_{\mathbf{k}}^{BZ} : \text{VFP-ARX}(69, 69)_{30}$
C	$\mathcal{M}_{\mathbf{k}}^{CY} : \text{VFP-ARX}(44, 44)_{30}$	$\mathcal{M}_{\mathbf{k}}^{CZ} : \text{VFP-ARX}(65, 65)_{30}$
Weighted Least Squares (WLS) estimation		
99 training experiments for damage topology A; 55 training experiments each for topologies B and C		
Frequency range [4 – 90] Hz, Sampling frequency $f_s = 256$ Hz		
Signal length $N = 1500$ samples (5.85 s)		

Table 4.6: The structure of the identified damage topology (mode) models.

Model order selection starts with the orders selected for the conventional ARX models representing the healthy structure, the final model orders being presently selected based on the BIC criterion (Fassois 2001) and model validation techniques, such as checking the whiteness (uncorrelatedness) and the normality of the model residuals (Matlab functions *acf.m* and *normplot.m*, respectively) (Fassois 2001, Ljung 1999). The functional subspaces are selected via a Genetic Algorithm (GA) based procedure (Matlab function *ga.m*). An extended functional subspace consisting of 45 Chebyshev Type II bivariate polynomial basis functions (see Appendix A of Chapter 3) is initially considered, with the GA aiming at selecting the optimal functional basis subset based on BIC minimization (see Section 3.4.1.2 – GA estimation details in Table 4.7).

The identified damage mode models are summarized in Table 4.6 and are as follows:

- (a) Point X – Point Y Dynamics: A VFP-ARX damage model is identified for each damage topology mode based on $N = 1500$ sample-long signals: a VFP-ARX(48, 48) for damage topology A, a VFP-ARX(57, 57) for damage topology B, and a VFP-ARX(44, 44) model for damage topology C. Each functional subspace consists of $p = 30$ Chebyshev Type II 2-dimensional polynomials.
- (b) Point X – Point Z Dynamics: A VF-ARX damage model is identified for each damage topology based on $N = 1500$ sample-long signals: a VFP-ARX(51, 51) for damage topology A, a VFP-ARX(69, 69) for damage topology B, and a VFP-ARX(65, 65) model for damage topology C. Like in the previous case, each functional subspace consists of $p = 30$ Chebyshev Type II 2-dimensional polynomials.

Indicative FRF magnitude curves obtained from damage topology A and the Point Y VFP-ARX(48, 48)₃₀ model (designated as $\mathcal{M}_{\mathbf{k}}^{AY}$) are, as functions of frequency, damage magnitude and location, depicted in Figure 4.4. Indicative AR parameters of the same model are depicted in Figure 4.5 as functions of damage magnitude and location. Similarly, indicative natural frequencies obtained by the model as functions of damage magnitude and location are presented in Figure 4.6 (also compare with Figure 4.3 and Table 4.5).

Population size	Elite count	Crossover fraction	Maximum number of generations
100	20	0.7	1000

Table 4.7: Genetic Algorithm (GA) details for functional subspace dimensionality estimation.

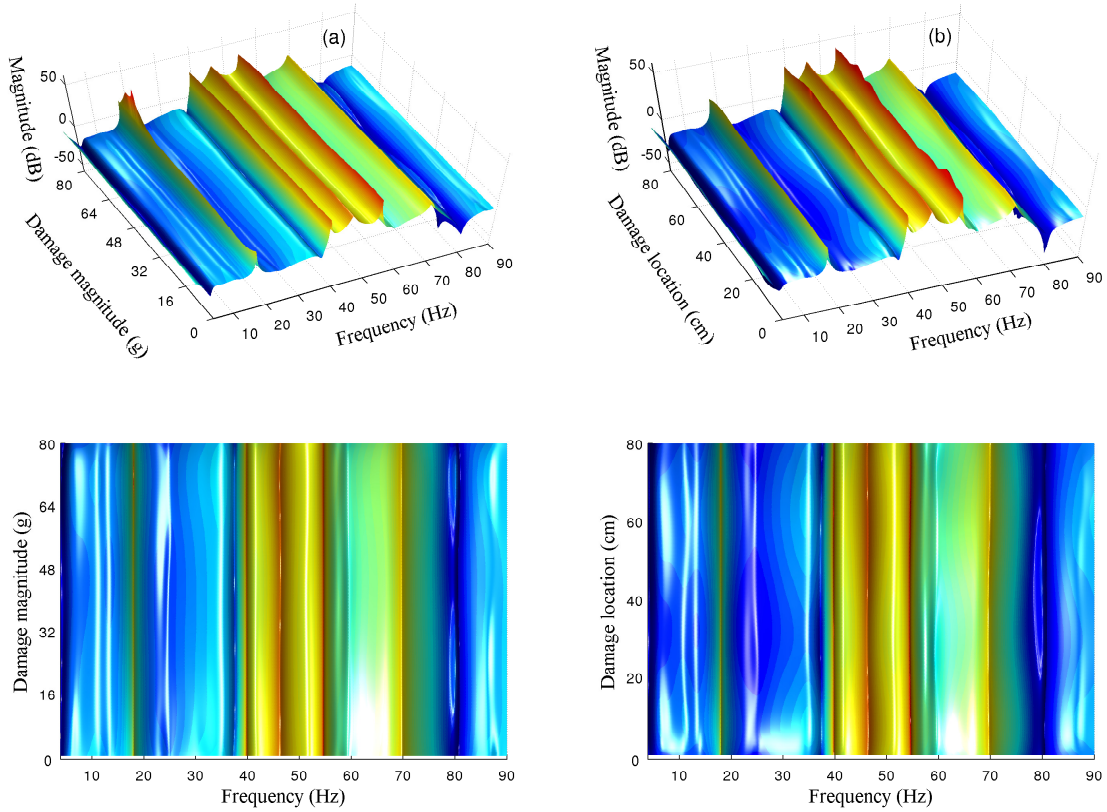


Figure 4.4: Damage topology A model ($\mathcal{M}_{\mathbf{k}}^{AY}$) based FRF magnitude versus frequency and (a) damage magnitude (for set location $k^2 = 0 \text{ cm}$) and (b) damage location (for set magnitude $k^1 = 48.792 \text{ g}$).

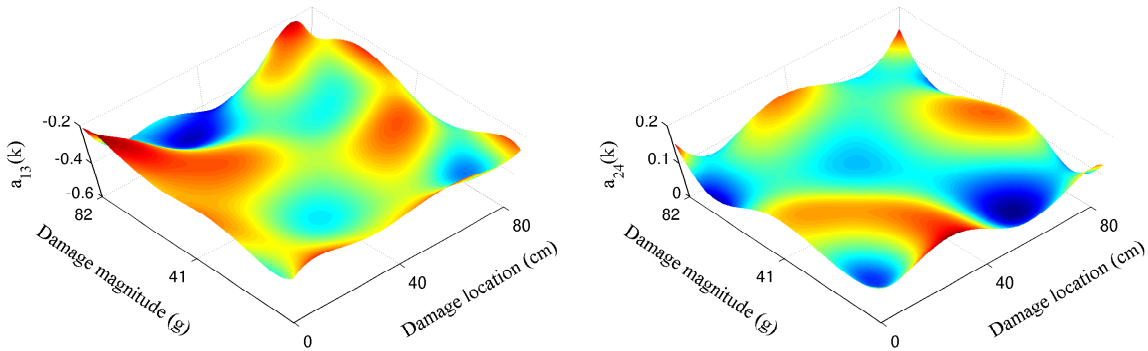


Figure 4.5: Typical damage topology A model ($\mathcal{M}_{\mathbf{k}}^{AY}$) AR parameters versus damage magnitude ($k^1 \text{ g}$) and location ($k^2 \text{ cm}$).

4.4.2 Inspection phase: damage detection, localization and magnitude estimation

The effectiveness of the damage diagnosis method is now assessed via the Test Cases of Table 4.4. It should be stressed that the damages associated with the Test Cases do *not* coincide with those used in the baseline (training) phase – apart from Test Case I that corresponds to the healthy structure. Each one of the first eight Test Cases (I – VIII) is considered twice: once using the Point Y sensor and once using the Point Z sensor. In this way each damage may be either “local” or “remote” depending on the sensor used, so that the capability of the method to operate under either one of the

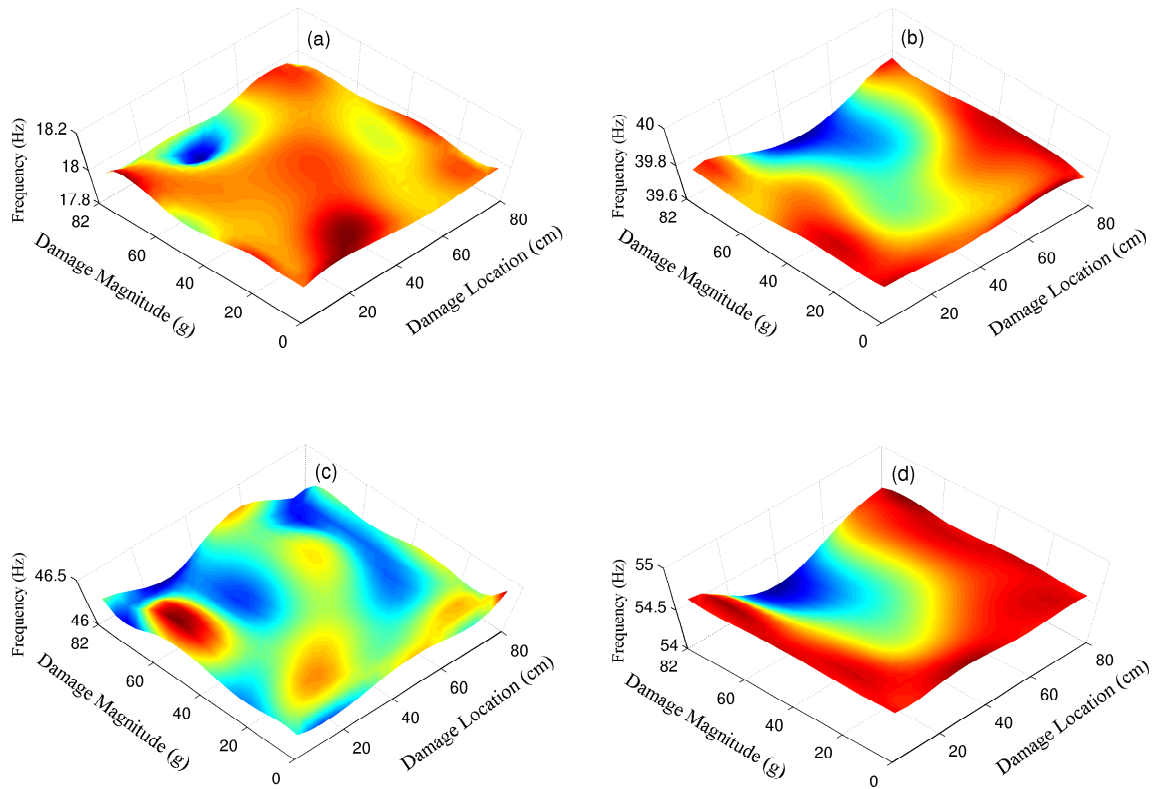


Figure 4.6: Indicative natural frequencies versus damage magnitude (k^1 g) and damage location (k^2 cm) based on the damage topology A (\mathcal{M}_k^{AY}) model: (a) second mode; (b) third mode; (c) fourth mode; and (d) fifth mode (compare with Table 4.5 and Figure 4.4).

two circumstances is assessed. The ninth Test Case (IX) in Table 4.4 is “unmodelled”, meaning that it does not belong to any one of the three (A, B, C) topologies. Still, it is particularly interesting to examine whether or not its presence can be detected, and whether or not it can be “negatively” localized, the latter meaning whether it can be actually concluded that it does not belong to any of the three considered topologies. An additional question is whether this can be achieved using any one of the three different topology (A or B or C) models; for this reason Test Case IX is considered three times (using both sensors) and the results are designated as IXa, IXb, IXc, respectively.

Damage detection results for each Test Case and each one of the two response sensors are presented in Figure 4.7. Evidently, damage is in all cases clearly detected as the t statistic is where it should be, that is within the dashed lines in the healthy Test Case (I) and beyond them in all damaged Test Cases (II – IXc). Notice that the color code in the bars indicates the actual topology of each considered damage. An important observation here is that all damages are detected, including the “unmodelled” damage, and this is irrespectively of the damage being “local” or “remote” to the sensor used. The importance of this result is related to the fact that even one (or a few, depending on the structure) sensor is sufficient for detecting damage, even if that is taking place at a “remote” location.

Damage topology (mode) identification results for each Test Case are pictorially presented in Figure 4.8 separately for each one of the two response sensors. The hypotheses of the current damage belonging to topology A, topology B, or topology C are considered in each Test Case (plot) using the corresponding topology VFP-ARX model. One of these hypotheses is accepted if the corresponding

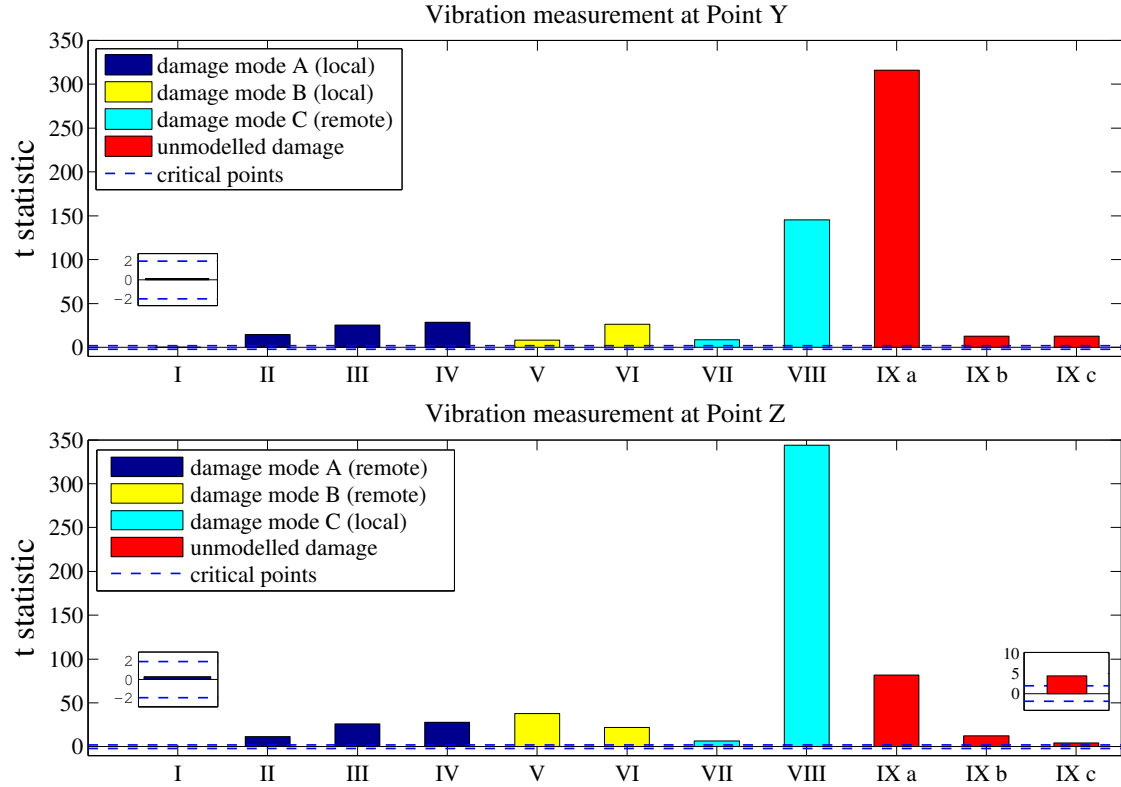


Figure 4.7: Damage detection results for the various Test Cases and each vibration measurement position (upper plot: Point Y; lower plot: Point Z): t statistic (bars) and the critical points (---) at the $\alpha = 0.05$ risk level. In each Test Case damage is detected if t exceeds the critical point.

Q statistic is lower than the critical point (dashed horizontal line). The actual damage and its characterization as either “local” or “remote” are indicated above each plot. The results of all Test Cases are remarkable, as the actual damage topology (mode) is correctly identified by each one of the two sensors. In the last two plots it is demonstrated that the “unmodelled” damage of Test Case IX is correctly rejected as being associated with one of the A, B, C topologies. These results demonstrate that correct damage topology identification is feasible based on any one of the two sensors, while the same is true for “negative” topology identification of the “unmodelled” damage.

Damage localization and magnitude interval estimation results are presented in Figure 4.9 for each Test Case and each one of the two response sensors (both shown in the same plot). It should be noticed that damage detection may be also re-confirmed based on these results, by simply examining whether or not the interval estimate of damage magnitude (at a certain risk level) includes the zero (no damage) – this is essentially equivalent to the test of Step I of the method. In Test Case I the structure is in fact healthy (F_o), hence the interval estimate of only the damage magnitude is depicted. Evidently, no damage is detected as the interval estimate at the $\alpha = 0.05$ risk level (shaded strip) includes the $k^1 = 0$ value (notice that the dashed vertical line designates the true damage magnitude while the middle line the point estimate and the left and right vertical lines the lower and upper confidence bounds, respectively). In the rest of the Test Cases the bivariate (k^1, k^2) estimates are presented both as point estimates (diamonds) and interval (uncertainty) estimates (ellipsoids) at the $\alpha = 0.05$ risk level. The results obtained by the “local” response sensor are shown as dark (blue), while those obtained by the “remote” sensor as light (magenta). A damage is, in each of these cases, correctly detected as the damage magnitude’s interval (uncertainty) estimate does not include the $k^1 = 0$ value (vertical axis). It should be further observed that impressively accurate estimates of the

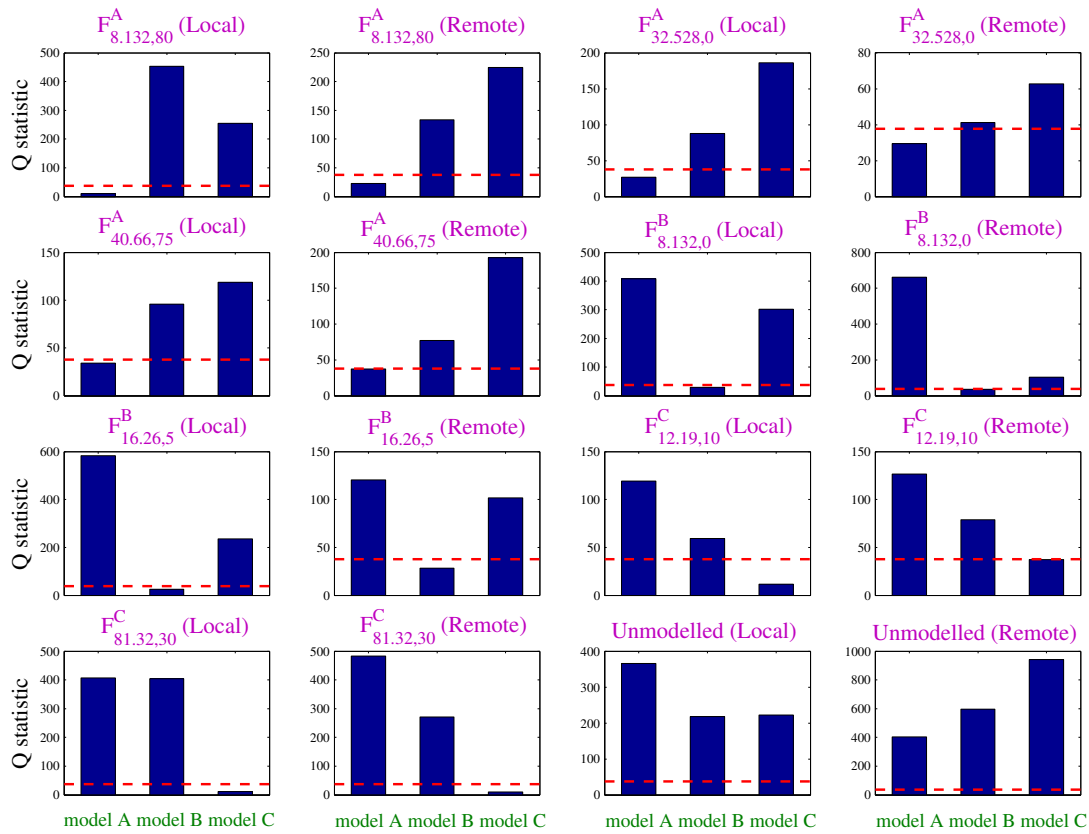


Figure 4.8: Damage topology identification results for various Test Cases and each vibration measurement position (Points Y and Z – to be read in rows): In each plot the Q statistic (bar) for the hypothesis of the current damage belonging to each one of the A, B, C topologies is shown relative to the critical point (- -) at the $\alpha = 0.05$ risk level. A hypothesis is accepted – and the corresponding damage topology is accepted as true – if the Q statistic lies below the critical point. The actual damage and its characterization as “local” or “remote” are indicated above each plot.

damage magnitude and location, also characterized by narrow uncertainties, are obtained. It is also observed that, in general, the “local” sensors achieve slightly better performance; yet the results are very impressive for all Test Cases.

4.5 Concluding remarks

A vibration based statistical time series method that is capable of effective damage detection, precise localization, and magnitude estimation within a unified stochastic framework has been introduced. The method is based on the novel extended class of Vector-dependent Functionally Pooled (VFP) models and proper statistical decision making schemes. VFP models are capable of accurately representing a structure in a damaged state for that state’s continuum of damage magnitudes and locations on a particular topology. In its inspection phase, the method operates in three distinct steps taking place within a unified framework: Step I involves damage detection, step II involves damage topology identification, and step III involves precise damage localization and magnitude estimation within the identified topology. Damage topologies are continuous, involving an infinite number of potential damage locations; they are presently confined to a single dimensionality but, of course, this may be properly generalized.

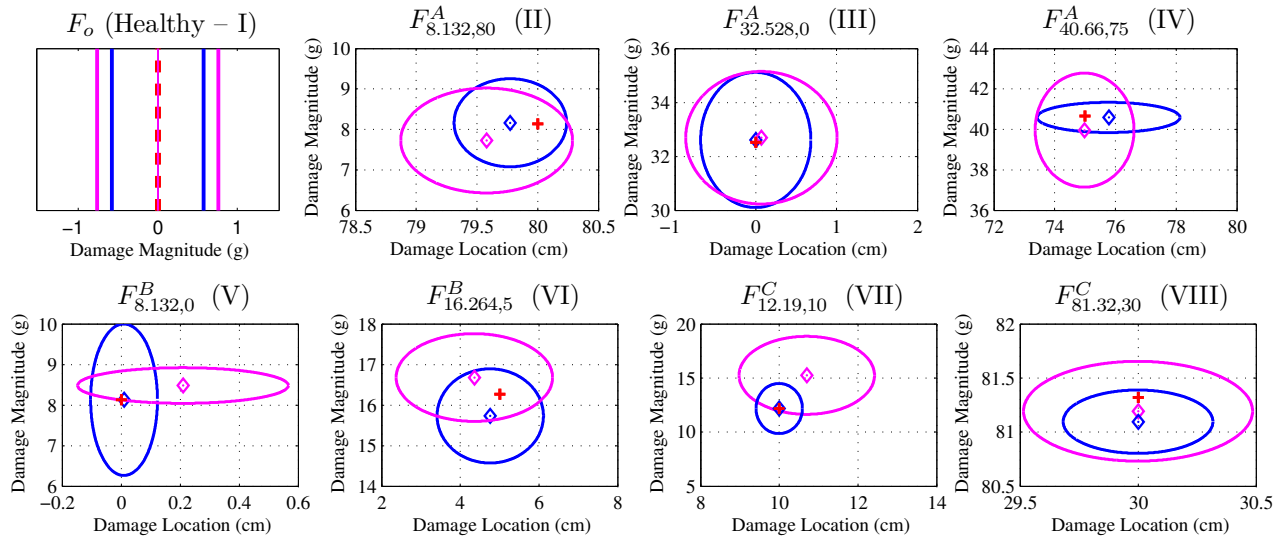


Figure 4.9: Damage localization and magnitude interval estimation results: In each plot results of a Test Case in terms of estimated damage magnitude and precise location are presented for two vibration measurement positions (Points Y and Z), one characterized as “local” damage (dark – blue) and the other as “remote” (light – magenta). Damage magnitude and location point estimates are indicated by diamonds and interval (uncertainty) estimates by ellipsoids at the $\alpha = 0.05$ risk level. Damage detection may be also re-confirmed by examining whether the damage magnitude uncertainty includes the zero (no damage) point. In each Test Case the actual damage is indicated by a cross in the diagram as well as above each plot.

The method allows, for the first time within the context of statistical time series and related methods, for complete and precise damage localization on any continuous topology of a structure of interest using a very limited – depending on the size and complexity of the structure – number of sensors. As demonstrated, for “simple” and “limited” size structures even a single pair of excitation-response sensors may be sufficient. Furthermore, estimator uncertainties are fully taken into account in all diagnostic phases, while uncertainty ellipsoids are provided for the damage location and magnitude.

The validity and effectiveness of the method have been experimentally assessed via a proof-of-concept application involving damage detection, precise localization, and magnitude estimation on a prototype GARTEUR type laboratory aircraft skeleton structure. Damages of different magnitudes occurring on various topologies on the structure (and involving an infinite number of locations within each topology) have been represented by small added masses simulating local stiffness reductions. Although the added masses have been quite small compared to the overall skeleton mass, with their effects on the dynamics being rather minor, the method has proved remarkably effective in detecting damage, identifying the correct damage topology, and then precisely localizing and accurately estimating the damage magnitude. No false alarm or missed damage events have been reported, while the corresponding uncertainty ellipsoids have been impressively accurate, while providing the user with a good feeling about estimation uncertainty.

The main *lessons learnt* and *conclusions drawn* from this chapter may be summarized as follows:

- (i) First and foremost, the study – including the proof-o-concept application – has demonstrated the important fact that effective damage detection, damage topology identification, and precise damage localization and magnitude estimation are possible based on *partial models* of the structural dynamics and a *very limited number of sensors* (even in a single excitation-response signal

pair). This is in sharp contrast to methods requiring detailed and “complete” models (such as FEMs) and a multitude of sensors.

- (ii) From a slightly different perspective, the study has demonstrated the very significant *amount of information* on the state of the structure embedded even in a single excitation-response signal pair. Thus an important message is that it may not be necessary to employ a “high” number of sensors for precise damage diagnosis; instead, a “few” sensors and powerful signal analysis for extracting the embedded information may be a much more practical and effective approach.
- (iii) The diagnostic performance in terms of damage detection, topology identification, and precise localization and magnitude estimation achieved in the proof-of-concept study (though under controlled laboratory conditions) has been impressive. Damage localization and magnitude estimation are not only excellent at the nominal (point estimation) level, but also at a probabilistic level that provides very accurate and tight uncertainty bounds (ellipsoids).
- (iv) A practically important observation is that the diagnosis performance characteristics do *not* appear significantly dependent on the *proximity* of the damage location to the sensor used. Although the uncertainty bounds have been somewhat tighter when estimated by “local”, rather than “remote”, sensors, this effect has been remarkably limited in the study.
- (v) “*Unmodelled*” damages, that is damages *not* belonging to any of the considered structural topologies (and thus not modelled in the baseline phase) have been very successfully detected and “negatively” identified as not belonging to the modelled topologies. This is very important as it provides detection and some localization information even for damages for which the method has not been trained.
- (vi) The fact that effective damage diagnosis is possible *without* the need for specifically designed excitations and special testing procedures is also very important. Combined with the use of often naturally occurring random excitation and the fact that good results may be obtained with even low/limited frequency bandwidth (4 – 90 Hz, which includes ten of the structural modes in the present study), allows for potentially *in-operation* damage diagnosis. The potential use of higher frequency range/bandwidth is expected to lead to further gain in performance.
- (vii) The method may operate on *any type* (acceleration, velocity, displacement) of vibration signals and may be modified to be applied to the *output-only case*, where only vibration response signal(s) is (are) available. Naturally, the difficulty is higher in this case, and performance is expected to be affected. This is an issue to be considered in future studies.
- (viii) The *price* to be paid for the aforementioned benefits mainly involves the *baseline* (training) phase, and more specifically the identification of the necessary VFP models – yet, this takes place only once, while the inspection phase is simple and automated. Nevertheless, user expertise is necessary in the baseline phase, along with the availability of excitation-response signal records. Although the former is expected to be reduced in the future via more automated procedures, excitation-response signal records still need to be obtained possibly through scale laboratory models or via Finite Element (FE) models. The advantages over alternative (including FE based) methods remain that the FEM is only needed in the baseline phase for inferring the partial and much more “compact” VFP models, and that no model updating is required in the inspection phase.
- (ix) Naturally, a number of issues remain open for future work. Among them are the treatment of multiple damage scenarios (the present method should have no problem with detection, but precise localization or magnitude estimation are not generally possible under the current formulation), as well as operation under varying operating conditions and significant uncertainties.

Chapter 5

A Sequential Statistical Time Series Method for Vibration Based Structural Health Monitoring

The goal of this chapter is the introduction and experimental assessment of a sequential statistical time series method for vibration based Structural Health Monitoring (SHM). The method is based on a combination of binary and multihypothesis versions of the statistically optimal Sequential Probability Ratio Test (SPRT), which employs the residual sequences obtained through a stochastic time series model of the healthy structure. In this work the full list of properties and capabilities of the SPRT are for the first time presented and explored in the context of vibration based damage detection, identification (localization) and quantification. The method is shown to achieve effective and robust damage detection, identification and quantification based on predetermined sampling plans, which are both analytically and experimentally compared and assessed. The method's performance is determined a priori via the use of the analytical expressions of the Operating Characteristic (OC) and Average Sample Number (ASN) functions in combination with baseline data records, while it requires on average a minimum number of samples in order to reach a decision compared to Fixed Sample Size (FSS) most powerful tests. The effectiveness of the proposed method is validated and experimentally assessed via its application on a lightweight aluminum truss structure, while the obtained results for three distinct vibration measurement positions prove the method's ability to operate based even on a single pair of measured excitation-response signals.

5.1 Introduction

Vibration based damage detection, identification and quantification, also collectively referred to as damage diagnosis, is of paramount importance for reasons associated with proper operation, reduced maintenance costs, increased safety, and improved dynamic performance (Doebbling *et al.* 1996, Doebbling *et al.* 1998, Farrar *et al.* 2001, Fassois and Sakellariou 2007, Fassois and Sakellariou 2009). The process of implementing a damage diagnosis strategy is referred to as Structural Health Monitoring (SHM). This process involves the online or periodical observation of a structure, the extraction of damage sensitive quantities (features) from these measurements, and the statistical analysis of these quantities in order to determine the current structural health state.

The need for global damage diagnosis methods that can be applied to “real” structures has led to the development of methods that examine changes in the structural vibration characteristics. Vibration based SHM methods are among the most accurate and effective (Doebbling *et al.* 1998, Farrar *et al.* 2001, Montalvão *et al.* 2006, Fassois and Sakellariou 2007, Fassois and Sakellariou 2009, Fan and Qiao 2011). Statistical time series SHM methods form an important and rapidly evolving class, withing the broader vibration based family of methods. Their three *main elements* are: (i) random excitation and/or vibration response signals (referred to as *time series*), (ii) statistical model building, and (iii) statistical decision making for inferring the health state of a structure. They offer a number of potential advantages, including no requirement for physics based or finite element models as they are *data based* (inverse type) methods, no requirement for complete modal models, effective treatment of uncertainties, and statistical decision making with specified performance characteristics (Fassois and Sakellariou 2007, Fassois and Sakellariou 2009, Sakellariou and Fassois 2008, Kopsaftopoulos and Fassois 2010*a*, Kopsaftopoulos and Fassois 2011*b*).

Statistical time series methods for SHM are based on random (stochastic) vibration signals under healthy and potentially damage structural states, identification of suitable (parametric or non-parametric) time series models describing the dynamics in each state, and extraction of a statistical characteristic quantity characterizing the structural state in each case (baseline phase). Damage diagnosis is accomplished in the inspection phase via statistical decision making consisting of comparing, in a statistical sense, the current characteristic quantity with that of each potential state as determined in the baseline phase. Non-parametric time series methods are those based on corresponding non-parametric time series representations, such as spectral estimates (Power Spectral Density, Frequency Response Function) (Sakellariou *et al.* 2001, Liberatore and Carman 2004, Bayissa and Haritos 2007, Rizos *et al.* 2008, Kopsaftopoulos and Fassois 2010*a*). On the other hand, parametric time series methods are those based on corresponding parametric time series representations, such as the AutoRegressive Moving Average (ARMA) models (Ljung 1999, Fassois 2001) and their principles have been used in a number of studies (Sohn and Farrar 2001, Sohn *et al.* 2003, Nair *et al.* 2006, Zheng and Mita 2007, Carden and Brownjohn 2008, Gao and Lu 2009, Sakellariou and Fassois 2008, Kopsaftopoulos and Fassois 2010*a*). For an extended overview of the main statistical time series methods for SHM the interested reader is referred to Fassois and Sakellariou (2007) and Fassois and Sakellariou (2009), while experimental assessments of various scalar and vector methods are provided in Kopsaftopoulos and Fassois (2010*a*), Kopsaftopoulos and Fassois (2011*b*) and Kopsaftopoulos and Fassois (2011*d*).

The vast majority of the work on statistical time series SHM methods literature is based on Fixed Sample Size (FSS) hypothesis testing procedures which are used during the statistical decision making phase for determining the actual health state of the structure. FSS hypothesis testing employs a constant amount of observations, which is determined *a priori* of the experimental data acquisition. On the other hand, sequential analysis is a method of statistical inference whose characteristic feature

is that the number of observations required by the procedure is not determined in advance of the experiment. The decision to terminate the experiment depends, at each stage, on the results of the observations previously made, thus the number of observations required by the test is not predetermined, but a *random variable*. If samples can be taken one at a time and the information from them accumulated, one would expect to be in a better position to make decisions than if no attempt were made to look at the data until a sample of fixed size had been taken. A merit of the sequential method, as applied to testing statistical hypotheses, is that test procedures can be constructed which require, on average, a substantially smaller number of observations than equally reliable test procedures based on a predetermined (fixed) number of observations (Wald 1947, Ghosh and Sen 1991, Lehmann and Romano 2008). Moreover, a potential advantage of a damage diagnosis method based on sequential analysis is its straightforward extension for online implementation, which may be of great interest with respect to current SHM application requirements.

In traditional Fixed Sample Size (FSS) hypothesis testing, after a random sample is observed one of two possible actions is taken: accept the null hypothesis H_0 , or accept the alternative hypothesis H_1 . In some cases the evidence may strongly support one of the hypotheses, whereas in other cases the evidence may be less convincing. Nevertheless, a decision must be made. In sequential tests there is a third possible course of action when the evidence is *ambiguous*, which is to take more observations (uncertainty zone). Such a test typically continues until the evidence strongly favors one of the considered hypotheses.

Wald (1947) introduced the Sequential Probability Ratio Test (SPRT), which is a statistically optimal test in the sense that it minimizes the expected sample size (stopping time of the test) both under the null and under the alternative hypotheses among all tests with the same or smaller error probabilities and with finite expected sample sizes under the two hypotheses (Wald 1947, Wald and Wolfowitz 1948, Ghosh and Sen 1991, Lehmann and Romano 2008). Although the SPRT was introduced over half a century ago its engineering applications have been limited to the surveillance of nuclear power plant components (Humenik and Gross 1990, Gross and Humenik 1991), while some numerical investigations of its performance with respect to anomaly detection in nuclear reactor noise signals have been presented in Schoonewelle *et al.* (1995), Schoonewelle *et al.* (1996) and Glöckler (1991). Furthermore, in the context of vibration based damage detection and Structural Health Monitoring (SHM), the SPRT, combined with extreme value statistics, has been applied in Sohn *et al.* (2003) for treating statistical damage classification in a laboratory three-story building model, as well as in Oh and Sohn (2009) for tackling damage diagnosis under environmental and operational variations using unsupervised support vector machines.

Although there are several situations, particularly in engineering applications, where more than two hypotheses are considered (such as different types of structural damage), the majority of current research on SHM employs binary FSS hypothesis testing procedures in order to face an actual multihypothesis testing problem. Obviously, this leads to statistically suboptimal solutions and ineffective use of the available data records. Nevertheless, there is a limited number of studies employing sequential multihypothesis testing methods with examples including target detection in multiple resolution radar (Marcus and Swerling 1962, Tartakovsky *et al.* 2003) and infrared systems (Emlsee *et al.* 1997), signal acquisition in direct sequence code-division multiple access systems (Veeravalli and Baum 1996), and statistical pattern recognition (Fu 1968).

The *goal* of the present chapter is the introduction and experimental assessment of a *sequential* statistical time series method for SHM capable of achieving effective and robust damage detection, identification and quantification under uncertainties. The method is based on a combination of binary and multihypothesis versions of the statistically optimal Sequential Probability Ratio Test (SPRT), which employs the residual sequences obtained through a stochastic time series model of the healthy

structure. Moreover, the full list of properties and capabilities of the SPRT are – for the first time – presented and explored in the context of vibration based SHM. The performance of the method is determined a priori via the use of the analytical expressions of the Operating Characteristic (OC) and Average Sample Number (ASN) functions in combination with baseline data records obtained under healthy and various damage structural states.

The effectiveness of the proposed method is validated and experimentally assessed via its application to a lightweight aluminum truss structure, while the results presented for *three* distinct vibration response positions confirm the method’s ability to operate based even on a single pair of measured excitation-response signals. The damage cases considered correspond to the loosening of various bolts connecting certain of the truss elements. Random force excitation is provided via an electromechanical shaker, while the vibration responses are measured at various positions via dynamic strain gauges. The method’s main features and operational characteristics are discussed along with practical issues, while its effectiveness is demonstrated via various test cases corresponding to different experiments, damage scenarios, and vibration measurement positions.

The main issues addressed in this chapter are summarized as follows:

- (a) Use – for the first time in the vibration based SHM context – of a combination of the binary and multihypothesis SPRT in order to propose a complete SHM method able to achieve effective and *robust* damage detection, identification and quantification under uncertainties.
- (b) The method’s performance is determined *a priori* via the use of the Operating Characteristic (OC) and Average Sample Number (ASN) functions, selected type I (false alarm) and II (missed damage) error probabilities, and available baseline data records of the structure under various potential states.
- (c) Assessment of the method in terms of its damage detection and identification capability under experimental uncertainties and various damage scenarios; *multiple* vibration measurement locations which are either “local” or “remote” with respect to damage location are employed; large number of experiments under each scenario (1200 data records for the healthy structure and 900 data records for each considered damage out of a total of five types).
- (d) Assessment of the ability of the method to accurately identify the actual damage type through “local” or “remote” sensors.

The rest of the chapter is organized as follows: a brief review of the basic theory on sequential analysis is outlined in Section 5.2, while the sequential statistical method for SHM is presented in Section 5.3. The experimental set-up is presented in Section 5.4 and the experimental assessment of the method is presented in Section 5.5. Concluding remarks are finally summarized in Section 5.6.

5.2 Basic theory on sequential analysis

Sequential analysis is a method of statistical inference whose characteristic feature is that the number of observations required by the procedure is not determined in advance of the experiment. The decision to terminate the experiment depends, at each stage, on the results of the observations previously made, thus the number of observations required by the test is not pre-determined, but a *random variable*.

In testing a hypothesis, the sequential method gives a rule of procedure for making one of the following three decisions at each stage of the experiment: (1) accept the hypothesis, (2) reject the hypothesis, or (3) continue the experiment by taking an additional observation.

A random experiment yields observations (data) x_1, x_2, \dots that are random variables (or vectors) not necessarily independent. Sequential analysis is concerned with the statistical theory and methods of analyzing such data in which the final number of observations need not be fixed in advance, but may depend in some specified way on the data as they become available. Two elements characterize a sequential statistical method (Ghosh and Sen 1991, Lehmann and Romano 2008, Mukhopadhyay and de Silva 2009):

- (i) a *stopping rule* that dictates whether experimentation should be stopped with (x_1, x_2, \dots, x_n) or continued with the additional observation x_{n+1} for each $n \geq 1$ and
- (ii) a *decision rule* that determines the terminal action to be taken about the given problem after experimentation has stopped.

Formally, a stopping rule gives rise to a stopping variable N , which is an extended random variable such that, for $n = 1, 2, \dots, \infty$, the event $N = n$ is in the sigma-field \mathcal{E}_n generated by (x_1, x_2, \dots, x_n) . A decision rule δ is then an \mathcal{E}_N -measurable function taking values in some well defined space. For a given problem there may exist more than one pair (N, δ) . The *goal* of sequential analysis is then to determine an “optimum” (N, δ) , or under a specified N , an “optimum” δ that meets certain desirable criteria.

Most experiments are intrinsically sequential in that they produce the observations in a temporal or spatial order. However, the majority of the statistical literature is concerned with the analysis of such data under fixed sample size (FSS) procedures.

5.2.1 Binary hypotheses sequential testing

It is well known that Wald’s SPRT based on iid observations minimizes the expected sample size both under the null and under the alternative hypotheses among all tests with the same or smaller error probabilities and with finite expected sample sizes under the two hypotheses (Wald 1947, Wald and Wolfowitz 1948). The reason for the advantage of the sequential approach over the Fixed Sample Size (FSS) approach lies in the ability of the sequential method to reach an early decision for samples that are favorable to either the null (H_o) or alternative (H_1) hypothesis. The SPRT frequently results in a saving of about 50% in the number of observations over the most efficient test procedure based on a fixed number of observations (Wald 1947, Ghosh and Sen 1991). The savings that can be realized by the sequential approach may be even greater than theory would indicate, as in “real life” experiments the actual outcome might heavily favor either H_o or H_1 (Hoel 1984, Mukhopadhyay and de Silva 2009).

Wald (1947) derived an *optimality* property for the SPRT which states that the test minimizes the average sample size under H_o and H_1 among all sequential tests with no greater type I and type II error probabilities. Moreover, although the SPRT is most commonly applied in the case of iid observations, there are important examples where this is not the case (Ghosh and Sen 1991, Chapter 3), as the observations need to be neither independent nor identically distributed.

5.2.1.1 The Sequential Probability Ratio Test (SPRT)

Consider a sequence of successive observations on x , denoted by x_1, x_2, \dots , having the common probability density function (pdf) $f(x/\theta)$ for $x \in \mathcal{X} \subseteq \mathbb{R}$ and $\theta \in \Theta \subseteq \mathbb{R}$. Let the hypothesis to be tested be

$$H_o : \theta = \theta_o \tag{5.1a}$$

and the alternative hypothesis

$$H_1 : \theta = \theta_1, \quad (5.1b)$$

with $\theta_o \neq \theta_1$ being two specified parameters in the parameter space Θ . Thus, the distribution of x under H_o (when H_o is true) is given by $f(x/\theta_o)$ and under H_1 (when H_1 is true) is given by $f(x/\theta_1)$. Moreover, let two preassigned values $0 < \alpha, \beta < 1$ with $\alpha + \beta < 1$, correspond to the type I and type II error probabilities.

For any positive value n the likelihood function of θ_o and θ_1 with respect to the sequence x_1, x_2, \dots, x_n is given by

$$\mathcal{L}(\theta_o/x_1, \dots, x_n) = \prod_{t=1}^n f(x_t/\theta_o) \quad \text{and} \quad \mathcal{L}(\theta_1/x_1, \dots, x_n) = \prod_{t=1}^n f(x_t/\theta_1), \quad (5.2)$$

respectively. In general, we write the likelihood function under the H_o and H_1 hypotheses as

$$\mathcal{L}(\theta_o/x_1, \dots, x_n) = \prod_{t=1}^n f(x_t/H_o) \quad \text{and} \quad \mathcal{L}(\theta_1/x_1, \dots, x_n) = \prod_{t=1}^n f(x_t/H_1), \quad (5.3)$$

respectively.

Having observed the sequence $\mathbf{x}_n = (x_1, x_2, \dots, x_n)$, the *most powerful* (MP) level α (type I error probability) test, according to the Neyman–Pearson lemma, is based on the likelihood ratio

$$\text{Reject } H_o \text{ if and only if } \Lambda = \frac{\mathcal{L}(\theta_1/\mathbf{x}_n)}{\mathcal{L}(\theta_o/\mathbf{x}_n)} = \frac{\prod_{t=1}^n f(x_t/H_1)}{\prod_{t=1}^n f(x_t/H_o)} \geq k, \quad (5.4)$$

where k ($k > 0$) is to be determined appropriately. The test given in Equation (5.4) is the best among FSS tests, for a sample size equal to n , at level α . Nevertheless, its type II error probability β can be quite larger than the preassigned target value. The Neyman-Pearson method chooses as critical region those sample points for which the likelihood ratio is larger than a certain constant k . The region in which this ratio is smaller than k constitutes the region for accepting H_o . The SPRT is constructed by extending this FSS approach to include a region for continuous sampling in order to meet both (α, β) error probabilities requirements.

Consider the sequence \mathbf{x}_t and the sequence of successive likelihood ratios:

$$\Lambda(t) = \frac{\mathcal{L}(\theta_1/\mathbf{x}_t)}{\mathcal{L}(\theta_o/\mathbf{x}_t)}, \quad t = 1, 2, \dots \quad (5.5)$$

By analogy to the FSS test, the acceptance region of H_o may be chosen for the sample points for which (5.5) is small, while the acceptance region of H_1 for the sample points for which (5.5) is large. The main idea in sequential testing is to use part of the sample space \mathfrak{X} for a third region such that if the sample point falls in this region the decision to accept H_o or H_1 will be postponed. Thus, the postponement region consists of those sample points for which (5.5) is neither small nor large.

The SPRT for testing H_o against H_1 is defined as follows:

Definition 5.2.1 (Sequential Probability Ratio Test) *Let A and B two positive constants with $B < A$. To test the hypothesis $H_o : \theta = \theta_o$ against the alternative $H_1 : \theta = \theta_1$, at each stage t ($t > 1$) of the experiment calculate the likelihood function ratio $\Lambda(t)$ and process as follows:*

$$(i) \quad \text{if} \quad \Lambda(t) \leq B \quad \text{accept } H_o \quad (5.6a)$$

$$(ii) \quad \text{if} \quad \Lambda(t) \geq A \quad \text{accept } H_1 \quad (5.6b)$$

$$(iii) \quad \text{if} \quad B < \Lambda(t) \leq A \quad \text{take an additional observation.} \quad (5.6c)$$

Then, the stopping time for the SPRT is defined as

$$\hat{N} = \min_t \inf \{n \mid \Lambda(t) \leq B \text{ or } \Lambda(t) \geq A, t > 1\}. \quad (5.7)$$

□

The above terminal decision rule works in practice, as it has been proved that the sampling terminates with probability one under both H_0, H_1 , thus N is finite with probability one (Wald 1947, Ghosh and Sen 1991, Mukhopadhyay and de Silva 2009).

In sequential testing the values of the type I and type II error probabilities (α, β) may be determined in advance, rather than fix the type I error probability and then be forced to calculate the type II, which is the case in FSS tests. The following theorem provides two inequalities satisfied by the quantities α, β, A and B (Wald 1947, Ghosh and Sen 1991, Mukhopadhyay and de Silva 2009):

Theorem 5.2.1

$$B \geq \frac{\beta}{1 - \alpha} \quad \text{and} \quad A \leq \frac{1 - \beta}{\alpha}. \quad (5.8)$$

□

For a proof of the theorem the interested reader may see Wald (1947), Ghosh and Sen (1991) and Mukhopadhyay and de Silva (2009).

The inequalities of Theorem 5.2.1 are derived under the assumption that the successive observations x_1, x_2, \dots, x_n are independent observations (Wald 1947). Nevertheless, the validity of the inequalities is by no means restricted to the case of independent observations. They are generally valid also for dependent observations (Wald 1947, Ghosh and Sen 1991, Lehmann and Romano 2008).

Theorem 5.2.2 (Wald 1947) *If a SPRT is desired such that the probability of an error of the first kind (type I error) does not exceed α , and the probability of an error of the second kind (type II error) does not exceed β , then use*

$$B = \frac{\beta}{1 - \alpha} \quad \text{and} \quad A = \frac{1 - \beta}{\alpha} \quad (5.9)$$

and carry out the SPRT as defined in Definition 5.2.1. □

Theorem 5.2.2 provides excellent approximations for the thresholds A and B , which are defined by the in advance specified type I and type II error probabilities (α, β). On the other hand, the sample required to reach a decision is unknown, as the sample size needed n is now a *random variable*. In subsection 5.2.1.3, a general formula for calculating the mean value of n will be presented, so that the sample size n may be determined in advance.

Since the original SPRT is purely sequential in nature, it may continue sampling for quite some time, even though $P(N < \infty / H_i) = 1, i = 0, 1$. Nevertheless, it may be possible that one decides to terminate sampling when the sample reaches a limit stopping time K . Determination of K may take into account sampling cost approaches and time constraints. The truncation of the SPRT is given by the following definition:

Definition 5.2.2 (Truncated Sequential Probability Ratio Test) *Implement the SPRT of definition 5.2.1 and let $T = \min\{N, K\}$, with N defined as in Equation (5.7) and K a user defined*

stopping time. Then:

$$(i) \quad \text{if } T = N \quad \text{decide as the SPRT of Definition 5.2.1} \quad (5.10a)$$

$$(ii) \quad \text{if } T = K \text{ and } \Lambda(K) \leq \frac{1}{2}(A + B) \quad \text{accept } H_o \quad (5.10b)$$

$$(iii) \quad \text{if } T = K \text{ and } \Lambda(K) \geq \frac{1}{2}(A + B) \quad \text{accept } H_1 \quad (5.10c)$$

□

In other words, once N reaches K but the original SPRT (Definition 5.2.1) still needs to continue sampling, it may be stopped at that stage and make the decision to accept H_o or H_1 depending on the closeness of $\Lambda(K)$ (likelihood ratio of \mathbf{x}_K) to B or A on an intuitive ground (Mukhopadhyay and de Silva 2009, Ghosh and Sen 1991). Such truncation will obviously affect the sizes of the attained type I and type II error probabilities. The size of the impact on the error probabilities largely depends on the magnitude of K (Mukhopadhyay and de Silva 2009, Tantaratana and Thomas 1977). For small probabilities of error truncating the SPRT at the sample size of the corresponding FSS test leaves the SPRT essentially unaffected when the samples are distributed according H_o and H_1 .

In the case where the hypotheses to be tested are composite, which this is the general case, hence $H_o : \theta \leq \theta_o$ and $H_1 : \theta \geq \theta_1$, and the preassigned values of type I and type II error probabilities are α whenever $\theta \leq \theta_o$ and β whenever $\theta \geq \theta_1$, respectively, the corresponding SPRT of strength (α, β) (see Definition 5.2.1) for testing $H_o : \theta = \theta_o$ and $H_1 : \theta = \theta_1$ should be employed.

In the next two subsections the Operating Characteristic (OC) and the Average Sample Number (ASN) functions of the SPRT will be presented, as their comparison aids in judging the relative merits of different test procedures.

5.2.1.2 The Operating Characteristic (OC) function

After a particular SPRT has been adopted (choice of strength (α, β)) the probability that the process will terminate with the acceptance of hypothesis H_o depends only on the distribution $f(x/\theta)$ of the random variable x under consideration. Since the distribution of x is determined by the parameter point θ , the probability of accepting H_o is a function of θ . This function is called the *Operating Characteristic (OC)* function and is denoted by $L(\theta)$ (Wald 1947, Ghosh and Sen 1991). Obviously, the probability of rejecting H_o is equal to $1 - L(\theta)$. The OC function is considered more favorable the higher the value of $L(\theta)$ for θ consistent with H_o and the lower the value of $L(\theta)$ for θ not consistent with H_o .

Definition 5.2.3 (Operating Characteristic (OC) function (Wald 1947)) Consider a parameter value θ and the parameter space Θ with $\theta \in \Theta$. Then, $L(\theta)$ is defined as the probability of accepting H_o when θ is the true parameter value. □

The OC function describes how well the test procedure achieves its objective of making correct decisions. It is clear that $L(\theta_o) = 1 - \alpha$ and $L(\theta_1) = \beta$. Moreover, if the points $(\theta, L(\theta)) \forall \theta \in \Theta$ are plotted, the corresponding figure is the OC function curve.

It is proved that if $A = \frac{1-\beta}{\alpha}$ and $B = \frac{\beta}{1-\alpha}$, an approximation of $L(\theta)$ is given by Wald (1947, pp. 48–52) and Mukhopadhyay and de Silva (2009, p. 42):

$$L(\theta) \approx \frac{\left(\frac{1-\beta}{\alpha}\right)^{h(\theta)} - 1}{\left(\frac{1-\beta}{\alpha}\right)^{h(\theta)} - \left(\frac{\beta}{1-\alpha}\right)^{h(\theta)}}. \quad (5.11)$$

For each value θ , the value of $h(\theta)$ is determined so that $h(\theta) \neq 0$ and

$$\int_{-\infty}^{+\infty} \left[\frac{f(x/\theta_1)}{f(x/\theta_o)} \right]^{h(\theta)} f(x/\theta) dx = 1. \quad (5.12)$$

5.2.1.3 The Average Sample Number (ASN)

It was pointed out before that the number of observations required by a sequential test is not predetermined, but a *random variable*, as at any stage of the experiment the decision to terminate the process depends on the results of the observations made so far. For any given test procedure of strength (α, β) the expected value of N depends only on the distribution of the sequence x . Since the distribution of x is determined by the parameter point θ , the expected value of N depends only on θ . For a parameter point θ , the expected value of N is denoted by $E_\theta(N)$.

Definition 5.2.4 (Average Sample Number (ASN) function (Wald 1947)) Consider a parameter value θ with $\theta \in \Theta$. Then, the Average Sample Number (ASN) function is defined as $E_\theta(N)$ when θ is the true parameter value. \square

The ASN function represents the price to be paid in terms of the number of observations required by the test. For a SPRT of strength (α, β) Wald proposed the following approximation formula (Wald 1947, pp. 52–54):

$$E_\theta\{N\} \approx \frac{L(\theta) \log \frac{\beta}{1-\alpha} + [1 - L(\theta)] \log \frac{1-\beta}{\alpha}}{E_\theta\{z\}} \quad (5.13)$$

with

$$E_\theta\{z\} = E_\theta\{\log \Lambda\} \quad (5.14)$$

designating the expected value of the logarithm of the likelihood ratio when θ is the true parameter value.

Under H_o and H_1 , the OC function equals to $L(\theta_o) = 1 - \alpha$ and $L(\theta_1) = \beta$, respectively, thus equation (5.13) may be further reduced to:

$$E_{\theta_o}\{N\} \approx \frac{(1 - \alpha) \log \frac{\beta}{1-\alpha} + \alpha \log \frac{1-\beta}{\alpha}}{E_{\theta_o}\{z\}} \quad (5.15a)$$

$$E_{\theta_1}\{N\} \approx \frac{\beta \log \frac{\beta}{1-\alpha} + (1 - \beta) \log \frac{1-\beta}{\alpha}}{E_{\theta_1}\{z\}}. \quad (5.15b)$$

One of the most celebrated results regarding the SPRT is referred to as its *optimality property* among all comparable tests, including the FSS most powerful test (Wald and Wolfowitz 1948, Lehmann and Romano 2008, Mukhopadhyay and de Silva 2009). The original result was proved in Wald and Wolfowitz (1948).

Theorem 5.2.3 (Optimality property of the SPRT) Consider the hypothesis test of $H_o : \theta = \theta_o$ versus $H_1 : \theta = \theta_1$. Then, among all tests, fixed sample size (FSS) or sequential, for which the type I error probability $\leq \alpha$, the type II error probability $\leq \beta$, and for which $E_\theta(N) < \infty$ when $\theta = \theta_o, \theta_1$, the SPRT with error probabilities α and β minimizes $E_\theta(N)$ when $\theta = \theta_o, \theta_1$ and $\alpha + \beta < 1$. \square

The main conclusion from the above theorem is that among all reasonable tests, including the most powerful FSS test, having type I and II error probabilities $\leq \alpha$ and $\leq \beta$, respectively, from a practical point of view the SPRT with error probabilities α, β would on average require the minimum number of observations at termination. Moreover, the SPRT beats Neyman-Pearson's most powerful test with comparable type I and II error probabilities (Wald and Wolfowitz 1948), (Mukhopadhyay and de Silva 2009, p. 44).

5.2.2 Sequential multihypothesis testing

The problem of sequential testing of multiple hypotheses is considerably more difficult than that of testing two hypotheses (Ghosh and Sen 1991, Chapter 9), (Lehmann and Romano 2008). Published work on this problem has taken two approaches. One approach has aimed at finding an optimal multihypothesis sequential test via a recursive solution to the optimization problem in Bayesian setting (Tartakovsky 1989, Zacks 1971, Lai 2000, Dragalin *et al.* 1999). However, this approach is very complex and impractical except in certain special cases. A second approach has been to extend and generalize the SPRT to the case of more than two hypotheses with "nearly optimal" procedures. Several such multihypothesis tests have been proposed and studied, namely the Sobel-Wald (Sobel and Wald 1949) and the Simons (Simons 1967) tests, which examine the case of three hypotheses in normal distributions, the Armitage test (Armitage 1950), the Lorden test (Lorden 1972), and m -SPRTs (Lorden 1976, Baum and Veeravalli 1994, Dragalin *et al.* 1999). A survey of several multihypothesis tests may be found in Ghosh and Sen (1991, Chapter 9).

Combinations of one-sided SPRT's are shown to be "nearly optimal" for problems involving a finite number of possible underlying distributions. For sequential decision problems simple explicit procedures are proposed which "do exactly what a Bayes solution would do" with probability approaching one as the cost per observation c goes to zero (Lorden 1977, Baum and Veeravalli 1994, Dragalin *et al.* 1999). It is well known that for binary hypotheses testing ($k = 2$) Wald's SPRT is optimal, in the sense that it simultaneously minimizes both expectations of the sample size among all tests, sequential and FSS tests, for which the probabilities of type I and II errors do not exceed predefined values (Wald 1947, Wald and Wolfowitz 1948, Ghosh and Sen 1991, Lehmann and Romano 2008). Unfortunately, if the number of hypotheses is greater or equal than three ($k \geq 3$) it is not clear if there even exists a test that minimizes the expected sample size for all hypotheses. Moreover, existing research indicates that even if such a test exists it would be very difficult to find its structure (Dragalin *et al.* 1999).

In the case of $k \geq 3$ hypotheses there are two different generalizations of the type I and II error probabilities α, β . There are the $k(k-1)$ error probabilities $\alpha_{ij} = P(\delta = H_i/H_j)$ for $i \neq j$, and there are the k correct decision probabilities $\alpha_{ii} = P(\delta = H_i/H_i)$, with δ denoting the decision rule of the sequential test. Furthermore, one can control the vector of correct decision probabilities (Sobel and Wald 1949) or the matrix of error probabilities (Armitage 1950, Simons 1967, Lorden 1972). It is generally impossible to duplicate the optimality of the SPRT, that is minimize the expected sample sizes under all hypotheses for $k \geq 3$ (Ghosh and Sen 1991, p. 231). Thus, in sequential multihypothesis testing the goal is to achieve specified bounds on either the error probabilities or the correct decision probabilities while controlling the expected sample size under all hypotheses "as well as possible". In general, it does not exist a multihypothesis test which is optimal in the sense that the SPRT is optimal in the case of two hypotheses (Ghosh and Sen 1991, Chapter 9).

In the present work the Armitage multihypothesis test (Armitage 1950) will be employed, as it constitutes a generalization of the SPRT that can be defined for any number of hypotheses.

5.2.2.1 The Armitage multihypothesis test

The Armitage multihypothesis test is a generalization of the SPRT that can be defined for any number of hypotheses (Armitage 1950),(Ghosh and Sen 1991, pp. 237–238). Consider k simple hypotheses H_1, H_2, \dots, H_k and denote the likelihood under hypothesis H_i (H_i is true) as \mathcal{L}_i . There are $\frac{1}{2}k(k-1)$ likelihood ratios for the various pairs of hypotheses, though each of these may be expressed in terms of $k-1$ independent likelihood ratios, which may be chosen in any one of a number of different ways:

$$\Lambda_{ij}(t) = \frac{\mathcal{L}_i(\theta_i/\mathbf{x}_t)}{\mathcal{L}_j(\theta_j/\mathbf{x}_t)}, \quad i, j = 1, 2, \dots, k, \quad i \neq j, \quad t = 1, 2, \dots \quad (5.16)$$

Definition 5.2.5 (Armitage multihypothesis test) Consider k simple hypotheses H_1, H_2, \dots, H_k . Let A_{ij} be the upper boundary, and let $B_{ij} = A_{ji}^{-1}$ be the lower boundary of the hypothesis H_i versus H_j . Each component SPRT is extended until for some j all $k-1$ SPRTs involving H_j simultaneously lead to the decision H_j . Since $\Lambda_{ij} = \Lambda_{ji}^{-1}$ and $B_{ij} = A_{ji}^{-1}$ the multihypothesis test is defined by the pair (N, δ) , where N is the stopping time and δ the final decision, which are defined in the following manner:

$$N = \min_{j=1, \dots, k-1} \inf \left\{ t \geq 1 : \Lambda_{ij}(t) \geq A_{ij} \quad \forall i \neq j \right\} \quad (5.17a)$$

with decision δ :

$$\delta = \arg \min_{j=1, \dots, k-1} N \quad (5.17b)$$

□

The interpretation of the multihypothesis SPRT is that it stops the first time t at which there exists some hypothesis H_j for which *each* likelihood ratio $\Lambda_{ij}(t)$ between H_i and H_j is greater than or equal to a chosen threshold A_{ij} . For the above sequential procedure it has been proved that the probability that no decision has been reached by the n^{th} stage tends to zero as n increases indefinitely (Armitage 1950).

Let a_{ij} the probability of accepting H_i when in fact H_j is true (error probabilities), that is $\alpha_{ij} = P(\delta = H_i/H_j)$, $i \neq j$, and let a_{ii} the probability of accepting H_i when in fact H_i is true (correct decision probabilities), that is $\alpha_{ii} = P(\delta = H_i/H_i)$. Armitage proved that $\alpha_{ij} \leq A_{ij}^{-1} = B_{ij}$ (Armitage 1950, Ghosh and Sen 1991), thus the error probabilities a_{ij} may be controlled via suitable selection of the A_{ij} 's:

$$\alpha_{ii} = 1 - \sum_{i \neq j} \alpha_{ij} \geq 1 - \sum_{i \neq j} A_{ij}^{-1}. \quad (5.18)$$

Using the above inequalities the Armitage test of Definition 5.2.5 can control the whole matrix of error probabilities α_{ij} , as well as the vector of correct decision probabilities α_{ii} . By choosing the A_{ij} sufficiently large, the probabilities of arriving at the correct conclusion, when any one of the H_i is true, can be made as large as we wish. These inequalities are, however, conservative, in the sense that the true probabilities may be considerably higher than the lower bound given in (5.18) (Armitage 1950).

5.3 A sequential statistical time series method for SHM

Like all statistical time series methods for SHM (Fassois and Sakellariou 2007, Fassois and Sakellariou 2009, Sakellariou and Fassois 2008, Kopsaftopoulos and Fassois 2010a, Kopsaftopoulos and Fassois 2011b), the sequential statistical time series method for SHM consists of two phases: (a) The *baseline*

phase, which includes modeling of the healthy structure, as well as the potential¹ modeling of the structure under predetermined damage types via stochastic time series models, and (b) the *inspection phase*, which is performed during the structure's service cycle or continuously (on-line), and includes the functions of damage detection, identification and quantification.

5.3.1 The workframe

Let S_o designate the structure under consideration in its *nominal* (healthy) state, S_A, S_B, \dots the structure under damage of *type* A, B, \dots and so on, and S_u the structure in an unknown (to be determined) state. Each damage type may include a continuum of damages which are characterized by common nature or location, for instance, damage in a specific structural element.

The sequential statistical time series method is based on discretized, scalar or vector, excitation $x[t]$ and/or response $y[t]$ (for $t = 1, 2, \dots, n$) random vibration data records. Note that t refers to discrete time, with the corresponding actual time being $(t - 1)T_s$, where T_s stands for the sampling period. Like before, a subscript (o, A, B, \dots, u) is used for designating the corresponding structural state that provided the signals. Note that all collected signals need to be suitably pre-processed (Fassois and Sakellariou 2007, Fassois and Sakellariou 2009, Doebling *et al.* 1998, Fassois 2001). This may include low or band-pass filtering within the frequency range of interest, signal subsampling (in case the originally used sampling frequency is too high), sample mean subtraction, as well as proper scaling (in the linear dynamics case). The latter is not only used for numerical reasons, but also for counteracting –to the extent possible– different operating (including excitation levels) and/or environmental conditions.

Damage detection, identification and quantification is based on the residual sequence obtained by driving the current (unknown) signal(s) $x_u[t], y_u[t]$ through a predetermined, in the baseline phase, model M_o corresponding to the healthy structural state. Let the residual series obtained by driving the current signals $x_u[t], y_u[t]$ through the healthy model M_o be designated as $e_{ou}[t]$ and characterized by variance σ_{ou}^2 . The first subscript designates the model employed, while the second the structural state corresponding to the current excitation and/or response signal(s) employed. The general idea is that the residual sequence obtained by a model that truly reflects the actual (current) structural state will be characterized by a standard deviation which becomes minimal, thus will be below a predetermined threshold.

Damage detection may be then based on the fact that under the H_o hypothesis (the structure being in its healthy state) the residual series generated by driving the current signal(s) $x_u[t], y_u[t]$ through the model M_o possesses the property:

$$\text{Under } H_o : e_{ou}[t] \sim \text{iid } \mathcal{N}(0, \sigma_{ou}^2) \quad (5.19)$$

with

$$\sigma_{ou}^2 < \sigma_{V_u}^2 \quad \text{for any structural state } V \quad (5.20)$$

thus, the corresponding residual variance (or standard deviation) will be minimal.

5.3.2 Baseline phase

5.3.2.1 Baseline modeling of the structure

The obtained data records are employed for the identification and validation of appropriate parametric time series models, which may be scalar (univariate) models in the case of a single vibration response

¹Modeling of the structure under predetermined damage types is not always necessary. See Section 5.3.3.2 for details.

measurement location, or vector (multivariate) models or an array of scalar models in the case of several vibration response measurement locations. In the *response-only* case, AutoRegressive (AR) or AutoRegressive Moving Average (ARMA) models may be employed (Box *et al.* 1994, pp. 52–53), which may be alternatively set into state space form (Box *et al.* 1994, pp. 163–164), (Ljung 1999, Section 4.3). In the excitation-response case, AutoRegressive with eXogenous excitation (ARX) or AutoRegressive Moving Average with eXogenous excitation (ARMAX) models may be used (Ljung 1999, Section 4.2), (Fassois 2001), or their corresponding state space representations (Ljung 1999, Section 4.3). For the case of vector time series models and their identification, the interested reader is referred to Lütkepohl (2005).

In this study an array of three single excitation and single response AutoRegressive with eXogenous excitation (ARX) models is used. An ARX(na, nb) model is of the form² (Fassois 2001, Ljung 1999):

$$y[t] + \sum_{i=1}^{na} a_i \cdot y[t-i] = \sum_{i=0}^{nb} b_i \cdot x[t-i] + e[t] \quad e[t] \sim \text{iid } \mathcal{N}(0, \sigma_e^2) \quad (5.21)$$

with t designating the normalized discrete time ($t = 1, 2, 3, \dots$ with absolute time being $(t-1)T_s$, where T_s stands for the sampling period), $x[t]$, $y[t]$ the measured excitation and vibration response signals, respectively, na , nb the AutoRegressive (AR) and eXogenous (X) orders, respectively, and $e[t]$ the stochastic model residual (one-step-ahead prediction error) sequence, that is a white (serially uncorrelated), Gaussian, zero mean with variance σ_e^2 sequence, uncorrelated with the excitation $x[t]$. The symbol $\mathcal{N}(\cdot, \cdot)$ designates Gaussian distribution with the indicated mean and variance, and iid stands for identically independently distributed.

The model is parameterized in terms of the parameter vector $\boldsymbol{\theta} = [a_i : b_i : \sigma_e^2]^T$ to be estimated from the measured signals (Fassois 2001, Ljung 1999). Model estimation may be achieved based on minimization of the Ordinary Least Squares (OLS) or the Weighted Least Squares (WLS) criteria (Fassois 2001, Ljung 1999). The modeling procedure involves the successive fitting of ARX(na, nb) models for increasing orders na and nb , until an adequate model is selected (Fassois 2001). Model order selection, which is crucial for successful identification, may be based on a combination of tools, including the Bayesian Information Criterion (BIC), which is a statistical criterion that penalizes model complexity (order) as a counteraction to a decreasing quality criterion (Fassois 2001), (Ljung 1999, pp. 505–507), monitoring of the RSS/SSS (Residual Sum of Squares / Signal Sum of Squares) criterion, monitoring of the residual autocorrelation function (MATLAB function *autocorr.m*) (Ljung 1999, p. 512), and use of “stabilization diagrams” which depict the estimated modal parameters (usually frequencies) as a function of increasing model order (Fassois 2001, Ljung 1999). Final model validation is based on formal verification of the residual (one-step-ahead prediction error) sequence uncorrelatedness (whiteness) hypothesis (Ljung 1999, pp. 512–513).

5.3.3 Inspection phase

Let $x_u[t]$, $y_u[t]$ ($t = 1, 2, \dots, n$) represent the current excitation and response signals, respectively, obtained from the structure in an *unknown* (to be classified) state. Damage detection, identification and quantification are based on the pre-determined in the baseline phase time series model for the healthy structure (M_o). The current excitation and response signals are driven through this model and estimates of the current residual series $e_{ou}[t]$ are obtained. Subsequently, these estimates are used for tackling the damage detection, identification and quantification tasks.

²Lower case/capital bold face symbols designate vector/matrix quantities, respectively.

5.3.3.1 Damage detection

The SPRT of Definition 5.2.1 is used in order to detect a change in the standard deviation σ_{ou} of the model residual sequence obtained by driving the current (unknown) excitation and response signals through the baseline healthy model M_o . By using the SPRT it is possible to specify two values σ_o and σ_1 for the residual standard deviation, such as the classification of the structure as healthy is considered whenever $\sigma_{ou} \leq \sigma_o$, while the classification of the structure as damaged is considered whenever $\sigma_{ou} \geq \sigma_1$. The zone between σ_o and σ_1 is the *uncertainty zone*, thus whenever σ_{ou} lies in this range the decision is postponed and the experiment continues by using an additional observation.

The probability of classifying the structure as damaged should not exceed a preassigned value α whenever $\sigma_{ou} \leq \sigma_o$ (type I error probability), while the probability of classifying the structure as healthy should not exceed a preassigned value β whenever $\sigma_{ou} \geq \sigma_1$ (type II error probability). The values σ_o and σ_1 are user defined values and express the increase of the standard deviation ratio $q = \sigma_1/\sigma_o$ for which the structure is considered to be in a damage state. For example, a ratio of $q = 1.1$ means that the structure is considered damaged whenever there is a increase of 10% in the standard deviation σ_{ou} of the current residual sequence compared to its nominal value σ_o .

Damage detection is based on the following hypothesis testing problem implemented via the SPRT of strength (α, β) , with α, β the type I (false alarm) and II (missed damage) error probabilities, respectively:

$$\begin{aligned} H_o &: \sigma_{ou} \leq \sigma_o && \text{(null hypothesis – healthy structure)} \\ H_1 &: \sigma_{ou} \geq \sigma_1 && \text{(alternative hypothesis – damaged structure)} \end{aligned} \quad (5.22)$$

with σ_o, σ_1 designating user defined values.

Under the null hypothesis the residuals $e_{ou}[t]$ are iid zero mean Gaussian with variance σ_{ou}^2 , hence:

$$\text{Under } H_o : e_{ou}[t] \sim \text{iid } \mathcal{N}(0, \sigma_{ou}^2) \quad t = 1, 2, \dots, n \quad (5.23)$$

and the probability density function of the residual sequence $e_{ou}[t]$ ($t = 1, 2, \dots, n$) is given by:

$$f(e_{ou}[t]/\sigma) = \frac{1}{(2\pi)^{\frac{n}{2}} \sigma^n} \exp\left\{ -\frac{1}{2\sigma^2} \sum_{t=1}^n e_{ou}^2[t] \right\}. \quad (5.24)$$

The likelihood ratio Λ is computed at each stage n of the experiment as follows:

$$\Lambda(n) = \frac{\mathcal{L}(\sigma_1/e_{ou}[1], \dots, e_{ou}[n])}{\mathcal{L}(\sigma_o/e_{ou}[1], \dots, e_{ou}[n])} = \frac{\prod_{t=1}^n f(e_{ou}[t]/\sigma_1)}{\prod_{t=1}^n f(e_{ou}[t]/\sigma_o)} = \frac{\frac{1}{(2\pi)^{\frac{n}{2}} \sigma_1^n} \exp\left\{ -\frac{1}{2\sigma_1^2} \sum_{t=1}^n e_{ou}^2[t] \right\}}{\frac{1}{(2\pi)^{\frac{n}{2}} \sigma_o^n} \exp\left\{ -\frac{1}{2\sigma_o^2} \sum_{t=1}^n e_{ou}^2[t] \right\}}$$

Taking logarithms and dividing by $(1/2\sigma_o^2) - (1/2\sigma_1^2)$ the logarithm of the likelihood ratio is obtained:

$$\log \Lambda(n) = n \cdot \log \frac{\sigma_o}{\sigma_1} + \frac{\sigma_1^2 - \sigma_o^2}{2\sigma_o^2 \sigma_1^2} \cdot \sum_{t=1}^n e_{ou}^2[t]. \quad (5.25)$$

The basis of the SPRT is the logarithm of the likelihood ratio function based on n samples with $\log \Lambda(n)$ designating the decision parameter of the method.

Based on the SPRT of Definition 5.2.1, the following test of strength (α, β) is constructed:

$$\begin{aligned} \log \Lambda(n) \leq \log B &&& \text{accept } H_o && \text{(healthy structure)} \\ \log \Lambda(n) \geq \log A &&& \text{accept } H_1 && \text{(damaged structure)} \\ \log B < \log \Lambda(n) \leq \log A &&& \text{no decision is made} && \text{(continue the test)} \end{aligned} \quad (5.26)$$

with $B = \frac{\beta}{(1-\alpha)}$ and $A = \frac{(1-\beta)}{\alpha}$ obtained from Theorem 5.2.2.

Then, the stopping time for the SPRT is defined as:

$$\widehat{N} = \min \inf_t \{n \mid \log \Lambda(t) \leq \log B \text{ or } \log \Lambda(t) \geq \log A, t > 1\}. \quad (5.27)$$

Following a decision at a stopping time \widehat{N} , it is possible to continue the test by resetting $\log \Lambda(\widehat{N} + 1)$ to zero and continue the experiment by using additional residual samples. Thus, by using finite vibration response data records $x_u[t], y_u[t]$ with $t = 1, 2, \dots, K$ and the corresponding residual sequences, the SPRT is able to take multiple decisions, hence multiple damage detections can be achieved.

The Operating Characteristic (OC) function

According to Definition 5.2.3, for any value σ , the OC function $L(\sigma)$ denotes the probability that the SPRT for damage detection will terminate with the acceptance of the null hypothesis H_o that the structure is in healthy state. For $A = \frac{1-\beta}{\alpha}$ and $B = \frac{\beta}{1-\alpha}$ and by applying the Equations (5.11) and (5.12) we obtain:

$$L(\sigma) = \frac{\left(\frac{1-\beta}{\alpha}\right)^h - 1}{\left(\frac{1-\beta}{\alpha}\right)^h - \left(\frac{\beta}{1-\alpha}\right)^h} \quad (5.28)$$

where h is the root of the equation:

$$\frac{1}{\sqrt{2\pi}\sigma} \frac{\sigma_o^h}{\sigma_1^h} \int_{-\infty}^{+\infty} \left(\frac{\exp\left\{-\frac{1}{2\sigma_1^2} e_{ou}^2[t]\right\}}{\exp\left\{-\frac{1}{2\sigma_o^2} e_{ou}^2[t]\right\}} \right)^h \exp\left\{-\frac{1}{2\sigma^2} e_{ou}^2[t]\right\} de = 1 \quad (5.29)$$

The integral on the left side of Equation (5.29) has a finite value only if $(h/\sigma_1^2) - (h/\sigma_o^2) + (1/\sigma^2) > 0$. Hence, Equation (5.12) may be written as:

$$\sigma \left(\frac{\sigma_1}{\sigma_o} \right)^h = \sqrt{\frac{1}{\frac{h}{\sigma_1^2} - \frac{h}{\sigma_o^2} + \frac{1}{\sigma^2}}}. \quad (5.30)$$

Instead of solving (5.30) with respect to h , it is solved with respect to σ . Thus, we obtain:

$$\sigma = \sqrt{\frac{\left(\frac{\sigma_o}{\sigma_1}\right)^{2h} - 1}{\frac{h}{\sigma_1^2} - \frac{h}{\sigma_o^2}}}. \quad (5.31)$$

Using Equations (5.28) and (5.31) the OC function curve may be plotted by computing the pair $(\sigma, L(\sigma))$ for a sequence of values h , which has to be sufficiently large in order to obtain enough OC function points.

Figure 5.1a presents the OC function for various residual standard deviation ratios $q = \sigma_1/\sigma_o$ and constant strength (α, β) , while Figure 5.2a presents the OC function for various strengths (α, β) and constant residual standard deviation ratio $q = \sigma_1/\sigma_o = 1.1$. By calculating the OC function of various candidate SPRT sampling plans of strength (α, β) (see Figure 5.1b) and residual standard deviation ratios $q = \sigma_1/\sigma_o$ (see Figure 5.1a), the user is able to determine the corresponding probabilities of acceptance of the null hypothesis H_o (healthy structure) and thus, compare in a systematic way the various sampling plans. Moreover, in the case that a number of baseline healthy data records

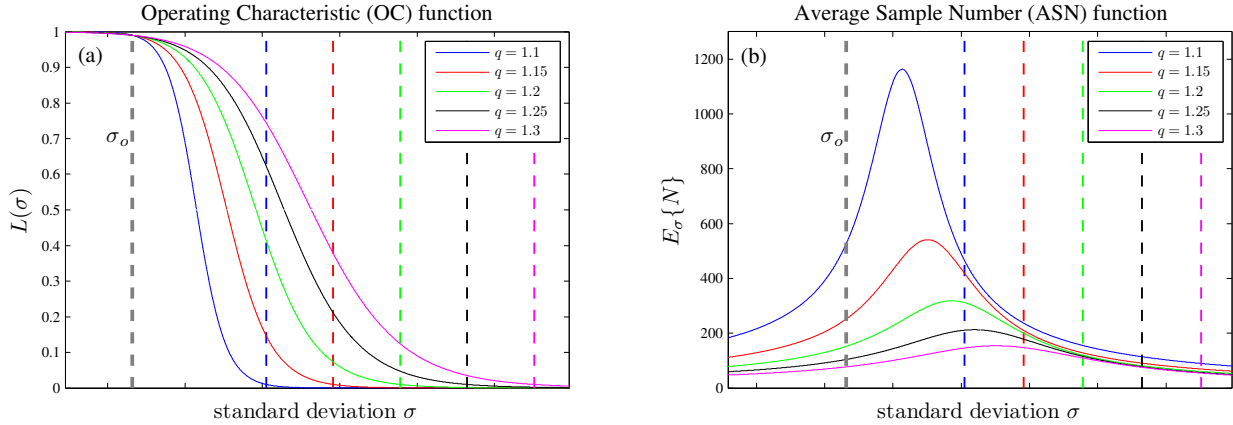


Figure 5.1: (a) Operating Characteristic (OC) and (b) Average Sample Number (ASN) functions for various residual standard deviation ratios $q = \sigma_1/\sigma_o$ and constant strength $(\alpha, \beta) = 0.01$. The vertical colored dashed lines designate the σ_1 values for the corresponding ratios q .

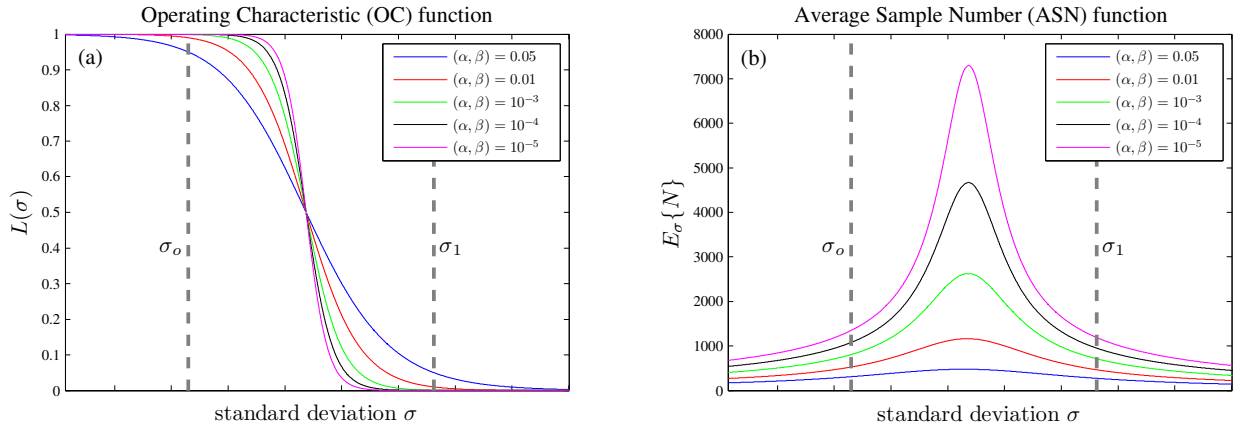


Figure 5.2: (a) Operating Characteristic (OC) and (b) Average Sample Number (ASN) functions for various strengths (α, β) and constant residual standard deviation ratio $q = \sigma_1/\sigma_o = 1.1$.

is available, the user may estimate the corresponding residual standard deviations and check the probability that the candidate SPRT sampling plans will accept them, indeed, as belonging to the healthy structural state. This way, using the available baseline data records, the behavior of various SPRT sampling plans may be investigated with respect to damage detection robustness and potential false alarm rates, and the sampling plan with the best performance may be selected for final implementation.

The Average Sample Number (ASN) function

The ASN function represents the average number of inspection samples required by the SPRT to reach a decision. As the number of observations required by a sequential test is not predetermined, but a *random variable*, the ASN is an approximation of the expected value $E_\sigma(N)$ of the number of residual samples required by a sampling plan of strength (α, β) and residual standard deviations σ_o, σ_1 in order to reach a terminal decision.

The expected value of the ASN function based on Equation (5.13) is given by Wald (1947, p.

131):

$$E_{\sigma}\{N\} \approx \frac{L(\sigma) \log \frac{\beta}{1-\alpha} + [1 - L(\sigma)] \log \frac{1-\beta}{\alpha}}{E_{\sigma}\{z\}} \quad (5.32)$$

where

$$z = \log \Lambda = \frac{\frac{1}{\sigma_1} \exp\left\{-\frac{1}{2\sigma_1^2} e_{ou}^2[t]\right\}}{\frac{1}{\sigma_o} \exp\left\{-\frac{1}{2\sigma_o^2} e_{ou}^2[t]\right\}} = \log \frac{\sigma_o}{\sigma_1} + \frac{1}{2} \left(\frac{1}{\sigma_o^2} - \frac{1}{\sigma_1^2} \right) e_{ou}^2[t]. \quad (5.33)$$

$E_{\sigma}(z)$ denotes the expected value of the likelihood ratio when σ is the standard deviation of the residual sequence, hence:

$$E_{\sigma}\{z\} = E_{\sigma}\{\log \Lambda\} = \log \frac{\sigma_o}{\sigma_1} + \frac{1}{2} \left(\frac{1}{\sigma_o^2} - \frac{1}{\sigma_1^2} \right) E\{e_{ou}^2[t]\} = \log \frac{\sigma_o}{\sigma_1} + \frac{1}{2} \left(\frac{1}{\sigma_o^2} - \frac{1}{\sigma_1^2} \right) \sigma^2. \quad (5.34)$$

From Equations (5.28), (5.31), (5.32) and (5.34) the ASN function of various candidate SPRT sampling plans may be calculated. This is of great importance in the design of a SPRT sampling plan for damage detection, as by pre-specifying the test strength (α, β) and the residual standard deviation ratio $q = \sigma_1/\sigma_o$ for which the structure is considered to be in a damage state, one may have an approximation of the expected number of residual samples that the SPRT needs in order to accept hypothesis H_o or H_1 and terminate. Hence, along with the OC function, the ASN function constitutes an additional analytical tool which may contribute to the optimal selection of a SPRT sampling plan. Figure 5.1b shows the ASN function for various residual standard deviation ratios $q = \sigma_1/\sigma_o$ and constant strength (α, β) , while Figure 5.2b depicts the ASN function for various strengths (α, β) and constant residual standard deviation ratio $q = \sigma_1/\sigma_o = 1.1$.

Based on Theorem 5.2.3, the SPRT of strength (α, β) minimizes, under H_o (healthy structure) and H_1 (damaged structure), the expected value $E_{\sigma}\{N\}$ of the ASN among all tests, FSS or sequential, for which the type I error probability is equal or less than α and the type II error probability is equal or less than β . Thus, in order to tackle damage detection and infer the health state of a structure, based on the adopted sampling plan of the SPRT, the above procedure requires a minimum number of observations for reaching a terminal decision.

The truncated SPRT

In the case that the expected number of samples $E_{\sigma}\{N\}$, as approximated by the ASN function, indicates that an increased number of residual samples is required by the adopted SPRT sampling plan with respect to the available or “desired” number of residual samples to be employed, then the truncated SPRT version of Definition 5.2.2 may be used. Moreover, the truncated SPRT may also be employed in the case where the SPRT stopping time N reaches the limit stopping time K (length of the current residual sequence $e_{ou}[t]$) and still needs to continue sampling to reach a terminal decision.

Based on the truncated SPRT of Definition 5.2.2, the following test of strength (α, β) is constructed based on a user defined stopping time K :

$$\begin{aligned} \log \Lambda(K) \leq \log \frac{1}{2}(A + B) & \quad \text{accept } H_o \quad (\text{healthy structure}) \\ \log \Lambda(K) \geq \log \frac{1}{2}(A + B) & \quad \text{accept } H_1 \quad (\text{damaged structure}) \end{aligned} \quad (5.35)$$

with $B = \frac{\beta}{(1-\alpha)}$ and $A = \frac{(1-\beta)}{\alpha}$ obtained from Theorem 5.2.2.

The truncation of the SPRT will affect the type I and II error probabilities α and β , respectively, and as a result of this the strength (α, β) of the test. Nevertheless, the size of the impact on the error probabilities depends on the number of samples K based on which the SPRT is truncated

(Mukhopadhyay and de Silva 2009). Hence, if the truncation is implemented for a large value of K the strength of the test will be practically unaffected. For small probabilities of type I (false alarm) and II (missed damage) errors, truncating the SPRT at stopping time K leaves the SPRT essentially unaffected when the samples are distributed under H_o (healthy structure) and H_1 (damaged structure) (Mukhopadhyay and de Silva 2009, Tantaratana and Thomas 1977). Furthermore, the truncated SPRT compares favorably with the corresponding FSS most powerful test when the probabilities of error are small (Tantaratana and Thomas 1977).

5.3.3.2 Damage identification and quantification

Consider k hypotheses H_A, H_B, \dots with each one indicating the acceptance of the corresponding, as determined in the baseline phase, damage type A, B, \dots , respectively, as current. Damage identification may be treated via two statistical procedures: (i) k pairwise binary SPRTs based hypothesis testing similarly to damage detection, and (ii) sequential multihypothesis testing. In this section both methods will be presented, along with their corresponding pros and cons.

Pairwise binary SPRT based method

The current excitation and response signals $x_u[t], y_u[t]$ ($t = 1, 2, \dots, n$), obtained from the structure under an unknown (to be classified) damage state are driven through predetermined, in the baseline phase, damage type models M_A, M_B, \dots . Afterwards, estimates of the current residual series $e_{Au}[t], e_{Bu}[t], \dots$ are obtained that are used for the damage identification task³.

Thus, damage identification may be achieved via similar to (5.26) pairwise SPRTs implemented using the corresponding residual series $e_{Au}[t], e_{Bu}[t], \dots$. For, say damage type V , the following test of strength (α, β) is used:

$$\begin{aligned} H_o &: \sigma_{Vu} \leq \sigma_o && \text{(null hypothesis – damage is of type } V) \\ H_1 &: \sigma_{Vu} \geq \sigma_1 && \text{(alternative hypothesis – damaged in not of type } V) \end{aligned} \quad (5.36)$$

with σ_o, σ_1 designating user defined values.

Then, the SPRT is implemented as follows:

$$\begin{aligned} \log \Lambda_V(n) \leq \log B &&& \text{accept } H_o && \text{(damage is of type } V) \\ \log \Lambda_V(n) \geq \log A &&& \text{accept } H_1 && \text{(damaged in not of type } V) \\ \log B < \log \Lambda_V(n) \leq \log A &&& \text{no decision is made} && \text{(continue the test)} \end{aligned} \quad (5.37)$$

with $B = \frac{\beta}{(1-\alpha)}$ and $A = \frac{(1-\beta)}{\alpha}$ obtained from Theorem 5.2.2 and

$$\log \Lambda_V(n) = n \cdot \log \frac{\sigma_o}{\sigma_1} + \frac{\sigma_1^2 - \sigma_o^2}{2\sigma_o^2\sigma_1^2} \cdot \sum_{t=1}^n e_{Vu}^2[t]. \quad (5.38)$$

The above testing procedure is used in order to detect a change in the standard deviation σ_{Vu} of the model residual sequence obtained by driving the current (unknown) excitation and response signals through the baseline damage type models M_A, M_B, \dots . The classification of the structural state as being under damage type V is considered whenever $\sigma_{Vu} \leq \sigma_o$, while the classification of the

³The first subscript designates the model employed and the second the structural state of the current excitation-response signals.

The upper bounds A_{ij} of the likelihood ratios are obtained via Equation (5.18) by defining the matrix of error probabilities a_{ij} (the probability of accepting H_i when in fact H_j is true), which also yields the vector of correct probabilities a_{ii} (the probability of accepting H_i when in fact H_i is true). Using Equation (5.18) the above testing procedure can control the whole matrix of error probabilities α_{ij} , as well as the vector of correct decision probabilities α_{ii} . By choosing the A_{ij} sufficiently large, the probabilities of arriving at the correct decision, when any one of the H_i is true, can be made as large as desired.

Notice that in the multihypothesis damage identification procedure no baseline damage type modeling for the considered damage structural states is involved, as this method employs just the nominal (healthy) model M_o of the structure in order to obtain the residual sequences. Hence, although multihypothesis testing is more elaborate than hypothesis binary testing, the proposed method avoids the potentially complicated task of damage type identification, which is necessary in the case of the binary hypothesis testing method.

Nevertheless, it is possible that different damage types may have a similar effect on the residual sequences $e_{ou}[t]$ and thus in the residual standard deviation σ_{ou} . In this case the multihypothesis method will not provide clear classification results for the corresponding damage types, nevertheless will provide an indication of the potential damage types. If it is desired to reach a single final decision with respect to the current “actual” damage type, the user may apply, in a second stage, the binary hypothesis damage identification method between the candidate damage types indicated by the multihypothesis testing.

Damage quantification is treated simultaneously with the damage identification task. The predetermined residual standard deviation values $\sigma_A, \sigma_B, \dots$ under the corresponding damage types constitute an indication of the damage severity. This is due to the fact that as damage severity increases the current structural dynamics deviate from the nominal healthy behavior, thus the nominal model M_o belonging to the healthy structure will not be able to accurately represent them, leading to increased residuals and corresponding standard deviation values. Moreover, by considering a nominal standard deviation σ_{oo} for the healthy structure, damage detection may also be considered. Nevertheless, in this case, the advantages of the SPRT based damage detection method (predetermined strength (α, β) , analytical comparison of candidate sampling plans via the OC and ASN functions) will be neglected.

Structural State	Description	Total Number of Data Sets
Healthy	—	1200 (100 baseline)
Damage type A	loosening of bolt A1	900 (100 baseline)
Damage type B	loosening of bolts A1 and B1	900 (100 baseline)
Damage type C	loosening of bolts C1 and C2	900 (100 baseline)
Damage type D	loosening of bolt D1	900 (100 baseline)
Damage type E	loosening of bolt E1	900 (100 baseline)
Sampling frequency: $f_s = 256$ Hz, Signal bandwidth: $[0.5 - 100]$ Hz		
Signal length N in samples (s): Non-parametric analysis: $N = 30\,720$ (120 s)		
Parametric analysis: $N = 1\,000$ (3.9 s)		

Table 5.1: The considered damage types, number of experiments, and vibration signal details.

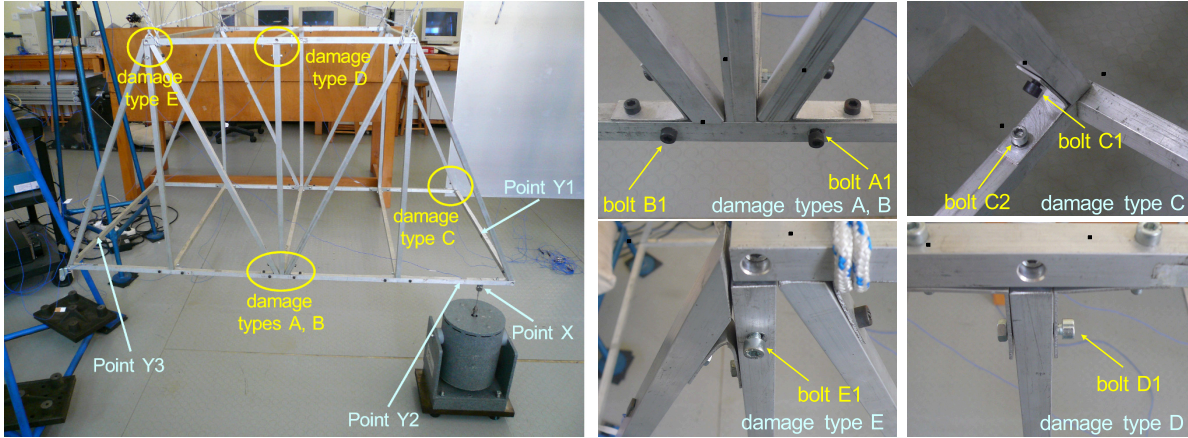


Figure 5.3: The aluminum truss structure and the experimental set-up: The force excitation (Point X), the vibration measurement positions (Points Y1 – Y3), and the considered damage types (A, B, C, D, and E).

5.4 The experimental set-up

5.4.1 The structure

The truss structure is depicted in Figure 5.3, suspended through a set of cords. It consists of twenty eight elements with rectangular cross sections (15×15 mm) jointed together via steel elbow plates and bolts. All parts are constructed from standard aluminum with the overall dimensions being $1400 \times 700 \times 800$ mm.

5.4.2 The damage types and the experiments

The damages considered correspond to the complete loosening of various bolts at different joints of the structure. Five distinct types are specifically considered (Figure 5.3): The first damage type, referred to as *damage type A*, corresponds to the loosening of bolt A1 joining together an horizontal with a vertical element. The second damage type, referred to as *damage type B*, corresponds to the loosening of bolts A1 and B1 joining together an horizontal with a vertical element. Damage type B affects the same elements as damage type A, but it is more severe, as loosening of two bolts is involved. The third damage type, referred to as *damage type C*, corresponds to the loosening of bolts C1 and C2 joining together an horizontal with a diagonal element. The fourth damage type, referred to as *damage type D*, corresponds to the loosening of bolt D1 joining together an horizontal with a vertical element. Finally, the fifth damage type, referred to as *damage type E*, corresponds to the loosening of bolt E1 joining together a vertical with a diagonal element. All damage types considered are summarized in Table 5.1.

The force excitation is a random Gaussian signal applied vertically at Point X (Figure 5.3) via an electromechanical shaker (MB Dynamics Modal 50A, max load 225 N) equipped with a stinger, and measured via an impedance head (PCB 288D01, sensitivity 98.41 mV/lb). The vibration responses are measured at different points via dynamic strain gauges (PCB ICP 740B02, 0.005–100 kHz, 50 mV/ $\mu\epsilon$; sampling frequency $f_s = 256$ Hz, signal bandwidth 0.5–100 Hz). The force and strain signals are driven through a signal conditioning device (PCB 481A02) into the data acquisition system (SigLab 20-42). In this study the damage detection, identification and quantification are results based on each one of the three vibration response signals (Points Y1, Y2 and Y3 – Figure 5.3). This allows the examination

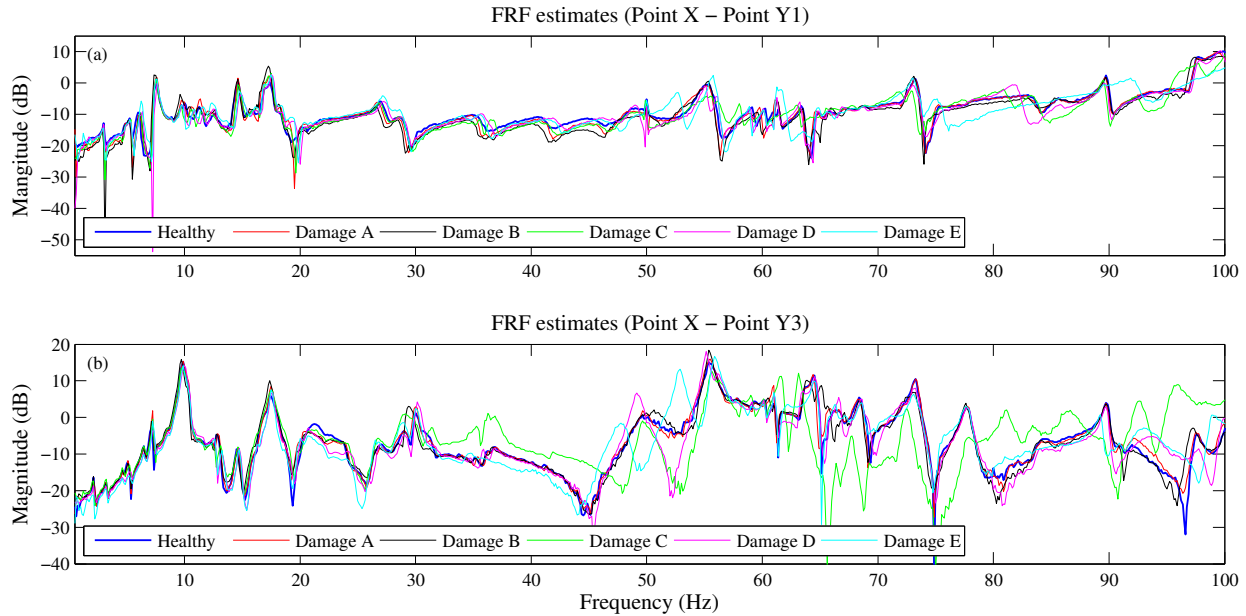


Figure 5.4: Frequency Response Function (FRF) magnitude estimates for the healthy and damage structural states: (a) Point X – Point Y1 and (b) Point X – Point Y3 transfer functions.

and assessment of the sequential method’s ability to achieve damage detection, identification and quantification with respect to the vibration response measurement locations employed. For this reason, the results are characterized as “local” or “remote” with respect to the distance between the damage and the response point employed.

A significant number of test cases is considered in the experimental assessment: In each test case a specific data set (out of a total of 1200 data sets for the healthy structure and 900 data sets for each damage state, with 100 from each category reserved for the baseline phase – Table 5.1) and a specific vibration response measurement position (Points Y1 – Y3, Figure 5.3) are employed. Experimental details are presented in Table 5.1. Notice that the sample mean is subtracted from each signal and scaling by the signal’s sample standard deviation is implemented.

5.5 Damage detection, identification and quantification results

Damage detection, identification and quantification results are based on a single excitation-response signal pair for each test case. The excitation force is always measured at Point X, but the vibration response measured either at Points Y1, Y2, or Y3 (Figure 5.3 is used in each test case. Depending on the distance of the employed sensor from the damage occurrence location, the damage is characterized either as “local” or “remote”. Of course, the interesting point being investigated here is whether the potential proximity of the sensor seems to provide a significant advantage in the damage detection robustness and the identification and quantification accuracy. The considered damage test cases are summarized in Table 5.1.

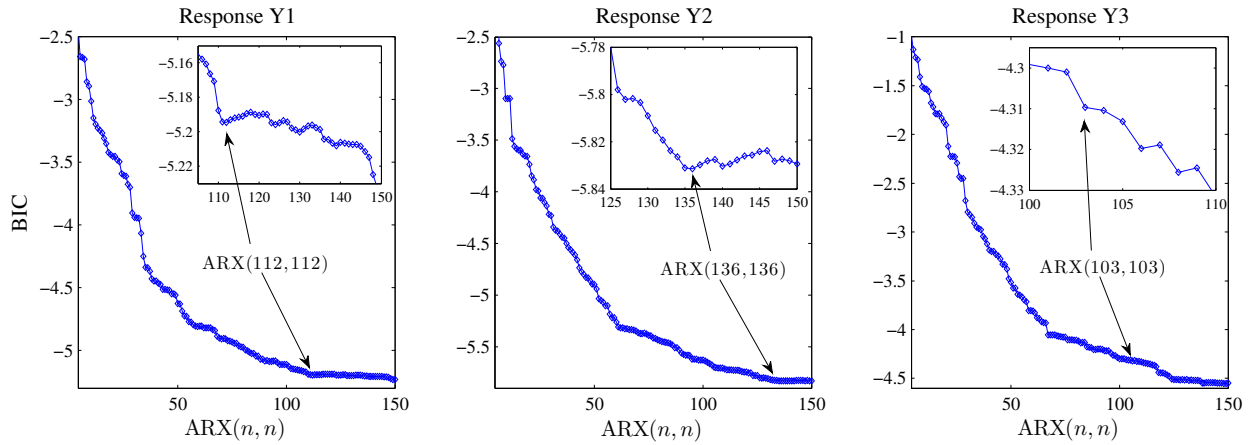


Figure 5.5: BIC order selection criterion for $ARX(n, n)$ type parametric models in the healthy case for all vibration response measurement locations.

5.5.1 Baseline phase: structural identification under the healthy structural state

5.5.1.1 Non-parametric identification

Non-parametric identification of the structure is based on $N = 30\,720$ (≈ 120 s) sample-long excitation-response signals. An $L = 2048$ sample-long Hamming data window with zero overlap is used (number of segments $K = 15$) for the FRF Welch based estimation (MATLAB function *tfestimate.m*). The obtained response FRF magnitude estimates for the healthy and damage states of the structure (Point X – Point Y1 and Point X – Point Y3 transfer functions) are depicted in Figure 5.4. As it may be observed, the healthy and damage curves are rather similar for both transfer functions in the 0.5 – 30 Hz range, where the first twelve modes are included. In the case of Point X – Point Y3 transfer function, significant differences between the healthy and damage types C, D and E curves are seen in the 30 – 58 Hz range, where the next three modes are included. Finally, in the 58 – 100 Hz range where the next eight modes are included, the Point X – Point Y1 FRF magnitude curves are quite similar except for the damage type E curve, while discrepancies are more evident for damage types C and E in the Point X – Point Y3 transfer function case.

5.5.1.2 Parametric identification

Parametric identification of the structural dynamics is based on $N = 10\,000$ (≈ 39 s) sample-long excitation and single response signals which are used for estimating AutoRegressive with eXogenous excitation (ARX) models (MATLAB function *arx.m*). The modeling strategy consists of the successive fitting of $ARX(na, nb)$ models (with na, nb designating the AR and X orders, respectively; in this study $na = nb = n$) until a suitable model is selected. Model parameter estimation is achieved by minimizing a quadratic Prediction Error (PE) criterion leading to a Least Squares (LS) estimator (Fassois 2001), (Ljung 1999, p. 206). Model order selection, which is crucial for successful identification, may be based on a combination of tools, including the Bayesian Information Criterion (BIC) (Figure 5.5), which is a statistical criterion that penalizes model complexity (order) as a counteraction to a decreasing quality criterion (Fassois 2001), (Ljung 1999, pp. 505–507), monitoring of the RSS/SSS (Residual Sum of Squares / Signal Sum of Squares) criterion, monitoring of the residual autocorrelation function (MATLAB function *autocorr.m*) (Ljung 1999, p. 512), and use of “stabilization diagrams” (Figure 5.6) which depict the estimated modal parameters (usually frequencies) as a function of increasing model order (Fassois 2001, Ljung 1999).

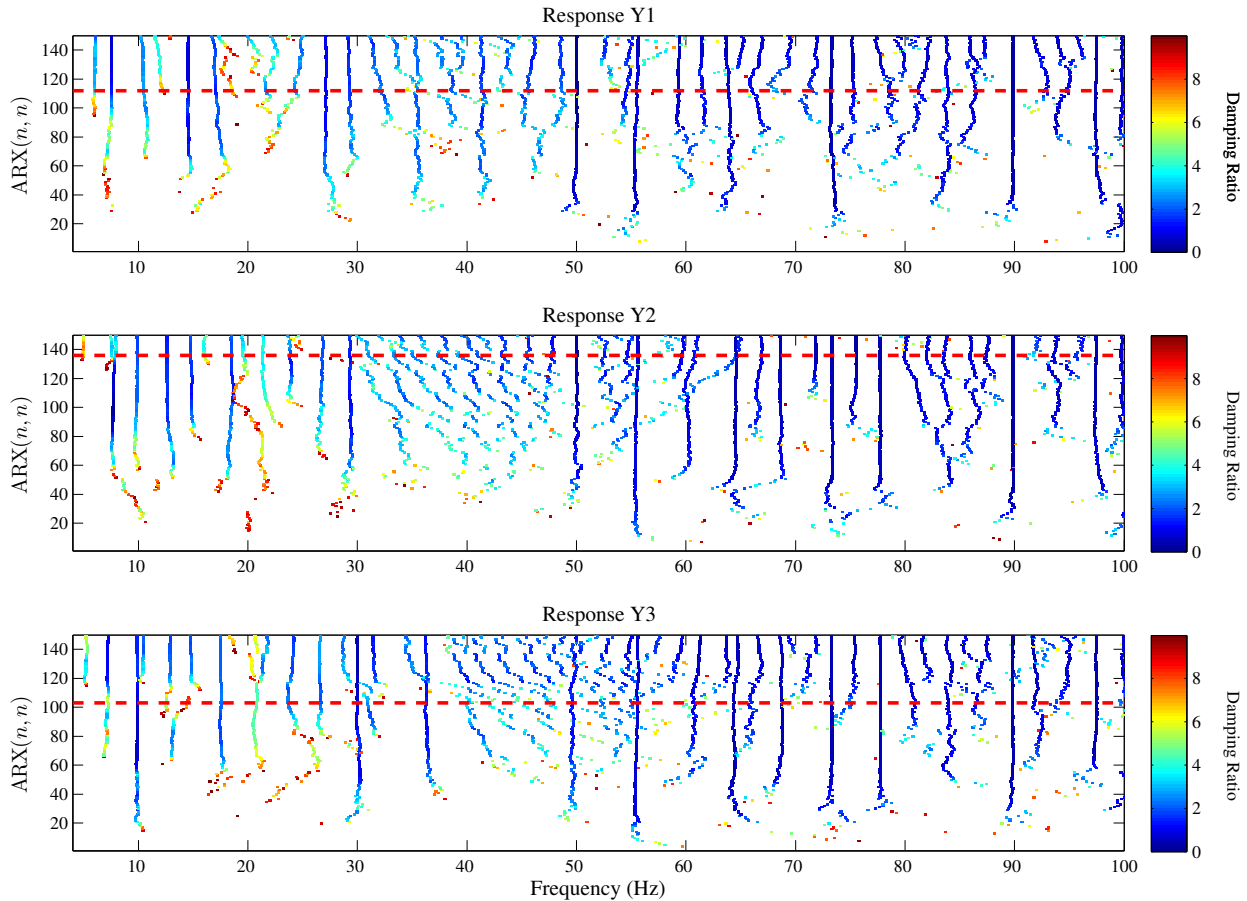


Figure 5.6: Frequency stabilization diagram for ARX(n, n) type models in the healthy case for all vibration response measurement locations. The dashed red lines indicate the selected model orders in each case.

An approximate plateau in the BIC sequences is achieved for model order $n > 100$ (Figure 5.5). Furthermore, as indicated in the frequency stabilization diagram of Figure 5.6, model orders of $n > 90$ are adequate for most natural frequencies to get stabilized. Notice the color bar in Figure 5.6, which demonstrates the damping ratios for each frequency for increasing model order. In the 0.5 – 50 Hz range, higher damping ratios for model order $n < 100$ are observed for certain structural modes.

The above identification procedure leads to the selection of an ARX(112, 112), ARX(136, 136) and ARX(103, 103) model for vibration measurement positions Y1, Y2 and Y3, respectively. The selected ARX models, as well as their estimation details and corresponding numbers of the estimated parameters, Sample Per Parameter (SPP), BIC, and RSS/SSS values are summarized in Table 5.2. Note that the identification procedure generally leads to different ARX models (including somewhat different model orders) for each vibration measurement position.

Response	Selected Model	No of estimated parameters	SPP	BIC	RSS/SSS (%)
Y1	ARX(112, 112)	225 parameters	44.4	-5.19	0.43
Y2	ARX(136, 136)	273 parameters	36.6	-5.83	0.22
Y3	ARX(103, 103)	207 parameters	48.3	-4.31	1.07

Parameter estimation method: Weighted Least Squares (WLS), QR implementation, $N = 10\,000$ samples

Table 5.2: Selected models and estimation details.

5.5.2 Inspection phase

5.5.2.1 Damage detection

Damage detection is based on the binary SPRT presented in Section 5.3.3.1. Prior to implementing the SPRT for tackling damage detection an appropriate sampling plan should be selected. The selection of the sampling plan involves the determination of the following three aspects: (i) the nominal residual standard deviation σ_o under which the structure is considered to be in its healthy state, (ii) the standard deviation ratio $q = \sigma_1/\sigma_o$, which constitutes the standard deviation increase under which the structure is determined to be in a damage state, and (iii) the SPRT strength (α, β) ,

The determination of the nominal residual standard deviation σ_o under which the structure is considered to be healthy is based on the available 100 baseline data records obtained from the healthy structure (Table 5.1). For each considered vibration measurement location (Figure 5.3, Points Y1, Y2 and Y3), the corresponding identified ARX model, as presented in Section 5.5.1.2 and Table 5.2, is employed in order to obtain the 100 baseline residual sequences. A typical selection for the nominal residual standard deviation could be $\sigma_o = E\{\hat{\sigma}_{ou}\} + 1.96 \cdot \text{std}\{\hat{\sigma}_{ou}\}$, which represents the 95% confidence interval of the standard deviation with respect to the baseline residual sequences. The selected nominal σ_o values for all three vibration responses are presented in Table 5.3.

The determination of the residual standard deviation ratio q may be based on the OC and ASN functions of the SPRT (Section 5.3.3.1) for various q ratios, along with the use of the baseline healthy data records. Figures 5.7a and 5.7b present, for vibration response Y2, the OC and ASN functions, respectively, for various candidate ratios q and constant SPRT strength $(\alpha, \beta) = 0.01$. In both figures, the σ_o value is shown as gray vertical dashed line, while the σ_1 values corresponding to the considered $q = \sigma_1/\sigma_o$ ratios are shown in colored vertical dashed lines. Along with the OC and ASN function curves, the standard deviation values obtained from the 100 baseline residual sequences are depicted in vertical cyan dashed lines.

In Figure 5.7a the intersections of the vertical lines, belonging to the residual standard deviation values, with the OC function curves for the various q ratios correspond to the probabilities of acceptance of the null hypothesis H_o (healthy structure) for each ratio, while in Figure 5.7b correspond to the expected number of residual samples required to reach a decision. The OC function (Figure 5.7a) is considered more favorable the higher the value of $L(\sigma)$ for σ consistent with H_o and the lower the value of $L(\sigma)$ for σ not consistent with H_o . Thus, by plotting the OC and ASN functions, not only do we may have an indication of the probability of acceptance for various residual standard deviations σ , but we also obtain an approximation of the number of residual samples that are required for reaching a terminal decision.

In order to design a robust, yet effective in detecting small damages, SPRT for damage detection, the lowest q ratio with the highest probabilities of acceptance of the null hypothesis H_o for the plotted baseline residual standard deviations should be selected. In a second stage, the expected number of residual samples required to reach a decision should be checked in order to assure that its value is in accordance with the experimental specifications and the potential online implementation requirements. Notice that the lower the selected ratio q , the greater is the expected number of the required samples

	Response Y1	Response Y2	Response Y3
Nominal σ_o	0.0866	0.0660	0.1168
σ_o obtained as mean value out of 100 baseline residual sequences.			

Table 5.3: Selected nominal residual standard deviation σ_o values for the damage detection SPRT.

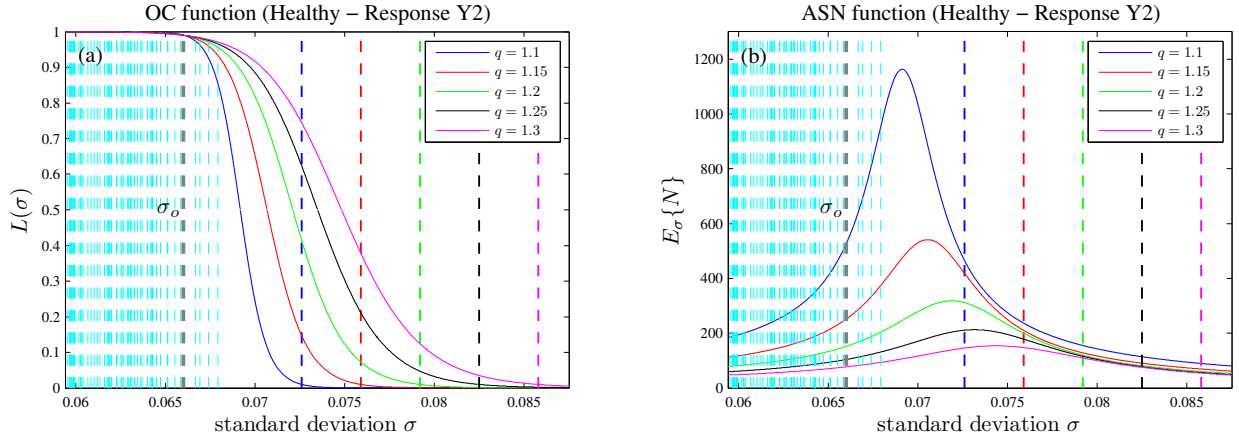


Figure 5.7: Healthy structure: (a) Operating Characteristic (OC) and (b) Average Sample Number (ASN) functions for various residual standard deviation ratios $q = \sigma_1/\sigma_o$ and constant strength $(\alpha, \beta) = 0.01$ (vibration response Y2). The vertical colored dashed lines designate the σ_1 values for the corresponding ratios q . The vertical cyan dashed lines represent the residual standard deviation values obtained from the 100 baseline healthy data sets.

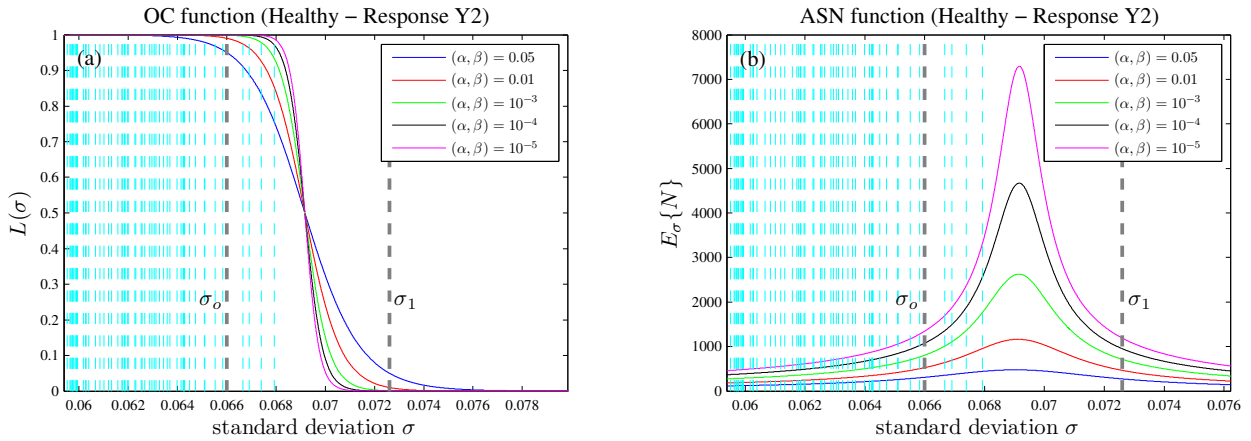


Figure 5.8: Healthy structure: (a) Operating Characteristic (OC) and (b) Average Sample Number (ASN) functions for various strengths (α, β) and residual standard deviation ratio $q = \sigma_1/\sigma_o = 1.1$ (vibration response Y2). The vertical cyan dashed lines represent the residual standard deviation values obtained from the 100 baseline healthy data sets.

to reach a terminal decision. Moreover, notice that the largest amount of residual samples required to reach a decision arises when the value of the current standard deviation σ lies in the middle of the (σ_o, σ_1) range. This is due to the fact that in this case the standard deviation σ favors neither the null H_o (healthy structure) nor the alternative H_1 (damaged structure) hypothesis.

For tackling damage detection in the aluminum truss structure a standard deviation ratio $q = \sigma_1/\sigma_o$ equal to 1.1 has been selected as adequate for the implementation of the SPRT.

After the selection of the residual standard deviation ratio q , the final SPRT strength (α, β) should be determined as well. Similarly to the q selection procedure, Figures 5.8a and 5.8b depict the OC and ASN functions, respectively, for various test strengths (α, β) and constant ratio $q = 1.1$. Again, the standard deviation values for the baseline residual sequences are shown in vertical cyan dashed lines. Based on the standard deviation acceptance probabilities under the null hypothesis H_o (Figure 5.8a) and the corresponding expected number of the required residual samples to reach

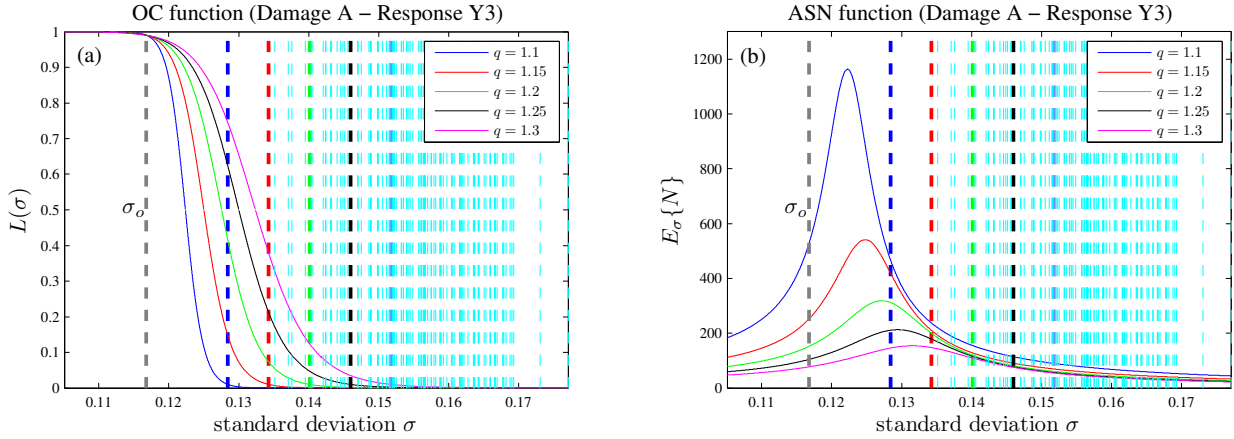


Figure 5.9: Damage type A: (a) Operating Characteristic (OC) and (b) Average Sample Number (ASN) functions for various residual standard deviation ratios $q = \sigma_1/\sigma_o$ and constant strength $(\alpha, \beta) = 0.01$ (vibration response Y3). The vertical cyan dashed lines represent the residual standard deviation values obtained from the 100 baseline damage type A data sets.

a decision (Figure 5.8b) the user may select an appropriate strength (α, β) . Notice that the lower the selected α, β values, the greater is the expected number of required samples to reach a terminal decision.

For tackling damage detection in the aluminum truss structure a SPRT strength equal to $(\alpha, \beta) = 0.01$ has been selected as adequate.

Figures 5.9a and 5.9b depict the OC and ASN function curves (response Y3), respectively, for various candidate ratios q and constant SPRT strength $(\alpha, \beta) = 0.01$, along with the standard deviation values (vertical cyan dashed lines) obtained from the 100 baseline residual sequences that belong to damage type A (see Table 5.1). In the case where baseline data from various potential damage types are available, either by corresponding experiments or tuned Finite Element (FE) models, Figure 5.9a constitutes an additional means of validation of the determined SPRT sampling plan for damage detection. If for the selected sampling plan the probability of acceptance of damage type A standard deviation values is considerably high (vertical axis of Figure 5.9a) then there is an increased probability of missed damage occurrence, as the adopted sampling plan will not be able to clearly distinguish the standard deviation values between the healthy and the damage structural state. Furthermore, Figure 5.9b depicts the expected number of residual samples that are required to reach a terminal decision versus the damage type A standard deviation values. As it may be observed, all the plotted baseline standard deviation values require less than 200 samples in order to accept the underlying alternative hypothesis H_1 (damaged structure).

Indicative damage detection results, for the vibration response of Point Y1, based on the implemented SPRT sampling plan of standard deviation ratio $q = 1.1$ and strength $(\alpha, \beta) = 0.01$ are presented in Figure 5.10. A damage is detected when the test statistic (vertical axis) exceeds the upper critical point (dashed horizontal lines), while the structure is determined to be in a healthy state when the test statistic exceeds the lower critical point. After a critical point is exceeded a decision is made, while the test statistic is reset to zero and the test continues. Hence, during testing multiple decisions are made, as each inspection residual sequence contains 1000 samples. Evidently, correct detection (Figure 5.10) is obtained in each test case, as the test statistic is shown to exceed multiple times (multiple correct decisions) the lower critical point in the healthy case, while it also exceeds multiple times the upper critical point (multiple correct damage detections) in the damage test cases. Inside each subplot of Figure 5.10 is indicated whether the corresponding damage type

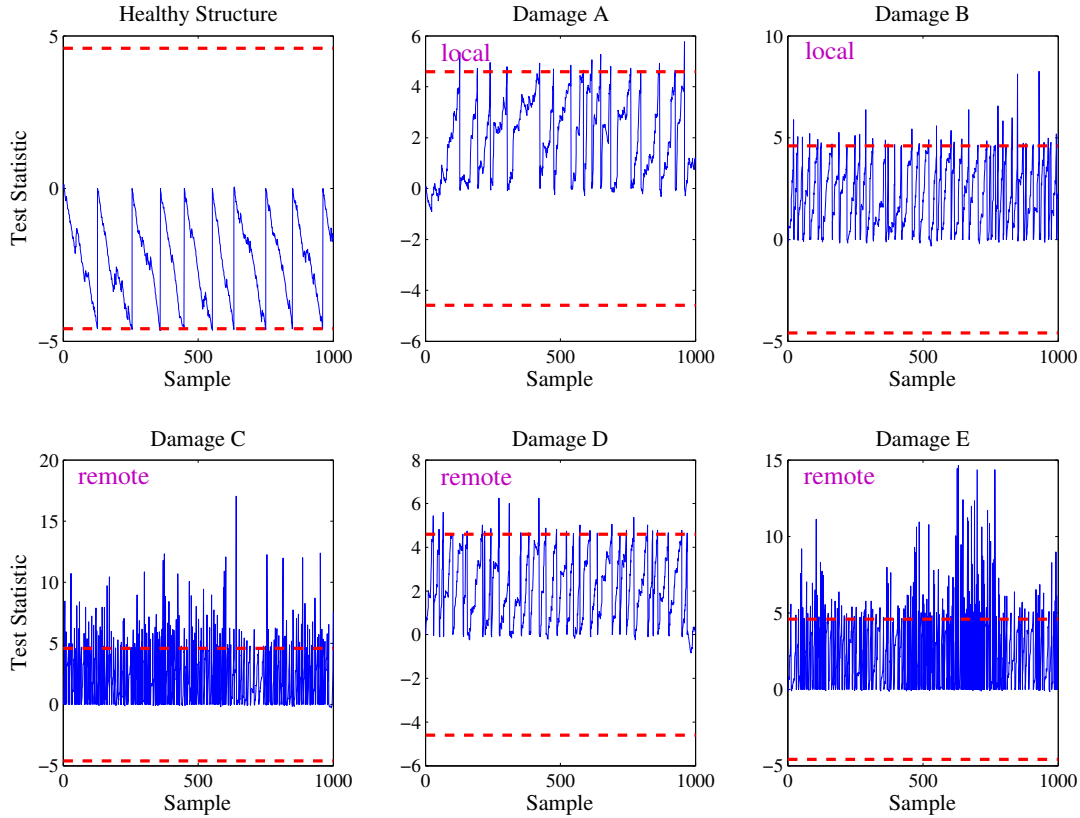


Figure 5.10: Indicative damage detection results for response Y2 at the $\alpha = \beta = 0.01$ risk levels ($q = \sigma_1/\sigma_o = 1.1$). The actual structural state is shown above each plot.

is “local” or “remote” with respect to the vibration sensor employed. Thus, damage types A and B are characterized as “local” with respect to sensor Y2, while damage type C, D and E as “remote”. Observe that damage type A (Table 5.1) appears harder to detect, as the number of detections in this case is the smallest one among all the damage test cases, while damage types C and E appear easier to detect. This is in agreement with the remarks made in subsection 5.5.1.1 and Figure 5.4.

Figure 5.11 depicts the average number of correct detections under the healthy structural state versus the residual standard deviation ratio q for various SPRT strengths (α, β). The dashed blue lines correspond to the experimental correct detection point estimates obtained from the 1100 healthy inspection data sets of 1000 samples each, while the gray shaded areas correspond to the ± 1.96 standard deviation confidence intervals. The dashed red lines correspond to the theoretical number of correct detections as approximated via the ASN function under the null hypothesis H_o (healthy structure). Notice that the greater the α, β error probabilities are, the larger is the number of correct detections per data set. Nevertheless, keep in mind that increased values of type I and II error probabilities may lead to an increased false alarms rates.

Moreover, notice that the theoretical numbers of correct detections for the various test strengths in Figure 5.11 are smaller than the corresponding experimental ones in all test cases. This is due to the fact that in “real life” applications the experimental data often heavily favor either the null (H_o) or the alternative (H_1) hypothesis. In this case, the experimental inspection data were obtained under the healthy structural state, thus the corresponding residual samples strongly favor the null hypothesis of the healthy structure. This constitutes a strong indication that the proposed method may actually perform effectively in “real life” applications, and thus evade from being exclusively used in laboratory assessments.

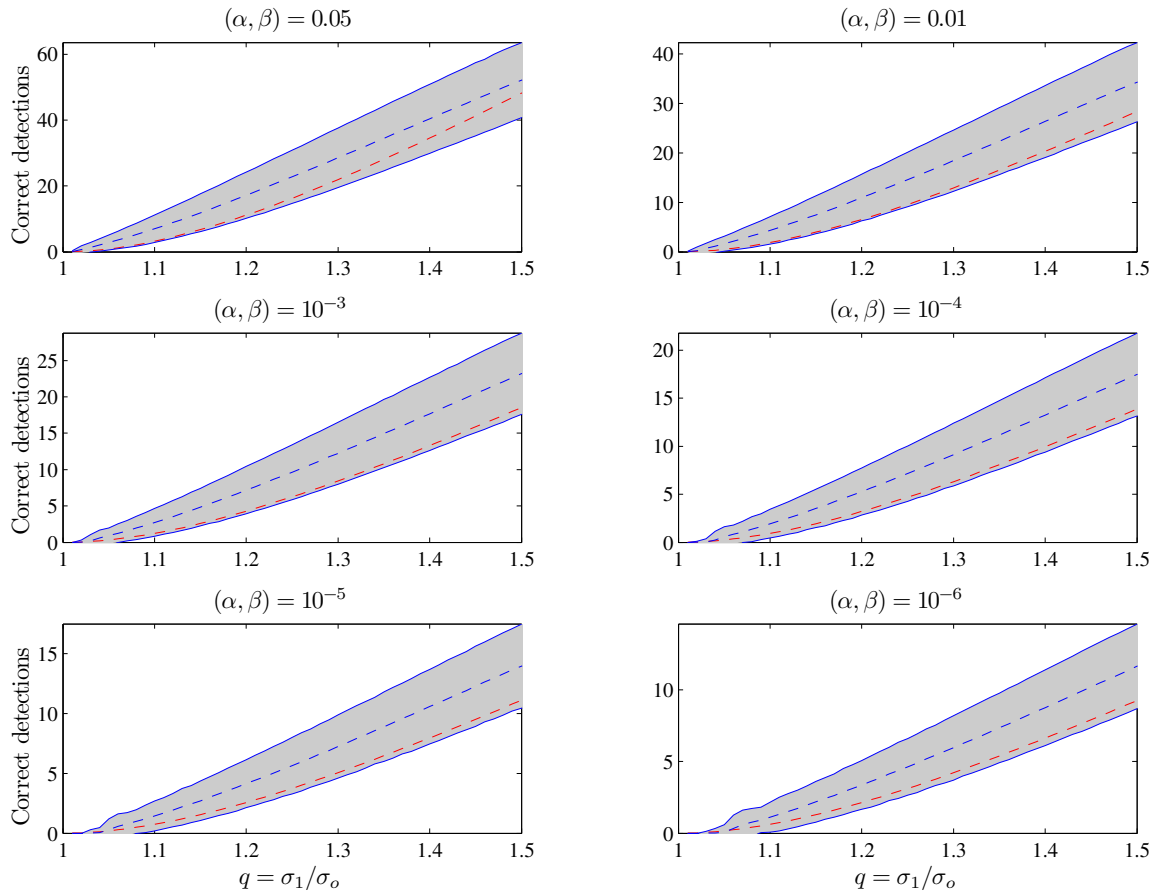


Figure 5.11: Average number of correct detections for the healthy structure (response Y2): experimental (dashed blue lines ± 1.96 standard deviation confidence intervals from 1100 inspection healthy data sets of 1000 samples each) and theoretical (dashed red lines) point estimates for various SPRT strengths (α, β) versus residual standard deviation ratio $q = \sigma_1/\sigma_o$. The actual strength is shown above each plot.

Figure 5.12 presents the false alarm percentages for all three vibration measurement locations versus the residual standard deviation ratio q for various SPRT strengths (α, β) . These rates have been extracted from the 1100 healthy inspection data records and the corresponding residual sequences. As the ratio q increases the false alarm percentages slightly increase too. This may seem awkward at first, as one would expect that as the standard deviation q increases the false alarm rates would decrease. Nevertheless, this is not the case, as by increasing the ratio q the number of correct detections largely increases (see Figure 5.11) and as a result, as the SPRT becomes more “sensitive”, there is a slight increase in the false alarms.

For the damage detection implemented SPRT of $q = 1.1$ and strength $(\alpha, \beta) = 0.01$ the false alarm percentages (green lines in Figure 5.12) for all vibration responses are practically zero, a fact that demonstrates the effectiveness and robustness of the designed test.

Finally, Figure 5.13 depicts the average number of correct detections for the three vibration responses and various test strengths (α, β) under damage type A versus the residual standard deviation ratio q . The lowest mean correct detection values are obtained for vibration response Y1, while the largest values are obtained for vibration response Y3. This implies that damage type A, which is the least severe among all considered damages, is easier detected via vibration response Y3 and harder via response Y1. Nevertheless, it is obvious from Figure 5.13 that the SPRT for damage

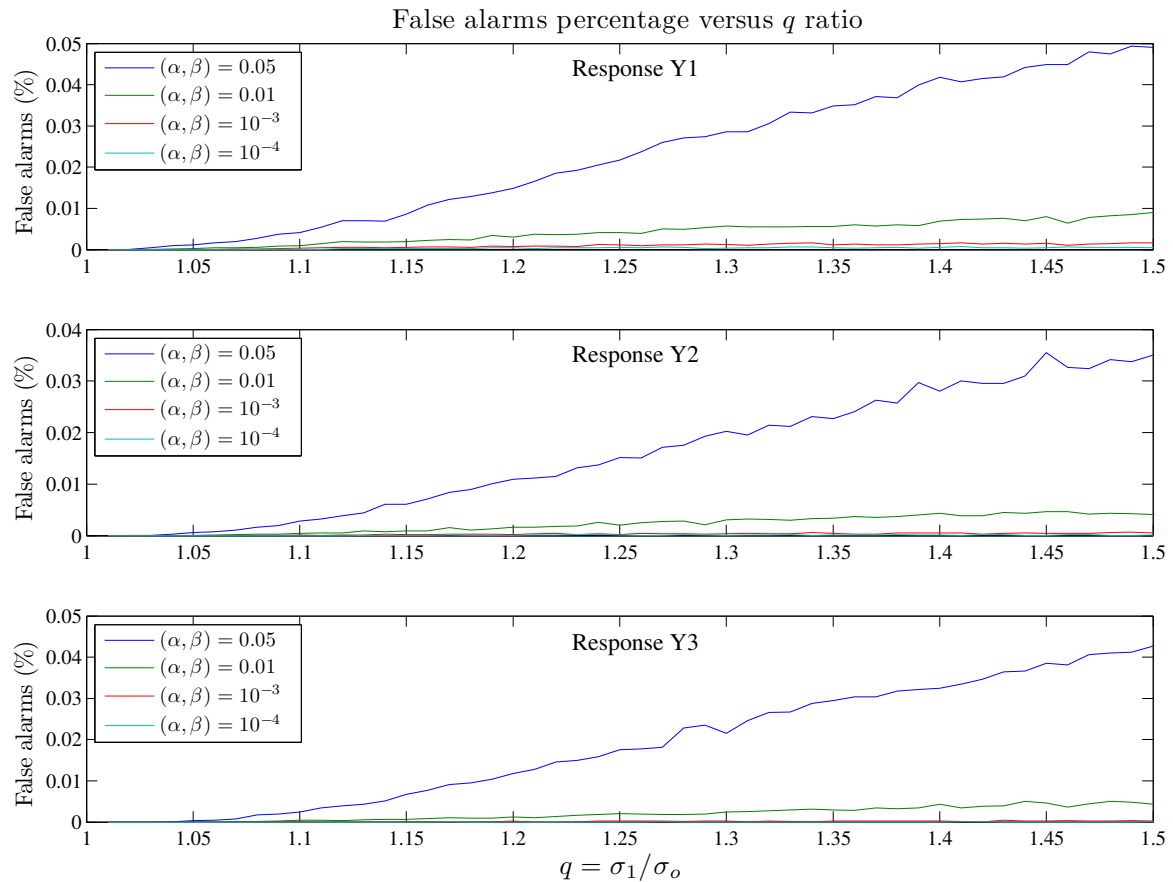


Figure 5.12: False alarms percentage for all vibration response measurement locations and various SPRT strengths (α, β) versus residual standard deviation ratio $q = \sigma_1/\sigma_o$; 1100 healthy inspection data sets are used.

detection is capable of accurately detecting the least severe damage type via all the considered vibration measurement locations.

The summarized damage detection results for each vibration response are presented in Table 5.4. The healthy detections and false alarm numbers are mean estimates per data set, as they are extracted from the 1100 healthy inspection data sets of 1000 samples each. For all the considered vibration responses the mean false alarm values are extremely low, as well as the mean missed damage

Response	Damage Detection						
	Mean healthy detections	Mean false alarms	Mean missed damage values				
			damage A	damage B	damage C	damage D	damage E
Y1	4.40	0.011	0.390	0	0	0	0
Y2	4.34	0.005	0.048	0	0	0	0
Y3	3.61	0.005	0	0	0	0	0

Test strength $(\alpha, \beta) = 0.01$; Residual standard deviation ratio $q = \sigma_1/\sigma_o = 1.1$.

Mean healthy detections and **false alarms** per data set out of 1100 healthy inspection data sets.

Mean missed damage values per data set out of 900 damage inspection data sets.

Table 5.4: Damage detection summary results for the three vibration responses (Y1, Y2 and Y3).

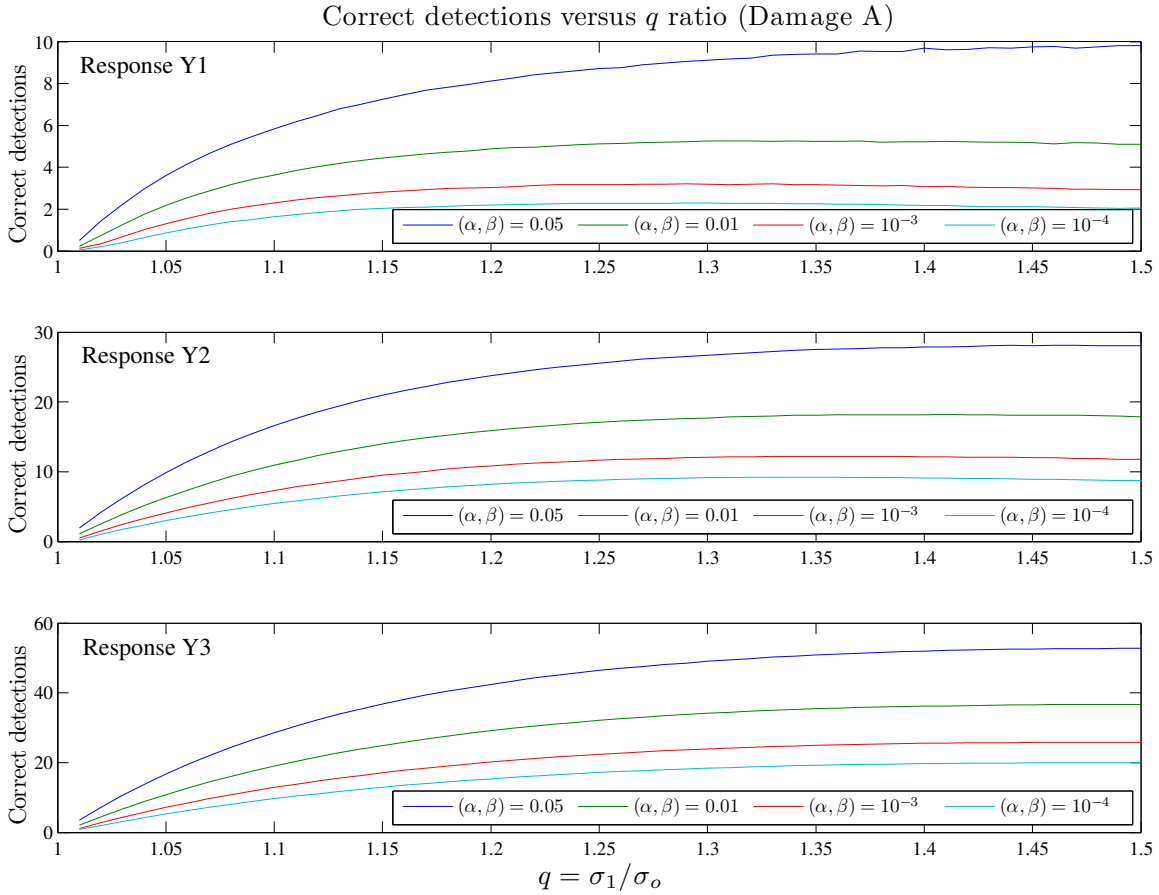


Figure 5.13: Average number of correct damage detections under damage type A for all vibration response measurement locations and various SPRT strengths (α, β) versus residual standard deviation ratio $q = \sigma_1/\sigma_o$; 800 damage type A inspection data sets are used.

values which are zero, except for the case of the less severe damage type A (see Figures 5.3, 5.4 and Table 5.1), which exhibits its maximum mean value of false alarms for response Y1 equal to 0.39.

Overall, the method exhibits excellent performance in tackling damage detection.

5.5.2.2 Damage identification and quantification

Damage identification and quantification is based on the multihypothesis SPRT presented in Section 5.3.3.2. Prior to implementing the multihypothesis test for tackling damage identification and quantification an appropriate sampling plan should be selected, similarly to the damage detection task. The selection of the sampling plan involves the determination of the following two aspects: (i) the nominal residual standard deviation values $\sigma_A, \dots, \sigma_E$ under which the structure is considered to be in the corresponding damage type A, \dots , E state, respectively, and (ii) the matrix of error probabilities α_{ij} (see Equation (5.18)). As it may be observed from Equation (5.18), the vector of correct decision probabilities α_{ii} is indirectly obtained via the determination of the error probabilities matrix.

The determination of the nominal residual standard deviation values $\sigma_A, \dots, \sigma_E$ under which the structure is considered to be under the corresponding damage type is based on the available 100 baseline data records obtained from the structure under each damage state (Table 5.1). For each considered vibration measurement location (Figure 5.3, Points Y1, Y2 and Y3), the corresponding

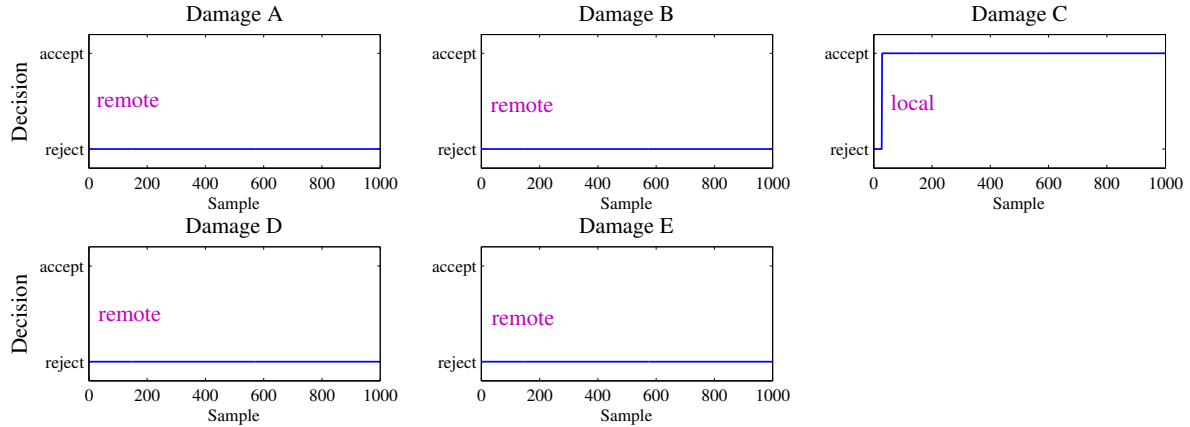


Figure 5.14: Indicative damage identification results for response Y1 at the $\alpha_{ij} = 0.01$ error probabilities level, with the actual damage being of type C. The actual structural state is shown above each plot.

identified ARX model, as presented in Section 5.5.1.2 and Table 5.2, is employed in order to obtain the 100 baseline residual sequences for each damage type. In the damage identification and quantification case the nominal residual standard deviation values $\sigma_A, \dots, \sigma_E$ that are needed to implement the multihypothesis test are selected as the mean values of the 100 baseline residual standard deviations under each damage type. The selected nominal $\sigma_A, \dots, \sigma_E$ values for all three vibration responses are presented in Table 5.5.

As it may be observed from Table 5.5 the nominal residual standard deviation values σ_B and σ_D , that belong to the corresponding damage types B and E, are quite similar for all three vibration responses. This is due to the fact that these two damage types have a similar effect on the residual sequences obtained by driving the baseline data under each damage type through the nominal models of the healthy structure (see Table 5.2).

Indicative damage identification results for vibration response Y1 at the $\alpha_{ij} = 0.01$ error probabilities level are presented in Figure 5.14, with the actual damage being of type C. Inside each subplot of Figure 5.14 is indicated whether the considered damage type is “local” or “remote” with respect to the vibration sensor employed (sensor Y1), hence damage type C is characterized as “local”, whereas damage types A, B, D and E are characterized as “remote”. The vertical axes in each subplot designate whether the corresponding hypothesis is accepted or rejected, while the horizontal axes indicate the 1000 residual samples under each damage type. Once the multihypothesis test reaches a terminal decision the corresponding damage type hypothesis is accepted, thus the sample for which this terminal decision is made constitutes the stopping time of the test (see Equations (5.41) and (5.42)). In Figure 5.14 the hypotheses belonging to damage types A, B, D, and E are correctly rejected, while the hypothesis that belongs to damage type C is correctly accepted. Moreover, notice that the stopping

Response	Nominal residual standard deviations				
	σ_A	σ_B	σ_C	σ_D	σ_E
Y1	0.1056	0.1617	0.2304	0.1492	0.3259
Y2	0.0991	0.1361	0.2672	0.1211	0.2806
Y3	0.1633	0.3377	1.7264	0.3475	0.4857

$\sigma_A, \dots, \sigma_E$ mean values out of 100 baseline damage data sets each.

Table 5.5: Nominal residual standard deviation values $\sigma_A, \dots, \sigma_E$ for damage identification.

time for the terminal decision of hypothesis C acceptance is reached before 50 samples (≈ 0.19 s), which demonstrates the ability of the multihypothesis test to arrive at an early decision.

Summary identification results for all vibration responses are presented in Table 5.6. The correct damage classification percentages are presented for all damage type inspection sets, along with the corresponding mean stopping times. As it may be observed the multihypothesis test damage classification results obtained for all vibration responses are very accurate for damage types A, C and E, as the percentages of correct classification are very high. Nevertheless, the method faces difficulties in accurately classifying damage types B and D. As already mentioned, this is due to the fact that these damage types have a similar effect on their corresponding residual standard deviation values obtained through the healthy models (see Table 5.2 and Table 5.5).

In this case, as presented and explained in Section 5.3.3.2, the user may apply the binary damage identification method for the candidate damage types. Nevertheless, this procedure would require the baseline modeling of at least one of these types.

Indicative damage identification results for damage types B and D via the binary damage identification method at the $\alpha = \beta = 0.01$ risk levels and $q = \sigma_1/\sigma_o = 1.1$ are presented in Figure 5.15 for vibration response Y2. The model orders that were employed for the ARX modeling of damage types B and D are the same that are used for the modeling of the healthy structure (Table 5.2). As it may be observed from Figure 5.15, although the multihypothesis method faces difficulties in correctly classifying these damage types, the binary damage identification method is capable of accurately identifying the actual damage type as current, while the summarized results exhibit zero misclassification numbers. Nevertheless, this method requires the baseline modeling of the potential damage structural states, a procedure which is avoided by the multihypothesis method.

Damage quantification is indirectly treated via the damage identification task. The nominal residual standard deviation values $\sigma_A, \dots, \sigma_E$, as determined in the multihypothesis damage identification method, constitute an indication of damage severity for the corresponding damage types. This is due to the fact that as damage severity increases the current structural dynamics deviate from the nominal healthy behavior, thus the nominal model M_o belonging to the healthy structure will not be able to accurately represent them, leading to increased residual sequence values and corresponding standard deviations.

Table 5.5 presents the selected nominal standard deviation values for all damage types (see also Figure 5.3). For vibration responses of Points Y1 and Y2 damage type E is the most severe followed by damage type C. Damage types B and D are of the same severity level, which justifies the misclassification issues for these types, while damage type A is the least severe and thus hardest to detect. For the vibration response of Point Y3 damage type C is the most severe, followed by damage type E. Again, damage types B and D are of the same severity level, while damage type A is the least

Actual damage	Damage Identification				
	Damage classification (%)				
	damage A	damage B	damage C	damage D	damage E
Type A	99.33/98.22/100	0.11/0/0	0/0/0	0.55/1.78/0	0/0/0
Type B	0/0/0	45.65/69.77/66.55	2.33/0/0	52/30.22/33.44	0/0/0
Type C	0/0/0	0/0/0	98.32/95.10/100	0/0/0	0.66/4.89/0
Type D	0/0/0	46.33/11.22/49.99	0/0/0	53.55/88.77/51.01	0/0/0
Type E	0/0/0	0/0/0	0.11/1.11/0.77	0/0/0	99.88/98.88/97.65
Mean \bar{N}	15.68/22.84/8.76	174.35/172.32/176.26	36.18/117.99/3.81	200.08/167.34/231.98	18.54/90.33/27.21

Damage classification percentage for points Y1/Y2/Y3 out of 800 inspection data sets; $\alpha_{ij} = 0.01$.

Mean stopping time in samples for points Y1/Y2/Y3 out of 800 inspection data sets of 1000 samples each.

Table 5.6: Damage identification summary results for the three vibration responses (Y1, Y2 and Y3).

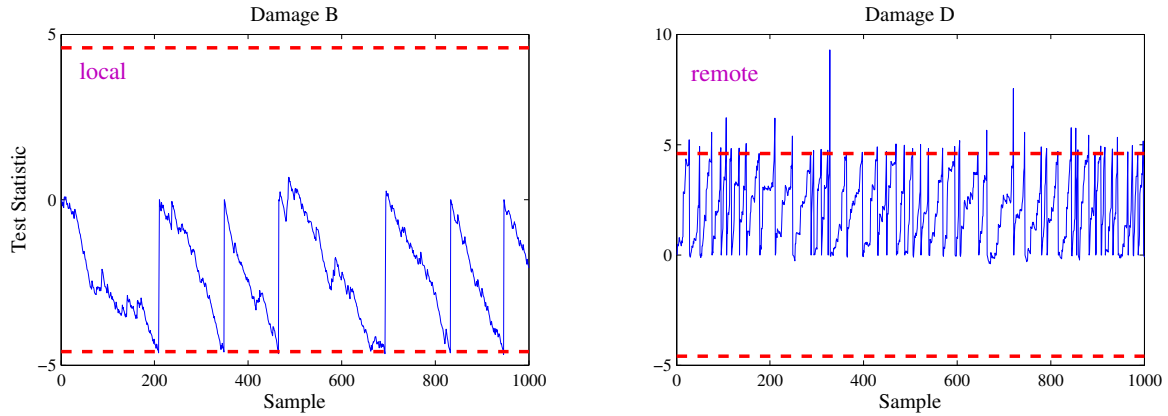


Figure 5.15: Indicative damage identification results for response Y2 at the $\alpha = \beta = 0.01$ risk levels ($q = \sigma_1/\sigma_o = 1.1$) for damage types B and D. The baseline model of damage type B is used with the actual structural state shown above each plot.

severe. The above conclusions are in agreement with the non-parametric FRFs presented in Figure 5.4 and the remarks of subsection 5.5.1.1.

5.6 Concluding remarks

A vibration based sequential statistical time series method for SHM was presented. The method, which is based on binary and multihypothesis versions of the statistically optimal SPRT, was shown to be capable of achieving effective and robust damage detection and accurate identification and quantification. The main conclusions drawn from this study may be summarized as follows:

- The method was shown to effectively tackle damage detection and identification, achieving excellent performance with practically zero false alarms and missed damage rates.
- An optimal sampling plan was determined *a priori* via the use of the Operating Characteristic (OC) and Average Sample Number (ASN) functions, selected type I (false alarm) and II (missed damage) error probabilities, and available baseline data records of the structure under various potential states.
- The method was shown to have global and robust damage detection capability, as it was able to detect both “local” and “remote” damage with respect to the sensor position employed.
- The multihypothesis damage identification procedure faced some difficulties in classifying two damage types with similar effects on the residual series, an issue that was tackled via the baseline modeling of these damage types and sequential binary hypothesis testing.
- The method was able to accurately quantify damage with respect to its effect on model residuals.
- The method was shown to achieve *early* damage detection and identification (< 0.19 s) as it required a minimum number of residual samples in order to reach a decision.
- The availability of baseline data records corresponding to various potential damage scenarios is necessary in order to treat damage identification. This may not always be possible with the actual structure itself, but laboratory scale models or analytical (Finite Element) models may be used for this purpose.

- Potential extension for online implementation is straightforward, as the method is based on simple conventional time series models (ARX, ARMAX, state space, and so on) and is characterized by computational simplicity.

Chapter 6

Conclusions

The final chapter of the thesis is divided into two sections: Section 6.1 contains a brief summary of the thesis chapters. Section 6.2 gives an overall discussion and outlook of the issues treated in this thesis, while Section 6.3 discusses the future perspectives of the main subjects of the thesis.

6.1 Thesis summary

Chapter I

Chapter I contains the thesis introduction. The general problem was divided into two main topics: (i) the vibration based damage diagnosis and (ii) the stochastic system identification under multiple operating conditions. The main focus of the thesis has been the development of novel vibration based statistical time series methods for SHM capable of effectively and robustly treating the damage detection, identification and quantification subproblems within a unified framework. The secondary focus of the thesis has been the postulation of generalized FP model structures for the identification of stochastic systems under multiple or varying operating conditions with the ultimate goal being to be employed in the damage diagnosis context. Furthermore, the current state-of-the-art was outlined and discussed, and the specific thesis goals were presented. Finally, the thesis chapters were analytically presented and their individual contributions outlined.

Chapter II

The goal of the second chapter was to provide an experimental assessment and critical comparison of vibration based statistical time series methods for SHM via their application to prototype laboratory structures. An overview of the principles and techniques of the main non-parametric and parametric methods was provided, including response-only and excitation-response, as well as scalar (univariate) and vector (multivariate) schemes. Damage detection and identification results for several distinct vibration measurement positions on the structures were presented. The non-parametric and parametric identification was presented, while the damage diagnosis methods' effectiveness was assessed via multiple experiments under various damage scenarios. The results of the study confirmed the high potential and effectiveness of statistical time series methods for SHM.

Chapter III

The goal of this chapter has been the identification of stochastic systems under multiple or varying operating conditions via Vector-dependent Functionally Pooled (VFP) models. Chapter III addressed the problem of identifying a globally valid and parsimonious system model based on input-output data records obtained under a sample of operating conditions characterized by more than one parameters (for instance operating temperature and humidity). Thus, models that include a *vector* characterization of the operating condition (*operating parameter vector*) were postulated. The problem was tackled within the novel Functional Pooling (FP) framework that postulates proper global models of the ARX and ARMAX types, data pooling techniques, and statistical parameter estimation. Corresponding Vector-dependent Functionally Pooled (VFP) ARX and ARMAX models were postulated, and proper estimators of the Least Squares (LS), Maximum Likelihood (ML), and Prediction Error (PE) types were developed. Model structure estimation was achieved via customary criteria, such as the Akaike and Bayesian information criteria (AIC and BIC, respectively), and a novel Genetic Algorithm (GA) based procedure. The strong consistency of the VFP-ARX least squares and maximum likelihood estimators was established, whereas the effectiveness of the complete estimation and identification method was demonstrated via two Monte Carlo studies.

Chapter IV

A vibration based statistical time series method that is capable of effective damage detection, precise localization, and magnitude estimation within a unified stochastic framework was introduced in Chapter IV. The method constitutes an important generalization of the recently introduced Functional Model Based Method (FMBM) in that it allows, for the first time in the statistical time series methods context, for complete and precise damage localization. More precisely, the proposed method was demonstrated to accurately localize damage anywhere on properly defined continuous topologies on the structure, instead of pre-defined specific locations. Estimator uncertainties were taken into account, and uncertainty ellipsoids were provided for the damage location and magnitude. To achieve its goal, the method is based on the extended class of Vector-dependent Functionally Pooled (VFP) models, which are characterized by parameters that depend on both damage magnitude and location, as well as on proper statistical estimation and decision making schemes. The method was validated and its effectiveness was experimentally assessed via its application to damage detection, precise localization, and magnitude estimation on a prototype GARTEUR-type laboratory scale aircraft skeleton structure. The damage scenarios considered consist of varying size small masses attached to various continuous topologies on the structure. The method was shown to achieve effective damage detection, precise localization, and magnitude estimation based on even a single pair of measured excitation-response signals.

Chapter V

The goal of this chapter has been the introduction and experimental assessment of a sequential statistical time series method for vibration based SHM. The method is based on a combination of binary and multihypothesis versions of the statistically optimal Sequential Probability Ratio Test (SPRT), which employs the residual sequences obtained through a stochastic time series model of the healthy structure. In this work the full list of properties and capabilities of the SPRT were for the first time presented and explored in the context of vibration based damage detection, identification and quantification. The method was shown to achieve effective and robust damage detection, identification and quantification based on predetermined sampling plans, which were both analytically and experimen-

tally compared and assessed. The method's performance was determined a priori via the use of the analytical expressions of the OC and ASN functions in combination with baseline data records, while it required on average a minimum number of samples in order to reach a decision (early damage detection) compared to most powerful Fixed Sample Size (FSS) tests. The effectiveness of the proposed method was validated and experimentally assessed via its application on a lightweight aluminum truss structure, while the obtained results for three distinct vibration measurement positions proved the method's ability to operate based even on a single pair of measured excitation-response signals.

Chapter VI

The final chapter of the thesis presents the general conclusions of the thesis, as well as the future perspectives.

6.2 Concluding remarks

6.2.1 General conclusions

The general conclusions drawn from this thesis may be summarized as follows:

- The experimental assessment and critical comparison of several non-parametric and parametric vibration based statistical time series SHM methods demonstrated their effectiveness and potential, as well their limitations with respect to damage detection, identification and quantification. The methods were shown to be able to achieve effective damage detection and identification (damage classification) using a limited number of vibration response sensors, although parametric methods demand increased user expertise and are more prone to experimental and modeling uncertainties. The methods are able to treat damage identification as a discrete classification problem.
- The novel FP framework was extended and improved via the VFP parametrization that includes a vector characterization of all the admissible operating conditions. VFP models now allow for the analytical inclusion of *both* damage location and damage magnitude effects on the dynamics. Appropriate estimators were developed, while their strong consistency was established. Model structure selection is treated via a GA procedure.
- Based on the postulated VFP parametrization, the extension and generalization of the FMBM was proposed, which is now capable of achieving – for the first time in the statistical time series methods context – unified and effective damage detection, along with complete and precise damage localization and magnitude estimation on continuous structural topologies. The method was experimentally validated and assessed via a proof-of-concept application on a prototype laboratory scale aircraft skeleton structure.
- A statistical sequential time series method was introduced capable of achieving effective and robust damage detection, identification and quantification under experimental, operational and modeling uncertainties. The method is more robust and less sensitive to uncertainties compared to FSS hypothesis testing based time series methods. Moreover, via its experimental application and assessment the method was shown to achieve early damage detection and identification, while its computational simplicity renders it suitable for online SHM implementation.

6.2.2 Chapter conclusions

The general conclusions obtained from comparative experimental assessment of vibration based statistical time series methods for SHM via their application to damage diagnosis in a lightweight aluminum truss structure and a scale aircraft skeleton structure may be summarized as follows:

- Statistical time series methods for SHM achieve damage detection and identification based on (i) *scalar* or *vector* random excitation and/or vibration response signals, (ii) statistical model building, and (iii) statistical decision making under uncertainty.
- Both non-parametric and parametric methods were shown to effectively tackle damage detection and identification, with parametric methods achieving excellent performance with zero false alarm, missed damage, and damage misclassification rates.
- Both scalar and vector statistical time series methods for SHM have been shown to effectively tackle damage detection and identification, with the vector methods achieving excellent performance with zero false alarm, missed damage and damage misclassification errors.
- Both non-parametric and parametric methods were shown to have global damage detection capability, as they are able to detect “local” and “remote” damage with respect to the sensor position used.
- Both scalar and vector methods have “global” damage detection capability, as they are able to detect “local” and “remote” damage (with respect to the sensor location being used).
- All methods were shown to be capable of correctly identifying the actual damage type, with the exception of the FRF based method which exhibited a small number of damage misclassification errors, irrespectively of the vibration measurement position used.
- Parametric time series methods are more elaborate and demand increased user expertise compared to their generally simpler non-parametric counterparts. Yet, they were shown to offer increased sensitivity and accuracy.
- The availability of data records corresponding to various potential damage scenarios is necessary in order to treat damage identification. This may not be possible with the actual structure itself, but laboratory scale models or analytical (Finite Element) models may be used for this purpose.

The main issues addressed with respect to the identification of stochastic systems under multiple or varying operating conditions and the postulated VFP model structure are the following:

- Extension of the FP models employing a scalar operating parameter to the Vector-dependent FP models employing the *operating parameter vector*.
- Model structure estimation was achieved via customary criteria such as the BIC and the AIC, as well as via a Genetic Algorithm (GA) based procedure offering potential automation and complete solution to the functional basis dimensionality subproblem.
- A new VFP model form was introduced in which the innovations sequence variance is projected to a functional subspace, so now it may be available not only for the sample of operating conditions (available data records), but it may be efficiently estimated for all the potential admissible operating conditions, thus for all the potential operating parameter vectors \mathbf{k} .

- The strong consistency of the least squares and the maximum likelihood estimators was established, as well as the asymptotic distribution of the all the considered estimators.
- Assessment of the proposed estimators and structure selection procedures via two Monte Carlo studies, investigating both the cases of complete and non-complete functional subspaces.
- Discussion of the estimators main features, as well as their corresponding computational times.

The main conclusions drawn from the generalized functional model based method for damage detection, precise localization, and magnitude estimation are the following:

- First and foremost, the study – including the proof-of-concept application – has demonstrated the important fact that effective damage detection, damage topology identification, and damage precise localization and magnitude estimation are possible based on *partial models* of the structural dynamics.
- The study has demonstrated the very significant *amount of information* on the state of the structure embedded even in a single excitation-response signal pair. Thus an important message is that it may not be necessary to employ a “high” number of sensors for precise damage diagnosis; instead, a “few” sensors and powerful signal analysis for extracting the embedded information may be a much more practical and effective approach.
- The diagnostic performance in terms of damage detection, topology identification, and precise localization and magnitude estimation achieved in the proof-of-concept study has been impressive. Damage localization and magnitude estimation are not only excellent at the nominal (point estimation) level, but also at a probabilistic level that provides very accurate and tight uncertainty bounds (ellipsoids).
- A practically important observation is that the diagnosis performance characteristics do *not* appear significantly dependent on the *proximity* of the damage location to the sensor used. Although the uncertainty bounds have been somewhat tighter when estimated by “local”, rather than “remote”, sensors, this effect has been remarkably limited in the study.
- “*Unmodelled*” damages, that is damages *not* belonging to any of the considered structural topologies (and thus not modelled in the baseline phase) have been very successfully detected and “negatively” identified as not belonging to the modelled topologies. This is very important as it provides detection and some localization information even for damages not formally accounted for by the method.
- The fact that effective damage diagnosis is possible *without* the need for specifically designed excitations and special testing procedures is also very important. Combined with the use of often naturally occurring random excitation and the fact that good results may be obtained with even low/limited frequency bandwidth (4 – 90 Hz, which includes ten of the structural modes in the present study), allows for potentially *in-operation* damage diagnosis. The possible use of higher frequency range/bandwidth is expected to lead to further gain in performance.
- The method may operate on *any type* (acceleration, velocity, displacement) of vibration signals and may be modified to be applied to the *output-only case*, where only vibration response signal(s) is (are) available. Naturally, the difficulty is higher in this case, and performance is expected to be affected. This is an issue to be considered in future studies.

- The *price* to be paid for the aforementioned benefits mainly involves the *baseline* (training) phase, and more specifically the identification of the necessary VFP models – yet, this takes place only once, while the inspection phase is simple and automated. Nevertheless, user expertise is necessary in the baseline phase, along with the availability of excitation-response signal records. Although the former is expected to be reduced in the future via more automated procedures, excitation-response signal records need to be obtained possibly through scale laboratory models or via Finite Element Models (FEMs). The advantages over alternative (including FEM based) methods remain that the FEM is only needed in the baseline phase for inferring the partial and much more “compact” VFP models, and that no model updating is required in the inspection phase.

The main conclusions drawn from the study on the vibration based sequential statistical time series method for SHM may be summarized as follows:

- The method was shown to effectively tackle damage detection and identification, achieving excellent performance with practically zero false alarms and missed damage rates.
- An optimal sampling plan was determined *a priori* via the use of the Operating Characteristic (OC) and Average Sample Number (ASN) functions, selected type I (false alarm) and II (missed damage) error probabilities, and available baseline data records of the structure under various potential states.
- The method was shown to have global and robust damage detection capability, as it was able to detect both “local” and “remote” damage with respect to the sensor position employed.
- The multihypothesis damage identification procedure faced some difficulties in classifying two damage types with similar effects on the residual series, an issue that was tackled via the baseline modeling of these damage types and sequential binary hypothesis testing.
- The method was able to accurately quantify damage with respect to its effect on model residuals.
- The method was shown to achieve *early* damage detection and identification (< 0.19 s) as it required a minimum number of residual samples in order to reach a decision.
- The availability of baseline data records corresponding to various potential damage scenarios is necessary in order to treat damage identification. This may not always be possible with the actual structure itself, but laboratory scale models or analytical (Finite Element) models may be used for this purpose.
- Potential extension for online implementation is straightforward, as the method is based on simple conventional time series models (ARX, ARMAX, state space, and so on) and is characterized by computational simplicity.

6.3 Future perspectives

The purpose behind this section is to focus on the issues that must be addressed by future research in order to make damage diagnosis using vibration measurements a viable, practical, and commonly implemented technology:

- The acquisition of baseline (training) data records is an extremely important issue, especially for the damage localization and quantification tasks. Excitation-response data records need to be obtained possibly through scale laboratory models or via analytical or tuned Finite Element (FE) models under potential damage structural states. This way the baseline phase of the statistical time series methods will be greatly facilitated. Nevertheless, while it is doubtful that all dependence on prior models and data can be eliminated, certainly steps can and should be taken to minimize the dependence on such information.
- As already demonstrated, statistical time series methods are capable of treating damage diagnosis based on limited or even on a single pair of excitation-response measurements and may also achieve a certain level of automation. Nevertheless, it is of critical importance that their performance on “real”, large scale structures should be further investigated in order to exist a chance for wide future implementation in aeronautical, engineering or civil infrastructure.
- The treatment of multiple damage scenarios on the same structure is another important issue. Current methods are able to detect multiple damage, nevertheless they fail to identify the distinct damages when they happen simultaneously on the same structure.
- The selection of the number and position of measurement sensors is another important issue. Several vibration based damage diagnosis techniques that appear to work well in test cases may perform poorly when subjected to the measurement constraints imposed by actual testing. Techniques that are to be seriously considered for implementation in the field should demonstrate that they can perform well under limitations of a small number of measurement positions and under the constraint that these positions should be selected a priori, without a priori knowledge of the damage location.
- The extension of the statistical time series methods to the more general *multivariate* case should be investigated. This case requires the use of corresponding vector models and multivariate statistical decision making procedures and needs to be fully investigated in the future.
- With regard to long-term SHM of large structures such as bridges and offshore platforms, the need to reduce the dependence on measurable excitation forces is noted. The ability to use vibrations induced by ambient environmental or operating loads for the assessment of structural integrity is an area that merits further investigation.
- The postulated VFP model identification needs to be further validated via data obtained from analytical or FE models, or –even better– by additional experimental set-ups under multiple operating conditions in order to fully understand and investigate the complete range of capabilities, pros and cons of this representation.
- The need for methods capable of working under varying operational and environmental conditions and “real” levels of uncertainties is extremely important and also the subject of current research (for instance see Hios and Fassois 2009a, Michaelides and Fassois 2008).

Bibliography

- Adams D. E., Farrar C. R., 2002, Classifying linear and nonlinear structural damage using frequency domain arx models, *Structural Health Monitoring*, **1**(2), 185–201.
- Akaike H., 1971, Information theory and an extension of the maximum likelihood principle, *Supplement to Problems of Control and Information Theory*, pp. 267–281.
- Alvandi A., Cremona C., 2006, Assessment of vibration-based damage identification techniques, *Journal of Sound and Vibration*, **292**, 179–202.
- Andersen P., 1997, *Identification of civil engineering structures using vector ARMA models*, PhD thesis, Department of Building Technology and Structural Engineering, Aalborg University, Denmark.
- Armitage P., 1950, Sequential analysis with more than two alternative hypotheses and its relation to discriminant function analysis, *Journal of the Royal Statistical Society: Series B (Methodological)*, **12**(1), 137–144.
- Balmes E., Wright J. R., 1997, Garteur group on ground vibration testing – results from the test of a single structure by 12 laboratories in europe, *Proceedings of ASME Design Engineering Technical Conferences*, Sacramento, U.S.A.
- Bamieh B., Giarre L., 2003, Identification of linear parameter varying models, *International Journal of Robust and Nonlinear Control*, **12**, 841–853.
- Basseville M., Mevel L., Goursat M., 2004, Statistical model-based damage detection and localization: subspace-based residuals and damage-to-noise sensitivity ratios, *Journal of Sound and Vibration*, **275**, 769–794.
- Baum C. W., Veeravalli V. V., 1994, A sequential procedure for multihypothesis testing, *IEEE Transactions on Information Theory*, **40**(6), 1994–2007.
- Bayissa W. L., Haritos N., 2007, Damage identification in plate-like structures using bending moment response power spectral density, *Structural Health Monitoring*, **6**(1), 5–20.
- Bendat J. S., Piersol A. G., 2000, *Random Data: Analysis and Measurement Procedures*, 3rd edition edn, Wiley-Interscience: New York.
- Benedetti M., Fontanari V., Zonta D., 2011, Structural health monitoring of wind towers: remote damage detection using strain sensors, *Smart Materials and Structures*, **20**, 13pp.
- Bently D. E., Hatch C. T., 2003, *Fundamentals of rotating machinery diagnostics*, ASME Press, New York.
- Bernstein D., 2005, *Matrix Mathematics*, Princeton University Press.

- Bodeux J. B., Golinval J. C., 2001, Application of armav models to the identification and damage detection of mechanical and civil engineering structures, *Smart Materials and Structures*, **10**, 479–489.
- Box G. E. P., Jenkins G. M., Reinsel G. C., 1994, *Time Series Analysis: Forecasting & Control*, third edn, Prentice Hall: Englewood Cliffs, NJ.
- Carden E. P., Brownjohn J. M., 2008, Arma modelled time-series classification for structural health monitoring of civil infrastructure, *Mechanical Systems and Signal Processing*, **22**(2), 295–314.
- Chipperfield A., Fleming P., Pohlheim H., Fonseca C., n.d., *Genetic Algorithm Toolbox: For Use With Matlab*.
- Coleman T. F., Zhang Y., n.d., *Optimization Toolbox 4: User's Guide*.
- Degener M., Hermes M., 1996, Ground vibration test and finite element analysis of the GARTEUR SM-AG19 testbed, *Technical Report IB 232-96 J 08*, Deutsche Forschungsanstalt für Aerolastic, Göttingen.
- Dielman T. E., 1989, *Pooled Cross-Sectional and Time Series Data Analysis*, Marcel Dekker, Inc.
- Doebling S. W., Farrar C. R., Prime M. B., 1998, A summary review of vibration-based damage identification methods, *Shock and Vibration Digest*, **30**(2), 91–105.
- Doebling S. W., Farrar C. R., Prime M. B., Shevitz D. W., 1996, Damage identification and health monitoring of structural and mechanical systems from changes in their vibration characteristics: A literature review, *Technical Report LA-13070-MS*, Los Alamos National Laboratory.
- Doherty J. E., 1987, Nondestructive evaluation, in A. S. Kobayashi, (ed.), *Handbook on experimental mechanics*, Society for experimental mechanics, chapter 12.
- Dragalin V. P., Tartakovsky A. G., Veeravalli V. V., 1999, Multihypothesis sequential probability ratio tests – Part I: asymptotic optimality, *IEEE Transactions on Information Theory*, **45**, 2448–2461.
- Dunkl C., Xu Y., 2001, *Orthogonal Polynomials in Several Variables*, Cambridge University Press.
- Emlsee B., Rogers S. K., DeSimio M. P., Raines R. A., 1997, Complete automatic target recognition system for tactical forward-looking infrared images, *Optical Engineering*, **36**, 2593–2603.
- Fan W., Qiao P., 2011, Vibration-based damage identification methods: A review and comparative study, *Structural Health Monitoring*, **10**(1), 83–111.
- Farrar C. R., Doebling S. W., Nix D. A., 2001, Vibration-based structural damage identification, *The Royal Society – Philosophical Transactions: Mathematical, Physical and Engineering Sciences*, **359**, 131–149.
- Farrar C. R., Jauregui D. A., 1998a, Comparative study of damage identification algorithms applied to a bridge: I. experiment, *Smart Materials and Structures*, **7**, 704–719.
- Farrar C. R., Jauregui D. A., 1998b, Comparative study of damage identification algorithms applied to a bridge: II. numerical study, *Smart Materials and Structures*, **7**, 720–731.
- Farrar C. R., Lieven N. A. J., 2007, Damage prognosis: the future of structural health monitoring, *The Royal Society – Philosophical Transactions: Mathematical, Physical and Engineering Sciences*, **365**, 623–632.

- Farrar C. R., Sohn H., Hemez F. M., Bement M. T., Cornwell P. J., Doebling S. W., Schultze J. F., Lieven N., Robertson A. N., 2003, Damage prognosis: Current status and future needs, *Technical Report LA-14051-MS*, Los Alamos National Laboratory.
- Farrar C. R., Worden K., 2007, An introduction to Structural Health Monitoring, *The Royal Society – Philosophical Transactions: Mathematical, Physical and Engineering Sciences*, **365**, 303–315.
- Fassois S. D., 2001, Parametric identification of vibrating structures, in S. Braun, D. Ewins, S. Rao, (eds), *Encyclopedia of Vibration*, Academic Press, pp. 673–685.
- Fassois S. D., Sakellariou J. S., 2007, Time series methods for fault detection and identification in vibrating structures, *The Royal Society – Philosophical Transactions: Mathematical, Physical and Engineering Sciences*, **365**, 411–448.
- Fassois S. D., Sakellariou J. S., 2009, Statistical time series methods for structural health monitoring, in C. Boller, F. K. Chang, Y. Fujino, (eds), *Encyclopedia of Structural Health Monitoring*, John Wiley & Sons Ltd., pp. 443–472.
- Fu K. S., 1968, *Sequential Methods in Pattern Recognition and Learning*, Academic Press, New York.
- Fugate M. L., Sohn H., Farrar C. R., 2001, Vibration-based damage detection using statistical process control, *Mechanical Systems and Signal Processing*, **15**(4), 103–119.
- Gao F., Lu Y., 2009, An acceleration residual generation approach for structural damage identification, *Journal of Sound and Vibration*, **319**, 163–181.
- Gertler J. J., 1998, *Fault Detection and Diagnosis in Engineering Systems*, Marcel Dekker.
- Ghosh B. K., Sen P. K., (eds) 1991, *Handbook of Sequential Analysis*, Marcel Dekker, Inc., New York.
- Gill P. E., Murray W., Wright M. H., 1981, *Practical Optimization*, London Academic Press.
- Glöckler O., 1991, Fault detection via sequential probability ratio test of multivariate autoregressive modeling-based residual time series, *Sixth Symposium on Nuclear Reactor Surveillance and Diagnostics*, Tennessee, U.S.A.
- Greene W. H., 2003, *Econometric Analysis*, 5th edn, Prentice–Hall.
- Gross K. C., Humenik K. E., 1991, Sequential probability ratio tests for nuclear plant component surveillance, *Nuclear Technology*, **93**, 131–137.
- Gul M., Catbas F. N., 2011, Structural health monitoring and damage assessment using a novel time series analysis methodology with sensor clustering, *Journal of Sound and Vibration*, **330**, 1196–1210.
- Hios J. D., Fassois S. D., 2009a, Statistical damage detection in a smart structure under different temperatures via vibration testing: a global model based approach, *Key Engineering Materials*, **Vols. 413–414**, 261–268.
- Hios J. D., Fassois S. D., 2009b, Stochastic identification of temperature effects on the dynamics of a smart composite beam: assessment of multi-model and global model approaches, *Smart Materials and Structures*, **18**(3), 035011 (15pp).
- Hoel P. G., 1984, *Introduction to Mathematical Statistics*, 5th edn, Wiley, New York.

- Humenik K. E., Gross K. C., 1990, Sequential probability ratio tests for reactor signal validation and sensor surveillance applications, *Nuclear Science and Engineering*, **150**, 383–390.
- Hwang H. Y., Kim C., 2004, Damage detection in structures using a few frequency response measurements, *Journal of Sound and Vibration*, **270**, 1–14.
- Jung U., Koh B. H., 2009, Structural damage localization using wavelet-based silhouette statistics, *Journal of Sound and Vibration*, **321**, 590–604.
- Kay S. M., 1988, *Modern Spectral Estimation: Theory and Application*, Prentice Hall: New Jersey.
- Kirikera G. R., Shinde V., Schulz M. J., Ghoshal A., Sundaresan M., Allemang R., 2007, Damage localisation in composite and metallic structures using a structural neural system and simulated acoustic emissions, *Mechanical Systems and Signal Processing*, **21**, 280–297.
- Kopsaftopoulos F. P., Fassois S. D., 2006a, Identification of stochastic systems under multiple operating conditions: The vector dependent FP-ARX parametrization, *Proceedings of 14th Mediterranean Conference on Control and Automation*, Ancona, Italy.
- Kopsaftopoulos F. P., Fassois S. D., 2006b, Vibration-based fault detection and assessment in a scale aircraft structure via stochastic VFP-ARX models, *Proceedings of the 3rd European Workshop on Structural Health Monitoring (EWSHM)*, Granada, Spain.
- Kopsaftopoulos F. P., Fassois S. D., 2007, Vibration-based structural damage detection and precise assessment via stochastic functionally pooled models, *Key Engineering Materials*, **347**, 127–132.
- Kopsaftopoulos F. P., Fassois S. D., 2008, Experimental assessment of time series methods for structural health monitoring (SHM), *Proceedings of the 4th European Workshop on Structural Health Monitoring (EWSHM)*, Cracow, Poland.
- Kopsaftopoulos F. P., Fassois S. D., 2010a, Vibration based health monitoring for a lightweight truss structure: experimental assessment of several statistical time series methods, *Mechanical Systems and Signal Processing*, **24**, 1977–1997.
- Kopsaftopoulos F. P., Fassois S. D., 2010b, Vibration based health monitoring for a lightweight truss structure: experimental assessment of several statistical time series methods, *Proceedings of the ISMA 2010 International Conference on Noise and Vibration Engineering*, Leuven, Belgium.
- Kopsaftopoulos F. P., Fassois S. D., 2010c, Vibration based health monitoring for a thin aluminum plate – a comparative assessment of statistical time series methods, *Proceedings of the 5th European Workshop on Structural Health Monitoring (EWSHM)*, Sorrento, Italy.
- Kopsaftopoulos F. P., Fassois S. D., 2011a, Identification of stochastic systems under multiple operating conditions: The Vector-dependent Functionally Pooled (VFP) parametrization, *under preparation for publication*, .
- Kopsaftopoulos F. P., Fassois S. D., 2011b, Scalar and vector time series methods for vibration based damage diagnosis in a scale aircraft skeleton structure, *Journal of Theoretical and Applied Mechanics*, **49**(3), 727–756.
- Kopsaftopoulos F. P., Fassois S. D., 2011c, A sequential statistical time series method for vibration based Structural Health Monitoring, *under preparation for publication*, .

- Kopsaftopoulos F. P., Fassois S. D., 2011*d*, Statistical time series methods for damage diagnosis in a scale aircraft skeleton structure: loosened bolts damage scenarios, *Proceedings of the 9th International Conference on Damage Assessment on Structures (DAMAS)*, Vol. 305 of *Journal of Physics: Conference Series*, Oxford, U.K.
- Kopsaftopoulos F. P., Fassois S. D., 2011*e*, A stochastic functional model based method for vibration based damage detection, precise localization, and magnitude estimation, *accepted in Mechanical Systems and Signal Processing*, .
- Kopsaftopoulos F. P., Magripis S. G., Amlianitis A. D., Fassois S. D., 2010, Scalar and vector time series methods for vibration based damage diagnosis in an aircraft scale skeleton structure, *Proceedings of the ASME 2010 10th Biennial Conference on Engineering Systems Design and Analysis*, Istanbul, Turkey.
- Kowalski M. A., 1982, The recursion formulas for orthogonal polynomials in n variables, *SIAM Journal on Mathematical Analysis*, **13**(2), 309–315.
- Krall H. L., Scheffer I. M., 1967, Orthogonal polynomials in two variables, *Annali di Matematica Pura ed Applicata (4)*, **76**, 325–376.
- Lai T. L., 2000, Sequential multiple hypotheses testing and efficient fault detection–isolation in stochastic systems, *IEEE Transactions on Information Theory*, **46**(2), 595–608.
- Lee J. W., Kirikera G. R., Kang I., Schulz M. J., Shanov V. N., 2006, Structural health monitoring using continuous sensors and neural network analysis, *Smart Materials and Structures*, **15**, 1266–1274.
- Lehmann E. L., Romano J. P., 2008, *Testing Statistical Hypotheses*, 3rd edn, Springer.
- Liberatore S., Carman G. P., 2004, Power spectral density analysis for damage identification and location, *Journal of Sound and Vibration*, **274**(3–5), 761–776.
- Lim Y. Y., Bhalla S., Soh C. K., 2006, Structural identification and damage diagnosis using self-sensing piezo-impedance transducers, *Smart Materials and Structures*, **15**, 987–995.
- Liu S., 1999, Matrix results on the Khatri–Rao and Tracy–Singh products, *Linear Algebra and its Applications*, **289**, 267–277.
- Liu S., Trenkler G., 2008, Hadamard, Khatri–Rao, Kronecker and other matrix products, *International Journal of Information and System Sciences*, **4**(1), 160–177.
- Ljung L., 1999, *System Identification: Theory for the User*, 2nd edn, Prentice–Hall.
- Loh C. H., Weng J. H., Liu Y. C., Lin P. Y., Huang S. K., 2011, Structural damage diagnosis based on on-line recursive stochastic subspace identification, *Smart Materials and Structures*, **20**, 10pp.
- Lois W. S., 1989, Pooled time series analysis, *Quantitative Applications in the Social Sciences*, SAGE Publications.
- Lorden G., 1972, Likelihood ratio tests for sequential k –decision problems, *Annals of Mathematical Statistics*, **43**, 1412–1427.
- Lorden G., 1976, 2–SPRTs and the modified kiefer-weiss problem of minimizing an expected sample size, *Annals of Statistics*, **4**(2), 281–291.

- Lorden G., 1977, Nearly-optimal sequential tests for finitely many parameter values, *Annals of Statistics*, **5**(1), 1–21.
- Lu Y., Gao F., 2005, A novel time-domain auto-regressive model for structural damage diagnosis, *Journal of Sound and Vibration*, **283**, 1031–1049.
- Lütkepohl H., 2005, *New Introduction to Multiple Time Series Analysis*, Springer-Verlag Berlin.
- Manson G., Worden K., Allman D., 2003, Experimental validation of a structural health monitoring methodology: Part III. damage location on an aircraft wing, *Journal of Sound and Vibration*, **259**(2), 365–385.
- Marcus M. B., Swerling P., 1962, Sequential detection in radar with multiple resolution elements, *IRE Transactions on Information Theory*, **IT-8**, 237–245.
- Mattson S. G., Pandit S. M., 2006a, Damage detection and localization based on outlying residuals, *Smart Materials and Structures*, **15**, 1801–1810.
- Mattson S. G., Pandit S. M., 2006b, Statistical moments of autoregressive model residuals for damage localization, *Mechanical Systems and Signal Processing*, **20**, 627–645.
- Mendel J. M., 1995, *Lessons in Estimation Theory for Signal Processing, Communications and Control*, Prentice Hall.
- Mevel L., Goursat M., Basseville M., 2003, Stochastic subspace-based structural identification and damage detection and localisation – application to the z24 bridge benchmark, *Mechanical Systems and Signal Processing*, **17**(1), 143–151.
- Michaelides P. G., Fassois S. D., 2008, Stochastic identification of structural dynamics from multiple experiments – experimental variability analysis, *Proceedings of the ISMA Conference on Noise and Vibration Engineering*, Leuven, Belgium.
- Montalvão D., Maia N. M. M., Ribeiro A. M. R., 2006, A summary review of vibration-based damage identification methods, *Shock and Vibration Digest*, **38**(4), 295–324.
- Montgomery D. C., 1997, *Introduction to statistical quality control*, John Wiley & Sons Inc.
- Mukhopadhyay N., de Silva B. M., 2009, *Sequential Methods and Their Applications*, Chapman and Hall/CRC.
- Nair K. K., Kiremidjian A. S., 2007, Time series based structural damage detection algorithm using gaussian mixtures modeling, *Journal of Dynamic Systems, Measurement, and Control*, **129**, 285–293.
- Nair K. K., Kiremidjian A. S., Law K. H., 2006, Time series-based damage detection and localization algorithm with application to the asce benchmark structure, *Journal of Sound and Vibration*, **291**, 349–368.
- Nauerz A., Fritzen C. P., 2001, Model based damage identification using output spectral densities, *Journal of Dynamic Systems, Measurement, and Control*, **123**, 691–698.
- Oh C. K., Sohn H., 2009, Damage diagnosis under environmental and operational variations using unsupervised support vector machine, *Journal of Sound and Vibration*, **328**, 224–239.

- Panopoulou A., Loutas T., Roulias D., Fransen S., Kostopoulos V., 2011, Dynamic fiber bragg gratings based health monitoring system of composite aerospace structures, *Acta Astronautica*, doi:10.1016/j.actaastro.2011.05.027.
- Perera R., Ruiz A., Manzano C., 2007, An evolutionary multiobjective framework for structural damage localization and quantification, *Engineering Structures*, **29**(10), 2540–2550.
- Petsounis K. A., Fassois S. D., 2001, Parametric time-domain methods for the identification of vibrating structures – A critical comparison and assessment, *Mechanical Systems and Signal Processing*, **15**, 1031–1060.
- Poulimenos A. G., 2007, *Modeling of non-stationary vibration signals via Functional Series (FS) TARMA models*, PhD thesis, Department of Mechanical Engineering and Aeronautics, University of Patras, Greece.
- Razi P., Esmaeel R. A., Taheri F., 2011, Application of a robust vibration-based non-destructive method for detection of fatigue cracks in structures, *Smart Materials and Structures*, **20**, 115017 (12pp).
- Reinsel G. C., 1993, *Elements of Multivariate Time Series Analysis*, Springer-Verlag Berlin.
- Rizos D. D., Fassois S. D., Marioli-Riga Z. P., Karanika A. N., 2008, Vibration-based skin damage statistical detection and restoration assessment in a stiffened aircraft panel, *Mechanical Systems and Signal Processing*, **22**, 315–337.
- Rytter A., 1993, *Vibration based inspection of civil engineering structures*, PhD thesis, Department of Building Technology and Structural Engineering, Aalborg University, Denmark.
- Sakellariou J. S., 2005, *Stochastic Functional Models: Identification methods and Application to Damage Diagnosis*, PhD thesis, Department of Mechanical Engineering and Aeronautics, University of Patras, Greece.
- Sakellariou J. S., Fassois S. D., 2006, Stochastic output error vibration-based damage detection and assessment in structures under earthquake excitation, *Journal of Sound and Vibration*, **297**, 1048–1067.
- Sakellariou J. S., Fassois S. D., 2007, A functional pooling framework for the identification of systems under multiple operating conditions, *Proceedings of 15th Mediterranean Conference on Control and Automation*, Athens, Greece.
- Sakellariou J. S., Fassois S. D., 2007b, Identification of dynamical systems under multiple operating conditions via Functionally Pooled ARMAX models, *Proceedings of 15th Mediterranean Conference on Control and Automation*, Athens, Greece.
- Sakellariou J. S., Fassois S. D., 2008, Vibration based fault detection and identification in an aircraft skeleton structure via a stochastic functional model based method, *Mechanical Systems and Signal Processing*, **22**, 557–573.
- Sakellariou J. S., Petsounis K. A., Fassois S. D., 2001, Vibration analysis based on-board fault detection in railway vehicle suspensions: a feasibility study, *Proceedings of First National Conference on Recent Advances in Mechanical Engineering*, Patras, Greece.
- Sakellariou J. S., Petsounis K. A., Fassois S. D., 2002, On-board fault detection and identification in railway vehicle suspensions via a functional model based method, *Proceedings of International Conference on Noise and Vibration Engineering*, Leuven, Belgium.

- Salawu O. S., 1997, Detection of structural damage through changes in frequency: a review, *Engineering Structures*, **19**(9), 718–72.
- Schoonewelle H., van der Hagen T. H. J. J., Hoogenboom J. E., 1995, Theoretical and numerical investigation into the sprt method for anomaly detection, *Annals of Nuclear Energy*, **22**(11), 731–742.
- Schoonewelle H., van der Hagen T. H. J. J., Hoogenboom J. E., 1996, A comparison of three time-domain anomaly detection methods, *Annals of Nuclear Energy*, **23**(2), 159–170.
- Schwarz G., 1978, Estimating the dimension of a model, *Annals of Statistics*, **6**, 461–464.
- Shull P. J., 2002, *Nondestructive evaluation theory, techniques, and applications*, Marcel Dekker, Inc., New York.
- Simons G., 1967, A sequential three hypothesis test for determining the mean of a normal population with known variances, *Annals of Mathematical Statistics*, **38**, 1365–1375.
- Sobel M., Wald A., 1949, A sequential dsign procedure for choosing one of three hypotheses concerning the unknown mean of normal distribution, *Annals of Mathematical Statistics*, **20**, 502–522.
- Söderström T., Stoica P., 1989, *System Identification*, Prentice–Hall.
- Sohn H., Allen D. W., Worden K., Farrar C. R., 2003, Statistical damage classification using sequential probability ratio tests, *Structural Health Monitoring*, **2**(1), 57–74.
- Sohn H., Czarnecki J. A., Farrar C. R., 2000, Structural health monitoring using statistical process control, *Journal of Structural Engineering*, **126**(11), 1356–1363.
- Sohn H., Farrar C., Hunter N., Worden K., 2001, Structural health monitoring using statistical pattern recognition techniques, *Journal of Dynamic Systems, Measurement, and Control*, **123**(4), 706–711.
- Sohn H., Farrar C. R., 2001, Damage diagnosis using time series analysis of vibration signals, *Smart Materials and Structures*, **10**, 446–451.
- Sorenson H. W., 1980, *Parameter Estimation Principles and Problems*, Marcel Dekker, Inc.
- Staszewski W. J., Boller C., Tomlinson G. R., (eds) 2004, *Health monitoring of aerospace structures: Smart sensor technologies and signal processing*, John Wiley & Sons Inc., Chichester, U.K.
- Tantaratana S., Thomas J. B., 1977, Truncated sequential probability ratio test, *Information Sciences*, **12**, 283–300.
- Tartakovsky A. G., 1989, Sequential testing of many simple hypotheses with independent observations, *Problems of Information Transmission*, **24**(4), 299–309.
- Tartakovsky A. G., Li X. R., Yarov G., 2003, Sequential detection of targets in multichannel systems, *IEEE Transactions on Information Theory*, **49**(4), 425–445.
- Toth R., 2010, *Modeling and Identification of Linear Parameter-Varying Systems*, Vol. 403 of *Lecture Notes in Control and Information Sciences*, Springer, Germany.
- Veeravalli V. V., Baum C. W., 1996, Hybrid acquisition of direct sequency cdma signals, *International Journal of Wireless Information Networks*, **3**, 55–65.

- Wald A., 1947, *Sequential Analysis*, Wiley, New York.
- Wald A., 2004, *Sequential Analysis*, Dover Publications Inc., New York.
- Wald A., Wolfowitz J., 1948, Optimum character of the sequential probability ratio test, *Annals of Mathematical Statistics*, **19**, 326–339.
- White H., 2001, *Asymptotic Theory for Econometricians*, 2nd edn, Academic Press.
- Worden K., 1997, Structural fault detection using a novelty measure, *Journal of Sound and Vibration*, **201**(1), 85–101.
- Xi F., Sun Q., Krishnappa G., 2000, Bearing diagnostics based on pattern recognition of statistical parameters, *Journal of Vibration and Control*, **6**, 375–392.
- Zacks S., 1971, *The Theory of Statistical Inference*, Wiley, New York.
- Zak A., Radzienski M., Krawczuk M., Ostachowicz W., 2012, Damage detection strategies based on propagation of guided elastic waves, *Smart Materials and Structures*, **21**, 035024 (18pp).
- Zepico-Valle J. L., Garcia-Diegez M., Gonzalez-Martinez M. P., Worden K., 2011, Experimental validation of a new statistical process control feature for damage detection, *Mechanical Systems and Signal Processing*, **25**, 2513–2525.
- Zhang Q. W., 2007, Statistical damage identification for bridges using ambient vibration data, *Computers and Structures*, **85**, 476–485.
- Zheng H., Mita A., 2007, Two-stage damage diagnosis based on the distance between arma models and pre-whitening filters, *Smart Materials and Structures*, **16**, 1829–1836.
- Zimmerman D. C., Kim H. M., Bartkowicz T. J., Kaouk M., 2001, Damage detection using expanded dynamic residuals, *Journal of Dynamic Systems, Measurement, and Control*, **123**, 699–705.

List of Figures

2.1	Workframe for statistical time series methods for Structural Health Monitoring.	18
2.2	Schematic for residual based statistical time series methods for SHM (the inspection phase is depicted outside the dashed boxes).	22
2.3	The aluminum truss structure and the experimental set-up: The force excitation (Point X), the vibration measurement positions (Points Y1 – Y3), and the considered damage types (A, B, C, D, and E).	25
2.4	(a) Power Spectral Density (PSD) and (b) Frequency Response Function (FRF) magnitude estimates for the healthy and damaged structural states (response Y1).	27
2.5	Order selection criteria for ARX(n, n) type parametric models in the healthy case (response: (a) BIC and (b) RSS/SSS).	28
2.6	Frequency stabilization diagram for ARX(n, n) type models in the healthy case (response Y1).	28
2.7	PSD based method (response Y1): Indicative damage detection results for six representative test cases (one healthy and five damaged) at the $\alpha = 10^{-4}$ risk level. The actual structural state is shown above each plot box. A damage is detected if the test statistic exceeds the critical points (dashed horizontal lines).	29
2.8	PSD based method (response Y1): Indicative damage identification results for five damage test cases at the $\alpha = 10^{-4}$ risk level, with the actual damage being of type A. Each considered test case is shown above each plot box. A damage type is identified as current when the test statistic does not exceed the critical points (dashed horizontal lines).	30
2.9	FRF magnitude based method (response Y1): Indicative damage detection results for six representative test cases (one healthy and five damaged) at the $\alpha = 10^{-5}$ risk level. The actual structural state is shown above each plot box. A damage is detected if the test statistic exceeds the critical points (dashed horizontal lines).	30
2.10	FRF magnitude based method (response Y1): Indicative damage identification results for five damage test cases at the $\alpha = 10^{-5}$ risk level, with the actual damage being of type C. Each considered test case is shown above each plot box. A damage type is identified as current when its test statistic does not exceed the critical points (dashed horizontal lines).	31
2.11	Model parameter based method (response Y1): Model parameter estimates for two healthy and five damage states (the dark lines represent point estimates and the shaded boxes ± 3 sample standard deviation confidence intervals).	32

2.12	Model parameter based method (response Y1): Indicative damage detection results for six representative test cases (one healthy and five damaged) at the $\alpha = 10^{-12}$ risk level. A damage is detected if the test statistic (bar) exceeds the critical point (dashed horizontal line).	32
2.13	Model parameter based method (response Y1): Indicative damage identification results for five damage test cases at the $\alpha = 10^{-12}$ risk level. Each bar corresponds to each considered hypothesis test, with the actual damage indicated within each subplot. A damage type is identified as current if the test statistic (bar) does not exceed the critical point (dashed horizontal line).	33
2.14	Residual variance based method (response Y1): Residual variance estimates based on ARX(103, 103) models for two healthy and five damaged states (the dark lines represent point variance estimates and the shaded boxes ± 3 sample standard deviation confidence intervals).	34
2.15	Residual variance based method (response Y1): Indicative damage detection results for six representative test cases (one healthy and five damaged) at the $\alpha = 10^{-12}$ risk level. A damage is detected if the test statistic (bar) exceeds the critical point (dashed horizontal line).	34
2.16	Residual variance based method (response Y1): Indicative damage identification results for five damage test cases at the $\alpha = 10^{-12}$ risk level. Each bar corresponds to each considered hypothesis test, with the actual damage indicated within each subplot. A damage type is identified as current if the test statistic (bar) does not exceed the critical point (dashed horizontal line).	35
2.17	Residual uncorrelatedness based method (response Y1): Normalized residual ACF estimates $\hat{\rho}[\tau]$ based on ARX(138, 138) models for one healthy and five damaged states. The dashed horizontal lines designate the limits within which the ACF can be accepted as being zero at the $\alpha = 0.05$ risk level.	35
2.18	Residual uncorrelatedness based method (response Y1): Indicative damage detection results for six representative test cases (one healthy and five damaged) at the $\alpha = 10^{-12}$ risk level (max lag $r = 25$). A damage is detected if the test statistic (bar) exceeds the critical point (dashed horizontal line).	36
2.19	Residual uncorrelatedness based method (response Y1): Indicative damage identification results for five damage test cases at the $\alpha = 10^{-12}$ risk level (max lag $r = 25$). Each bar corresponds to each considered hypothesis test, with the actual damage indicated within each subplot. A damage type is identified as current if the test statistic (bar) does not exceed the critical point (dashed horizontal line).	36
2.20	The scale aircraft skeleton structure and the experimental set-up: The force excitation (Point X), the vibration measurement locations (Points Y1 – Y4), and the bolts connecting the various elements of the structure.	40
2.21	Non-parametric Welch-based Frequency Response Function (FRF) magnitude estimates for the healthy and damaged structural states (Point X – Point Y2 transfer function).	41
2.22	Bayesian Information Criterion (BIC) for VARX(n, n) type parametric models in the healthy case.	42
2.23	PSD based method: Representative damage detection results (sensor Y1) at the $\alpha = 10^{-4}$ risk level. The actual structural state is shown above each plot.	44

2.24	PSD based method: Representative damage identification results (sensor Y3) at the $\alpha = 10^{-4}$ risk level, with the actual damage being of type A. Each considered damage hypothesis is shown above each plot.	44
2.25	FRF based method: Representative damage detection results (sensor Y4) at the $\alpha = 10^{-6}$ risk level. The actual structural state is shown above each plot.	45
2.26	FRF based method: Representative damage identification results (sensor Y2) at the $\alpha = 10^{-6}$ risk level, with the actual damage being of type E. Each considered damage hypothesis is shown above each plot.	46
2.27	Residual variance based method: Representative damage detection results (sensor Y2; healthy – 60 experiments; damaged – 200 experiments). A damage is detected if the test statistic exceeds the critical point (dashed horizontal line).	47
2.28	Residual variance based method: Representative damage identification results (sensor Y3; 240 experiments), with the actual damage being of type D. A damage is identified as type D if the test statistic is below the critical point (dashed horizontal line).	47
2.29	SPRT based method: Representative damage detection results (sensor Y1) at the $\alpha = \beta = 0.01$ risk levels ($\sigma_1/\sigma_o = 1.1$). The actual structural state is shown above each plot.	48
2.30	SPRT based method: Representative damage identification results (sensor Y4) at the $\alpha = \beta = 0.01$ risk levels ($\sigma_1/\sigma_o = 1.1$) with the actual damage being of type B. Each considered damage hypothesis is shown above each plot.	49
2.31	Model parameter based method: Representative damage detection results for three structural states (healthy – 60 experiments; damaged – 80 experiments). A damage is detected if the test statistic exceeds the critical point (dashed horizontal line).	50
2.32	Model parameter based method: Representative damage identification results (240 experiments), with the actual damage being of type F. A damage is identified as type F if the test statistic is below the critical point (dashed horizontal line).	50
2.33	Residual likelihood function based method: Representative damage detection results (healthy – 60 experiments; damaged – 200 experiments). A damage is detected if the test statistic exceeds the critical point (dashed horizontal line).	51
2.34	Residual likelihood function based method: Representative damage identification results (240 experiments), with the actual damage being of type A. A damage is identified as type A if the test statistic is below the critical point (dashed horizontal line).	52
3.1	Schematic representation of the problem showing the operating points on the (k^1, k^2) plane, an excitation-response data set corresponding to a particular operating point, and the VFP-ARMAX model structure.	59
3.2	The ARX model structure.	61
3.3	Statistical hypothesis testing based on a χ^2 distributed statistic (one-tail test).	76
3.4	Functional basis dimensionality selection criteria for VFP-ARX(4, 1) ₆ models: (a) BIC and (b) RSS/SSS versus functional subspace dimensionality p (each cross (+) designates the value from one simulation run; 500 runs for each p). In the close-ups inside each plot the mean values for each p are depicted (\diamond).	82

- 3.5 Indicative VFP-ARX(4,1)₆ model validation results: Q statistic versus the 320 cross-section at the $\alpha = 0.01$ (99%) confidence level (maxlag = 50). The model is valid when the test statistics lie below the critical point (dashed red line) for the selected confidence level. 82
- 3.6 Indicative VFP-ARX(4,1)₆ model validation results: (a) top line plots: cross correlation function between various model residual series $e_{\mathbf{k}}[t]$ pairs at the $\alpha = 0.01$ (99%) confidence level, and (b) bottom line plots: cross correlation function between various input $x_{\mathbf{k}}$ and residual series $e_{\mathbf{k}}[t]$ pairs at the $\alpha = 0.01$ (99%) confidence level (maxlag = 50). 83
- 3.7 Indicative VFP-ARX(4,1)₆ projection coefficient estimation results by the OLS, WLS and ML methods (Monte Carlo results based on 500 runs per method): sample mean estimates ± 1.96 sample standard deviations (shaded boxes), along with the corresponding true values (dashed red lines - - -) and the theoretical asymptotic WLS standard deviations (dashed blue lines - - -), which coincide with the Cramer-Rao lower bound. 84
- 3.8 Indicative VFP-ARX(4,1)₆ residual variance results by the OLS, WLS and ML methods (Monte Carlo results based on 500 runs per method): sample mean estimates ± 1.96 sample standard deviations (shaded boxes), along with the corresponding residual true values (dashed red lines - - -). 85
- 3.9 VFP-ARX(4,1)₆ model parameter a_1 estimates versus k^1 and k^2 series: (a) true system, (b) mean OLS estimate, (c) mean WLS estimate and (d) mean ML estimate (mean parameters over 500 runs). 86
- 3.10 VFP-ARX(4,1)₆ model parameter b_0 estimates versus k^1 and k^2 series: (a) true system, (b) mean OLS estimate, (c) mean WLS estimate and (d) mean ML estimate (mean parameters over 500 runs). 87
- 3.11 VFP-ARX(4,1)₆ second natural frequency ω_2 versus k^1 and k^2 series: (a) true system, (b) mean OLS estimate, (c) mean WLS estimate and (d) mean ML estimate (mean parameters over 500 runs). 88
- 3.12 VFP-ARX(4,1)₆ first damping ratio ζ_1 versus k^1 and k^2 series: (a) true system, (b) mean OLS estimate, (c) mean WLS estimate and (d) mean ML estimate (mean parameters over 500 runs). 89
- 3.13 VFP-ARX(4,1)₆ based frequency response magnitude versus frequency and k^1 series (k^2 is set to k_3^2): (a) true system, (b) mean OLS estimate, (c) mean WLS estimate and (d) mean ML estimate (mean parameters over 500 runs). 90
- 3.14 Indicative VFP-ARX(4,1)₉ model validation results: (a) top line plots: cross correlation function between various model residual series $e_{\mathbf{k}}[t]$ pairs at the $\alpha = 0.01$ (99%) confidence level, and (b) bottom line plots: cross correlation function between various input $x_{\mathbf{k}}$ and residual series $e_{\mathbf{k}}[t]$ pairs at the $\alpha = 0.01$ (99%) confidence level (maxlag = 50). 90
- 3.15 Indicative VFP-ARX(4,1)₉ projection coefficient estimation results by the OLS, WLS and ML methods (Monte Carlo results based on 500 runs per method): sample mean estimates ± 1.96 sample standard deviations (shaded boxes), along with the corresponding true values (dashed red lines - - -) and the theoretical asymptotic WLS standard deviations (dashed blue lines - - -), which coincide with the Cramer-Rao lower bound. 91

3.16	Indicative VFP-ARX(4, 1) ₉ residual variance results by the OLS, WLS and ML methods (Monte Carlo results based on 500 runs per method): sample mean estimates ± 1.96 sample standard deviations (shaded boxes), along with the corresponding residual true values (dashed red lines - - -).	92
3.17	VFP-ARX(4, 1) ₉ model parameter a_4 estimates versus k^1 and k^2 series: (a) true system, (b) mean OLS estimate, (c) mean WLS estimate and (d) mean ML estimate (mean parameters over 500 runs).	93
3.18	VFP-ARX(4, 1) ₉ model parameter b_0 estimates versus k^1 and k^2 series: (a) true system, (b) mean OLS estimate, (c) mean WLS estimate and (d) mean ML estimate (mean parameters over 500 runs).	94
3.19	VFP-ARX(4, 1) ₉ second natural frequency ω_2 versus k^1 and k^2 series: (a) true system, (b) mean OLS estimate, (c) mean WLS estimate and (d) mean ML estimate (mean parameters over 500 runs).	95
3.20	VFP-ARX(4, 1) ₉ first damping ratio ζ_1 versus k^1 and k^2 series: (a) true system, (b) mean OLS estimate, (c) mean WLS estimate and (d) mean ML estimate (mean parameters over 500 runs).	95
3.21	VFP-ARX(4, 1) ₉ based frequency response magnitude versus frequency and k^2 series (k^1 is set to k_8^1): (a) true system, (b) mean OLS estimate, (c) mean WLS estimate and (d) mean ML estimate (mean parameters over 500 runs).	96
C.1	AutoRegressive (AR) VFP-ARX(4, 1) ₆ true model parameters versus k^1 and k^2 series.	105
C.2	Exogenous (X) VFP-ARX(4, 1) ₆ true model parameters versus k^1 and k^2 series.	105
C.3	The two VFP-ARX(4, 1) ₆ true model natural frequencies ω versus k^1 and k^2 series.	106
C.4	The two VFP-ARX(4, 1) ₆ true model damping ratios ζ versus k^1 and k^2 series.	106
C.5	VFP-ARX(4, 1) ₆ based frequency response magnitude versus frequency and k^2 series (k^1 is set to k_8^1): (a) true system, (b) mean OLS estimate, (c) mean WLS estimate and (d) mean ML estimate (mean parameters over 500 runs).	106
C.6	AutoRegressive (AR) VFP-ARX(4, 1) ₉ true model parameters versus k^1 and k^2 series.	107
C.7	Exogenous (X) VFP-ARX(4, 1) ₉ true model parameters versus k^1 and k^2 series.	107
C.8	The two VFP-ARX(4, 1) ₉ true model natural frequencies ω versus k^1 and k^2 series.	107
C.9	The two VFP-ARX(4, 1) ₉ true model damping ratios ζ versus k^1 and k^2 series.	108
C.10	VFP-ARX(4, 1) ₉ based frequency response magnitude versus frequency and k^1 series (k^2 is set to k_5^2): (a) true system, (b) mean OLS estimate, (c) mean WLS estimate and (d) mean ML estimate (mean parameters over 500 runs).	108
4.1	Flowchart representation of the VFP-ARX model based method.	119
4.2	(a) The scale aircraft skeleton structure and the experimental set-up; (b) the right wing-tip with the force excitation (Point X), the first vibration measurement position (Point Y), and the aa' and bb' axes that define the A and B damage topologies, respectively; (c) the horizontal stabilizer with the second vibration measurement position (Point Z) and the cc' axis that defines the C damage topology.	121

4.3	The effects of two topology A damages on parametrically obtained FRF magnitude curves corresponding to each one of the Point X – Point Y (a – b) and Point X – Point Z (c – d) transfer functions. The gray zones depict 95% confidence intervals (uncertainty zones) for the healthy FRF magnitudes. The (b) and (d) subplots are blow ups of (a) and (c), respectively.	123
4.4	Damage topology A model ($\mathcal{M}_{\mathbf{k}}^{AY}$) based FRF magnitude versus frequency and (a) damage magnitude (for set location $k^2 = 0$ cm) and (b) damage location (for set magnitude $k^1 = 48.792$ g).	126
4.5	Typical damage topology A model ($\mathcal{M}_{\mathbf{k}}^{AY}$) AR parameters versus damage magnitude (k^1 g) and location (k^2 cm).	126
4.6	Indicative natural frequencies versus damage magnitude (k^1 g) and damage location (k^2 cm) based on the damage topology A ($\mathcal{M}_{\mathbf{k}}^{AY}$) model: (a) second mode; (b) third mode; (c) fourth mode; and (d) fifth mode (compare with Table 4.5 and Figure 4.4).	127
4.7	Damage detection results for the various Test Cases and each vibration measurement position (upper plot: Point Y; lower plot: Point Z): t statistic (bars) and the critical points (---) at the $\alpha = 0.05$ risk level. In each Test Case damage is detected if t exceeds the critical point.	128
4.8	Damage topology identification results for various Test Cases and each vibration measurement position (Points Y and Z – to be read in rows): In each plot the Q statistic (bar) for the hypothesis of the current damage belonging to each one of the A, B, C topologies is shown relative to the critical point (---) at the $\alpha = 0.05$ risk level. A hypothesis is accepted – and the corresponding damage topology is accepted as true – if the Q statistic lies below the critical point. The actual damage and its characterization as “local” or “remote” are indicated above each plot.	129
4.9	Damage localization and magnitude interval estimation results: In each plot results of a Test Case in terms of estimated damage magnitude and precise location are presented for two vibration measurement positions (Points Y and Z), one characterized as “local” damage (dark – blue) and the other as “remote” (light – magenta). Damage magnitude and location point estimates are indicated by diamonds and interval (uncertainty) estimates by ellipsoids at the $\alpha = 0.05$ risk level. Damage detection may be also re-confirmed by examining whether the damage magnitude uncertainty includes the zero (no damage) point. In each Test Case the actual damage is indicated by a cross in the diagram as well as above each plot.	130
5.1	(a) Operating Characteristic (OC) and (b) Average Sample Number (ASN) functions for various residual standard deviation ratios $q = \sigma_1/\sigma_o$ and constant strength $(\alpha, \beta) = 0.01$. The vertical colored dashed lines designate the σ_1 values for the corresponding ratios q	148
5.2	(a) Operating Characteristic (OC) and (b) Average Sample Number (ASN) functions for various strengths (α, β) and constant residual standard deviation ratio $q = \sigma_1/\sigma_o = 1.1$	148
5.3	The aluminum truss structure and the experimental set-up: The force excitation (Point X), the vibration measurement positions (Points Y1 – Y3), and the considered damage types (A, B, C, D, and E).	153
5.4	Frequency Response Function (FRF) magnitude estimates for the healthy and damage structural states: (a) Point X – Point Y1 and (b) Point X – Point Y3 transfer functions.	154

5.5	BIC order selection criterion for ARX(n, n) type parametric models in the healthy case for all vibration response measurement locations.	155
5.6	Frequency stabilization diagram for ARX(n, n) type models in the healthy case for all vibration response measurement locations. The dashed red lines indicate the selected model orders in each case.	156
5.7	Healthy structure: (a) Operating Characteristic (OC) and (b) Average Sample Number (ASN) functions for various residual standard deviation ratios $q = \sigma_1/\sigma_o$ and constant strength $(\alpha, \beta) = 0.01$ (vibration response Y2). The vertical colored dashed lines designate the σ_1 values for the corresponding ratios q . The vertical cyan dashed lines represent the residual standard deviation values obtained from the 100 baseline healthy data sets.	158
5.8	Healthy structure: (a) Operating Characteristic (OC) and (b) Average Sample Number (ASN) functions for various strengths (α, β) and residual standard deviation ratio $q = \sigma_1/\sigma_o = 1.1$ (vibration response Y2). The vertical cyan dashed lines represent the residual standard deviation values obtained from the 100 baseline healthy data sets.	158
5.9	Damage type A: (a) Operating Characteristic (OC) and (b) Average Sample Number (ASN) functions for various residual standard deviation ratios $q = \sigma_1/\sigma_o$ and constant strength $(\alpha, \beta) = 0.01$ (vibration response Y3). The vertical cyan dashed lines represent the residual standard deviation values obtained from the 100 baseline damage type A data sets.	159
5.10	Indicative damage detection results for response Y2 at the $\alpha = \beta = 0.01$ risk levels ($q = \sigma_1/\sigma_o = 1.1$). The actual structural state is shown above each plot.	160
5.11	Average number of correct detections for the healthy structure (response Y2): experimental (dashed blue lines ± 1.96 standard deviation confidence intervals from 1100 inspection healthy data sets of 1000 samples each) and theoretical (dashed red lines) point estimates for various SPRT strengths (α, β) versus residual standard deviation ratio $q = \sigma_1/\sigma_o$. The actual strength is shown above each plot.	161
5.12	False alarms percentage for all vibration response measurement locations and various SPRT strengths (α, β) versus residual standard deviation ratio $q = \sigma_1/\sigma_o$; 1100 healthy inspection data sets are used.	162
5.13	Average number of correct damage detections under damage type A for all vibration response measurement locations and various SPRT strengths (α, β) versus residual standard deviation ratio $q = \sigma_1/\sigma_o$; 800 damage type A inspection data sets are used.	163
5.14	Indicative damage identification results for response Y1 at the $\alpha_{ij} = 0.01$ error probabilities level, with the actual damage being of type C. The actual structural state is shown above each plot.	164
5.15	Indicative damage identification results for response Y2 at the $\alpha = \beta = 0.01$ risk levels ($q = \sigma_1/\sigma_o = 1.1$) for damage types B and D. The baseline model of damage type B is used with the actual structural state shown above each plot.	166

List of Tables

1.1	Thesis chapters.	9
2.1	Workframe setup: structural state, vibration signals used, and the characteristic quantity (baseline and inspection phases).	17
2.2	Statistical hypothesis testing problems for the damage detection and identification tasks.	18
2.3	Estimation of non-parametric statistical time series models.	20
2.4	The considered damage types, number of experiments, and vibration signal details.	26
2.5	Non-parametric estimation details.	27
2.6	Selected models and estimation details (response Y1).	29
2.7	Damage detection and identification summary results for three responses (Y1, Y2 and Y3).	37
2.8	The damage scenarios and experimental details.	40
2.9	Non-parametric estimation details.	41
2.10	Characteristics of the employed statistical time series methods for SHM	43
2.11	Scalar methods: damage detection and identification summary results.	53
2.12	Vector methods: damage detection and identification summary results.	53
3.1	Functional subspaces of bivariate polynomials up to fourth degree (see Appendix A).	80
3.2	Indicative Monte Carlo estimation results for the VFP-ARX(4,1) ₆ model (selected coefficients of projection; 500 runs per method; mean estimate ± 1 standard deviation).	81
3.3	Genetic Algorithm (GA) details for functional subspace determination of Test Case I.	81
3.4	CPU and relative (test case I/test case II) CPU times for the OLS, WLS and ML estimation methods as percentage of the total ML time (single run).	85
3.5	Indicative Monte Carlo estimation results for the VFP-ARX(4,1) ₉ model (selected coefficients of projection; 500 runs per method; mean estimate ± 1 standard deviation).	86
3.6	Genetic Algorithm (GA) details for functional subspace determination of Test Case II.	88
4.1	Dimensions of the scale aircraft skeleton structure.	121
4.2	The considered damage topologies (modes) – see Figure 4.2b-c.	122
4.3	Signal pre-processing and details.	122

4.4	The considered test cases [†]	123
4.5	Global modal characteristics (natural frequencies and damping ratios) of the structure based on the identified ARX(48, 48) model of the healthy structure.	124
4.6	The structure of the identified damage topology (mode) models.	125
4.7	Genetic Algorithm (GA) details for functional subspace dimensionality estimation. . .	125
5.1	The considered damage types, number of experiments, and vibration signal details. . .	152
5.2	Selected models and estimation details.	156
5.3	Selected nominal residual standard deviation σ_o values for the damage detection SPRT. . .	157
5.4	Damage detection summary results for the three vibration responses (Y1, Y2 and Y3). . .	162
5.5	Nominal residual standard deviation values $\sigma_A, \dots, \sigma_E$ for damage identification. . . .	164
5.6	Damage identification summary results for the three vibration responses (Y1, Y2 and Y3).	165

Curriculum Vitae

Personal information

Fotis P. Kopsaftopoulos

Mechanical & Aeronautical Engineer

Date of Birth: 26/06/1980

Place of Birth: Athens, Greece

Citizenship: Greek

E-mail: fkopsaf@mech.upatras.gr

Education

- Ph.D. in Mechanical Engineering and Aeronautics
Department of Mechanical Engineering & Aeronautics, University of Patras, Patras, Greece
October 2004 – September 2011
Ph.D. Thesis Title: Advanced Functional and Sequential Statistical Time Series Methods for Damage Diagnosis in Mechanical Structures.
Supervisor: Prof. Spilios D. Fassois
- Diploma in Mechanical Engineering and Aeronautics
Department of Mechanical Engineering & Aeronautics, University of Patras, Patras, Greece
October 1998 – June 2004
M.Sc. Thesis Title: Parametric Identification of a Scale Aircraft Skeleton Structure via Multi-variate ARX and ARMAX Models.
Supervisor: Prof. Spilios D. Fassois

Research interests

stochastic system identification, damage detection & identification, Structural Health Monitoring (SHM), signal processing, fault detection & diagnosis in systems/structures, vibration testing, modal analysis, identification of stochastic systems under multiple operating conditions and uncertainties

Research experience

- FP7 Research Project: 4 Dimension Contract – Guidance and Control (4DCo–GC).
January – January 2012
- FP7 Research Project: The Personal Plane (PPlane) project: Assessment and validation of pioneering concepts for personal air transport systems.
January – April 2010
- FP6 Research Project: Structural Health Monitoring (SHM) in Action.
January 2007 – December 2009
- Greek General Secretariat for Research & Development: Pythagoras II Grant – Development of smart mechanical structures with stochastic damage self-diagnosis capabilities.
January 2005 – December 2007

Academic experience

- Teaching assistant for the “Systems & Automatic Control I” laboratory exercises (fourth year undergraduate course).
2004 – 2009
- Teaching assistant for the “Mechatronics” laboratory exercises (third year undergraduate course).
2006 – 2009

Administrative experience

Supervision of a number of diploma thesis students (> 10) in the Stochastic Mechanical Systems & Automation (SMSA) laboratory of the Mechanical Engineering & Aeronautics Department of University of Patras.

Awards

State Scholarship Foundation (I.K.Y.) 1998 – 1999

Language Skills

- Greek (mother tongue)
- English (CAE, Advanced level)
- French (DELFF A1–A6, Advanced level)

Publications

Journal publications

1. Kopsaftopoulos F.P. and Fassois S.D., “**Scalar and vector time series methods for vibration based damage diagnosis in a scale aircraft skeleton structure**”, *invited paper to Journal of Theoretical and Applied Mechanics*, Vol. 49, No. 3, pp. 727–756, 2011.
2. Kopsaftopoulos F.P. and Fassois S.D., “**Vibration based health monitoring for a light-weight truss structure: experimental assessment of several statistical time series methods**”, *Mechanical Systems and Signal Processing (ISMA Special Issue)*, Vol. 24, pp. 1977–1997, 2010.
3. Kopsaftopoulos F.P. and Fassois S.D., “**Vibration based structural damage detection and precise assessment via stochastic functionally pooled models**”, *Key Engineering Materials*, Vol. 347, pp. 127–132, 2007.
4. Kopsaftopoulos F.P. and Fassois S.D., “**A stochastic functional model based method for vibration based damage detection, precise localization, and magnitude estimation**”, accepted for publication, *Mechanical Systems and Signal Processing*, 2011.
5. Kopsaftopoulos F.P. and Fassois S.D., “**A sequential statistical time series method for vibration based Structural Health Monitoring**”, *under preparation for publication*.
6. Kopsaftopoulos F.P. and Fassois S.D., “**Identification of stochastic systems under multiple operating conditions: The Vector-dependent Functionally Pooled (VFP) parametrization**”, *under preparation for publication*.

Conference publications

1. Kopsaftopoulos F.P. and Fassois S.D., “**Vector-dependent Functionally Pooled ARX models for the identification of systems under multiple operating conditions**”, *accepted in the 16th IFAC Symposium on System Identification (SYSID)*, Brussels, Belgium, July 2012.
2. Kopsaftopoulos F.P. and Fassois S.D., “**Statistical time series methods for damage diagnosis in a scale aircraft skeleton structure: loosened bolts damage scenarios**”, *Journal of Physics: Conference Series 305 (2011) 012056, Proceedings of the 9th International Conference on Damage Assessment of Structures (DAMAS)*, St. Anne’s College, Oxford, U.K., July 2011.
3. Kopsaftopoulos F.P., Apostolellis P.G., and Fassois S.D., “**Output-only parametric identification of a scale cable-stayed bridge structure: A comparison of vector AR and state space methods**”, *Proceedings of the 4th International Operational Modal Analysis Conference (IOMAC)*, Istanbul, Turkey, May 2011.
4. Kopsaftopoulos F.P. and Fassois S.D., “**Vibration based health monitoring for a thin aluminum plate – A comparative assessment of statistical time series methods**”, *Proceedings of the 5th European Workshop on Structural Health Monitoring (EWSHM)*, Sorrento, Italy, July 2010.
5. Kopsaftopoulos F.P. and Fassois S.D., “**Vibration based health monitoring for a light-weight truss structure: experimental assessment of several statistical time series methods**”, *Proceedings of the ISMA 2010 International Conference on Noise and Vibration Engineering*, Leuven, Belgium, September 2010.

6. Kopsaftopoulos F.P., Magripis S.G., Amlianitis A.D., and Fassois S.D., “**Scalar and vector time series methods for vibration based damage diagnosis in an aircraft scale skeleton structure**”, *Proceedings of the ASME 2010 10th Biennial Conference on Engineering Systems Design and Analysis (ESDA)*, Istanbul, Turkey, July 2010.
7. Kopsaftopoulos F.P. and Fassois S.D., “**Experimental assessment of time series methods for structural health monitoring (SHM)**”, *Proceedings of the 4th European Workshop on Structural Health Monitoring (EWSHM)*, Cracow, Poland, 2008.
8. Kopsaftopoulos F.P. and Fassois S.D., “**Vibration based structural damage detection and precise assessment via stochastic functionally pooled models**”, *Proceedings of the 7th International Conference on Damage Assessment of Structures (DAMAS)*, Torino, Italy, 2007.
9. Kopsaftopoulos F.P. and Fassois S.D., “**Identification of stochastic systems under multiple operating conditions: the Vector-dependent FP-ARX parametrization**”, *Proceedings of the 14th Mediterranean Conference on Control and Automation (MCCA)*, Ancona, Italy, 2006.
10. Kopsaftopoulos F.P. and Fassois S.D., “**Vibration-based fault detection and assessment in a scale aircraft structure via stochastic VFP-ARX models**”, *Proceedings of the 3rd European Workshop on Structural Health Monitoring (EWSHM)*, Granada, Spain, 2006.